Activator and inhibitor interactions and expression during trichome patterning in *Arabidopsis thaliana*

Inaugural-Dissertation

zur

Erlangung des Doktorgrades

der Mathematisch-Naturwissenschaftlichen Fakultät

der Universität zu Köln

vorgelegt von

Hanna Bechtel

aus Neunkirchen (Saar)

Köln, 2024

Berichterstatter/in: Prof. Dr. Martin Hülskamp

Prof. Dr. Ute Höcker

Prüfungsvorsitzender: Prof. Dr. Kay Hofmann

Tag der mündlichen Prüfung: 09.09.2024

Table of Contents

List of Tables

List of Figures

List of Abbreviations

α	alpha
°C	degree Celsius
Δ	delta, deletion
µg	microgram
µl	microliter
µs	microseconds
4-MU	4-Methylumbelliferone
A	adenosine
aa	amino acid
ABA	abscisic acid
AC	Activator complex
approx	approximately
A. thaliana	Arabidopsis thaliana
A. tumefaciens	Agrobacterium tumefaciens
bHLH	Basic helix-loop-helix
BiFC	Bimolecular fluorescence complementation
bp	Base pair
BSA	bovine serum albumin
C	cysteine
$CaCl_2$	Calcium chloride
Carb.	Carbenicillin
ccdB	Control of cell death protein B, inhibitor of DNA gyrases
CFP	Cyan fluorescent protein
ChIP	Chromatin immunoprecipitation
C. hirsuta	Cardamine hirsuta
Chlor.	Chloramphenicol
cm	centimetre
Col-0	Columbia-0
CPC	CAPRICE
CRE	Cis-regulatory element
CRISPR	Clustered Regularly Interspaced Short Palindromic Repeats
ddH_2O	Double distilled water
DNA	Deoxyribonucleic acid
dNTPs	deoxyribonucleotides
DMF	dimethylformamide
DMSO	dimethyl sulfoxide
E. coli	Escherichia coli

e.g.	exempli gratia
E2A	2A sequence originated from equine rhinitis A virus
EDTA	ethylenediaminetetraacetic acid
EGL3	ENHANVER OF GLABRA3
et al.	et alii; “and others”
ETC1	ENHANCER OF TRY AND CPC 1
ETC2	ENHANCER OF TRY AND CPC 2
ETC3	ENHANCER OF TRY AND CPC 3
EtOH	ethanol
Ex.	exon
F2A	2A sequence originated from foot-and-mouth disease virus
g	gram
G	guanine
GA	Gibberellic acid
Gent.	Gentamycin
GL1	GLABRA1
GL2	GLABRA2
GL3	GLABRA3
GUS	β-glucuronidase
GW	Gateway
h	hour/hours
H2B	histone 2B
HCl	hydrogen chloride; in aqueous solutions: hydrochloric acid
HY5	ELONGATED HYPOCOTYL 5
Hygro.	Hygromycin
Hz	Hertz
IC	Inhibitor complex
i. e.	id est, “in other words”
In.	intron
Kan.	Kanamycin
kb	kilo base
kbp	kilo base pair
KCl	Potassium chloride
kDa	kilodaltons
KikGR	Kikume GreenRed
KOH	Potassium hydroxide
l	liter
LB	Lysogeny broth
Ler	Landsberg erecta

m	monomeric
M	molar concentration
MBW	MYB, bHLH, WD40
MeOH	methanol
MES	2-(*N*-morpholino) ethanesulfonic acid
mg	milligram
MG132	Cbz-leu-leu-leucinal; proteasome inhibitor
$MgCl_2$	magnesium chloride
$MgSO_4$	magnesium sulfate
min	minute/minutes
mKikGR	monomeric Kikume GreenRed
ml	millilitre
mm	millimetre
mM	millimole
ms	milliseconds
MS	Murashige and Skoog
MUG	4-Methylumbelliferyl-β-D-glucuronic acid dihydrate
MYB	myeloblastosis
MYC	myelocytomatosis
n	number
Na_2HPO_4	disodium hydrogen phosphate
NaH_2PO_4	sodium dihydrogen phosphate
NaCl	sodium chloride
NaOAc	sodium acetate
NaOCl	sodium hypochloride
NaOH	sodium hydroxide
N. benthamiana	Nicotiana benthamiana
ng	nanogram
NLS	nuclear localization signal
nm	nanometre
OD	optical density
OD_{600}	absorbance measured at 600 nm wavelength
Ox	Oxford
p	Promoter, probability value
p35S	35S promoter of the Cauliflower mosaic virus
P2A	2A sequence originated from porcine teschovirus-1
PCR	polymerase chain reaction
PFD	perfluorodecalin
PIPES	piperazine-N,N'-bis(2-ethanesulfonic acid)

PLACE	plant cis-acting regulatory DNA elements
pmol	picomole
psi	pound-force per square inch
RCI2A	RARE-COLD-INDUCIBLE 2A
RFP	red fluorescence protein
Rif.	Rifampicin
ROI	Region of interest
rpm	rounds per minute
SDS	sodium dodecyl sulfate
sec	second/seconds
S/MAR	Scaffold/matrix attachment region
T2A	2A sequence originated from thosea asigna virus
T	thymine
T_A	annealing temperature
TAE	Tris base, acetic acid and EDTA.
TCL1	TRICHOMELESS1
TCL2	TRICHOMELESS2
TF	transcription factor
TFP	teal fluorescence protein
T_M	melting temperature
Tris	Tris (hydroxymethyl) aminomethane
TRY	TRIPTYCHON
TSS	transcription start site
TTG1	TRANSPARENT TESTA GLABRA1
TTG2	TRANSPARENT TESTA GLABRA2
U	uridine
UTR	untranslated region
V	volt
w/o	without
WD40	tryptophane-aspartic acid repeat
WER	WEREWOLF
WRKY	tryptophan-arginine-lysine-tyrosine domain
(w/v)	(weight/volume)
x g	gravitational acceleration
X-Gluc	5-Bromo-4-chloro-1H-indol-3-yl β-D-glucopyranosiduronic acid
YEB	yeast extract beef
YFP	yellow fluorescent protein

Zusammenfassung

Die Etablierung des Trichomschicksals ist ein gut untersuchter *de novo*-Musterungsprozess im Modellorganismus *A. thaliana*. Die regulatorischen Netzwerke, die der Musterungsmaschinerie zugrunde liegen, sind umfassend erforscht, aber einige Prozesse bleiben schwer fassbar. Das Zusammenspiel zwischen mathematischen Modellen, die biologische Muster beschreiben, und experimentellen Beobachtungen führte zur Etablierung von Trichommusterbildungsmodellen. Diese Modelle können das Trichommuster des Wildtyps präzise vorhersagen, haben jedoch Einschränkungen bei der Erklärung komplexerer Trichomphänotypen. Darüber hinaus werden bestimmte Parameter in diesen Modellen geschätzt und basieren nicht auf experimentellen Daten, wie z. B. Proteinproduktion und Abbauraten. Darüber hinaus wurden einige Annahmen der Modelle noch nicht in biologischen Experimenten verifiziert, wie z. B. eine positive Rückkopplungsschleife von Aktivatoren auf ihre eigene Genexpression oder die Bewegung von Aktivatoren. In der vorgestellten Studie wurden verschiedene Aspekte der Trichommusterbildung untersucht, um einige ungelöste Fragen zu beleuchten. Um Daten zur Proteinstabilität, -produktion und -abbauraten zu generieren, wurden virale „Selbstspaltungsstellen“ verwendet, um gewünschte Trichommusterbildungsgene in einer ratiometrischen Menge mit einer internen Kontrolle zu exprimieren. Diese Experimente zeigten eine Stabilisierung von MYB-Proteinen in Gegenwart von bHLH-Proteinen, aber nicht umgekehrt. Darüber hinaus wurde eine Destabilisierung des bHLH-Proteins GL3 durch sich selbst aufgedeckt. Diese Stabilitätsänderungen erwiesen sich als abhängig von Protein-Protein-Interaktionen, und es wurde ein mutmaßlicher Zusammenhang mit dem proteasomalen Abbau dieser Proteine entdeckt. Zusätzlich zu den Proteinstudien wurde die Genexpression mehrerer regulatorischer Sequenzen, die an der Trichommusterbildung beteiligt sind, hinsichtlich ihrer cis-regulatorischen Elemente und der Transaktivierung durch verschiedene Musterbildungsgene untersucht. Die Mutation von WRKY-Bindungsstellen im zweiten Intron von *GL3* ergab, dass sie nicht an der *GL3*-Expressionskontrolle beteiligt sind, was auf andere Mechanismen hindeutet. Insgesamt wurde die *GL3*-Expression durch die Gegenwart der getesteten Trichommusterbildungsgene nicht in hohem Maße beeinflusst, und was noch wichtiger ist: In diesem Aufbau konnte eine Verringerung der GL3-Expression durch die eigene Gegenwart nicht nachgewiesen werden. Interessanterweise könnte die Untersuchung verschiedener *GL1*-regulatorischer Sequenzen auf ein fehlendes Enhancer-Element hinweisen. Die untersuchte Genomsequenz von *GL1* kann Silencer-Elemente enthalten, die aufgrund der bisher verwendeten experimentellen Verfahren maskiert sind. Zusätzlich wurde für *GL1* eine positive Rückkopplungsschleife in Kombination mit der Expression von *GL3*, *TTG1* und *TTG2* beobachtet, was ein fehlendes Bindeglied in Bezug auf Musterbildungsmodelle sein könnte. Schließlich führten Rettungsexperimente mit Cardamine R2R3MYB-Sequenzen zur überraschenden teilweisen Rettung

der Trichomphänotypen von *Arabidopsis gl1* Mutanten, was auf konservierte Proteinfunktionen sowie ein gewisses Maß konservierter regulatorischer Sequenzen über Arten hinweg hinweist. Interessanterweise konnte *ChWER* Trichome in *gl1* induzieren, was eine mögliche Divergenz in der Trichom- und Wurzelhaarbildung zwischen Arten aufzeigte.

Abstract

The establishment of trichome fate is a well-studied *de novo* patterning process in the model organism *A. thaliana*. The regulatory networks underlying the patterning machinery are extensively researched but some processes remain elusive. The interplay between mathematic models describing biological patterns and experimental observations led to the establishment of trichome patterning models. These models can precisely predict the wildtype trichome pattern but face limitations in explaining more complex trichome phenotypes. Additionally, variables in these models are estimated and not based on experimental data, such as protein production and degradation rates. Moreover, some assumptions of the models have not been verified in biological experiments yet, like a positive feedback loop of activators on their own gene expression or the movement of activators. In the presented study, different aspects of trichome patterning were examined to shed light on some unresolved questions. To generate data on protein stability, production, and degradation rates, viral "self-cleavage" sites were utilized to express desired trichome patterning genes in a ratiometric amount with an internal control. These experiments revealed stabilization of MYB proteins in the presence of bHLH proteins but not vice versa. Moreover, a destabilization of the bHLH protein GL3 through itself was uncovered. These stability changes were found to be dependent on protein-protein interactions, and a putative link to the proteasomal degradation of these proteins was discovered. Additionally to protein studies, the gene expression of several regulatory sequences involved in trichome patterning was examined regarding their cis-regulatory elements and transactivation by various patterning genes. Mutation of WRKY-binding sites in the second intron of *GL3* revealed that they are not involved in *GL3* expression control, indicating other mechanisms. Overall, *GL3* expression was not affected to a high degree by the presence of any tested trichome patterning gene, and more importantly, in this setup, a decrease of GL3 expression by its own presence could not be verified. Interestingly, the rescue experiments using different *GL1* regulatory sequences may indicate a missing enhancer element due to low rescue efficiency. The examined genomic sequence of *GL1* may include silencer elements that are masked due to the experimental procedures using artificially increased gene expression for rescue experiments. Additionally, for *GL1*, a positive feedback loop was observed in combination with *GL3*, *TTG1*, and *TTG2* expression; which may resolve one missing link regarding patterning models. Finally, rescue experiments using *Cardamine* R2R3MYB sequences led to the surprising partial rescue of *Arabidopsis gl1* mutant trichome phenotypes, indicating conserved protein functions as well as a degree of conserved regulatory sequences across species. Interestingly, *ChWER* was able to induce trichomes in *gl1*, revealing a potential divergence in trichome and root hair formation between species.

1. Introduction

The development of an organism relies on cell differentiation, cell growth, organ formation, and a variety of other processes. Cell differentiation into specialized cells is highly regulated. This differentiation does not happen randomly but is dependent on clues conferring, for example, spatial or temporal information to form a non-random pattern of different cells (Campos-Ortega, 1993; Ghysen et al., 1993; Oates et al., 2012; Uriu, 2016). Especially *de novo* patterns are interesting regarding their regulation, as per definition, they do not rely on spatial information, and the pattern is formed out of a uniform cell layer (Davies, 2017). Regulatory networks controlling *de novo* patterning are hard to decipher completely, and interactions are often complex and possess feedback loops (Gierer & Meinhardt, 1972; Meinhardt & Gierer, 1974, 2000; Turing, 1952). Examples of such *de novo* patterns are the formation of nitrogen-fixing cells (heterocysts) in cyanobacteria (Zhang et al., 2006) or the formation of trichomes in *A. thaliana* (Hülskamp & Schnittger, 1998; Larkin et al., 1997; Marks, 1997; Schnittger et al., 1999).

1.1. Trichomes develop in a *de novo* non-random pattern in *A. thaliana*

Leaf hairs, also called trichomes, are appendages of epidermal cells on above-ground plant organs (Johnson, 1975). They are present in a variety of plant species and display a wide morphological range (Wang et al., 2021). Trichomes can be composed of one or multiple cells and can be glandular or non-glandular (Barthlott et al., 2009; Theobald et al., 1980). For instance, in cotton, the seed trichomes are the cotton fibers which are a valued agricultural resource (Guan et al., 2014; Wang et al., 2013). In tea (*Camellia sinensis*), the presence of trichomes is essential to ensure high product quality (Li et al., 2020). Generally, trichomes are thought to play a role in protecting the plant against various biotic and abiotic stresses. An increased UV protection can be achieved by trichomes absorbing the UV radiation and reflecting light (Karabourniotis et al., 1992; Tattini et al., 2000; Yan et al., 2012). Additionally, trichomes can be beneficial in resistance against drought by retaining moist air between their branches (Fernández et al., 2014; Guerfel et al., 2009). The presence of trichomes can also render the respective plant less attractive to insects, even sometimes leading to insect death (Dalin et al., 2008; Levin 1973).

In *Arabidopsis*, trichomes are specialized cells that emerge from a homogenous cell layer of epidermal cells, and on rosette leaves, they differentiate without known positional information (Hülskamp et al., 1994). The *Arabidopsis* trichomes develop in a so-called *de novo* pattern that is highly regulated, non-random, and was shown to be independent of cell lineage (Larkin et al., 1996; Schnittger et al., 1999). Under laboratory conditions, the absence of trichomes does not lead to decreased plant fitness. Therefore, they pose an ideal system to study cell differentiation (Hülskamp et al., 1999; Marks, 1997).

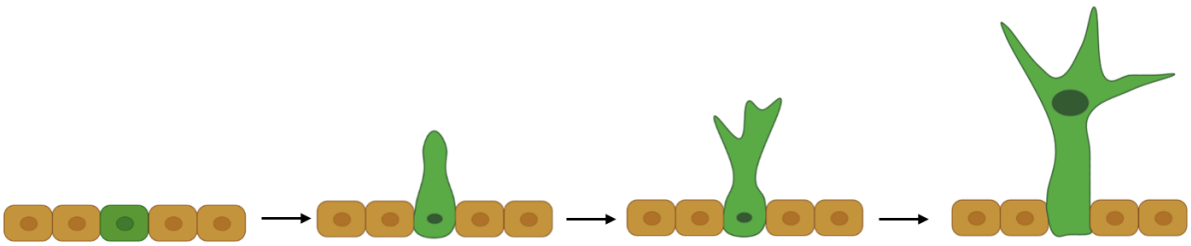

Figure 1. Trichome development in leaf epidermal cells. From left to right: In a homogenous cell layer, gene fluctuation leads to the establishment of trichome fate (green cell). The future trichome cell starts to grow out perpendicular to the leaf axis, undergoes several endoreduplications, and after two branching events, the mature trichome has developed. Figure based on Hülskamp, 1994.

On rosette leaves, trichomes are formed from pluripotent epidermal cells in a so-called patterning zone at the base of each young leaf (Figure 1; Hülskamp et al., 1994; Larkin et al., 1996; Schnittger et al., 1999). Small fluctuations in gene expression start the process of establishing the trichome fate (Greese et al., 2012; Meinhardt & Gierer, 2000; Turing, 1952). The destined trichome cell grows out vertically and undergoes several rounds of endoreduplication, resulting in an enlarged cell size with a DNA content of 32C (Hülskamp et al., 1994; Melaragno et al., 1993). After two branching events and the re-localization of the nucleus into the trichome apex, the mature trichome has developed (Folkers et al., 1997).

Two sets of genes regulate trichome cell fate: activators, which promote trichome fate, and inhibitors, which inhibit trichome fate. These two categories of genes were first identified in trichome mutant screens (Hülskamp et al., 1994). The genes activating trichome fate encode for three different protein classes: bHLH transcription factors, R2R3MYB transcription factors, and WD40 proteins. These proteins can form a complex called MBW complex (MYB/bHLH/WD40 complex). The only WD40 protein known to play a role in trichome patterning is TRANSPARENT TESTA GLABRA 1 (TTG1; Walker et al., 1999). In contrast, several bHLH transcription factors are involved in trichome patterning. GLABRA 3 (GL3) and its functional redundant homolog ENHANCER of GLABRA3 (EGL3) (Bernhardt et al., 2005; Payne et al., 2000; Zhang et al., 2003) are thought to be the major players of this protein class. Another bHLH transcription factor involved in trichome patterning is MYC1 (Morohashi & Grotewold, 2009; Symonds et al., 2011; Urao et al., 1996). Additionally, three R2R3MYB transcription factors are involved in trichome patterning: the redundant TFs GLABRA 1 (GL1) and MYB23, as well as MYB82 (Kirik et al., 2001, 2005; Liang et al., 2014; Li et al., 2009; Oppenheimer et al., 1991). All inhibitors known so far belong to the class of small R3 single-repeat MYB transcription factors, lacking an activation domain (Kirik et al., 2004a, b; Schellmann et al., 2002; Wada et al., 1997; Wang et al., 2007). The seven identified inhibitors are TRIPTYCHON (TRY), CAPRICE (CPC), ENHANCER OF TRIPTYCHON AND CAPRICE (ETC1), ETC2 and ETC3 as well as TRICHOMLESS 1 (TCL1) and TCL2 (Esch et al., 2004; Gan et al., 2011;

Kirik et al., 2004a, b); Schellmann et al., 2007; Simon et al., 2007; Tominaga et al., 2008; Wada, 1997; Wang et al., 2007, 2008; Wester et al., 2009).

1.2. Trichome mutants reveal distinct gene functions and redundancies

Although several protein classes are involved in trichome patterning, not all genes encoding these proteins are equally important in this process, as seen for the bHLH transcription factors GL3, EGL3, and MYC1. Single *gl3* mutants still develop trichomes, but the pattern is irregular with fewer and smaller under-branched trichomes that undergo fewer rounds of endoreduplication than wildtype (Hülskamp et al., 1994; Payne et al., 2000). The *egl3* single mutant develops a slightly reduced number of trichomes with a minor decrease in branches. However, the *gl3 egl3* double mutant lacks all trichomes, revealing the redundancy between GL3 and EGL3 (Zhang et al., 2003). In *myc1* mutants, a decrease in trichome number can be observed, even more drastic than the reduction observed in *gl3* or *egl3* (Zhao et al., 2012).

Also, the two involved R2R3MYB transcription factors GL1 and MYB23 have different effects on the patterning process. The *gl1* mutant displays a nearly glabarous phenotype, whereas *myb23* only seems to be impaired in trichome branching (Kirik et al., 2005; Koornneef et al., 1982; Oppenheimer et al., 1991). However, the *gl1 myb23* mutant, showing glabarous leaves, revealed the redundancy between GL1 and MYB23 in initiating trichomes at the leaf edges and petioles (Kirik et al., 2005). This leads to the assumption that GL1 plays a more pronounced role in trichome patterning than MYB23. Mutants of *MYB82* are not affected regarding their trichome pattern. However, overexpression of a chimeric construct containing MYB82 and a repressor domain led to a decreased trichome number and thus revealed the activator role of MYB82 (Liang et al., 2014).

In mutant screens, the inhibitors *TRY* (Schnittger et al., 1998) and *CPC* (Wada et al., 1997) were discovered. Plants possessing a mutation in *TRY* display a decreased number of trichomes but a high increase in cluster number. The *cpc* mutant, on the other hand, shows a drastic increase in trichomes but no difference in cluster frequency compared to wild-type plants (Schellmann et al., 2002). This led to the assumption that TRY is more involved in short-range trichome inhibition and CPC more in a long-range context. Interestingly, the *cpc try* double mutant displays massive clusters and a high cluster frequency but a decreased trichome number compared to the wild type (Schellmann et al., 2002). Three closely related genes are also involved in inhibiting trichome fate: *ETC1*, *ETC2,* and *ETC3*. The *etc1* single mutant displays a wild-type phenotype and the double mutants *etc1 try* and *ect1 cpc* possess the same phenotype as *try* and *cpc* plants, respectively. Interestingly, the triple mutant *etc1 try cpc*, forms clusters that nearly cover the whole leaf surface. Expression pattern analysis revealed a closer similarity with *CPC* expression than with *TRY*. Both, CPC and ETC1, are expressed in trichome

precursor cells and developing trichomes, as well as non-root hair cells (N-cells) in roots (Kirik et al., 2004a). Consequentially, ETC1 may be involved in long-range inhibition together with CPC (Kirik et al., 2004a). The *etc2* single mutant, as well as the double mutants *etc2 try* and *etc2 cpc*, display a higher number of trichomes compared to wildtype or the respective single mutants. However, the triple mutant *etc2 try cpc* is comparable to the *cpc try* double mutant regarding cluster size and number of trichomes but develops ectopic trichomes at the leaf margin and on the petioles. Expression analysis of *ETC2* revealed a similar expression pattern as TRY, both are expressed ubiquitously in young leaves and trichomes (Kirik et al., 2004b). The *etc3* single mutant displays a higher trichome number than the wild type. In the double mutant *etc3 try*, a weak synergistic phenotype can be observed that is absent in the *etc3 cpc* mutant. The *etc1 etc2 etc3* mutant possesses more trichomes than the single mutants, revealing the redundancy between the *ETCs* (Wester et al., 2009). Interestingly, the overexpression of any of the *ETCs* leads to a glabrous phenotype (Kirik et al., 2004a, b; Wester et al., 2009). The expression pattern of ETC3 is comparable to TRY expression. ETC3 is expressed in the patterning zone of young leaves and developing trichomes, but no expression was detected in mature trichomes (Wester et al., 2009). Additionally, TCL1 and TCL2 are involved in trichome inhibition. The *tcl1* mutant does not display any change in trichome pattern on rosette leaves, however trichome formation on pedicels and inflorescence stems is impaired (Wang et al., 2007). Also, the *tcl2* mutant does not display a trichome phenotype on rosette leaves (Gan et al., 2011). However, overexpression of *TCL1* or *TCL2* leads to a glabrous phenotype (Gan et al., 2011; Wang et al., 2007).

1.3. Regulation of trichome patterning in *Arabidopsis*

Currently, two models have been published that individually are sufficient to explain the observed trichome pattern in wildtype *Arabidopsis* plants: The Activator-Inhibitor (AI) model and the Activator-Depletion (AD) model (Figure 2; Pesch & Hülskamp, 2009).

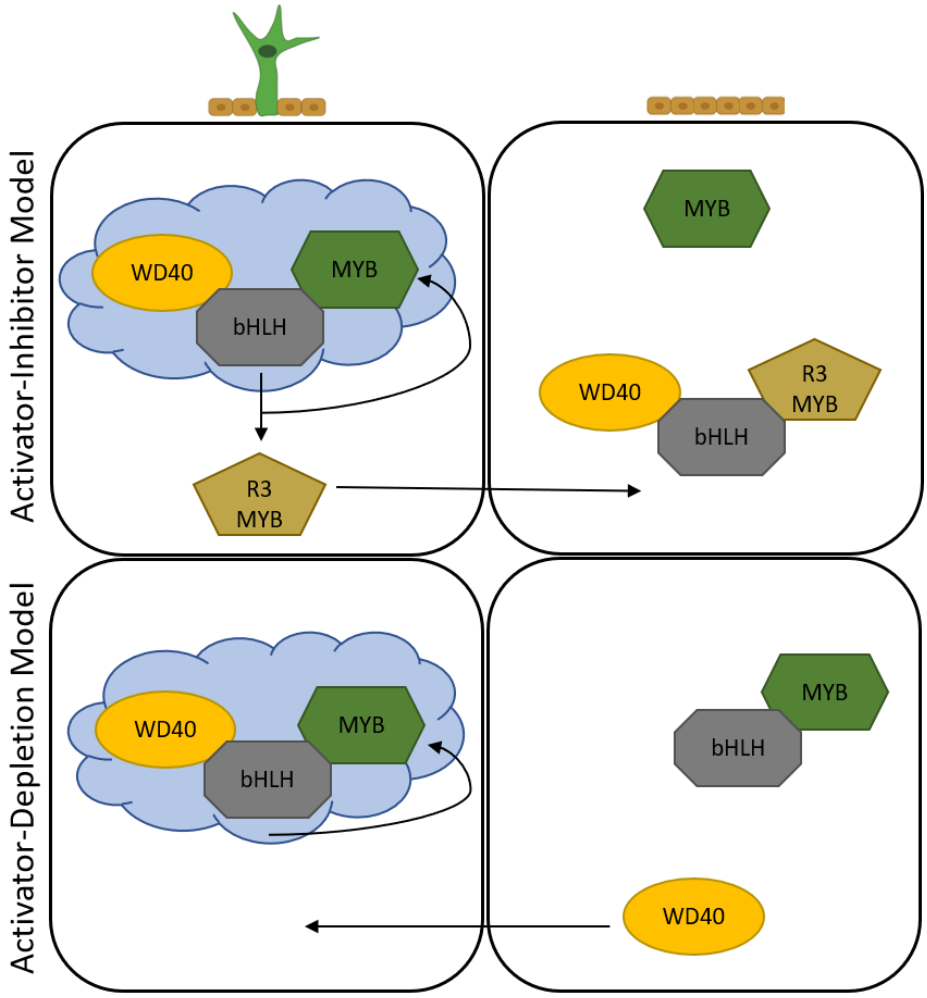

Figure 2. Models to describe trichome patterning in *A. thaliana*. Two simple models are published that can describe the wildtype trichome pattern in *Arabidopsis* rosette leaves: the activator-inhibitor model (AI; top row) and the activator-depletion model (AD, bottom row). In the AI model, the activator proteins (WD40, bHLH, MYB) form an active complex (indicated by the blue cloud) that activates the gene expression of its own components and of inhibitors (R3MYB). These inhibitors then move to neighbouring cells (right column) and replace the MYB in the active complex, thus rendering it inactive. The active complex leads to the activation of downstream genes and thus promotes trichome formation. The inactive complex leads to the maintenance of epidermal cell fate. In the AD model, the same active complex is formed but rendered inactive by the recruitment of the WD40 protein into the future trichome cell (left column). Figure based on Pesch & Hülskamp, 2009.

In the AI model, the activators form the active MBW complex consisting of the WD40, a bHLH, and an R2R3MYB protein. This active complex activates the gene expression of downstream genes that initiate the trichome fate, such as GLABRA2 (GL2), a transcription factor belonging to HD-ZIP homeobox family (Cristina et al., 1996; Masucci et al., 1996; Rerie et al., 1994), or the WRKY transcription factor TRANSPARENT TESTA GLABRA 2 (TTG2; Ishida et al., 2007; Johnson et al., 2002). Moreover, this active complex also activates the gene expression of the inhibitors as well as the expression of the activators that form the MBW complex. The inhibitor proteins then migrate into neighbouring cells and replace the R2R3MYB transcription factor in the active complex by binding to the bHLH protein, thus rendering the complex inactive. In these cells, no downstream genes are activated, and they retain their epidermal cell fate.

In the AD model, the active complex is also formed by the WD40 protein, a bHLH, and an R2R3MYB transcription factor. Contrary to the AI model, the active complex in the AD model is rendered inactive by the absence of the WD40 protein. The active complex recruits TTG1 into the future trichome cell and, therefore, disables the formation of an active complex in the surrounding cells (Balkunde et al., 2010, 2011; Hülskamp, 2004; Pesch & Hülskamp, 2004, 2009).

As illustrated in the description of the two patterning models, it is obvious that the trichome patterning genes and proteins have to interact with each other via protein-DNA and protein-protein interactions. Many publications are available in which protein-protein interactions in trichome patterning were examined. In these studies, it was observed that GL1, TTG1, and MYB23 each interact with GL3/EGL3 (Digiuni et al., 2008; Kirik et al., 2005; Payne et al., 2000; Zhang et al., 2003; Zhao et al., 2008; Zimmermann et al., 2004) and that GL3/EGL3 interact with all known inhibitors (Digiuni et al., 2008; Gan et al., 2011; Tominaga et al., 2008; Wang & Chen, 2008; Wester et al., 2009). Moreover, there are some indications for protein-protein interactions between TRY and GL1 (Digiuni et al., 2008), as well as between GL1 and TTG1 (Zhao et al., 2008). In addition to the protein-protein interactions, cross-regulatory interactions on the transcriptional level were observed. GL3/EGL3 positively influence the expression of several genes, either in concert with other proteins or alone (Pesch & Hülskamp, 2009). For instance, together with TTG1, it promotes the expression of *TRY*, as well as the expression of *CPC* together with GL1 (Pesch et al., 2015). *MYB23* expression seems to be influenced by GL1 and TTG1 (Kirik et al., 2005). Moreover, GL3 seems to negatively influence its own gene expression (Morohashi et al., 2007; Zhao et al., 2008).

1.4. The MBW complex regulates five different traits in *Arabidopsis*

In *Arabidopsis,* the MBW complex is involved in trichome formation but also regulates four additional traits: root hair formation, seed coat mucilage production as well as proanthocyanidin and anthocyanidin biosynthesis (Broun, 2005; Ramsay & Glover, 2005; Zhang & Schrader, 2017; Figure 3).

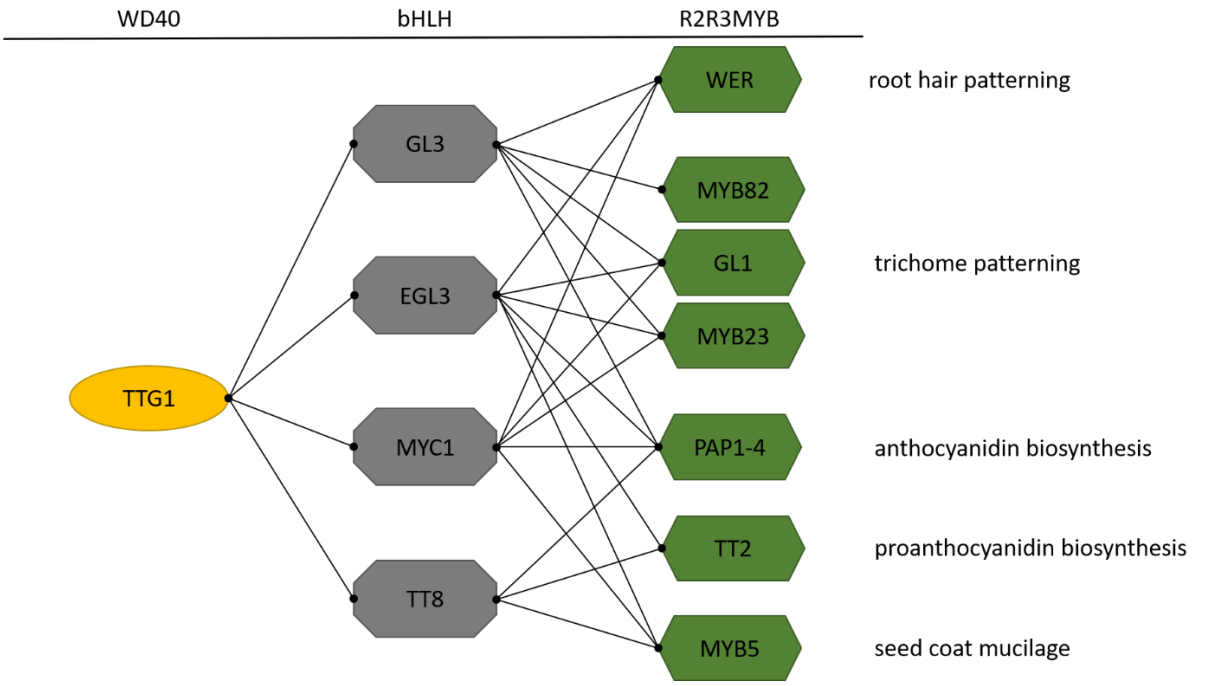

Figure 3. TTG1-dependent gene regulatory network in *A. thaliana*. The WD40 protein TTG1 regulates five different traits in Arabidopsis: root hair formation, trichome patterning, anthocyanidin & proanthocyanidin biosynthesis, and seed coat mucilage production. The regulated trait depends on the interaction partners, such as different bHLH transcription factors (GL3, EGL3, MYC1, TT8) and R2R3MYB transcription factors (WER, MYB82, GL1, MYB23, PAP 1-4, TT2, MYB5). Figure based on Zhang & Schrader, 2017.

While TTG1 is the core protein necessary for all complexes (Walker et al., 1999), bHLH TFs are involved in multiple traits, and the R2R3MYBs confer specialization for single traits. Together with the bHLH TFs TRANSPARENT TESTA 8 (TT8), MYC1 and ENHANCER OF GLABRA 3 (EGL3) as well as the R2R3MYB MYB5 seed coat mucilage production is regulated (Li et al., 1996; Morohashi & Grotewold, 2009; Nesi et al., 2000; Shirley et al., 1995; Symonds et al., 2011; Urao et al., 1996; Zhang et al., 2003). The same bHLHs are also active in proanthocyanidin production, but the involved R2R3MYB is TRANSPARENT TESTA 2 (TT2; Debeaujon et al., 2003; Nesi et al., 2001). Anthocyanidin production is regulated by the bHLH TFs TT8, MYC1, GLABRA 3 (GL3), and EGL3 and the R2R3MYBs PRODUCTION OF ANTHOCYANIN PIGMENT 1 (PAP1) and PAP2 as well as MYB113 (PAP3) and MYB114 (PAP4; Borevitz et al., 2000; Gonzalez et al., 2008; Stracke et al., 2001; Teng et al., 2005). In trichome and root hair formation, similar genes play a role in establishing specialized cell fate. In both patterning processes, TTG1 and the bHLH TFs MYC1, GL3, and EGL3 are involved. In trichome patterning, as described above, the R2R3MYBs GL1, MYB23, and MYB82 are involved (Kirik et al., 2001; Liang et al., 2014; Oppenheimer et

al., 1991). Root hair initiation is controlled by the R2R3MYB WERWOLF (WER; Lee & Schiefelbein, 1999). Interestingly, the principle of pattern initiation is reversed in roots. The MBW complex leads to the formation of normal epidermal cells in roots (Pesch & Hülskamp, 2004; Schiefelbein, 2003), meaning it represses the root hair cell fate (Masucci et al., 1996). Whereas in trichome patterning, the complex formation leads to the establishing of trichome fate (Pesch & Hülskamp, 2004; Schiefelbein, 2003).

1.5. Regulation of gene expression in plants

The MBW complex leads to the expression of specific genes dependent on its components. In general, gene expression depends on the accessibility of the DNA encompassing the gene of interest and its regulatory sequences, as well as the presence and binding of transcription factors and co-factors to *cis*-regulatory elements (CREs) to recruit the transcription machinery (Cirillo et al., 2002; Kaufmann et al., 2010; Lambert et al., 2018; Marand et al., 2023; Nolis et al., 2009; Quevedo et al., 2019; Schmitz et al., 2022). The DNA accessibility based on chromatin structure just recently gained more attention in plants, in animals epigenome maps and chromatin arrangement are extensively researched (De Laat & Duboule, 2013; Klemm et al., 2019; Schmitz et al., 2022; Shlyueva et al., 2014). CREs, however, are known to occur in the genome in so-called cis-regulatory modules (CRMs) and influence the expression of noncoding RNA genes or protein-coding genes (Andersson & Sandelin, 2020; Della Rosa & Spivakov, 2020; Kopp & Mendell, 2018; Shlyueva et al., 2014).

Some CREs are known binding sites for a specific class of transcription factors, such as W-boxes as WRKY-TF binding sites, MYB- or MYC-TF binding sites, and binding motifs for homeodomain-containing proteins (H. Abe et al., 2003; Eulgem et al., 1999, 2000; Johannesson et al., 2001; Rushton et al., 2010; Sablowski et al., 1994; Sessa et al., 1993; Stalberg et al., 1996; Sun et al., 2003; Urao et al., 1993; Yamamoto et al., 2004; Zhu et al., 2003). Other motifs are associated with genome organization, such as scaffold/matrix attachment sites (SMAR), or associated with transcription, such as poly(A) signals or putative splice junctions (Brown, 1986; Gasser, 1989; Joshi, 1987; Loke et al., 2005; O'Neill et al., 1990).

For basic gene expression, the core promoter is important, which is located in very close proximity to the transcription start site (TSS) and is needed for the recruitment of the pre-initiation complex (PIC, Brooks et al., 2023). The PIC contains RNA polymerase II and general transcription factors (Brooks et al., 2023). Formation of the PIC is initiated at specific core promoter elements, such as TATA boxes or downstream promoter elements (DPEs; Jores et al., 2021; Kumari & Ware, 2013; Porto et al., 2014). Promoters either possess a TATA box or a DPE (Brooks et al., 2023). TATA boxes are normally found 30-70 bp upstream of the TSS (Jores et al., 2021; Kumari & Ware, 2013). A subunit of the transcription factor IID (TFIID), the TATA-binding protein (TBP), recruits the RNA polymerase II by binding to the

TATA box. This initiates the formation of the PIC, and transcription starts (Brooks et al., 2023). In *Arabidopsis*, TATA box-containing promoters are often associated with tissue-specific expression (Molina & Grotewold, 2005). In DPE-containing promoters, the RNA polymerase II is recruited to DPE upon TFIID binding. DPEs are usually situated 30 bp downstream of the TSS, and often DPE-containing promoters are associated with stimulus-response (Burke & Kadonaga, 1996; Porto et al., 2014). In *Arabidopsis,* initiator elements (Inr) and Y-patches are often associated with promoters containing TATA boxes (Yamamoto et al., 2009). A Y-patch is an 8 pb long motif that is defined by the presence of C and T dimers, and it is normally located 1-100 bp upstream of the TSS (Yamamoto et al., 2007). The initiator element is also closely situated to the TSS and, together with either the DPE or TATA box, enables TFIID to bind and assemble the PIC (Nakamura et al., 2002; Smale & Kadonaga, 2003). The CCAAT (or CAAT, CAT) box can also be part of the core promoter (Brooks et al., 2023). It is the binding site for nuclear transcription factor Y (NF-Y), also known as CCAAT-binding factor (CBF). Binding of NF-Y to the CCAAT box can cause an increase or decrease in gene expression (Laloum et al., 2013).

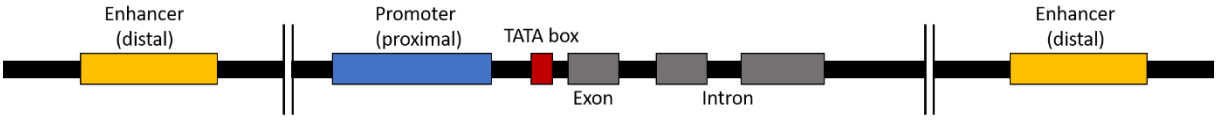

Figure 4. Structure of the promoter and enhancer regions in plants. Figure based on Porto et al., 2014.

Additionally to the core promoter, other regulatory sequences can play a role in gene expression regulation. Upstream to the TSS and core promoter, proximal promoter sequences can be localized. Enhancer/silencer elements can be located up- or downstream of the gene sequence (Porto et al., 2014). Interestingly, the directionality and distance of the silencer or enhancer often do not play a role (Brooks et al., 2023). Enhancer sequences alone cannot initiate transcription, but upon activation by specific transcription factor binding, they enhance the transcription of the core promoter. This is most likely achieved by increasing the transcription initiation frequency and not the amount of mRNA transcribed (Haberle & Stark, 2018). Silencers are harder to detect, and thus less studied (Marand et al., 2017, 2023; Pajoro et al., 2014; Weber et al., 2016; Xiao et al., 2017). They can lead to gene silencing, either by silencing enhancers or by directly silencing the gene (Harris et al., 2016; Ngan et al., 2020; Pang & Snyder, 2020).

However, transcription not only needs to be initiated but also terminated. This is orchestrated by terminators to ensure translation efficiency and stability, as well as 3' end processing and the transport of the mRNA from the nucleus into the cytoplasm (Zhao et al., 1999). The terminator is localized in the 3'-UTR (untranslated region) and encompasses one or more poly(A) signals. After gene transcription, a site-specific cleavage happens in the terminator and enables further processing or the mRNA (Mandel et al., 2008).

In *Arabidopsis*, due to the small genome, CRMs are often localized close to the gene they regulate. However, with increasing genome size, the distance between CRMs and regulated genes also increases (Li et al., 2019; Oka et al., 2017; Ricci et al., 2019). Different transcription factor binding sites are defined as CREs. The binding of a different set of TFs binding in different plant tissues at specific developmental stages, the gene expression is orchestrated accordingly (Brooks et al., 2023; Marand et al., 2023; Porto et al., 2014; Schmitz et al., 2022). A wide variety of CREs are already identified and can be searched for in sequences of interest by utilizing databases, such as PLACE and PlantCARE (Higo et al., 1999; Lescot et al., 2002). However, the lone presence of a CRE does not automatically determine the outcome of gene regulation, as different CREs together define a certain CRM and, in concert with chromatin structure and other binding proteins, regulate gene expression (Brooks et al., 2023; Marand et al., 2023; Porto et al., 2014; Schmitz et al., 2022). Interestingly, computational prediction of CREs seems to decrease the chance to find functional motifs. A high number of CREs is predicted but only a few of them are actually active in the examined sequence array. Thus, experiments to find and characterize the individual CRE function are needed (Hu et al., 2005; Tompa et al., 2005).

1.6. Regulation of protein stability in plants

In addition to the regulation of gene expression, protein function, properties, and translation, play important roles in determining the outcome of biological processes like trichome patterning. Protein turnover is essential for proper eukaryotic cell function and includes the degradation of proteins that are denatured, misfolded, or no longer needed (Ciechanover, 1998; Glickman & Ciechanover, 2002). Preferably, these proteins are recycled by the cell (Goldberg, 2003). Two main pathways orchestrate the degradation of proteins: The ubiquitin-proteasome pathway and the lysosome/vacuole pathway (Levine et al., 2011; Pickart & Eddins, 2004). Most plant proteins are degraded via the ubiquitin-proteasome pathway (Moon et al., 2004). The lysosome/vacuole pathway deals with the degradation of cell organelles or protein aggregates that are too large to be degraded via the ubiquitin-proteasome pathway (Levine et al., 2011).

Proteasomal degradation is dependent on the ubiquitination of lysine residues in the target protein (Glickman & Ciechanover, 2002; Hershko & Ciechanover, 1998; Scheffner et al., 1995; Wang et al., 2006). This ubiquitination is orchestrated by three enzymes: the ubiquitin-activating enzyme (E1), the ubiquitin-conjugating enzyme (E2), and the ubiquitin-protein ligase (E3) (Scheffner et al., 1995). The E1 activates ubiquitin in an ATP-dependent manner and transfers it to the E2, which then transfers the activated ubiquitin either directly to the target protein or first to the E3. Both transfers involve the binding of E2 to E3 (Smalle & Vierstra, 2004; Wilkinson, 2000). Two classes of E3 ligases are known: HECT (homology to E6-AP C terminus; Pickart & Eddins, 2004) and RING/U-box (Real Interesting New

Gene; Freemont, 2000; Seol et al., 1999). HECT E3 ligases receive the ubiquitin from E2 and transfer it; RING/U-box E3 ligases act as bridges to enable the E2 to transfer the ubiquitin to the substrate (Moon, 2004). Ubiquitinated proteins can then be recognized by the 26S proteasome. The 26S proteasome consists of three main subunits, a cylindrical core proteasome (20S) and two regulatory cap particles (19S) situated at each end of the core proteasome (Groll & Huber, 2003; Voges et al., 1999; P. Yang et al., 2004). The core proteasome is subdivided into α and β units, forming the cylindrical chamber. In this chamber, the proteins are degraded, and recycling can proceed (Voges et al., 1999; P. Yang et al., 2004). The 19S regulatory caps are divided into two more subunits, responsible for substrate recognition (the lid subunit) and substrate unfolding (the base component; Groll & Huber, 2003). In *A. thaliana,* a staggering number of around 1400 genes are involved in the proteasome pathway (Smalle & Vierstra, 2004). The majority of these genes, around 90%, are responsible for substrate specificity, as they encode subunits of the E3 ubiquitin ligases (Smalle & Vierstra, 2004).

In mathematical pattern models, the differential equations often include a term for degradation rates of the model components (Deneer, 2022; Gierer & Meinhardt, 1972; Meinhardt & Gierer, 1974; Turing, 1952). So far, regarding trichome patterning, these parameters were estimated and tested for their ability to induce a normal pattern (personal communication with A. Deneer). Interestingly, there are indications that GL3/EGL3 interact with UBIQUITIN PROTEIN LIGASE3 (UPL3, KAKTUS, KAK) and thus are degraded via the 26S proteasome (Patra et al., 2013b). Also, for GL1, there may be some indications that it is a target of KAKTUS as well (Jaime, 2007). Preferably, experimentally determined values for protein production, degradation, or stability should be used in the mathematical models. However, determining these parameters is challenging.

One such method to determine protein production, degradation, and stability could utilize viral “self-cleavage” sites (Szymczak et al., 2004). These so-called 2A sequences were first discovered in the foot-and-moth-disease virus (Ryan et al., 1991). This virus, as well as many others, possesses a polyprotein coding sequence, meaning all genes within a certain region are transcribed and translated as one sequence in a 1:1 ratio (Kim et al., 2011a). During translation, the proteins are cleaved, mostly by virus-encoded proteinases (Ryan et al., 1991). However, one of the first cleavage events is mediated by the 2A sequence itself, presumably by causing ribosomal skipping of the glycyl-propyl bond (Donnelly et al., 2001a, b). After cleavage, the N-terminal protein has nearly the whole 2A sequence attached to its C-term, whereas the C-terminal protein has an additional proline on its N-term (Atkins et al., 2007). Additionally to the 2A sequence found in the foot-and-mouth-disease virus (F2A), other 2A sequences with self-cleavage activity were identified: E2A from equine rhinitis A virus, P2A from porcine teschovirus-1, and T2A from the thosea asigna virus (de Lima & Lanza, 2021; Lewis et al., 2015; Nibert, 2007; Szymczak & Vignali, 2005). Alignment of the 2A sequences identified a conserved cleavage motif,

which is essential to all 2A sequences (Donnelly, et al., 2001a, b). An GSG motif was artificially added to the N-term of the 2A sequence and functions as a linker motif to increase cleavage efficiency (Szymczak et al., 2004).

Another method for the determination of protein degradation and production while also monitoring movement, expression, and co-localization, would be utilizing photoconvertible fluorescence proteins (Hofmann et al., 2005; Schwentker et al., 2007; Wu et al., 2011; Zhang et al., 2007). The conversion of the photoconvertible protein can be either reversible or irreversible and is often induced by UV light (Chudakov et al., 2010). A variety of photoconvertible proteins are available such as Kaede and Dendra (Ando et al., 2002; Gurskaya et al., 2006). Most photoconvertible proteins are switchable from green to red upon illumination with UV light (Mizuno et al., 2003). However, there are also some variants available that switch from none to green fluorescence upon UV irradiation, such as Dronpa and PA-CFP (Ando et al., 2004; Patterson & Lippincott-Schwartz, 2002).

1.7. Regulation of trichome patterning in different Brassicaceae species

Establishment of trichome fate, trichome development as well as trichome morphology are extensively researched in the model plant *Arabidopsis* (Hülskamp et al., 1994; Pesch & Hülskamp, 2009; Wang et al., 2021). However, trichomes are formed in various plant species and are even used to categorize angiosperms taxonomically (Judd et al., 1999; Tutin et al., 1993). Two Brassicaceae closely related to *Arabidopsis* also form trichomes and have fully sequenced genomes (Hay et al., 2014; Jiao et al., 2017;Willing et al., 2015): *Arabis alpina* diverged from *A. thaliana* around 26-40 million years ago (Beilstein et al., 2010; Koch et al., 2006), and *Cardamine hirsuta* diverged from *A. thaliana* around 32 million years ago (Baumgarten et al., 2023; Koch et al., 2001; Koch et al., 2006). While *Arabidopsis* and *Cardamine* are annual plants inhibiting similar geographic regions (Fulgione & Hancock, 2018; Fuster-Pons et al., 2024; Lee et al., 2017), *Arabis* is a perennial plant adapted to survive harsh environmental conditions, e. g. low temperatures (Koch 2006, Wang 2009). Although all three species form trichomes, they differ morphologically. *Cardamine*, similar to half of all Brassicaceae, forms unbranched trichomes (Huang et al., 2016; Tutin et al. 1993). Contrastingly, *Arabis* and *Arabidopsis* form three branched trichomes (Chopra et al., 2014; Hülskamp et al., 1994). Interestingly, *Arabidopsis* and *Cardamine* only possess one class of leaf trichomes (Hay et al., 2014; Hay & Tsiantis, 2016; Hülskamp et al., 1994), *Arabis* on the other hand, seems to possess two distinct classes (Chopra et al., 2014). While trichome and root hair formation are extensively researched in Arabidopsis, only a few studies exist for *Arabis* (Chopra et al., 2014, 2019; Mapar et al., 2021). In Cardamine, just recently, leaf trichomes were analyzed in more detail on the largest and terminal leaflet (Fuster-Pons et al., 2024) and root hair patterning was only superficially examined in a study from the early 19th century (Leavitt, 1904).

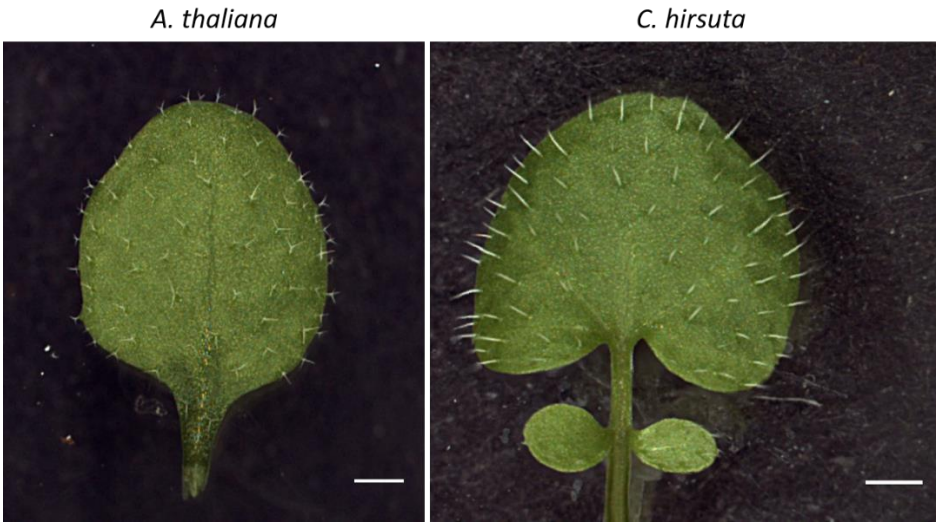

Figure 5. *A. thaliana* and *C. hirsuta* rosette leaf & terminal leaflet. Scale bar refers to 1 mm.

Several orthologous trichome patterning genes of *Arabidopsis* were identified in *Cardamine* and *Arabis* (Chopra et al., 2014, 2019; Fuster-Pons et al., 2024; Mapar et al., 2021). In addition, EMS mutagenesis screens facilitated the identification of multiple patterning genes involved in trichome patterning in *Arabis*: *AaTTG1*, *AaGL3*, *AaEGL3,* and potentially *AaTRY* and *AaGL2* (Chopra et al., 2019). Mutations in *AaTTG1* and *AaGL3* caused glabrous leaves, indicating conserved roles as trichome fate activators (Chopra et al., 2019). Interestingly, in *Arabidopsis*, *gl3* is not glabrous but displays fewer trichomes than wild-type leaves. Only the double mutant *gl3 egl3* displays a glabrous phenotype (Zhang et al., 2003). This indicates a redundant role of *GL3* and *EGL3* in *Arabidopsis* but not *Arabis*. Root hair patterning in *Arabis* is also regulated by *AaTTG1*, identical to the TTG1-dependent pathways in *Arabidopsis* (Chopra et al., 2014).

For *Cardamine*, orthologues of *GL1*, *WER,* and *MYB23* were identified by synteny analysis (Pietsch, 2022). In a recent study, the same gene, *CARHR149430*, was identified as *ChGL1* and in a GWAS approach, other genes associated with trichome pattern regulation were identified (Fuster-Pons et al., 2024). Fuster-Pons and colleagues (2024) indicated that trichome patterning is a genetic mechanism partially conserved between *Cardamine* and *Arabidopsis*. However, some differences were observed regarding environmental adaptation. In *Arabidopsis*, higher temperatures and radiation combined with low precipitation lead to an increased trichome density (Arteaga et al., 2022). In contrast, *Cardamine* produced a higher trichome density when exposed to low temperatures and high precipitation (Fuster-Pons et al., 2024). Consistently, these contrasting adaptations to environmental conditions were also observed in various other species producing unbranched trichomes (Hufford et al., 2013; Tan et al., 2020).

1.8. Aim of the study

Although genes involved in the regulation of trichome patterning and some general principles are known, some links are still missing to fully explain the trichome patterning network. Therefore, in this study, the regulatory mechanisms underlying trichome patterning in *Arabidopsis* were examined on the DNA and protein levels.

The effect of other trichome patterning proteins on the gene expression of *GL1*, *GL3*, *ETC1*, *ETC2,* and *ETC3* was studied via quantitative GUS assays in cell suspension cultures of *A. thaliana*. Moreover, the regulatory sequences were analyzed via PLACE analysis and, in the case of *GL1*, were used in rescue experiments to identify the minimal regions needed for proper gene expression. Also, for *GL3*, the effect of mutations in its second intron was studied regarding their influence on gene expression. Additionally, interspecies comparisons between the MYBs GL1, MYB23, and WER in *Arabidopsis* and *Cardamine* were conducted to shed light on their evolutionary relation. The first introns were analyzed via PLACE analysis, and *Cardamine* constructs were used to test their ability to rescue *gl1*, *myb23*, and *gl1 myb23* trichome phenotypes in *Arabidopsis*.

On the protein level, the protein-protein interactions of trichome patterning proteins were studied regarding their effects on protein stability. To examine this, the viral P2A “self-cleavage” system was utilized. Furthermore, photoconvertible proteins were tested as an alternative method to study protein production and degradation rates. Utilizing the “self-cleavage” 2A sequences and photoconvertible proteins in two independent experimental approaches may open new ways to determine protein stabilities and production and degradation rates. Additionally, GL1 and GL3 were analyzed regarding their degradation via the ubiquitin-proteasomal pathway.

Finally, to facilitate the development of published mathematic models regarding trichome patterning, weak *ttg1* mutants and the double mutant *cpc try* were analyzed in more detail regarding their cluster phenotypes. In wildtype plants the depletion of the mutated TTG1 were examined in leaf epidermal cells and trichomes. The *cpc try* double mutant was analyzed regarding cluster formation and expression pattern of inhibitors were examined.

2. Material and Methods

2.1. Material

2.1.1. List of chemicals

Table 1. List of chemicals used in this study.

Chemical	Manufacturer
4-Methylumbelliferyl-β-D-glucuronide hydrate (4-MUG)	Roth
Acetosyringon (Dimethoxy4-hydroxyacetophenon)	Sigma-Aldrich
Acetyl-coenzyme A	Biomol
Adenosine 5'-triphosphate	Sigma-Aldrich
Agar (Micro agar)	Duchefa
Agar (Plant agar)	Duchefa
Agarose (LE Agarose)	Biozym
Bacto-Peptone	Roth
Bacto-Yeast-Extract	Difco
BP enzyme mix	Thermo Fisher Scientific
Calcium chloride dihydrate ($CaCl_2$*$2H_2O$)	Sigma-Aldrich
Dimethyl sulfoxide (DMSO)	Thermo Fisher Scientific
Disodium phosphate (Na_2HPO_4)	Roth
1,4-Dithiothreitol (DTT)	Roth
Ethylenediaminetetraacetic acid (EDTA)	Roth
Ethidium bromide	Roth
Ethanol (EtOH) absolute	VWR Chemicals
Gamborg B5 Vitamin Mix	PlantMediabioWORLD
Glacial acetic acid	Roth
D-Glucose	Sigma-Aldrich
Glutamine	Sigma-Aldrich
Glycerol	Roth
Gold particle	BioRad
LR enzyme mix	Thermo Fisher Scientific
Magnesium sulfate heptahydrate	Roth
Methanol	Roth
D-Mannitol	Sigma-Aldrich
MES (2-(N-morpholino) ethane sulfonic acid)	Roth
Magnesium chloride hexahydrate ($MgCl_2$*H_2O)	Roth
Magnesium carbonate pentahydrate ($MgCO_3$*$5H_2O$)	Roth
Magnesium sulfate heptahydrate ($MgSO_4$*$7H_2O$)	Roth

Magenta-Glc	Duchefa
Orange G	Sigma-Aldrich
Perfluorodecalin	Sigma-Aldrich
Potassium chloride (KCl)	Roth
Potassium ferricyanide (K-FerriCyanid)	Sigma-Aldrich
Potassium ferrocyanide (K-FerroCyanid)	Sigma
Sucrose	Roth
Sodium chloride (NaCl)	Roth
Sodium dihydrogen phosphate (NaH_2PO_4)	Roth
Sodium hydroxide	Roth
Spermidine	Duchefa
Tricine	Roth
Tris base	Roth
Triton X-100	Roth
X-Gluc	Thermo Fisher Scientific
Xylene cyanol	Roth

2.1.2. List of plasmids

List of general plasmids

Table 2. List of general plasmids used in this study. Kan – kanamycin, Gent – gentamycin, Carb – carbenicillin, Chlor – chloramphenicol, Hygro - hygromycin

Plasmid	Description	Resistance	Publication/Origin
pDONR201	Gateway entry vector	Kan	Invitrogen
pDONR207	Gateway entry vector	Gent	Invitrogen
pENTR1A	Gateway entry vector	Kan	Invitrogen
pENTR4	Gateway entry vector	Kan	Invitrogen
pAMPAT	Gateway expression vector; p35S followed by GW cassette	Carb, Chlor	Based on GenBank ID AY436765
pENSG-CFP	Gateway expression vector; p35S followed by CFP and GW cassette	Carb, Chlor	(Feys et al., 2005)
pENSG-YFP	Gateway expression vector; p35S followed by YFP and GW cassette	Carb, Chlor	(Feys et al., 2005)
PARB	Gateway expression vector; GW cassette followed by minimal p35S-TATA box and GUS	Carb, Chlor	(Pesch & Hülskamp, 2011)
pGWB2	Gateway expression vector; p35S followed by GW cassette	Kan, Hygro, Chlor	(Nakagawa et al., 2007)
pGWB3	Gateway expression vector; GW cassette followed by GUS	Kan, Hygro, Chlor	(Nakagawa et al., 2007)

List of specific plasmids used in this study

Table 3. List of expression vectors used in this study.

Plasmid	Purpose	Provided/generated by
pAMPAT-pCPC:GUS	Stable lines	J. Pietsch
pAMPAT-pTRY:GUS	Stable lines	J. Pietsch
pGWB2 GW	Transformation cell culture	C. Dietzen
pGWB3 GW	Transformation cell culture	C. Dietzen
pGWB2-p35S:GUS	Transformation cell culture	this study
pGWB2-p35S:CPC	Transformation cell culture	this study
pGWB2-p35S:TRY	Transformation cell culture	this study
pGWB2-p35S:GL1	Transformation cell culture	this study
pGWB2-p35S:GL3	Transformation cell culture	this study
pGWB2-p35S:TTG1	Transformation cell culture	this study
pGWB2-p35S:TTG2	Transformation cell culture	this study
pGWB2 w/o ccdB	Transformation cell culture	this study
pGWB3 w/o ccdB	Transformation cell culture	this study

pGWB3-pETC1:GUS	Transformation cell culture	this study
pGWB3-pETC2:GUS	Transformation cell culture	this study
pGWB3-pETC3:GUS	Transformation cell culture	this study
pGWB3-pTRY:GUS	Transformation cell culture	this study
pGWB3-pTRY_mini:GUS	Transformation cell culture	this study
pGWB3-pCPC_mini:GUS	Transformation cell culture	this study
pGWB3-pGL1 Wang:GUS	Transformation cell culture	this study
pGWB3-pGL3:GUS	Transformation cell culture	this study
pGWB3-pGL3-EX1+2-In2-Ex3(10bp):GUS	Transformation cell culture	this study
pGWB3-Intron1_GL1:GUS	Transformation cell culture	this study
pGWB3-3'enhancer Wang:GUS	Transformation cell culture	this study
pGWB3-3' enhancer box Larkin:GUS	Transformation cell culture	this study
pGWB3-pGL3-EX1+2-IN2(1-138)-Ex3(10bp):GUS	Transformation cell culture	this study
pGWB3-pGL3-EX1+2-IN2(1-138)-Ex3(10bp)_Mut1&2:GUS	Transformation cell culture	this study
pGWB3-3'enhancer_Wang-GW:GUS	Transformation cell culture	this study
pGWB3-3' enhancer-pGL1:GUS	Transformation cell culture	this study
pGWB3-pGL1-Ex1-In1-Ex2(11bp):GUS	Transformation cell culture	this study
pGWB3-3'enhancer-pGL1-Ex1-In1-Ex2(11bp):GUS	Transformation cell culture	this study
pGWB3-pGL1+intron1:GUS	Transformation cell culture	this study
pGWB3-3'enhancer-pGL1+intron1:GUS	Transformation cell culture	this study
pENSG-p35S:YFP-ccdB-P2A-NLSNLS-mCherry GW	Protein stability	I. Schultheiß Araújo
pENSG-p35S:YFP-ccdB-P2A-RFP-NLS GW	Protein stability	I. Schultheiß Araújo
pENSG-p35S:YFP-TRY-P2A-NLSNLS-mCherry	Protein stability	I. Schultheiß Araújo
pENSG-p35S:YFP-CPC-P2A-NLSNLS-mCherry	Protein stability	I. Schultheiß Araújo
pENSG-p35S:YFP-GL1-P2A-NLSNLS-mCherry	Protein stability	I. Schultheiß Araújo
pENSG-p35S:YFP-GL3-P2A-NLSNLS-mCherry	Protein stability	this study
pENSG-p35S:YFP-EGL3-P2A-NLSNLS-mCherry	Protein stability	this study
pENSG-p35S:YFP-MYB23-P2A-NLSNLS-mCherry	Protein stability	this study
pENSG-p35S:YFP-TTG1-P2A-NLSNLS-mCherry	Protein stability	this study
pENSG-p35S:YFP-GL1R97D-P2A-NLSNLS-mCherry	Protein stability	this study
pENSG-p35S:NLSNLS-mCherry-P2A-YFP GW	Protein stability	this study
pENSG-p35S:NLSNLS-mCherry-P2A-EGL3	Protein stability	this study
pENSG-p35S:NLSNLS-mCherry-P2A-TTG1	Protein stability	this study
pENSG-p35S:YFP-HY5-P2A-RFP-NLS	Protein stability	this study
pENSG-p35S:YFP-GL1-P2A-RFP-NLS	Protein stability	this study

pENSG-p35S:YFP-GL3-P2A-RFP-NLS	Protein stability	I. Schultheiß Araújo
pENSG-p35S:CFP w/o	Protein stability	this study
pENSG-p35S:CFP-TRY	Protein stability	this study
pENSG-p35S:CFP-CPC	Protein stability	this study
pENSG-p35S:CFP-GL1	Protein stability	this study
pENSG-p35S:CFP-TTG1	Protein stability	this study
pENSG-p35S:CFP-GL3	Protein stability	I. Schultheiß Araújo
pENSG-p35S:CFP-EGL3	Protein stability	this study
pENSG-p35S:CFP-MYB23	Protein stability	this study
pENSG-p35S:CFP-Δ96 GL3	Protein stability	this study
pENSG-p35S:CFP-GL1-R97D	Protein stability	this study
pENSG-p35S:CFP-GL3Δ78 (Δ360-437)	Protein stability	this study
pENSG-p35S:CFP-KAK	Protein stability	J. Pietsch
pENSG-p35S:moxDendra2 GW	Protein stability	this study
pENSG-p35S:moxDendra2-GL1	Protein stability	this study
pENSG-p35S:moxDendra2-GL3	Protein stability	this study
pENSG-p35S:Dendra2 GW	Protein stability	this study
pENSG-p35S:Dendra2-GL1	Protein stability	this study
pAMPAT-p35S:Dendra2	Protein stability	this study
pAMPAT-p35S:moxDendra2	Protein stability	this study
PARB GW	Rescue experiments	M. Pesch
PARB-GL1 CDS GW	Rescue experiments	this study
PARB-GL1 gDNA GW	Rescue experiments	this study
PARB-pGL1 Wang -35S TATA-GL1 CDS-3'enhancer Wang	Rescue experiments	this study
PARB-pGL1 Wang-35S TATA-GL1 gDNA-3'enhancer Wang	Rescue experiments	this study
PARB-pGL1 1.4 kb Wang:GL1 CDS	Rescue experiments	this study
PARB-pGL1 Wang:GL1 gDNA	Rescue experiments	this study
PARB w/o 35S TATA & GUS GW	Rescue experiments	this study
PARB-pGL1 Wang:35S TATA:GL1 CDS-BglII 3‘enhancer Larkin	Rescue experiments	this study
PARB-pGL1 Wang:35S TATA:GL1 gDNA-BglII 3‘enhancer Larkin	Rescue experiments	this study
PARB-3‘enhancer Larkin SpeI-pGL1 Wang:35S TATA:GL1 CDS	Rescue experiments	this study
PARB-3’enhancer Larkin SpeI-pGL1 Wang:35S TATA:GL1 gDNA	Rescue experiments	this study
PARB-pGL1 Wang-GL1 gDNA-3'enhancer Wang	Rescue experiments	this study
PARB-pGL1 Wang et al.-GL1 CDS-3'enhancer Wang	Rescue experiments	this study

PARB-intron1-3‘enhancer Larkin SpeI-pGL1 Wang:35S TATA:GL1 CDS	Rescue experiments	this study
PARB-3‘enhancer Larkin SpeI-pGL1 Wang:35S TATA:GL1 CDS-intron1	Rescue experiments	this study
pAMPAT-pTTG1:TTG1-YFP	Rescue experiments	R. Balkunde
pAMPAT-pTTG1:TTG1ΔC26-YFP	Rescue experiments	R. Balkunde
pAMPAT-pTTG1:TTG1(S282F)-YFP	Rescue experiments	R. Balkunde
pAMPAT-pTTG1:TTG1(G43R)-YFP	Rescue experiments	R. Balkunde
pAMPAT-pTTG1:TTG1(G149R)-YFP	Rescue experiments	R. Balkunde
pAMPAT-pGL1-GL1 gDNA-3‘enhancer_ Cardamine	Rescue experiments	this study
pAMPAT-pMYB23-MYB23 gDNA3‘enhancer_ Cardamine	Rescue experiments	this study
pAMPAT-pWER-WER gDNA-3‘enhancer_ Cardamine	Rescue experiments	this study

2.1.3. List of oligonucleotides

Table 3. List of oligonucleotides used in this study.

Oligo-nucleotide	Sequence 5' to 3'	Provided by
ANS11	CGGGGAAGAAGTGGCTGATCTCAGC	A. Schrader
ANS44	CCTGCTTTTTTGTACAAA	A. Schrader
ANS99	CTCAGGAGAGCGTTCACCGACAAACAAC	A. Schrader
ANS142	CATTGGGATATATCAACGGTGG	A. Schrader
ANS218	GTCGCCGTCCAGCTCGACCAGGATG	A. Schrader
ANS299	TCTGAACCATGGTTACAAGCTAGCGTAATCTGGAACATCGTATGGGTAAGCGAATTCGATC	A. Schrader
ANS406	ATTACATGCTTAACGTAATTCAACAG	A. Schrader
J1475	TTATTAGCTATTGCTTCACCGCCTTA	M. Jakoby
J1649	CTTGTCAAGTCTCAATCCAATTATCC	M. Jakoby
H007	AGCGAAACCCTATAAGAAC	A. Friede
H010	CGGCGAAAACGGCAACTGTTTCATC	A. Friede
H011	GTACACATACAAATGGACGAACGGATAAACC	A. Friede
H013	AGTTCCAAACGTAAAACGGCTTGTCC	A. Friede
H023	GGGGACAAGTTTGTACAAAAAAGCAGGCTTACGATCACTCAAATAGTAATA	this study
H034	ACAAGTTTGTACAAAAAAGCAGGCT	this study
H035	ACCACTTTGTACAAGAAAGCTGGGT	this study
H036	TCGCGTTAACGCTAGCATGGATCTC	this study
H037	GTAACATCAGAGATTTTGAGACAC	this study
H038	GTTAAAACTGCCTGGCACAGCAAT	this study
H041	GCTTCCGGCTCGTATGTTGT	this study
H146	GGGGCTCGAGGTCGACGGTATCGAATAAGCTTATAATGCCAAAGAAGAAAAGAAA	this study
H148	GGAAGCGGAGCTACTAACTTCAGCCTGCTGAAGCAGGCTGGAGACGTGGAGGAGAACCCTGGACCTATGGTGAGCAAGGGCGAGGAG	this study
H149	CCCCGAATTCCGGATGAGCATTCATC	this study
H153	GGGGCTCGAGATGAGAATAAGGAGAAGAGATGAAAA	this study
H154	GGGGGAGCTCCTAAAGGCAGTACTCAACATCACCAG	this study
H155	GGGGACAAGTTTGTACAAAAAAGCAGGCTTAATAATTGTTTGTACTTTCTCGAGTTAGTC	this study
H164	ATAGAAGGAATCAGAGAATAAAAAAAGAATGAGAATAAGGAGAAGAGATGAAAA	this study
H165	TTTTCATCTCTTCTCCTTATTCTCATTCTTTTTTTATTCTCTGATTCCTTCTAT	this study
H167	CTGGTGATGTTGAGTACTGCCTTTAGTTGATGTTTTGAATTTGTCTTTGAATTT	this study
H170	GGGGAGATCTATCTTCCGCGTAGGTTTTCATTTA	this study
H171	GGGGAGATCTACCACTTTCATCTTAAATATTTTA	this study

H172	GGGGACTAGTATCTTCCGCGTAGGTTTTCATTTA	this study
H173	GGGGACTAGTACCACTTTCATCTTAAATATTTTA	this study
H174	AAATGAACACATAAATTTTGTGGTCTA	this study
H175	TTTTAAAAGTTCATGAGGTTACCCTCT	this study
H176	ACTATAAATTGGTCATTAATTACTCAAA	this study
H177	TGTATGTCCCTATGTGTAAATTAACTAC	this study
H178	TCTAGACAAATGGGCTAAGCAAAAATTAGACCAACTTTCTCATGT	this study
H179	GCCTACATGTATTACACACATGGTCTATAATACAGGTCCA	this study
H180	TGGACCTGTATTATAGACCATGTGTGTAATACATGTAGGC	this study
H181	CAGTCTTTACTTGTCAACTCTC	this study
H182	GATTTGGCCGGTTAAGTTGA	this study
H183	CCGGGAAGAACAGATAACCA	this study
H185	TCTTTTTGTTTCTGTGGAAG	this study
H186	ATCCGTTCGACCCGGCACTC	this study
H187	CTTGCTTGGTAACACATG	this study
H188	CAAGGCCGGGTGGGGGGACA	this study
H189	CTGCTACGTACATACCCC	this study
H190	GGAACCCTAAATTGCTTGAG	this study
H191	CCAGACTGAGAAGCAGAGAC	this study
H194	AGTTATTGCGATGAAATGTTGCAGAGAATTATTACCCCTCTT	this study
H195	AGGATTGGGTCAAAATCTGTTTGCCAGCAAAGTCAAAGATTT	this study
H196	TCTCCCATAGTTGGTCATAAACATAAATTAAGAACAACAATAATTC	this study
H197	CCCGGTACTCTTTTAGCTATCAAAGCCCATCTAATTTTTTGGAAAAACAATATC	this study
H199	TCAAGCTTGGAGTTTTTTGAATTTGTGGAGTTCGAAGATATGTGGCG	this study
H213	GGGGTCTAGAGCTCTTATTGTTTGCCTCCCTGCTGC	this study
H214	GGGGCCCGGGCGACGGATGGTGATCCCCC	this study
H216	CACTCGTAATGATGAATTTTGCTTCTGGTGATGTTGAGTACTGCCTTTAGTTGAT GTTTTGAATTTGTCTTTGAATTT	this study
H218	GGGGCTCGAGCCGGTGGATTCAGGGAGTTTCTTTAACCAGAGAA	this study
H228	CTAAAGGCAGTACTCAACATCACCAGAAGCAAAATTC	this study
H232	GGGGGAGCTCTTACTTGTACAGCTCGTCCATGCCGAGAGTGATCCC	this study
H234	GGGGGAGCTCCTTGTACAGCTCGTCCATGCCGAGAGTGATCCC	this study
H239	GGGGCACGTGTCACGAAAACCCATCATAAGTTCACTACTCATAATCTCTTTC	this study
H240	GGGGCCGCGGTAACTAACTTATTTTTCACATTCGGTAAAACTTAATGCTCTTTAA ATAGTATAAAGAAGTAC	this study
H244	GGCGCGCCAATTGAATTGAACTATTTTGTTTTATAAAAAATTGATAATTCAACAT ACGATTAATTAATTAACAATCCACACATCGGGATCCGAGAATAATTAATAC	this study
H246	GGGGGGGCCCGTACTCTTTCTCTCTCTCGC	this study
H247	GGGGGGGCCCCTATCAACGAATCAAATTTA	this study
H248	GGGGGAGCTCGTACTCTTTCTCTCTCTCGC	this study
H249	GGGGGAGCTCCTATCAACGAATCAAATTTA	this study
H250	GGGGGGCGCGCCAGTCTAGCTCAACAGAGCTTTTAACCCAAATTGG	this study
H251	GGGGCTCGAGCTGTTAATCAGAAAAACTCAGATTAATCGACAAATTC	this study
H255	GGGGACCACTTTGTACAAGAAAGCTGGGTTTCCAGGCATTCTGCAAAAAG	this study
H262	AGTTATTGCGATGAAATGTTGCAGAGAATTATTACCCCTCTTATTAACTCAAATC CACCGTGAGAGTTTAATATGTCTTGAATTTTAAATGTGCCAG	this study

H263	AGGATTGGGTCAAAATCTGTTTGCCAGCAAAGTCAAAGATTTTGGCAGAAAGTG AAATTTCAGCATTTGAAGACCAATGTGGCCGATGCGAAAGGG	this study
H279	GGGGGGCGCGCCAGAGTTTGGTATCACGGATG	this study
H280	TGCCAGCACTTTTGAAACAT	this study
H286	GGGGAAGCTTTTGATGTTTTGAATTTGTCTTTGAATTTTTGAG	this study
H287	GGGGAAGCTTTTCGGTTAGGGTAGATTATATTGAATTGATTG	this study
H294	GGGGACCACTTTGTACAAGAAAGCTGGGTTCTATCAACGAATCAAATTTAGTCT AACTGAGATATATTTATATATGAACTAGCTAGAGAC	this study
H295	GGCTAATGATTTCAAACAATATATTTTAC	this study
H296	CATATATTAATATTAGCGTACG	this study
H327	GACCTTAGGCGACTTTTGAACGCGC	this study
H328	GTCTGTTCTCCCCGGCACTCTC	this study
H331	CCTGTTTTCACTTATTGGC	this study
H332	CCCAACGGACGAGGCTCTGGTC	this study

2.1.4. Bacterial strains

Table 4. List of organisms used in this study

Organism	Strain	Property	Reference
E. coli	DH5α	F-, φ80lacZ ΔM1, Δ(lacZYA-argF), U169, deoR, recA1, endA1, hsdR17, (rk-, mk+), phoA, supE44, thi-1, gyrA96, relA1, -λ	Hanahan, 1983
	DB3.1	F-gyrA462 endA1 glnV44 Δ(sr1-recA) mcrB mrr hsdS20(rB-, mB-) ara14 galK2 lacY1 proA2 rpsL20(Smr) xyl5 Δleu mtl1	Bernard & Couturier, 1992; Miki et al., 1992
A. tumefaciens	GV3101:pMP90RK	pTiC58ΔT-DNA	Koncz & Schell, 1986
	RK19	Anti-silencing strain; P19 protein	Voinnet et al., 1999
	LBA4404.pBBR1MCS virGN54D	VirG wild-type, constitutive N54D and supersensitive I77V mutant virG genes in plasmid pBBR1MCS	Van Der Fits et al., 2000

2.1.5. Wildtype and mutant plants

Table 5. Arabidopsis thaliana wildtype and mutant lines used in this study.

Line	Ecotype	Target ID	Reference/Source
Col-0	*Col-0*		
cpc-2 try	*Col-0*	AT2G46410 / AT5G53200	J. Pitesch
gl1	*Col-0*	AT3G27920	I. Schultheiß Araújo
gl1 myb23	*Col-0*	AT3G27920 / AT5G40330	V. Kirik
myb23-1	*Col-0*	AT5G40330	V. Kirik

Experiments involving *Cardamine hirsuta* were always conducted with the *Ox* ecotype, provided by J. Pietsch (originally from M. Tsiantis).

2.1.6. Stably transformed *A. thaliana* lines

The constructs used to generate stable lines are listen in Table 3 with the respective provider.

Table 6. List of stable A. thaliana lines used in this study.

Construct	Background	Source/Reference
pAtML1:mCitrine-RCI2A, pAtML1:H2B-TFP	*Col-0*	Roeder et al., 2010
pAtML1:mCitrine-RCI2A, pAtML1:H2B-TFP	*cpc try*	this study
pAMPAT-pTTG1:TTG1-YFP	*Col-0*	this study
pAMPAT-pTTG1:TTG1ΔC26-YFP	*Col-0*	this study
pAMPAT-pTTG1:TTG1(S282F)-YFP	*Col-0*	this study
pAMPAT-pTTG1:TTG1(G43R)-YFP	*Col-0*	this study
pAMPAT-pTTG1:TTG1(G149R)-YFP	*Col-0*	this study
pAMPAT-pGL1-GL1 gDNA-3‘enhancer_Cardamine	*gl1*	this study
pAMPAT-pGL1-GL1 gDNA-3‘enhancer_Cardamine	*myb23*	this study
pAMPAT-pGL1-GL1 gDNA-3‘enhancer_Cardamine	*gl1 myb23*	this study
pAMPAT-pMYB23-MYB23 gDNA3‘enhancer_Cardamine	*gl1*	this study
pAMPAT-pMYB23-MYB23 gDNA3‘enhancer_Cardamine	*myb23*	this study
pAMPAT-pMYB23-MYB23 gDNA3‘enhancer_Cardamine	*gl1 myb23*	this study
pAMPAT-pWER-WER gDNA-3‘enhancer_Cardamine	*gl1*	this study
pAMPAT-pWER-WER gDNA-3‘enhancer_Cardamine	*myb23*	this study
pAMPAT-pWER-WER gDNA-3‘enhancer_Cardamine	*gl1 myb23*	this study
pAMPAT-pCPC:GUS	*cpc try*	this study
pAMPAT-pTRY:GUS	*cpc try*	this study
pAMPAT-pCPC:GUS	*Col-0*	this study
PARB-pGL1 Wang -35S TATA-GL1 CDS-3' enhancer Wang	*gl1*	this study
PARB-pGL1 Wang-35S TATA-GL1 gDNA-3' enhancer Wang	*gl1*	this study
PARB-pGL1 Wang-GL1 gDNA-3' enhancer Wang	*gl1*	this study
PARB-pGL1 Wang et al.-GL1 CDS-3' enhancer Wang	*gl1*	this study
PARB-pGL1 Wang:35S TATA:GL1 CDS-BglII 3‘enhancer Larkin	*gl1*	this study
PARB-pGL1 Wang:35S TATA:GL1 gDNA-BglII 3‘enhancer Larkin	*gl1*	this study
PARB-3‘enhancer Larkin SpeI-pGL1 Wang:35S TATA:GL1 CDS	*gl1*	this study
PARB-3’enhancer Larkin SpeI-pGL1 Wang:35S TATA:GL1 gDNA	*gl1*	this study
PARB-intron1-3‘enhancer Larkin SpeI-pGL1 Wang:35S TATA:GL1 CDS	*gl1*	this study
PARB-3‘enhancer Larkin SpeI-pGL1 Wang:35S TATA:GL1 CDS-intron1	*gl1*	this study
pENSG-p35S:YFP-MYB23-P2A-NLSNLS-mCherry	*Col-0*	this study

2.2. Solutions and media

2.2.1. Antibiotics

Table 7. List of antibiotics.

Antibiotics	Stock conc. [mg/ml]	Stored in	Conc. *E. coli* [µg/ml]	Conc. *A. tumefaciens* [µg/ml]
Carbenicillin	50	H_2O	50	50
Chloramphenicol	35	70 % EtOH	35	35
Gentamycin	25	H_2O	25	-
Hygromycin	25	H_2O	25	25
Kanamycin	50	H_2O	50	50
Rifampicin	50	MeOH	-	25-150

2.2.2. LB Media

20 g Bacto-Yeast-Extract, 40 g Bacto-Peptone, and 40 g NaCl were mixed, and water was added up to 4 liters. If necessary, the pH was adjusted to pH 7.0 using NaOH. To generate LB plates, 6.4 g Micro agar was added to 400 ml LB media. Any LB media was subsequently autoclaved for 20 min.

2.2.3. YEB Media

20 g Beef-Extract, 4 g Bacto-Yeast-Extract, 20 g Sucrose, 20 g Bacto-Peptone, and 8 ml 1 M Magnesium sulfate heptahydrate were mixed, and water was added up to 4 liters. To generate YEB plates, 6.4 g Micro agar was added to 400 ml YEB media. Any YEB media was subsequently autoclaved for 20 min.

2.2.4. MS Media

40 g Sucrose and 17.6 g MS were mixed, and water was added up to 4 liters to generate 1 % MS media. To generate ½ MS media, 20 g sucrose, and 8.8 g MS were mixed and filled up to 4 liters with water. For both media, the pH was adjusted to 5.8 using 2 M KOH. To generate MS plates, 3.2 g Plant agar was added to 400 ml of either 1% MS or ½ MS. Any MS media was subsequently autoclaved for 20 min.

2.2.5. TA Media

4.3 g MS basal salts, 4 ml Gamborg's Vitamin Solution, 1 mg 2,4-Dichlorophenoxyacetic acid, and 30 g sucrose were mixed, and water was added up to one liter. The pH was adjusted to 5.8 using 0.5 M KOH. The TA media was subsequently autoclaved for 12 min.

2.3. Solutions & Buffers

2.3.1. 50x TAE Buffer

242 g Tris base, 57.1 ml Glacial acetic acid, and 100 ml 500 mM EDTA (pH 8.0) were mixed, and water was filled up to one liter.

2.3.2. Sørensen's Phosphate ($NaPO_4$) buffer

To generate a phosphate buffer with 7.2 pH, 28 ml of NaH_2PO_4 and 72 ml of Na_2HPO_4 stock solutions of the same concentration were mixed.

2.3.3. 10x DNA loading dye

6.25 ml 80% (w/v) Glycerol, 1 ml 0.5 M EDTA (pH 8.0), 10 mg Xylene cyanol, 25-50 mg Orange G, and 100 µl 1M Tris/HCl (pH 8.0) were mixed, and water was added up to 10 ml.

2.3.4. GUS staining solution for plant material

82 ml water, 2 ml 10% Triton X-100, 10 ml 0.5 M $NaPO_4$ buffer (pH 7.2), 2 ml 100 mM Potassium ferrocyanide, 2 ml 100 mM Potassium ferricyanide, and 2 ml of 100 mM X-Gluc were mixed for 100 ml of GUS solution.

2.3.5. GUS staining solution for cell suspension culture

10 mg X-Gluc were dissolved in 1 ml DMF.

2.3.6. Lysis buffer for extracts from plant cell culture

To extract one sample harvested from the transformed cell suspension culture, 1 ml of 50 mM $NaPO_4$ buffer (pH 7.2), 20 µl 0.5 M EDTA (pH 8.0), and 100 µl 10% Triton X-100 were mixed.

2.3.7. Assay buffer for quantitative GUS assays

Quantitative GUS assays were performed using an assay buffer consisting of lysis buffer used for extracts from plant cell suspension culture (2.5.9) and 1.5 mM MUG.

2.3.8. Agromix

For 10x Agromix, 2.03 g of MgCl2*6H2O and 1.95 g MES were mixed, and water was added until 100 ml was reached. The pH was adjusted to 5.6 using 1 M NaOH. For 10 ml of 1x Agromix, 0.9 ml of 10x Agromix, 0.1 ml of Acetosyringon (3 mg/ml in 100% EtOH), and 9 ml were mixed freshly before tobacco infiltration.

2.3.9. $CaCl_2$-solution for competent *E. coli*

60 mM $CaCl_2$ and 10 mM PIPES pH 7 were mixed, and the pH was adjusted to 7 using NaOH. Glycerol was added to a final concentration of 15 %. The solution was autoclaved for 15 min.

2.3.10. Extraction buffer for genomic DNA extraction

For 50 ml extraction buffer, 10 ml 1 M Tris (pH 8.0), 2.5 ml 5 M NaCl, 2.5 ml 0.5 M EDTA (pH 8.0), 2.5 ml 10 % SDS, and 32.5 ml water were mixed.

2.3.11. Magic buffer for genomic DNA extraction

For 100 ml Magic buffer, 5 ml 1 M Tris/HCl (pH 7.2), 6 ml 5 M NaCl, and 10 g sucrose were mixed, and water was filled up to a volume of 100 ml.

2.4. Molecular methods

2.4.1. Extraction of genomic DNA for cloning

A small amount of plant material (one leaf < 1 cm) was frozen in liquid nitrogen together with three glass beads in a 2 ml Safe Seal Eppendorf tube. The plant material was shredded in a TissueLyser (Qiagen) at 30 Hz for 1.5 min. 125 µl extraction buffer (0) was added, and the Eppendorf tube was inverted three times. 38.5 µl 3 M NaOAc (pH 5.5) was added, the Eppendorf tube was inverted another three times, and the sample was centrifuged for 10 min at 14680 rpm. After discarding the supernatant, the pellet was washed with 500 µl 70 % EtOH and centrifuged for 2 min at 14680 rpm. Subsequently, to remove the supernatant, the pellet was dried for approximately 30 min at room temperature. Finally, the pellet was resuspended in 20 µl ddH_2O and stored at -20 °C.

2.4.2. Extraction of genomic DNA for genotyping

A small amount of plant material (one leaf < 1 cm) was harvested and placed in a 1.5 ml Safe Seal Eppendorf tube together with 3-4 glass beads. 300 µl Magic buffer were added and the sample was shredded in a TissueLyser (Qiagen) at 30 Hz for 1.5 min. This DNA extract was used to amplify genomic DNA from *Cardamine* samples and was only stored briefly at -20 °C.

2.4.3. PCR

Amplification of DNA was achieved by performing polymerase chain reactions (PCRs). Depending on the later usage of the PCR product and the properties of the amplicon, different DNA polymerases were used in this study.

Phusion Polymerase PCR

Due to the low error rate during amplification, the Phusion™ High-Fidelity DNA polymerase from Thermo Fisher Scientific was used to amplify DNA sequences destined for cloning and sequencing. The following PCR reaction mix and reaction program were used.

Table 8. Reaction mix and conditions for PCR using Phusion™ polymerase.

PCR reaction mix		**PCR program**		
DNA template	1 µl	98 °C	1 min	
Forward primer [10 µM]	0.5 µl	98 °C	10 sec	35 cycles
Reverse primer [10 µM]	0.5 µl	T_A	30 sec	
dNTPs [10 mM]	0.5 µl	72 °C	15-30 sec/kb	
5x High Fidelity buffer	5 µl	72 °C	10 min	
Phusion™ Polymerase [2 U/ µl]	0.3 µl	4 °C	∞	
ddH_2O	17.2 µl			

PrimeSTAR® GXL DNA Polymerase PCR

For amplification of especially long and GC-rich sequences, the PrimeSTAR® GXL DNA Polymerase was used. The following reaction mix and PCR program were applied.

Table 9. Reaction mix and conditions for PCR using PrimeSTAR® GXL DNA Polymerase.

PCR reaction mix		**PCR program**		
Template DNA	1 µl	10 sec	98 °C	30 cycles
5x PrimeSTAR GXL buffer	10 µl	15 sec	55 °C/60 °C	
Forward primer [10 µM]	1 µl	1 min/kb	68 °C	
Reverse primer [10 µM]	1 µl			
dNTPs [10 mM]	4 µl			
PrimeSTAR® GXL DNA polymerase	32 µl			

The T_A used in the protocol depended on the melting temperature of the used primer calculated by the following formula: T_M (°C) = [(the number of A and T) x 2] + [(the number of G and C) x 4]. If the calculated T_M was less than 55 °C, the T_A was set to 55 °C, and if the T_M was higher than 55 °C the T_A was set to 60 °C.

Fusion PCR

The fusion of two PCR products containing overlapping DNA sequences into one was achieved with a special fusion PCR protocol using the Phusion™ High-Fidelity DNA polymerase. The following PCR reaction mix and reaction program was used.

Table 10. PCR reaction mix and program for fusion PCR using Phusion™ polymerase.

PCR reaction mix		**PCR program**		
PCR product A	1 µl	98 °C	10 min	
PCR product B	1 µl	58 °C	10 min	
Forward primer [10 µM]	2 µl	72 °C	10 min	
Reverse primer [10 µM]	2 µl	98 °C	30 sec	35 cycles
dNTPs [10 mM]	1 µl	58 °C	30 sec	
5x High Fidelity buffer	10 µl	72°C	15-30 sec/kb	
Phusion™ Polymerase [2 U/ µl]	1 µl	72 °C	5 min	
DMSO	1.5 µl	12 °C	∞	
$MgCl_2$ [50 mM]	1.5 µl			
ddH_2O	29 µl			

PCR-mediated site-directed mutagenesis

Mutation of 1-3 base pairs in a DNA sequence was achieved using a primer pair containing the desired mutation in a PCR. The primers were designed with the following criteria: the 5'-end can be as close as 4 bp from the mutation, the 3'-end should be at least 8 bp away from the mutation, a minimum of 8 non-overlapping bp should be added to the 3'-end of each primer, each primer should contain a minimum of one G or C at each end, and the primer should possess a $T_A \geq 78°C$. The following PCR mixture containing Phusion™ DNA polymerase and PCR program were used to amplify the whole plasmid.

Table 11. PCR reaction mix and program for site-directed mutagenesis using Phusion™ DNA polymerase.

PCR reaction mix		**PCR program**		
DNA template	0.5 µl	98 °C	30 sec	
Forward primer [10 µM]	1 µl	98 °C	10 sec	
Reverse primer [10 µM]	1 µl	60 °C	30 sec	20 cycles
dNTPs [10 mM]	1 µl	72 °C	30 sec/kb	
5x High Fidelity buffer	10µl	72 °C	5 min	
Phusion™ Polymerase [2 U/ µl]	0.5 µl	4 °C	∞	
DMSO	1 µl			
ddH_2O	35 µl			

To destroy any template DNA, 1 µl DpnI was added to 50 µl PCR mix and incubated for 30 min at 37 °C. After heat-inactivation for 20 min at 80 °C, 1 µl of PCR mix was used for transformation.

PCR for AT-rich sequences

Amplification of AT-rich sequences can be challenging. To optimize such PCRs, the following PCR mixture and program were applied using the Phusion™ DNA polymerase.

Table 12. PCR mix and program for AT-rich sequences.

PCR reaction mix		**PCR program**		
Genomic DNA	2 µl	98 °C	1.5 min	
Forward primer [10 µM]	0.8 µl	98 °C	30 sec	35 cycles
Reverse primer [10 µM]	0.8 µl	Gradient (T_A+5 °C to 72°C)	3 min	
dNTPs [10 mM]	0.4 µl	Gradient (T_A+5 °C to 72°C)	7 min	
5x High Fidelity buffer	4 µl	12 °C	∞	
Phusion™ Polymerase [2 U/ µl]	0.2 µl			
$MgCl_2$ [50 mM]	1.2 µl			
ddH_2O	10.6 µl			

2.4.4. Blunting of 5'- and 3'-overhangs using T4 DNA polymerase

Generating blunt ends by filling in 5'-overhangs or removal of 3'-overhangs was achieved utilizing the 3' to 5' exonuclease activity of T4 DNA polymerase (Thermo Fischer Scientific). The following reaction mix was incubated at room temperature for 5 min and then heat-activated at 75 °C for 10 min.

Table 13. Reaction mix for blunting of DNA sequences using T4 DNA polymerase.

5x T4 DNA polymerase buffer	4 µl
dNTPs [10 mM]	0.8 µl
T4 DNA polymerase [5 U/µl]	0.2 µl
Linearized DNA or PCR product	200-400 ng
Water	add to 20 µl

2.4.5. Gel electrophoresis

Gel electrophoresis was performed to separate or visualize DNA fragments after PCR or restriction digestion. Typically, 1 % agarose gels were prepared with 1x TAE (in water diluted 50x TAE buffer) buffer. Small plasmid fragments were separated using 2 % agarose gels. DNA-staining was achieved by adding either ethidium bromide (0.25 µg/ml) or Thiazole-Orange (0.14 µg/ml) to the gel. The agarose gel was placed in an electrophoresis chamber filled with 1x TAE, the DNA samples were mixed with 10x DNA loading dye (0), and an electric current was applied with a voltage of 120-150 V. As a size reference, DNA ladders GeneRuler 1 kb or GeneRuler 1 kb Plus from Thermo Fisher Scientific were used. In the case of ethidium bromide, visualization was achieved using BioRad Universal Hood II (Quantity One software version 4.5.0) or the INTAS Gel Jet Imager (Intas GDS Touch 2 version 2.1.4). In the case of Thiazole-Orange, the INTAS Gel Jet Imager (Intas GDS Touch 2 version 2.1.4) was used to visualize the DNA.

2.4.6. DNA gel extraction

Isolation of PCR products or digested plasmid DNA was achieved by cutting out the desired band from an agarose gel. For extraction, the GeneJET Gel Extraction Kit from Thermo Fisher Scientific was used according to the manufacturer's manual.

2.4.7. DNA plasmid preparation

To isolate plasmid DNA, 5 ml cultures of single bacterial colonies in selective media were incubated overnight at 37 °C or 28 °C at 220 rpm. The cultures were centrifuged for 2 min at 8000 rpm, and the GeneJET Plasmid-Miniprep-Kit from Thermo Fisher Scientific was used according to the manufacturer's manual.

2.4.8. Restriction digest

Verification of cloning and vector integrity was achieved by performing restriction digests. All used restriction enzymes were from Thermo Fisher Scientific. For classic restriction digestion, 2 µl plasmid, 2 µl enzyme specific buffer, 0.3 µl restriction enzyme, and 15.7 µl ddH_2O were mixed and incubated for 1 h at 37 °C. For FastDigest enzymes, the reaction mix consisted of 2 µl plasmid, 2 µl FastDigest buffer, 1 µl FastDigest Enzyme and 15 µl ddH_2O. Double digests were performed according to the manufacturer's instructions.

2.4.9. Linearization of vectors

Linearization of larger vectors can be beneficial for cloning efficiency. Therefore, larger vectors (e.g., pGWB2) were linearized by mixing 1.5 µl plasmid, 1 µl enzyme specific buffer, 0.15 µl enzyme, and 7.85 µl ddH_2O. After incubation at 37 °C for 30 min, the enzymatic reaction was heat inactivated (20 min at 80 °C). For subsequent LR reaction, 1 µl linearized plasmid was used.

2.4.10. Cloning

Gateway Cloning

All vectors used in this study were Gateway-capable vectors. This vector system is based on the recombination strategy used by phage λ and was developed by Invitrogen. A sequence of interest is first equipped with flanking recombination sites via PCR and then used in a BP reaction to integrate the sequence of interest into a vector. This so-called entry vector can then be used in an LR reaction to transfer the sequence of interest into different expression vectors. The BP and LR reaction mixes are listed in Table 14.

Table 14. BP and LR reaction mixes.

BP reaction mix		**LR reaction mix**	
BP enzyme mix	0.5 µl	**LR enzyme mix**	0.5 µl
Donor vector	0.25 µl	**Donor vector**	0.5 µl
PCR product	1.75 µl	**Destination vector**	0.25 µl
		Water	1.25 µl

The BP and LR reactions were incubated at room temperature for 1-16 h, and subsequently, the whole volume was used to transform DH5α *E. coli* cells.

Ligation

Restriction site-based cloning was performed using T4 DNA ligase (Thermo Fisher Scientific) and DNA fragments harboring the appropriate restriction sites. After linearization with restriction enzymes, 50

ng of vector were mixed with a 1:1 to 1:5 ratio with the cut insert. The amount of insert was calculated using the following equation:

$$\frac{250\ \text{ng} * \text{bp insert}}{\text{bp vector}} = \text{ng insert}$$

The reaction mix was prepared according to the manufacturer's protocol, depending on sticky- or blunt-end ligation. After 10-60 min incubation at room temperature, 5 µl reaction mix was used to transform 50 µl *E. coli* cells, either DB3.1 or DH5α.

Cloning of donor vectors

The generation of donor vectors used for Gateway cloning that were not generated by a simple PCR followed by BP are described below.

pDONR207-pGL3:Ex1+2-In2-Ex3(10bp)

The insert was amplified as two separate PCR products. One was attB1-pGL3 with a 32bp overlap of exon 1 at the 3' end, which was amplified using the primers H023 and H283 and pEXSG-pGL3:2xmVenus GW as template. The other one was Ex1+2-In2-Ex3(10bp)-attB2 with a 30 bp overlap of pGL3 at the 5' end, which was amplified using the primers H282 and H255 and pDONR201-Ex1+2-In2-Ex3(10bp) as template. Subsequently, both PCR products were fused to one sequence via fusion PCR using the primers H023 and H255. This PCR product was then used in a BP reaction to generate pDONR207-pGL3:Ex1+2-In2-Ex3(10bp).

pDONR201-GL3 Ex1+2-In2(1-138)-Ex3(10bp) mutation W-boxes

Both W-boxes in the n-terminal part of intron 2 of *GL3* were sequentially mutated via site-directed mutagenesis. The most n-terminal W-box was mutated from 5' TTGAC 3' to 5' GGGCC 3' using the primers H273 and H274. After successful mutagenesis, the second W-box was changed from 5' TGTCA 3' to 5' GGGCC 3' using the primers H275 and H276.

pDONR201-pGL1 Wang:GL1 CDS-3'enhancer Wang

The gDNA from GL1 was cut out of pDONR201-pGL1:GL1 gDNA-3'enhancer Wang using PmlI and SacII. The sequence overlap-PmlI-GL1 CDS-SacII-overlap was amplified in three steps because extensions needed to be added to regenerate the cut-out sequences from the backbone. The first PCR was performed using the primers H235 and H236 using pENTR1A-GL1 as the template. This PCR product was used as the template in the following PCR and amplified with the primers H237 and H238. Finally, the second PCR product was amplified using primers H239 and H240. This final PCR product was cut with PmlI and SacII and used in a ligation reaction with the cut pDONR201 pGL1:GL1 gDNA-3'enhancer Wang, resulting in pDONR201 pGL1:GL1 CDS-3'enhancer Wang.

Cloning of expression vectors

The generation of expression vectors that are not the result of a simple LR reaction or the generation of new Gateway-capable vectors are described below.

pENSG-p35S:NLSNLS-mCherry-P2A-YFP-GW

A swap construct of the original pENSG-p35S:YFP-GW-P2A-NLSNLS-mCherry vector was cloned to enable a correct cleavage process for EGL3- and TTG1-containing constructs. To generate this vector, the insert XhoI-NLSNLS-mCherry-P2A-YFP-GW-EcoRI was cloned by amplifying two separate sequences. The first sequence contained XhoI-NLSNLS-mCherry-P2A and was amplified using the primers H146 and H148, utilizing pENSG-p35S:YFP-GW-P2A-NLSNLS-mCherry as the template. The second sequence, P2A-YFP-GW-EcoRI, was amplified using the primers H148 and H149, utilizing the vector pENSG-YFP GW as the template. This sequence contained a piece of the chloramphenicol resistance gene up to the EcoRI restriction site. After individual amplification, both PCR products were used in a fusion PCR reaction to create XhoI-NLSNLS-mCherry-P2A-YFP-GW-EcoRI. As vector backbone, pENSG-p35S:YFP GW was cut with XhoI and EcoRI, cutting out YFP and a part of the gateway cassette. This backbone was then used with the cut PCR product XhoI-NLSNLS-mCherry-P2A-YFP-GW-EcoRI in a ligation reaction, creating pENSG-p35S:NLSNLS-mCherry-P2A-YFP-GW.

PARB-attR1-pGL1 Wang-attR2:p35S TATA-GL1 CDS-3' enhancer Wang

The GUS sequence was cut out of the PARB vector using XhoI and SacI. The XhoI-GL1 CDS-SacI fragment was amplified using the primers H153 and H154 and pENTR1A-GL1 as the template. Subsequently, the PCR product was cut with XhoI and SacI and used for a ligation reaction with the XhoI/SacI cut PARB vector. This PARB-GW-GL1 CDS vector was then used in a LR reaction with pDONR201-pGL1 Wang, leading to PARB-pGL1 Wang:p35S TATA-GL1 CDS. SacI-3‘enhancer Wang-SacI was amplified with the primers H168 and H169, using genomic DNA from *Col-0*. The resulting PCR product was cut with SacI and used in a ligation reaction with the SacI-linearized PARB-pGL1 Wang:GL1 CDS.

PARB-attR1-pGL1 Wang-attR2:p35S TATA-GL1 gDNA-3' enhancer Wang

The GUS sequence was cut out of the PARB vector using XhoI and SacI. The XhoI-GL1 gDNA-SacI fragment was amplified using the primers H153 & H154 and using genomic Col-0 DNA as the template. Subsequently, the PCR product was cut with XhoI and SacI and used for a ligation reaction with the XhoI/SacI cut PARB vector. This PARB-GW-GL1 gDNA vector was then used in a LR reaction with pDONR201-pGL1 Wang, leading to PARB-pGL1 Wang:p35S TATA-GL1 gDNA. SacI-3‘enhancer Wang-SacI was amplified with the primers H168 and H169 using genomic DNA from Col-0. The resulting PCR

product was cut with SacI and used in a ligation reaction with the SacI-linearized PARB-pGL1 Wang:GL1 gDNA.

PARB-GW w/o p35S TATA-box & GUS

The p35S TATA box and GUS sequence were cut out of the PARB vector using HindIII and SacI. The resulting sticky ends were blunted using T4 DNA ligase, and the vector was closed. This vector was used to generate PARB-pGL1 Wang:GL1 CDS-3'enhancer Wang and PARB-pGL1 Wang:GL1 gDNA-3'enhancer Wang via LR reactions.

PARB-attR1-pGL1 Wang-attR2-p35S TATA-GL1 CDS-3'enhancer Larkin

The BglII-3'enhancer Larkin-BglII sequence was amplified using the primers H170 and H171 with genomic Col-0 DNA. Subsequently, the PCR product was cut with BglII and used with a BglII-linearized PARB-pGL1 Wang:p35S TATA-GL1 CDS in a ligation reaction to clone PARB-attR1-pGL1 Wang-attR2-p35S TATA-GL1 CDS-3'enhancer Larkin.

PARB-attR1-pGL1 Wang-attR2-p35S TATA-GL1 gDNA-3' enhancer Larkin

The BglII-3'enhancer Larkin-BglII sequence was amplified using the primers H170 and H171 with genomic Col-0 DNA. Subsequently, the PCR product was cut with BglII and used with a BglII-linearized PARB-pGL1 Wang:p35S TATA-GL1 gDNA in a ligation reaction to clone PARB-attR1-pGL1 Wang-attR2-p35S TATA-GL1 gDNA-3'enhancer Larkin.

PARB-3' enhancer Larkin-attR1-pGL1 Wang-attR2-p35S TATA-GL1 CDS

The SpeI-3'enhancer Larkin-SpeI sequence was amplified using the primers H172 and H173 using genomic Col-0 as the template. This PCR product and PARB-pGL1 Wang:p35S TATA-GL1 CDS were cut with SpeI and used in a ligation reaction to clone PARB-3' enhancer Larkin-attR1-pGL1 Wang-attR2-p35S TATA-GL1 CDS.

PARB-3' enhancer Larkin-attR1-pGL1 Wang-attR2-p35S TATA-GL1 gDNA

The SpeI-3'enhancer Larkin-SpeI sequence was amplified using the primers H172 and H173 using genomic Col-0 as the template. This PCR product and PARB-pGL1 Wang:p35S TATA-GL1 gDNA were cut with SpeI and used in a ligation reaction to clone PARB-3' enhancer Larkin-attR1-pGL1 Wang-attR2-p35S TATA-GL1 gDNA.

PARB-intron1-3'enhancer Larkin-attR1-pGL1 Wang-attR2-p35S TATA:GL1 CDS

The first intron of the genomic *GL1* sequence was amplified with flanking ApaI restriction sites. Therefore, a PCR was performed using the primers H246 and H247 and PARB-GW-GL1 gDNA as the template. This PCR product and PARB-3' enhancer Larkin-attR1-pGL1 Wang-attR2-p35S TATA-GL1 CDS

were cut with ApaI and used in a ligation reaction to clone PARB-intron1-3‘enhancer Larkin-attR1-pGL1 Wang-attR2-p35S TATA:GL1 CDS.

PARB-3‘enhancer Larkin-attR1-pGL1 Wang-attR2-p35S TATA:GL1 CDS-intron1

The first intron of the genomic *GL1* sequence was amplified with flanking SacI restriction sites. Therefore, a PCR was performed using the primers H248 and H249 and PARB-GW-GL1 gDNA as the template. This PCR product and PARB-3' enhancer Larkin-attR1-pGL1 Wang-attR2-p35S TATA-GL1 CDS were cut with SacI and used in a ligation reaction to clone PARB-3‘enhancer Larkin-attR1-pGL1 Wang-attR2-p35S TATA:GL1 CDS-intron1.

Cardamine MYBs in pAMPAT GW

Three different *MYBs* from *C. hirsuta* were amplified, namely *GL1*, *MYB23,* and *WER*. Each *MYB* sequence consisted of a 1.5 kb 5’ promoter region, the genomic *MYB* sequence, and a 3 kb 3’ enhancer sequence. The *GL1* and *WER* sequences were amplified using the phosphorylated primer pairs H196 + H199 and H194 + H195, respectively. The *MYB23* sequence was amplified with the primers H244 and H178, introducing a SgsI restriction site upstream of the promoter sequence and an XbaI restriction site downstream of the 3’enhancer sequence. All three *Cardamine* sequences were introduced into the pAMPAT expression vector. The Gateway cassette and the upstream two *35S* promoters were extracted from the vector using the SgsI and XbaI restriction sites. The amplified *MYB23* sequence was introduced into the cut pAMPAT vector via ligation utilizing the complementary restriction sites. For the *GL1* and *WER* sequences, the sticky ends of the cut pAMPAT vector were blunted using T4 DNA ligase, and the Cardamine sequences were subsequently introduced via ligation utilizing the blunt ends.

Promoter exchanges in pAMPAT-based vectors

All standard expression vectors used in this study possess one or two 35S promoters in front of the gateway cassette. These 35S promoters were cut out using SgsI and XhoI, and new promoter sequences were inserted utilizing these restriction sites.

pGWB3-3’enhancer Wang-GW:GUS

The 3‘enhancer region was amplified with flanking HindIII restriction sites using the primers H286 and H287, and pDONR201-pGL1 Wang:GL1 CDS-3‘enhancer Wang as the template. The PCR product was cut, and the expression vector pGWB3-GW:GUS was linearized with HindIII. Afterward, both were used in a ligation reaction cloning pGWB3-3’enhancer Wang-GW:GUS.

2.4.11. Generation of heat-shock competent bacteria

Generation of competent E. coli

A 5 ml pre-culture of LB medium without antibiotics was inoculated with 50 µl competent *E. coli* cells and incubated overnight at 37 °C shaking at 220 rpm. The next day, 200 ml LB medium without antibiotics was inoculated with 2 ml of the pre-culture and incubated at 37 °C shaking at 200 rpm. After 2h, the OD_{600} was measured and should not exceed 0.4. Subsequently, the main culture was divided into 4 Falcons, each containing 50 ml culture, and centrifuged for 7 min at 4 °C at 1600 g. The supernatant was discarded, and the pellet was resuspended in 10 ml ice-cold $CaCl_2$ solution (0). Following centrifugation at 4 °C and 1100 g for 5 min, the supernatant was discarded, and the pellet was again resuspended in 10 ml ice-cold $CaCl_2$ solution. The cells were incubated on ice for 30 min, and a centrifugation step (5 min, 4 °C, 1100 g) was performed. Each pellet was resuspended in 2 ml $CaCl_2$ solution and the solutions were unified. The cells were aliquoted at 6 °C, frozen in liquid nitrogen, and stored at -70 to -80 °C.

Generation of competent A. tumefaciens

A 5 ml pre-culture of YEB medium with appropriate antibiotics was inoculated with 50 µl competent *A. tumefaciens* cells and incubated overnight at 28 °C and 220 rpm. The next day, 200 ml YEB medium with appropriate antibiotics was inoculated with 2 ml pre-culture and incubated at 28 °C and 220 rpm. The OD_{600} was measured regularly until a value of 0.5 – 0.6 was reached. Subsequently, the culture was divided into 4 Falcons and centrifuged for 10 min at 4°C and 4000 rpm. Each pellet was resuspended in 5 ml ice-cold 0.15 M NaCl, and two pellets were pooled. After 15 min of incubation on ice, the cells were centrifuged for 10 min at 4 °C and 4000 rpm. The supernatant was discarded, and the cells were resuspended in a total volume of 15 ml ice-cold 20 mM $CaCl_2$. The cells were aliquoted at 6 °C, frozen in liquid nitrogen, and stored at -70 to -80 °C.

2.4.12. Transformation of heat-shock competent bacteria

Transformation of competent E. coli

50 µl competent cells were thawed on ice, and either 0.5 µl plasmid or the total BP/LR reaction volume was added. After the cells were incubated on ice for 20-30 min, a heat shock at 42 °C for 1.5 min was applied. Immediately, 300 µl LB media without antibiotics was added, and the solution was incubated at 37 °C and 600 rpm for 1 h. Subsequently, the cells were centrifuged at 8000 rpm for 5 min. The supernatant was discarded, and the cells were resuspended in the remaining liquid and plated on selective LB media. The plates were incubated overnight at 37 °C.

Transformation of competent A. tumefaciens

50 µl competent cells were thawed on ice, and 2-8 µl plasmid were added. After the cells were incubated on ice for 20-30 min, a heat shock at 42 °C for 1.5 min was applied. Immediately, 700 µl YEB media without antibiotics was added, and the solution was incubated at 28 °C and 650 rpm for 1.5 h. Subsequently, 100 µl were plated on selective YEB plates and incubated for 3-4 days at 28 °C.

2.4.13. Glycerol stocks

Overnight cultures of 5 ml selective LB or YEB media were inoculated with *E. coli* or *A. tumefaciens* single colonies, respectively. After incubation overnight shaking at 220 rpm at either 37 °C or 28 °C, 800 µl culture was mixed with 400 µl 60 % glycerol. The mixture was vortexed and immediately frozen in liquid nitrogen. The glycerol stocks were stored at -70 °C.

2.5. Plant Methods

2.5.1. Growth conditions

A. thaliana, C. hirsuta & N. benthamiana

The Arabidopsis and Cardamine plants were grown in the greenhouse on soil under long-day conditions.

A. thaliana cell suspension culture

The *A. thaliana Ler* cell suspension culture was grown in AT media and darkness at 21 °C, 60 % humidity, and 160 rpm. The suspension culture used in this study was maintained and cultivated by Irene Klinkhammer. Once a week, the cultures were freshly diluted 1:5 in AT media.

2.5.2. Seed sterilisation

Seed sterilisation with chlorine gas

Eppendorf tubes were filled with seeds and placed open in a desiccator. The seeds were spread out to maximize the exposed surface. 20 ml 12 % NaOCl solution was filled into a glass beaker and placed in the desiccator. Next, 2.5 ml of 37 % hydrochloric acid was added, and the desiccator was immediately closed. Seeds were incubated for 3-4 h.

Seed sterilisation with ethanol

Seeds were filled into Eppendorf tubes, and an appropriate amount of 70 % EtOH with 0.1 % SDS was added. The seeds were incubated shaking or rotating at 6 °C for 10-30 min. After incubation, the liquid was removed, and 100 % EtOH with 0.1 % SDS was added. Again, the seeds were incubated shaking or rotating for 10-30 min at 6 °C. Lastly, the seeds were distributed onto sterile Whatman paper, and after evaporation of EtOH, the seeds were collected in a clean Eppendorf tube for further use.

2.5.3. Generation of stably transformed *A. thaliana* by floral dipping

Agrobacteria containing the desired construct were used to inoculate a 5 ml overnight culture of selective YEB medium. After incubation at 28 °C and 220 rpm, the pre-culture was used to inoculate 200 ml of selective YEB medium. The main culture was incubated at 28 °C and 220 rpm at least overnight, until the culture was opaque. Subsequently, 10 g sucrose and 40 µl Silwet L-77 were added to each culture and incubated under the conditions above for 10 min. *A. thaliana* plants were dipped upside down into the bacterial solution for approximately 25 sec to ensure full coverage of the flowers. Plants were stored horizontally in a humid and dark place until the next day, when they were put into greenhouse conditions. Seeds obtained from dipped plants were tested for integration of the desired construct. Therefore, seeds were sown on soil and, after 7-8 days, either exposed to a 0.1 % Basta solution containing 0.001 % Tween-20 or a 1 mM Glyphosate solution. Approximately 7-10 days later, surviving plants were put in single pots and propagated.

2.5.4. Crossing of A. *thaliana*

Flowering Arabidopsis plants were emasculated by removing the anthers but leaving the petals intact. The stigma of the emasculated plants was pollinated with pollen from the crossing partner. Crossed plants were grown until seed production under greenhouse conditions.

2.5.5. *Agrobacterium*-mediated infiltration of *N. benthamiana* leaves

Agrobacteria containing the desired construct and the anti-silencing strain RK19 were used to inoculate 25 ml selective YEB medium and incubated 24-36 h at 28 °C and 220 rpm. The cultures were centrifuged for 15 min at 4000 rpm. Each culture was resuspended in 3-5 ml 1x Agromix (0), and the OD_{600} was adjusted to 0.7 – 0.8 with 1x Agromix. The desired combinations of Agrobacteria were mixed in a 1:1 ratio, including RK19 for each combination. After incubation at room temperature for 2-6 h, the abaxial side of *N. benthamiana* leaves was inoculated using a syringe. The infiltrated plants were further grown in the greenhouse, and fluorescence microscopy was performed 2-3 days after infiltration.

2.5.6. MG132 treatment of *N. benthamiana*

Proteasomal inhibitor treatment was performed using MG132 to infiltrate *N. benthamiana* leaves. The tobacco plants were infiltrated with agrobacteria containing the gene of interest two days prior. MG132 was stored in a 10 mM stock solution dissolved in DMSO at -70 °C. For treatment, the MG132 was diluted in 10 mM $MgCl_2$ solution to a concentration of 100 µM. The same leaf area formerly infiltrated with agrobacteria was infiltrated with the 100 µM MG132 solution. As a mock treatment, the same amount of DMSO as MG132 stock was added to 10 mm $MgCl_2$ solution and used for infiltration. After 8-24 h small samples were collected, frozen in liquid nitrogen and stores at -70 °C for potential later protein analysis. With the rest of the transformed *N. benthamiana* leaves fluorescence confocal microscopy was performed.

2.5.7. Particle bombardment

Transient transformation of leek epidermis or *A. thaliana* leaf epidermis was achieved by particle bombardment. For this, 1 ml 70 % EtOH was added to 30 mg of gold particles (1 µm), vortexed, and incubated on ice for 15 min. After centrifugation at 13000 rpm for 15 sec, the supernatant was discarded, and 1 ml ddH_2O was added. The gold particles were vortexed and centrifuged at 10000 rpm for 10 sec. The supernatant was removed and another wash step was carried out. Following resuspension in 1 ml ddH_2O, the gold particles were sonicated for 3 sec. Finally, the gold was aliquoted, frozen in liquid nitrogen, and stored at -20 °C. For each particle bombardment shot, 600 ng or 1 µl of each DNA was added for transformation of Arabidopsis, or 400 ng of each DNA was added for leek transformation. To the DNA, 5 µl gold (30 mg/ml), 10 µl 2.5 M $CaCl_2$, 4 µl 0.1 M Spermidine, and water to a final volume of 25 µl were added. The solution was mixed for 3-10 min at 1400 rpm and centrifuged at 13200 rpm for 17 sec. Afterwards, the supernatant was discarded, and 50 µl 70 % EtOH was added. The coated gold particles were resuspended, centrifuged at 13200 rpm for 17 sec, and the supernatant discarded. 20 µl 100 % EtOH was added, and the gold particles were resuspended and centrifuged at 13200 rpm for 17 sec. Finally, the supernatant was discarded, and the gold was resuspended in 12 µl 100 % EtOH. The DNA-coated gold particles were placed on the macro carrier (BioRad) and situated in the macro carrier holder. Arabidopsis leaves were placed on ½ MS plates without sugar with the abaxial site up, white pieces of leek were placed on wet Whatman paper in round petri dishes. Particle bombardment was performed using the Biolistic Particle Delivery System (Model PDS-1000/He, BioRad) and according to the manufacturer's instructions. For the transformation of Arabidopsis and leek leaves, 900 PSI and 650 PSI rupture discs were used, respectively. All plant material was stored in darkness at room temperature until the next day.

2.5.8. GUS staining of plant material

Plant material expressing *β-Glucuronidase* was submerged in GUS staining solution (0) and incubated at 37 °C in darkness for 1-24 h. Afterwards, the plant material was de-stained with 70 % EtOH at 50 °C. The samples were stored at room temperature in 70 % EtOH.

2.5.9. *Agrobacterium*-mediated transformation of dark-grown *A. thaliana* cell suspension culture

Transformation of Arabidopsis cell suspension culture was exclusively performed using LBA4404.pBBR1MCS virGN54D *A. tumefaciens*. These *A. tumefaciens* were transformed with pGWB2 or pGWB3 vectors and plated on selective YEB plates. Single colonies were cultivated in overnight cultures, and plasmid isolation followed by sequencing was performed to ensure the successful transformation. Positive clones were stored as glycerol stocks and plated freshly for each cell culture transformation. From YEB plates containing selective antibiotics, 3 ml cultures of YEB with antibiotics were inoculated and incubated at 28 °C overnight, shaking at 220 rpm. In addition to the agrobacteria expressing the genes of interest, the anti-silencing strain RK19 was also inoculated. The cultures were centrifuged at 4 °C for 15 min and 4000 rpm. After discarding the supernatant, each pellet was resuspended in 800 µl AT medium. The OD_{600} was measured and adjusted with AT medium to the lowest value of each experiment. 3 ml of freshly diluted dark-grown cell suspension culture was pipetted in each well of a 6-well plate. 20 µl of each agrobacterium solution was added into each well to include the desired combinations, including RK19. Each combination was transformed three times to generate biological triplicates. Per well, the same volume of agrobacteria was used. If the desired agrobacteria combination would amount to less volume, the missing volume was filled with an empty pGWB2 expressing agrobacterium. The 6-well plates were covered with a lid, sealed with micropore tape, and wrapped in aluminum foil before incubating for 4 days at 22 °C and 160 rpm. After incubation, 1 ml sample per well was collected and centrifuged at 4 °C for 15 min at 15000 rpm. The supernatant was discarded, and the sample was frozen in liquid nitrogen and stored at -70 °C until further analysis.

2.5.10. GUS staining of dark-grown *A. thaliana* cell suspension culture

After *agrobacterium*-mediated transformation, incubation for 4 days, and sample collection, qualitative GUS staining was performed. Therefore, 50 µl of GUS staining solution (0) was added per well and incubated at 37 °C in darkness. Each transformation of cell culture contained a positive control expressing *pGWB2-p35S:GUS*. GUS staining was examined after 2 h for the positive control to ensure the sufficient health of the cell culture and the successful transformation. The other transformations were incubated overnight at 37 °C before staining examination.

2.5.11. Quantitative GUS assay of dark-grown *A. thaliana* cell suspension culture

Samples of transformed cell suspension culture were used to extract a crude protein extract (2.3.6). This protein extract was used to measure GUS enzyme activity over time, thus comparing different promoter activities. To define the GUS activity, two standard curves were generated.

Protein standard curve using BSA

The correlation of enzyme activity to enzyme amount was achieved by measuring the protein amount using the absorbance at 562 nm and a standard curve to determine the total protein amount of each sample. The Pierce™ BCA Protein Assay Kit from Thermo Fisher Scientific was used to determine protein amounts and establish standard curves. A BSA stock of 2 mg/ml in water was stored at -20 °C and used for a dilution series shown in Table 15.

Table 15. Dilution series for BSA protein standard curve.

	[BSA] mg/ml	[BSA] µg/ml	Volume of previous solution	Volume diluent
1	2	2000	200 µl of stock (10 mg/ml)	800 µl
2	1.5	1500	750 µl of dilution 1	250 µl
3	1	1000	666.7 µl of dilution 2	333.3 µl
4	0.75	750	750 µl of dilution 3	250 µl
5	0.5	500	666.7 µl of dilution 4	333.3 µl
6	0.25	250	500 µl of dilution 5	500 µl
7	0.125	125	500 µl of dilution 6	500 µl
8	0.025	25	200 µl of dilution 7	800 µl
9	0	0	0.0 used as blank	10000 µl

Protein measurement was performed in a 96-well plate according to the manufacturer's manual. The values from the dilution series were used to generate a standard curve. One such standard curve used in this study is shown in Figure 6.

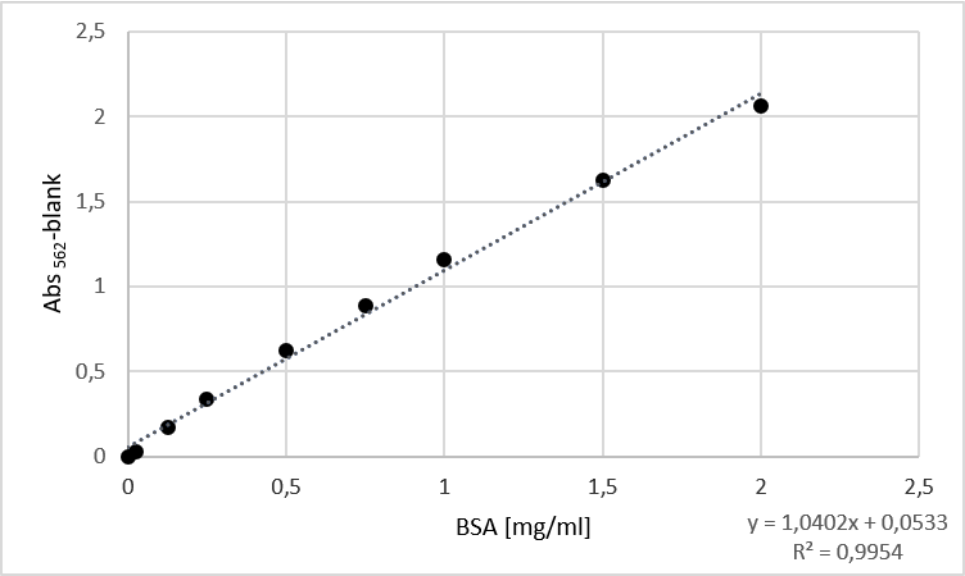

Figure 6. BSA standard curve . Absorption measurements at 562 nm of the BSA dilution series. The slope and coefficient of determination are displayed in the right bottom corner.

Substrate standard curve using 4-MU

The correlation of the amount of fluorescence product to fluorescence intensity was achieved by generating a standard curve using the fluorescent substrate 4-MU. The following dilution series was used in this study.

Table 16. Dilution series for 4-MU standard curve.

	4-MU [nM]	Volume of previous concentration	Volume of extraction buffer
1	10,000	10 µl of the stock 1mM	990 µl
2	5,000	500 µl of dilution 1	500 µl
3	1,000	200 µl of dilution 2	800 µl
4	500	500 µl of dilution 3	500 µl
5	250	500 µl of dilution 4	500 µl
6	50	200 µl of dilution 5	800 µl
7	25	500 µl of dilution 6	500 µl
8	5	200 µl of dilution 7	800 µl
9	2.5	500 µl of dilution 8	500 µl
10	0.5	200 µl of dilution 9	800 µl
11	0.0	0.0 µl (used as blank)	1000 µl

For measurement, 225 µl of each dilution was used. Fluorescence intensity was measured using a black 96-well plate. As mode, “Fluorescence Top Reading” was used. The temperature was set at 37 °C, and the measurements were delayed until a temperature in the range of 36.5 – 37.5 °C was reached. Measurements were conducted for 36 cycles with an interval time of 5 min, and at the start of each

cycle, the plate was shaken linearly for 10 sec with a linear amplitude of 1 mm. The excitation wavelength was set to 365 nm, and the emission wavelength detected was 455 nm. The excitation bandwidth was set to 9 nm and the emission bandwidth to 20 nm. A manual gain of 20 was used. Integration time was set to 20 µs, lag time was set to 0 µs, and the settle time to 0 ms. An exemplary 4-MU standard curve is shown in Figure 7.

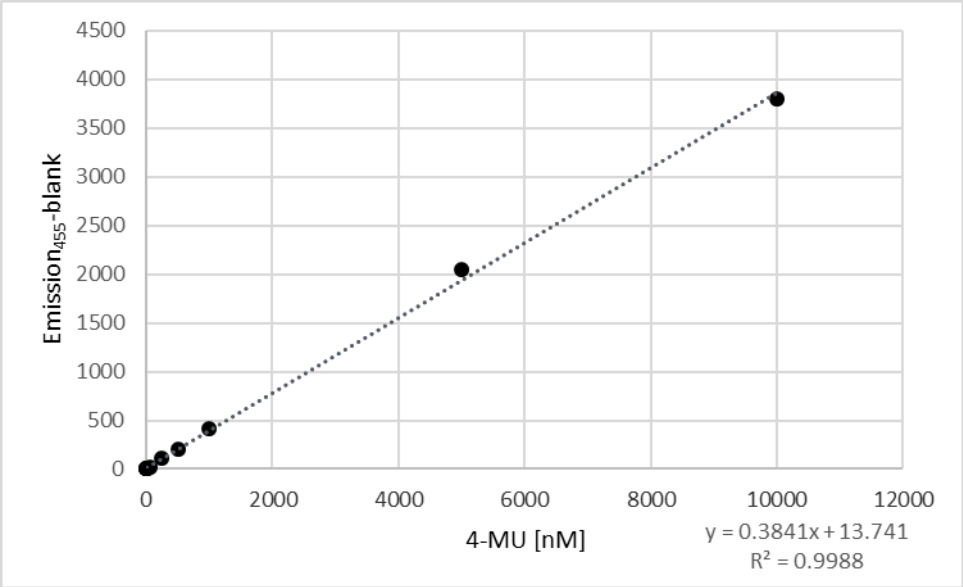

Figure 7. 4-MU standard curve. Emission measurements at 455 nm of the dilution series. The slope and coefficient of determination are displayed in the right bottom corner.

Tecan measurements

Quantitative GUS assays were performed using 25 µl of crude protein extract from cell suspension cultures and 200 µl assay buffer (0) per well in a black 96-well plate. Each sample was measured in three wells. As blank, 25 µl extraction buffer (2.3.6) in 200 µl assay buffer were used. The Tecan settings were identical to those used for the 4-MU standard curve. Additionally, the protein amount was determined for each sample by using the Pierce™ BCA Protein Assay Kit from Thermo Fisher Scientific in a 96-well plate according to the manufacturer's instructions. Each sample was measured in triplicates.

Calculation of promoter activity

First, the mean fluorescence intensity of each well for each time point was calculated, and the respective blank was subtracted. The amount of fluorescent substrate present at each time point was determined by subtracting the y-axis intercept of the 4-MU standard curve from the mean fluorescence and subsequently dividing this value by the slope of the 4-MU standard curve. The substrate amount per minute (nM/min) was determined by calculating the slope of substrate as a function of time. As a control, the coefficient of determination was calculated. The protein present in

25 µl sample was determined by utilizing the BSA standard curve, resulting in values of µg protein in 25 µl for each sample. The substrate amount per minute (nM/min) was divided by the protein concentration and multiplied by 1000 to determine the final nM/mg protein*min value. This value was calculated for each sample, and finally, the three biological replicates were summarized as mean values with corresponding standard deviations. The samples were normalized to the control (no added p35S constructs) and the reporter activity in percent was determined. Statistical analysis was performed by Student's t-tests ($p \leq 0.05$).

2.5.12. Leaf preparation for microscopy and growth assays

For microscopy of small leaves (leaf 3 or 4) in which trichome patterning still takes place, 6-8 days old seedlings grown on soil were prepared. The cotyledons, leaves 1 and 2, as well as all plant material covering the small leaf of interest, were cut off using a syringe needle. Only the hypocotyl with roots was left attached to the leaf of interest. The sample was transferred onto a microscope depression slide containing ½ MS with 1% sugar. The root was inserted into the MS media, and the hypocotyl was placed flat onto the media, exposing the leaf of interest. For microscopy, the sample was submerged in PFD (95%, ready to-use solution) and covered with a cover slip. After CLSM, the sample was stored in a square petri dish on wet paper. The dish was sealed and transferred to a long-day plant chamber. Leaf preparation and subsequent sample handling is based on (Harline & Roeder, 2023).

2.5.13. Phenotypic analysis of trichome rescue lines in T1 generation

Mutant *A. thaliana* plants were transformed using different rescue constructs. The T1 generation was Basta selected, and the rescue ability of the used constructs was determined. If possible, 50 T1 plants were analyzed for each rescue construct. To this end, leaf 4 of each plant was imaged in the same or very similar developmental state using the automated z-stack function of the Leica MZ16 F. Subsequently, the trichome number and leaf area were determined using ImageJ. Normal distribution was tested using the Kolmogorov-Smirnov test ($\alpha = 0.05$). If the data was normally distributed, a one-way ANOVA was performed. If the data was not normally distributed, Mann-Whitney U tests was performed.

2.5.14. Seed coat mucilage staining

A ruthenium red staining was performed to visualize seed coat mucilage production. Under gentle shaking, seeds were hydrated in water. After 5 min, the water was removed, and the ruthenium red solution (0.1 mg/ml) was added. The seeds were incubated for 5 min and subsequently washed twice with water (Zhao et al., 2017).

2.6. In-silico Methods

2.6.1. PLACE analysis

Analysis of regulatory sequences to find cis-acting regulatory DNA elements was performed using the New PLACE online tool (Higo et al., 1999).

2.6.2. Analysis of YFP/mCherry fluorescence ratios

P2A constructs expressing a gene of interest were transiently expressed together with CFP-tagged genes of interest using particle bombardment or tobacco infiltration. Fluorescence intensities were determined using CLSM images and the ImageJ software. Leek cells displaying fluorescence were surrounded using the polygon selection tool, and the fluorescence intensity was measured as the mean grey value in all used fluorescence channels. Minimal and maximal grey values were also determined, and cells containing more than five saturated pixels were excluded from the following analysis. The YFP/mCherry mean grey value ratios were calculated for each cell. All measured cells of the control (P2A construct + CFP-w/o) were used to determine the mean value. This mean was used to normalize the control and the other combinations. However, this normalization was only performed for combinations in the same microscope session/experiment. The Kolmogorov-Smirnov test ($\alpha = 0.05$) was used to determine normal distribution. If the data was normally distributed, a one-way ANOVA was performed. If the data was not normally distributed, Mann-Whitney U tests were performed.

2.6.3. Analysis of fluorescence intensity in trichomes & surrounding tiers in TTG1 stable lines

Col-0 plants were transformed with the following constructs to create stable lines: pAMPAT-pTTG1:TTG1-YFP, pAMPAT-pTTG1:TTG1ΔC26-YFP, pAMPAT-pTTG1:TTG1(S282F)-YFP, pAMPAT-pTTG1:TTG1(G43R)-YFP, and pAMPAT-pTTG1:TTG1(G149R)-YFP. These constructs refer to wild-type TTG1 and the TTG1 versions present in weak *ttg1* alleles. The resulting stable lines were imaged using the DM6000 CS Microscope and the TCS-SP8 imaging system equipped with the LAS X software (version 3.5.7). Small leaves were imaged using the 20x water immersion objective and the automated z-stack function with a step size of 1-1.5 µm. Only trichomes without any branches and their surrounding cell tiers were of interest. Fluorescence intensity measurements were performed using ImageJ. To this end, maximum projections were created displaying the trichome and surrounding cell tiers most accurately. Fluorescence intensity was measured as mean grey values by manually placing regions of interest (ROIs), three elliptical ROIs per trichome, and three polygonal ROIs for each cell tier (1st, 2nd, and 3rd tier). For each trichome and cell tier, the mean grey value was calculated. The fluorescence intensity in the trichome was set to 100 %, and the fluorescence intensity for each cell tier was normalized to that. This was determined for each TTG1 variant (TTG1 n=12, TTG1-9 n=19,

TTG1-11 n=28, TTG1-12 n=15) and the standard deviations were calculated. Normal distribution was determined using the Kolmogorov-Smirnov test ($\alpha = 0.05$), and subsequent one-sample t-tests ($p = 0.002$) were performed.

2.6.4. Cloning & Sequencing analysis

All *in-silico* cloning, alignments, phylogenetic trees, and sequence analysis, including analysis of sequencing results, were performed using the CLC DNA Workbench 5.6.1 and the CLC Main Workbench 22 software.

2.7. Microscopy

2.7.1. Light Microscopy

The LEICA MZ16 F was used to image whole leaves for trichome phenotype and GUS staining using the automated z-stack function. For documentation, the LEICA DFC420 C imaging system and the Leica Application Suite X (3.4.2 build 18368) were used. Images of GUS staining were also documented by using the Leica DMRB equipped with an Olympus EP50 camera. The camera was controlled via the EPview Software (version 1.4). Root phenotypes were examined using the Leica DM5000 B equipped with the DFC360 FX imaging system. For documentation, the Leica Application Suite Advanced Fluorescence (version 2.7.0.9329) was used.

2.7.2. Confocal laser scanning microscopy

For confocal laser scanning microscopy two different systems were used. Images used for protein stability measurements were generated using the Leica DMRE Fluorescence Microscope with the TCS-SPE imaging system equipped with the Leica LAS AF (version 2.6.0) software. Whole leaf images or images used for movement analysis were generated using DM6000 CS Microscope with the TCS-SP8 imaging system equipped with the LAS X software (version 3.5.7).

3. Results

3.1. Patterning proteins influence each other's stabilities

The trichome patterning process is tightly regulated on the transcriptional and protein level (Pesch & Hülskamp, 2009). Mathematic models of trichome patterning so far rely on estimated values for production, degradation, and stability rates for trichome patterning proteins (Balkunde et al., 2020). However, incorporating experimentally generated data into these models would be far more accurate. To examine if trichome patterning proteins display changed stability upon co-expression with other patterning proteins, the viral "self-cleavage" system of *2A* sequences as utilized in this study (Ryan et al., 1991). Using this system, two separate fusion proteins can be expressed from one plasmid or, rather, one mRNA (Ahier & Jarriault, 2014; Daniels et al., 2014). During translation, this mRNA is cleaved via ribosomal skipping at the end of the P2A sequence, and two separate proteins are translated in a 1:1 ratio (Donnelly et al., 2001a, b).

In former studies, 2A sequences from different viruses were used for gene expression in several organisms (Ahier & Jarriault, 2014; Kim et al., 2011). In publications only the 2A sequence from foot-and-mouth disease virus was expressed in plants (Samalova et al., 2006). But recently two different 2A sequences were tested regarding expression and cleavage efficiency in plants (Pietsch, 2022). The 2A sequences from porcine teschovirus-1 (P2A) displayed a higher cleavage efficiency in plants compared to the 2A sequence from foot-and-mouth disease virus (F2A) (Pietsch, 2022). The concept of determining differences in protein stability by utilizing P2A sequences flanked by fluorescence-tagged proteins was demonstrated (Pietsch, 2022). Therefore, in this study, the P2A sequence is used to determine differences in protein stability by measuring the amount of protein A compared to protein B in the presence or absence of other proteins. The protein amount is measured via fluorescence intensity, as proteins A and B are labelled differently.

3.1.1. The position of the P2A sequence may affect protein function and cleavage efficiency

The P2A plasmids used in this study usually exhibited the following composition: after a *35S* promoter, the gene of interest was N-terminally tagged with *YFP* and followed by the P2A sequence, and subsequently, *NLSNLS-mCherry* completed the construct. Initially, all trichome patterning genes were expressed using this orientation of the plasmid, which had been studied before (Pietsch, 2022). However, in the case of TTG1, this led to an aberrant cell localization (Figure 6) and, for EGL3, to the lack of mCherry signal in leek epidermal cells (Figure 46). The latter may be caused by insufficient cleavage during translation, as it is suspected that the N-terminal protein influences the P2A cleavage efficiency (Ryan et al., 1991, 2001).

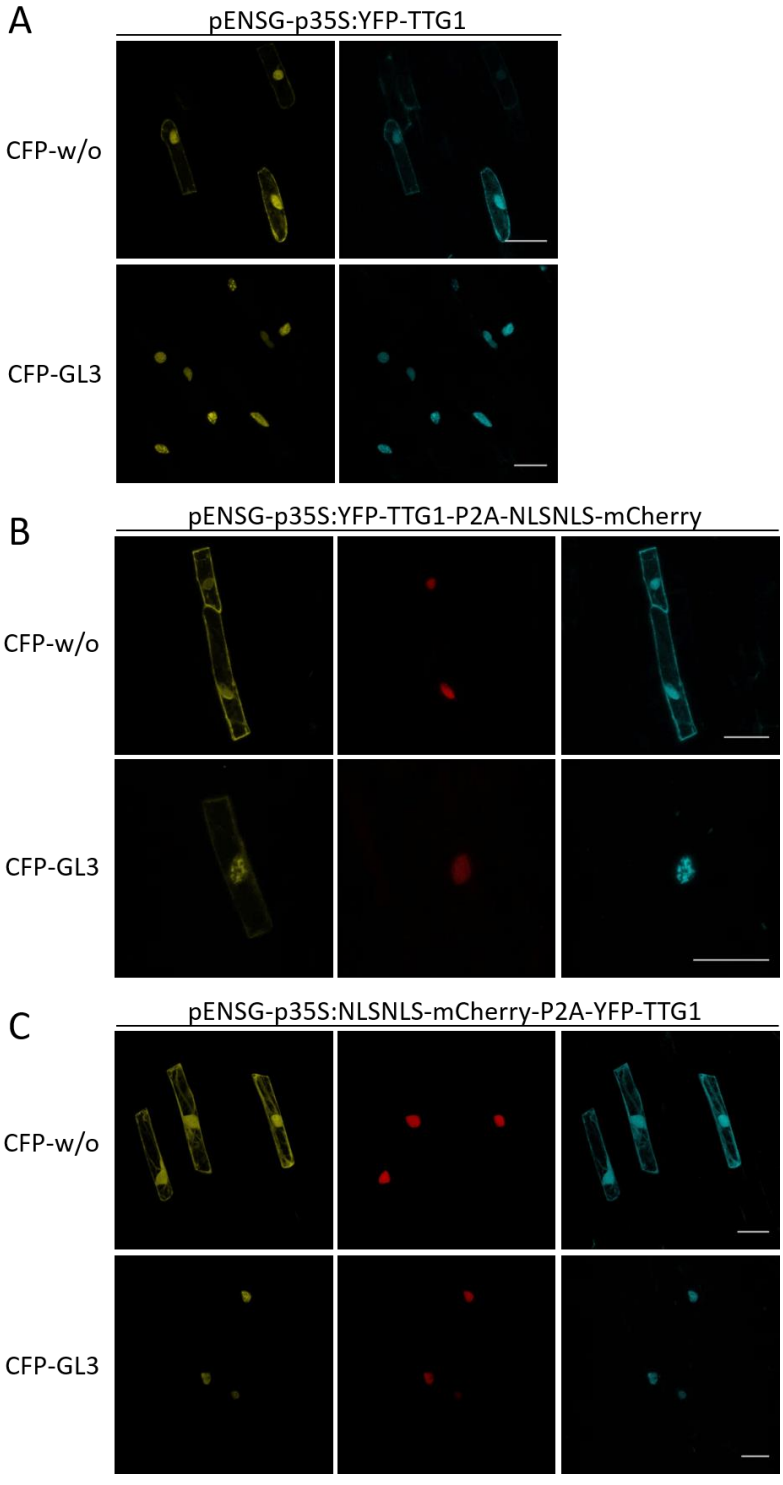

Figure 8. Subcellular localization of TTG1 in the presence or absence of GL3. A) CLSM images of leek epidermal cells transiently expressing *pENSG-p35S:YFP-TTG1* and *pENSG-p35S:CFP w/o* (top row) *or pENSG-p35S:CFP-GL3* (bottom row). YFP-TTG1 is displayed in the left column, and CFP or CFP-GL3 is displayed in the right column. B) CLSM images of leek epidermal cells transiently expressing *pENSG-p35S:YFP-TTG1-P2A-NLSNLS-mCherry* and *pENSG-p35S:CFP w/o* (top row) or *pENSG-p35S:CFP-GL3* (bottom row). YFP-TTG1 is displayed in the left column, NLSNLS-mCherry in the middle column, and CFP or CFP-GL3 in the right column. C) CLSM of leek epidermal cells transiently expressing *pENSG-p35S:NLSNLS-mCherry-P2A-YFP-TTG1* and *pENSG-p35S:CFP w/o* (top row) or *pENSG-p35S:CFP-GL3* (bottom row). YFP-TTG1 is displayed in the left column, NLSNLS-mCherry in the middle column, and CFP or CFP-GL3 in the right column. The scale bars indicate 100 µm.

The N-terminal attachment of a fluorophore did not usually cause any shift in cellular localization for TTG1, which is localized in the cytoplasm and nucleus in plant cells. Upon exposure to GL3, TTG1 is recruited into the nucleus by binding of GL3 to its C-term (Balkunde et al., 2011). Therefore, it was assumed that the C-terminal attachment of the majority of the P2A sequence might lead to an altered protein function or hindrance of protein interactions. To test this, a "swap" P2A construct was generated in which the NLSNLS-mCherry fusion is followed by the P2A sequence and the YFP-tagged gene of interest. This would only lead to adding a proline at the N-terminal end of YFP, whereas most of the P2A sequence would be attached to the C-terminal end of the mCherry protein. TTG1 expressed from this "swap" construct localized in the published fashion when expressed alone or together with GL3.

Since the P2A construct used to express *EGL3* N-terminally of the cleavage site resulted in no detectable mCherry fluorescence, EGL3 was also expressed using the "swap" construct. This resulted in a clear and strong nuclear mCherry signal (Figure 19). Interestingly, the cleavage problem was unique for EGL3, as the closely related bHLH protein GL3 did not seem to influence cleavage efficiency. Both proteins are highly similar in amino acid frequencies and share a 74 % identity (Figure 47).

3.1.2. Regulation of core activators and inhibitors in trichome patterning

Protein stabilities were determined by transient expression of the P2A system in leek epidermal cells. Fluorescence was detected using a CLSM, and intensity was measured using ImageJ. The reference was measured individually for each set and used to normalize the stabilities detected in the presence of other proteins. This means the protein of interest was tagged with YFP and, as an internal control to determine changes in YFP fluorescence intensity, NLSNLS-mCherry was used to determine a YFP/mCherry ratio. It can be assumed that NLSNLS-mCherry does not influence the ability of the CFP-tagged proteins to interact with the protein of interest or is interacting with the CFP-tagged proteins. Therefore, the YFP/mCherry ratio in the presence of free CFP (CFP w/o) can be used as a reference to determine changes in the YFP/mCherry fluorescence ratio upon the addition of CFP fused to another protein. Therefore, the YFP/mCherry ratio in the presence of CFP w/o is used for the normalization of the other combinations. This normalization was performed for each CLSM session individually, as the same microscope settings change if the device is switched off (personal communication J. Pietsch). Each set of combinations was transiently expressed at least two independent times.

GL1 is stabilized by activators and inhibitors in leek epidermal cells

One of the core components of trichome patterning is the R2R3MYB transcription factor GL1 (Oppenheimer et al., 1991). Stability changes of GL1 were observed in leek epidermal cells by transient expression of GL1 and other trichome patterning proteins, using the P2A system.

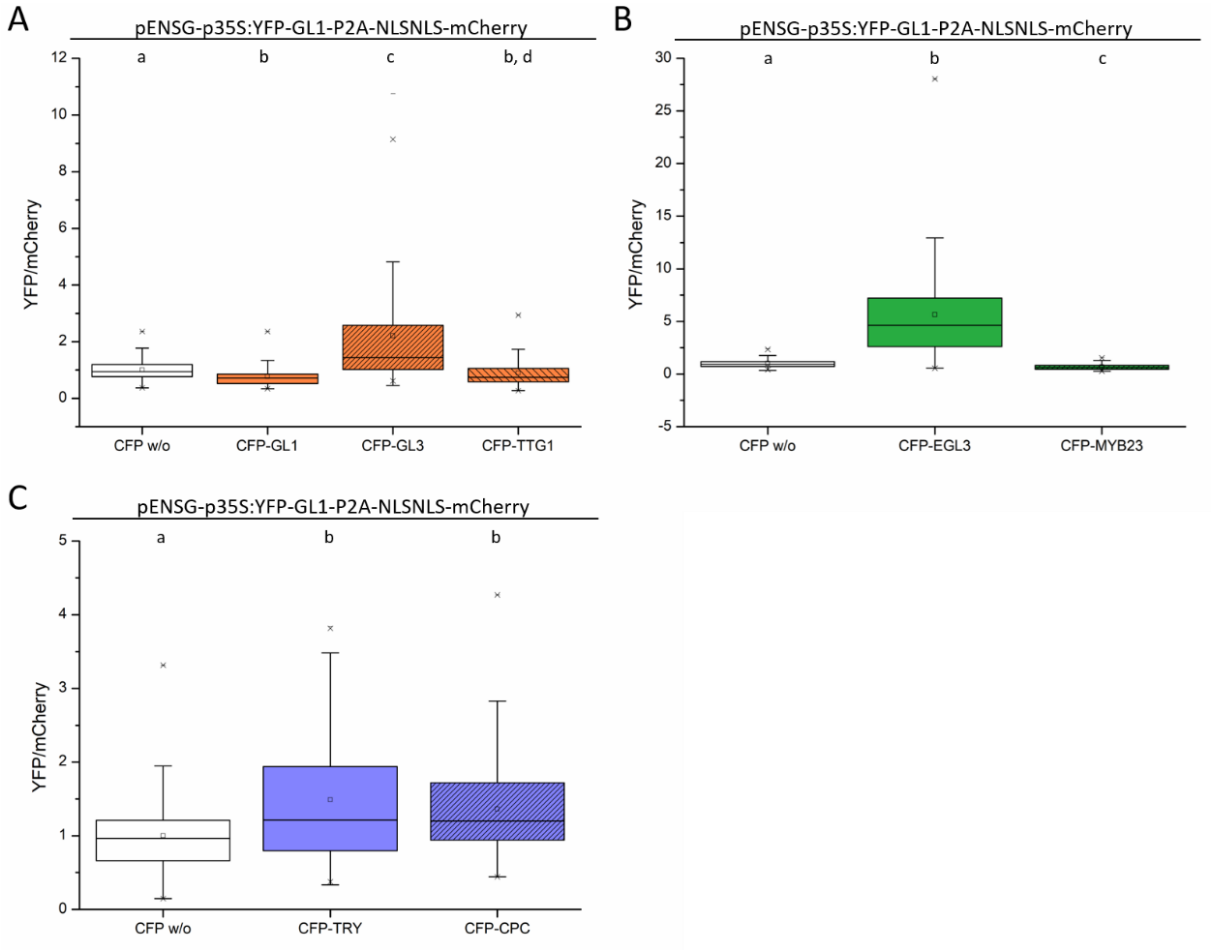

Figure 9. Stability of GL1 in leek epidermal cells. A) Box plot graph displaying the normalized YFP/mCherry fluorescence ratios of *pENSG-p35S:YFP-GL1-P2A-NLSNLS-mCherry* co-expressed with pENSG-p35S:CFP constructs expressing CFP w/o (n=61, median=0.76), CFP-GL1 (n=68, median=0.73), CFP-GL3 (n=103, median=1.43) and CFP-TTG1 (n=92, median=0.74). B) Box plot graph displaying the normalised YFP/mCherry fluorescence ratios of *pENSG-p35S:YFP-GL1-P2A-NLSNLS-mCherry* co-expressed with pENSG-p35S constructs expressing CFP w/o (n=104, median=0.92), CFP-EGL3 (n=97, median=4.64) and CFP-MYB23 (n=54, median=0.65). C) Box plot graph displaying the normalized YFP/mCherry fluorescence ratios of *pENSG-p35S:YFP-GL1-P2A-NLSNLS-mCherry* co-expressed with pENSG-p35S constructs expressing CFP w/o (n=63, median=0.96), CFP-TRY (n=120, median=1.21) and CFP-CPC (n=83, median=1.2). Statistical analysis was performed by Mann-Whitney U tests, and statistical differences are indicated by compact letter display ($p \leq 0.05$). In all box plots, the mean is displayed as a small square. Maximum and minimum values are indicated as horizontal lines at the end of the whiskers, and the 1% and 99% percentiles are displayed by crosses. Outliers are displayed as small horizontal lines.

In the first sets of experiments, *pENSG-p35S:YFP-GL1-P2A-NLSNLS-mCherry* (referred to as GL1-P2A in the following paragraphs) was expressed in the presence of other activators and the YFP/mCherry fluorescence ratios were determined and normalized to the control (CFP w/o). An increased ratio indicated a higher amount of YFP-tagged protein compared to NLSNLS-mCherry, indicating an increase in stability. A decreased ratio indicates a decrease in stability for the YFP-tagged protein. In Figure 9 A, the YFP/mCherry ratio of samples containing GL1-P2A and CFP-GL1 display a significant decrease in stability compared to the control. The mean fluorescence ratio in the presence of CFP-GL1 was 0.77 ($p=3.02*10^{-6}$). In the presence of CFP-GL3, GL1-P2A was stabilized significantly from 1 to a mean fluorescence ratio of 2.21 ($p=2.4*10^{-9}$). TTG1 led to a slight but statistically significant decrease in stability to 0.9 (p=0.004). Additionally, GL1-P2A was co-expressed with CFP-EGL3 and CFP-MYB23

(Figure 9 B). The presence of CFP-EGL3 very drastically increased the GL1 stability to 5.64 ($p=2.78*10^{-34}$). On the contrary, CFP-MYB23 led to a significant decrease stability to 0.68 ($p\leq7.17*10^{-8}$). GL1-P2A was also co-expressed with the inhibitors TRY and CPC (Figure 9 C). CFP-TRY led to a slight but statistically significant increase in stability of GL1-P2A of 1.49 ($p=3.99*10^{-4}$), and CFP-CPC led to a similar increase to 1.36 ($p=9.32*10^{-5}$).

Patterning activators differentially affect GL3 stability

Another key component of the trichome patterning machinery is the bHLH transcription factor GL3 (Payne et al., 2000). It is considered one of the essential proteins needed for the functionally active MBW complex, while its homolog EGL3 seems to play a minor role in trichome patterning (Bernhardt et al., 2005; Zhang et al., 2003). Therefore, in this study, GL3 stability was examined in leek epidermal cells.

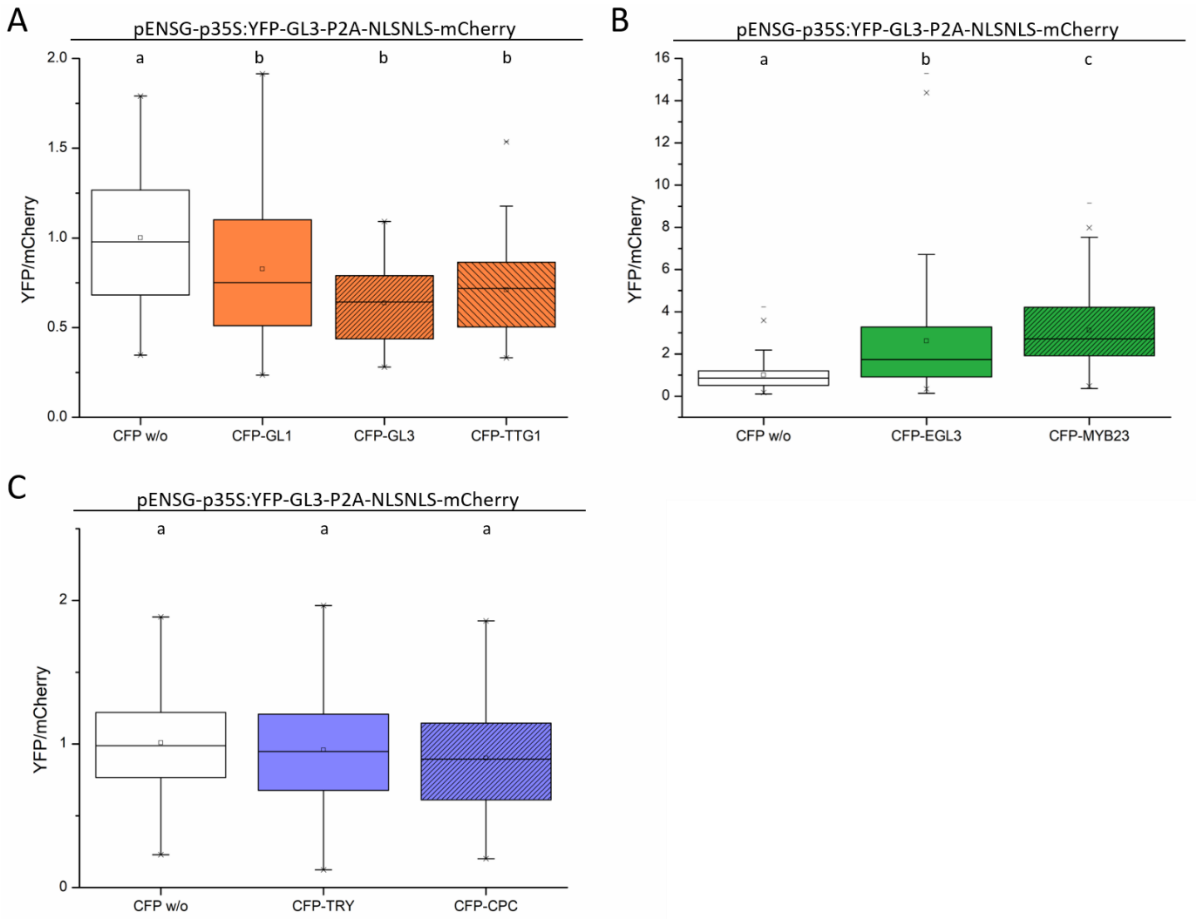

Figure 10. Stability of GL3 in leek epidermal cells. A) Box plot graph displaying the normalised YFP/mCherry fluorescence ratios of *pENSG-p35S:YFP-GL3-P2A-NLSNLS-mCherry* co-expressed with pENSG-p35S:CFP constructs expressing CFP w/o (n=56, median=0.98), CFP-GL1 (n=49, median=0.75), CFP-GL3 (n=44, median=0.64) and CFP-TTG1 (n=46, median=0.72). B) Box plot graph displaying the normalised YFP/mCherry fluorescence ratios of *pENSG-p35S:YFP-GL3-P2A-NLSNLS-mCherry* co-expressed with pENSG-p35S constructs expressing CFP w/o (n=220, median=0.85), CFP-EGL3 (n=191, median=1.74) and CFP-MYB23 (n=122, median=2.71). C) Box plot graph displaying the normalized YFP/mCherry fluorescence ratios of *pENSG-p35S:YFP-GL3-P2A-NLSNLS-mCherry* co-expressed with pENSG-p35S constructs expressing CFP w/o (n=78, median=0.99), CFP-TRY (n=66, median=0.95) and CFP-CPC (n=48, median=0.89). Statistical analysis was performed by Mann-Whitney U tests for A) and B) and by a OneWay ANOVA for C). Statistical differences are indicated by compact letter display ($p \leq 0.05$). In all

box plots, the mean is displayed as a small square. Maximum and minimum values are indicated as horizontal lines at the end of the whiskers, and the 1% and 99% percentiles are displayed by crosses. Outliers are displayed as small horizontal lines.

In experiments expressing *pENSG-p35S:YFP-GL3-P2A-NLSNLS-mCherry* (GL3-P2A) and the activators GL1, GL3, and TTG1 (Figure 10 A) tagged with CFP, different effects on protein stabilities were observed compared to GL1. GL3-P2A was significantly de-stabilized in the presence of all three activators. In the case of CFP-GL1, the mean stability decreased to 0.83 (p=0.021), in the presence of CFP-GL3 it even decreased to 0.64 ($p=6.06*10^{-7}$), and CFP-TTG1 led to a decrease to 0.71 ($p=3.1*10^{-5}$). Additionally, the activators EGL3 and MYB23 were tested regarding their effect on GL3-P2A stability (Figure 10 B). Interestingly, both activators stabilized GL3. CFP-EGL3 addition led to a significant increase in GL3 stability to 2.62 ($p=1.83*10^{-22}$), whereas CFP-MYB23 significantly increased the stability of GL3-P2A to a ratio of 3.12 ($p=1.57*10^{-45}$). The co-expression of CFP-TRY (mean=0.96, p=0.39) and CFP-CPC (mean=0.9, p=0.11) led to no statistically significant changes in the stability of GL3-P2A (Figure 10 C).

TTG1 is destabilized by itself and GL1, but stabilized by other patterning proteins

Another trichome patterning protein that was examined regarding differences in stability in leek epidermal cells was TTG1. This protein is the centre of the MBW network that controls five different traits in *Arabidopsis* (Zhang & Schrader, 2017), thus differential regulation of TTG1 stability may have wide ranging effects.

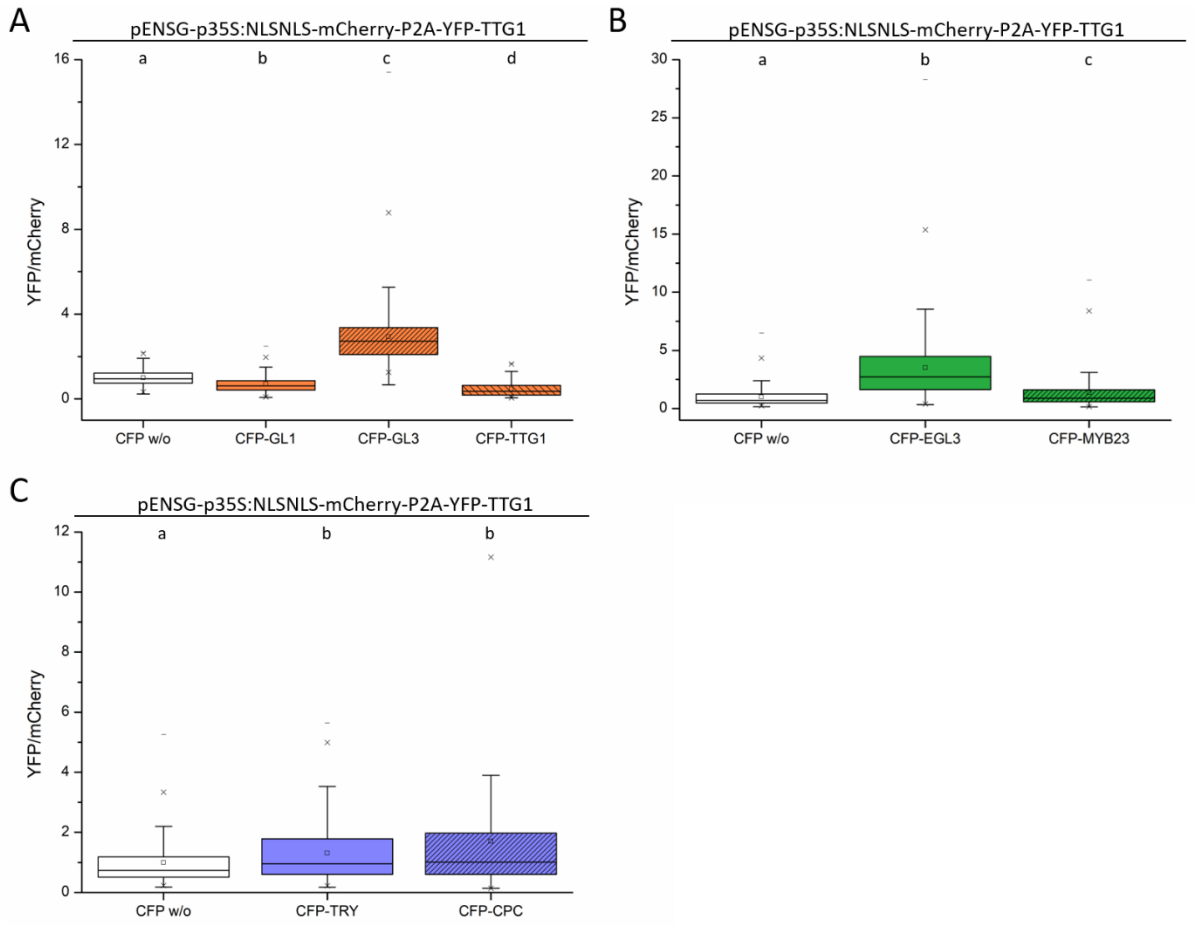

Figure 11. Stability of TTG1 in leek epidermal cells. A) Box plot graph displaying the normalized YFP/mCherry fluorescence ratios of *pENSG-p35S:NLSNLS-mCherry-P2A-YFP-TTG1* co-expressed with pENSG-p35S:CFP constructs expressing CFP w/o (n=178, median=0.95), CFP-GL1 (n=147, median=0.63), CFP-GL3 (n=262, median=2.73) and CFP-TTG1 (n=138, median=0.36). B) Box plot graph displaying the normalized YFP/mCherry fluorescence ratios of *pENSG-p35S:NLSNLS-mCherry-P2A-YFP-TTG1* co-expressed with pENSG-p35S constructs expressing CFP w/o (n=277, median=0.7), CFP-EGL3 (n=240, median=2.72) and CFP-MYB23 (n=260, median=0.88). C) Box plot graph displaying the normalized YFP/mCherry fluorescence ratios of *pENSG-p35S:NLSNLS-mCherry-P2A-YFP-TTG1* co-expressed with pENSG-p35S constructs expressing CFP w/o (n=156, median=0.73), CFP-TRY (n=202, median=0.96) and CFP-CPC (n=177, median=1.00). Statistical analysis was performed by Mann-Whitney U tests and statistical differences are indicated by different letters at the top of each graph ($p \leq 0.05$). In all box plots, the mean is displayed as a small square. Maximum and minimum values are indicated as horizontal lines at the end of the whiskers, and the 1% and 99% percentiles are displayed by crosses. Outliers are displayed as small horizontal lines.

In the first set of experiments, *pENSG-p35S:NLSNLS-mCherry-P2A-YFP-TTG1* (P2A-TTG1) was transiently expressed together with the activators GL1 and GL3, as well as TTG1 (Figure 11 A). The presence of CFP-GL1 led to a significant decrease in the mean TTG1 stability from 1 to 0.71 ($p=6.23*10^{-14}$). Expressing CFP-TTG1 additionally to P2A-TTG1 led to an even more drastic decrease in stability to 0.47 ($p=2.13*10^{-30}$). In contrast, CFP-GL3 addition led to a significant increase in TTG1 stability to a mean ratio of 2.93 ($p=2.74*10^{-101}$). Additionally, the activators EGL3 and MYB23 were co-expressed with TTG1-P2A and the stability was examined (Figure 11 B). In the presence of CFP-EGL3, TTG1-P2A was significantly stabilized to a mean YFP/mCherry ratio of 3.5 ($p=3.51*10^{-60}$). CFP-MYB23 also led to a significant increase in stability to 1.35 ($p=3.07*10^{-4}$). Interestingly, TTG1 is stabilized in the

presence of both tested inhibitors. CFP-TRY led to an increase in stability to 1.31 (p=0.002) and CFP-CPC even to a more drastic increase to 1.7 ($p=4.9*10^{-4}$, Figure 11 C).

EGL3 is stabilized profoundly by CPC

EGL3 was also tested for differential stability upon co-expression with other trichome patterning proteins, as it is also a core component of the trichome patterning network (Zhang & Schrader, 2017).

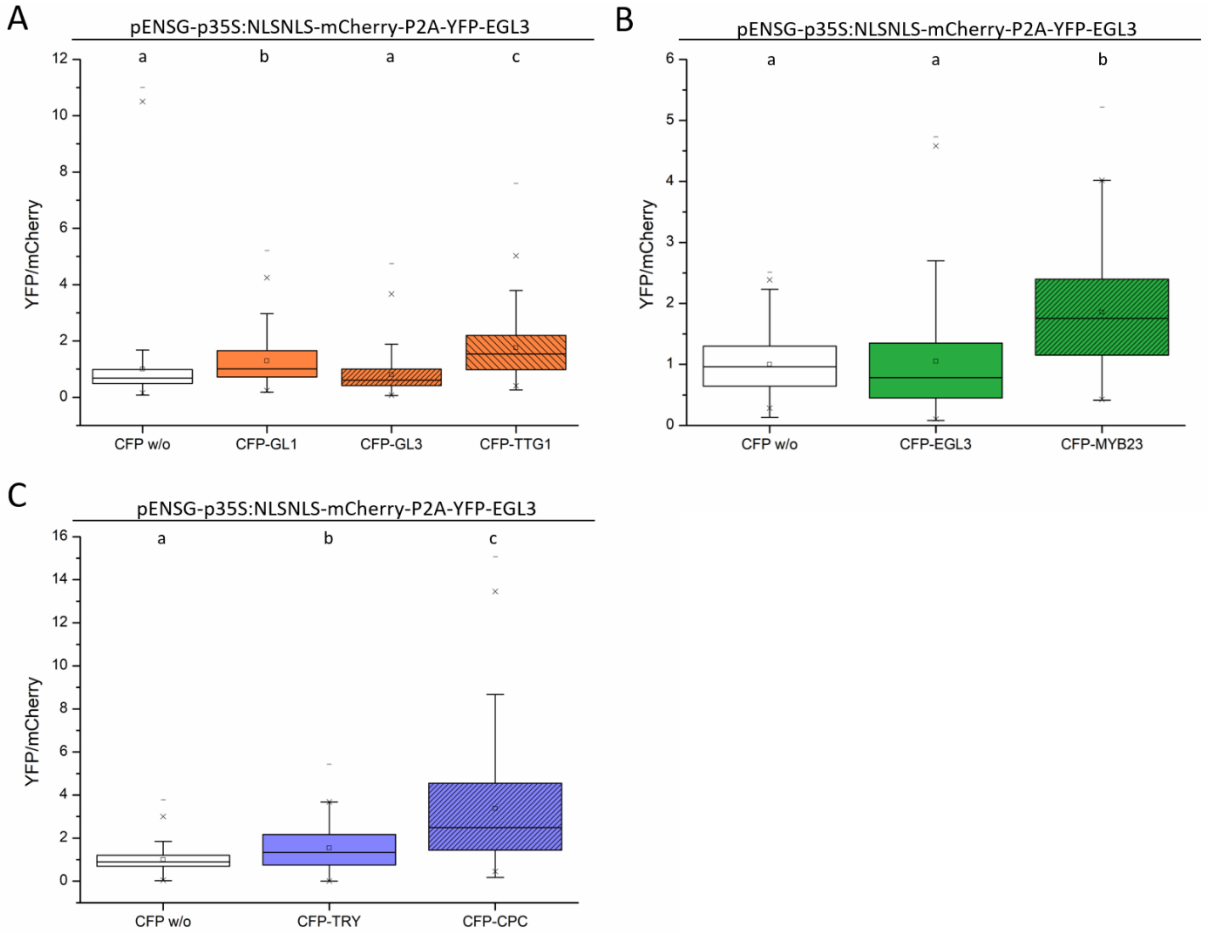

Figure 12. Stability of EGL3 in leek epidermal cells. A) Box plot graph displaying the normalized YFP/mCherry fluorescence ratios of *pENSG-p35S:NLSNLS-mCherry-P2A-YFP-EGL3* co-expressed with pENSG-p35S constructs expressing CFP w/o (n=183, median=0.68), CFP-GL1 (n=180, median=1.01), CFP-GL3 (n=185, median=0.61) and CFP-TTG1 (n=174, median=1.54). B) Box plot graph displaying the normalized YFP/mCherry fluorescence ratios of *pENSG-p35S:NLSNLS-mCherry-P2A-YFP-EGL3* co-expressed with pENSG-p35S constructs expressing CFP w/o (white box, n=105, median=0.96), CFP-EGL3 (n=188, median=0.78) and CFP-MYB23 (n=112, median=1.75). C) Box plot graph displaying the normalized YFP/mCherry fluorescence ratios of *pENSG-p35S:NLSNLS-mCherry-P2A-YFP-EGL3* co-expressed with pENSG-p35S constructs expressing CFP w/o (n=172, median=0.89), CFP-TRY (n=109, median=1.34) and CFP-CPC (n=147, median=2.47). Statistical analysis was performed by Mann-Whitney U tests, and statistical differences are indicated by different letters at the top of each graph ($p \leq 0.05$). In all box plots, the mean is displayed as a small square. Maximum and minimum values are indicated as horizontal lines at the end of the whiskers, and the 1% and 99% percentiles are displayed by crosses. Outliers are displayed as small horizontal lines.

The co-expression of *pENSG-p35S:NLSNLS-mCherry-P2A-YFP-EGL3* (P2A-EGL3) with the bHLH TFs GL3 and EGL3 surprisingly did not lead to a statistically significant change in protein stability. However, the co-expression of CFP-GL1 significantly increased the EGL3 stability to a mean ratio of 1.29 ($p=6.8*10^{-10}$). Remarkably, TTG1 led to an even higher stability of EGL3 to 1.75 ($p=1.2*10^{-26}$, Figure 12 A). The last

activator tested that changed EGL3 stability was CFP-MYB23 (Figure 12 B), increasing the stability to 1.86 ($p=3.2*10^{-16}$). In a final set of experiments, the two inhibitors TRY and CPC were examined regarding their effect on P2A-EGL3 stability (Figure 12 C). Interestingly, both seem to stabilize EGL3 but to a different extent. In the case of CFP-TRY, the mean stability significantly increased to 1.54 ($p=1.3*10^{-6}$) and in the case of CFP-CPC, the increase was even more drastic to 3.37 (p=0).

MYB23 is stabilized by the other MYBs, especially GL3

The last core activator that was tested for stability changes, was MB23. Although MYB23 does not affect trichome patterning as drastic as GL1, it is still considered a core patterning protein and is tightly embedded in the patterning network by protein-protein interactions and gene expression regulation (Kirik et al., 2001, 2005; Li et al., 2009b). Therefore, changes in MYB23 protein stability might influence patterning mechanisms.

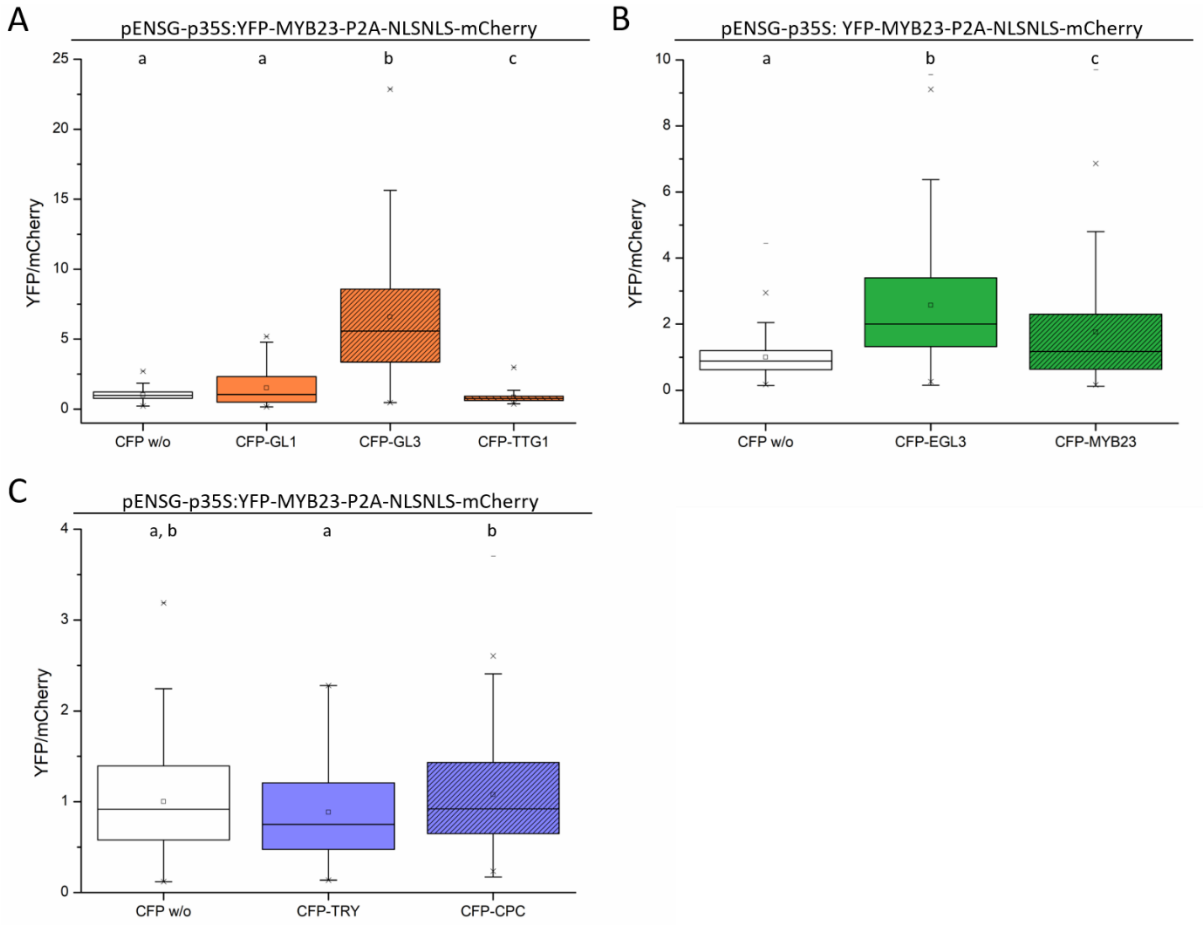

Figure 13. Stability of MYB23 in leek epidermal cells. A) Box plot graph displaying the normalized YFP/mCherry fluorescence ratios of *pENSG-p35S:YFP-MYB23-P2A-NLSNLS-mCherry* co-expressed with pENSG-p35S constructs expressing CFP w/o (n=97, median=0.98), CFP-GL1 (n=47, median=1.05), CFP-GL3 (n=94, median=5.58) and CFP-TTG1 (n=80, median=0.76). B) Box plot graph displaying the normalized YFP/mCherry fluorescence ratios of *pENSG-p35S:YFP-MYB23-P2A-NLSNLS-mCherry* co-expressed with pENSG-p35S constructs expressing CFP w/o (n=313, median=0.88), CFP-EGL3 (n=199, median=2) and CFP-MYB23 (n=240, median=1.17). C) Box plot graph displaying the normalized YFP/mCherry fluorescence ratios of *pENSG-p35S:YFP-MYB23-P2A-NLSNLS-mCherry* co-expressed with pENSG-p35S constructs expressing CFP w/o (n=95, median=0.92), CFP-TRY (n=61, median=0.75) and CFP-CPC (n=133, median=9.92). Statistical analysis was performed by Mann-Whitney U

tests, and statistical differences are indicated by different letters at the top of each graph ($p \leq 0.05$). In all box plots, the mean is displayed as a small square. Maximum and minimum values are indicated as horizontal lines at the end of the whiskers, and the 1% and 99% percentiles are displayed by crosses. Outliers are displayed as small horizontal lines.

Co-expression of *pENSG-p35S:YFP-MYB23-P2A-NLSNLS-mCherry* (MYB23-P2A) with the other R2R3MYB TF, GL1, did not lead to significant changes in MYB23 stability (Figure 13 A). However, CFP-GL3 and CFP-TTG1 led to opposite effects on MYB23 stability. CFP-TTG1 decreased the stability slightly, but still significantly, to 0.87 ($p=4.0*10^{-4}$). CFP-GL3 on the other side, drastically increased the stability to 6.58 ($p=2.1*10^{-41}$). In contrast to GL1, MYB23 influenced the stability of the MYB23-P2A protein positively by increasing the mean fluorescence ratio to 2.57 ($p=4.8*10^{-39}$). CFP-EGL3 also significantly increased the stability of MYB23 to 1.76 ($p=2*10^{-7}$, Figure 13 B). The addition of neither CFP-TRY nor CFP-CPC led to a significant change of MYB23 stability (Figure 13 C).

TRY is drastically stabilized by the bHLHs GL3 and EGL3

The first inhibitor examined regarding protein stability changes was TRY. TRY is known to act redundantly with the other R3MYB inhibitors but also regulates short-range trichome initiation, which sets it apart from e.g. CPC (Schellmann et al., 2002).

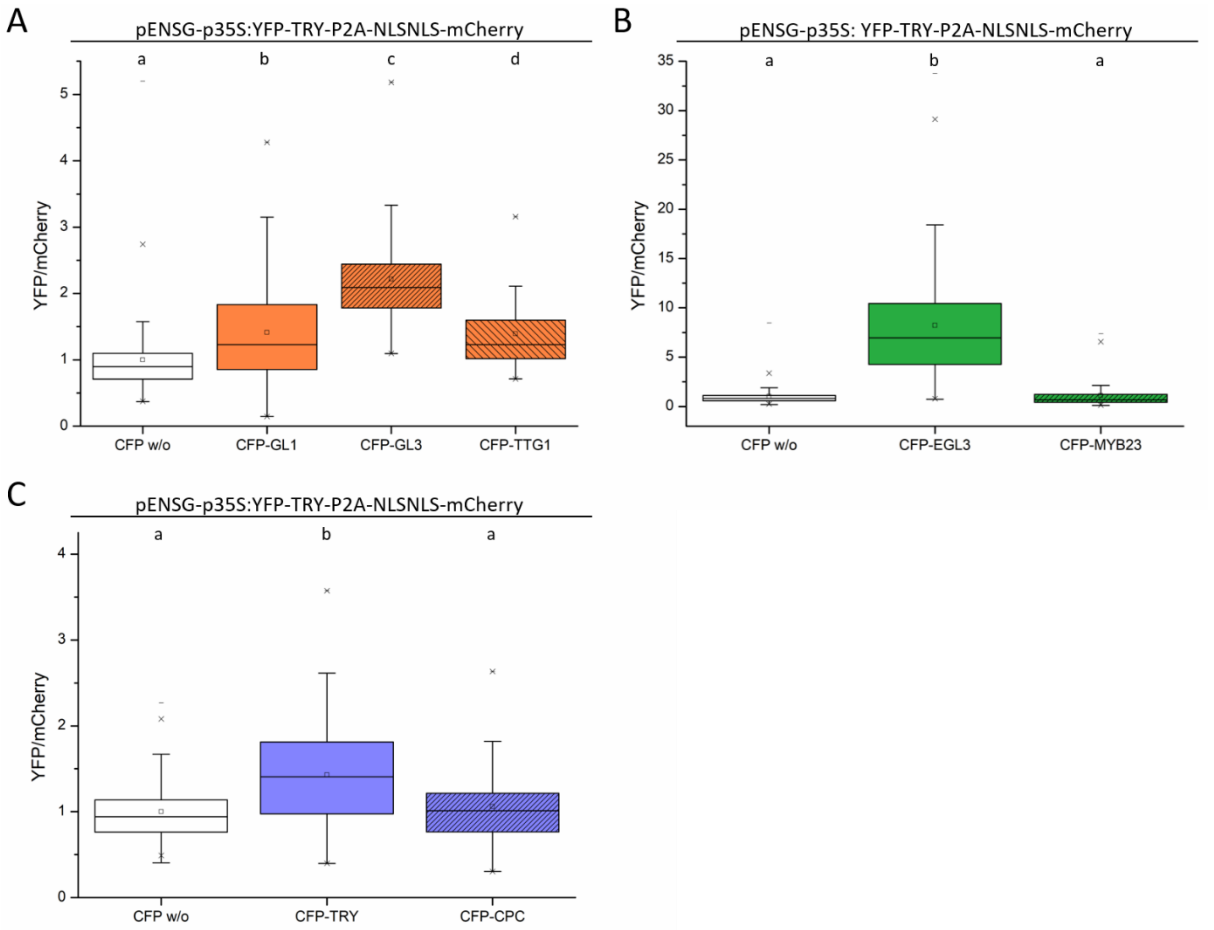

Figure 14. Stability of TRY in leek epidermal cells. A) Box plot graph displaying the normalized YFP/mCherry fluorescence ratios of *pENSG-p35S:YFP-TRY-P2A-NLSNLS-mCherry* co-expressed with pENSG-p35S constructs expressing CFP w/o (n=130,

median=0.89), CFP-GL1 (n=98, median=1.23), CFP-GL3 (n=86, median=2.09) and CFP-TTG1 (n=75, median=1.23). B) Box plot graph displaying the normalized YFP/mCherry fluorescence ratios of *pENSG-p35S:YFP-TRY-P2A-NLSNLS-mCherry* co-expressed with pENSG-p35S constructs expressing CFP w/o (n=210, median=0.80), CFP-EGL3 (n=168, median=6.95) and CFP-MYB23 (n=130, median=0.67). C) Box plot graph displaying the normalized YFP/mCherry fluorescence ratios of *pENSG-p35S:YFP-TRY-P2A-NLSNLS-mCherry* co-expressed with pENSG-p35S constructs expressing CFP w/o (n=106, median=0.94), CFP-TRY (n=95, median=1.41) and CFP-CPC (n=87, median=1.01). Statistical analysis was performed by Mann-Whitney U tests, and statistical differences are indicated by different letters at the top of each graph ($p \leq 0.05$). In all box plots, the mean is displayed as a small square. Maximum and minimum values are indicated as horizontal lines at the end of the whiskers, and the 1% and 99% percentiles are displayed by crosses. Outliers are displayed as small horizontal lines.

The co-expression of *pENSG-p35S:YFP-TRY-P2A-NLSNLS-mCherry* (TRY-P2A) with all tested activators except MYB23, led to a significant change in protein stability of TRY-P2A. All activators increased the stability of TRY (Figure 14 A and B). TRY-P2A was slightly but significantly stabilized to 1.4 in the presence of GL1 ($p=5.0*10^{-6}$) and TTG1 ($p=2.6*10^{-11}$). The presence of CFP-GL3 led to a higher protein stability increase of 2.2 ($p=6.4*10^{-41}$). Co-expression of CFP-EGL3 increased the mean YFP/mCherry fluorescence ratio very drastically to 8.22 ($p=5.7*10^{-79}$). Interestingly, only CFP-TRY influenced its own stability, but CFP-CPC did not change the fluorescence ratio significantly. When CFP-TRY was co-expressed with TRY-P2A, TRY stability increased to 1.43 ($p=2.4*10^{-9}$, Figure 14 C).

CPC is stabilized by EGL3 and MYB23

The last trichome patterning protein examined regarding stability changes was the inhibitor CPC, which is suspected to play a role in the long-range trichome inhibition (Schellmann et al., 2002).

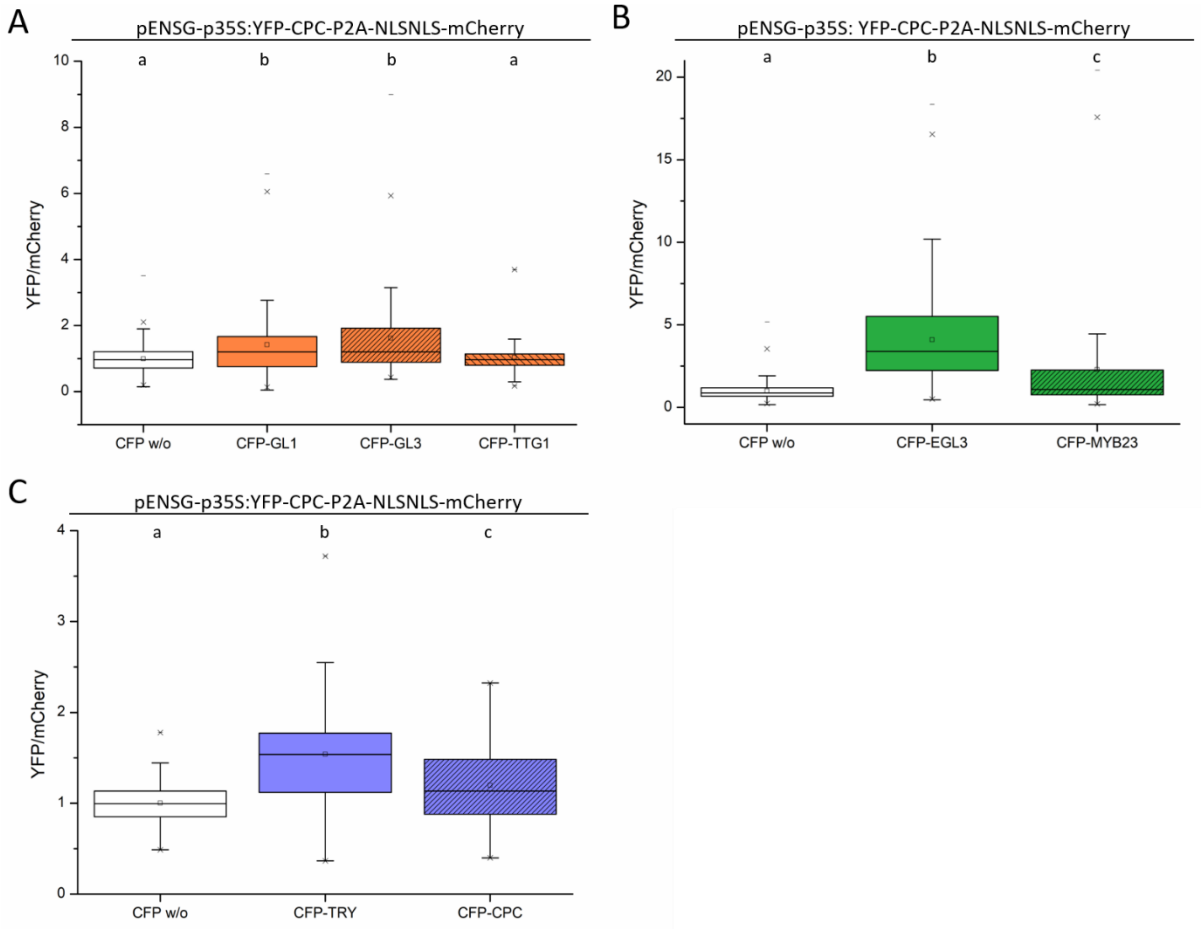

Figure 15. Stability of CPC in leek epidermal cells. A) Box plot graph displaying the normalized YFP/mCherry fluorescence ratios of *pENSG-p35S:YFP-CPC-P2A-NLSNLS-mCherry* co-expressed with pENSG-p35S constructs expressing CFP w/o (n=145, median=0.97), CFP-GL1 (n=101, median=1.2), CFP-GL3 (n=120, median=1.2) and CFP-TTG1 (n=99, median=0.96). B) Box plot graph displaying the normalized YFP/mCherry fluorescence ratios of *pENSG-p35S:YFP-CPC-P2A-NLSNLS-mCherry* co-expressed with pENSG-p35S constructs expressing CFP w/o (n=242, median=0.88), CFP-EGL3 (n=198, median=3.39) and CFP-MYB23 (n=113, median=1.08). C) Box plot graph displaying the normalized YFP/mCherry fluorescence ratios of *pENSG-p35S:YFP-CPC-P2A-NLSNLS-mCherry* co-expressed with pENSG-p35S constructs expressing CFP w/o (n=63, median=1), CFP-TRY (n=120, median=1.54) and CFP-CPC (n=83, median=1.13). Statistical analysis was performed by Mann-Whitney U tests, and statistical differences are indicated by different letters at the top of each graph ($p \leq 0.05$). In all box plots, the mean is displayed as a small square. Maximum and minimum values are indicated as horizontal lines at the end of the whiskers, and the 1% and 99% percentiles are displayed by crosses. Outliers are displayed as small horizontal lines

Co-expression of *pENSG-p35S:YFP-CPC-P2A-NLSNLS-mCherry* (CPC-P2A) with any tested activators, except TTG1, led to a statistically significant increase in mean YFP/mCherry fluorescence ratio (Figure 15 A and B). The extent of this increase, however, differed. The presence of CFP-GL1 led to an increase in the mean fluorescence ratio to 1.41 ($p=0.00125$), and CFP-GL3 increased the stability to 1.62 ($p=2.4*10^{-6}$). Interestingly, CFP-EGL3 and CFP-MYB23 increase TRY stability even more. EGL3 led to a mean fluorescence ratio of 4.09 ($p=2.3*10^{-70}$) and MYB23 to a ratio of 2.3 ($p=6.5*10^{-5}$). Also, the co-

expression of both tested inhibitors increased the protein stability of TRY. CFP-TRY more drastically stabilized TRY-P2A to a mean ratio of 1.54 ($p=1.1*10^{-10}$), whereas CFP-CPC only slightly but significantly raised the mean fluorescence ratio to 1.2 (p=0.004, Figure 15 C).

3.1.3. Proteasomal degradation may be the cause for changed fluorescence ratios

So far, the changed fluorescence ratios have been referred to as changed protein stabilities. This can be reasoned by considering that YFP and mCherry are expressed from one plasmid and co-translationally cleaved into two proteins in an equimolar manner. YFP and mCherry possess different quantum yields and brightness (Kremers et al., 2006; Shaner et al., 2004) but using the control (CFP w/o) as a normalization factor, this was taken into consideration. Therefore, any change in YFP/mCherry fluorescence ratio is caused by a change in fluorophore amount. NLSNLS-mCherry is very unlikely to be specifically targeted for protein degradation, therefore changes in fluorescence ratio are most likely caused by changes in the protein amount of YFP-tagged fusion protein. Protein amount is determined by production and degradation rates. However, an increase in production would also lead to an equimolar increase in NLSNLS-mCherry. Thus, no change in fluorescence ratio would be observed. However, a changed degradation would be indicated by a changed fluorescence ratio. Specific protein degradation is often mediated trough the 26S proteasome pathway (Moon et al., 2004) and for GL1, GL3 and TTG1 proteasomal degradation was suggested (Jaime, 2007; Patra et al., 2013a, b). To test the proteasomal degradation using the P2A system proteasomal inhibitor treatments were performed in transiently transformed *N. benthamiana* leaves. A well-established proteasomal inhibitor is MG-132, also known as Cbz-leu-leu-leicinal. As a cell-permeable and potent substrate analog of the 26S proteasome it inhibits reversibly the chymotrypsin-like activity of the proteasome by blocking its transition state (Lee & Goldberg, 1996, 1998; Rock et al., 1994). In these inhibitor treatments, a P2A construct expressing *RFP* instead of *mCherry* was used due to the availability of antibodies for possible further experiments.

To test the efficiency of the inhibitor treatment tobacco leaves were transiently transformed to express *pENSG-p35S:YFP-HY5-P2A-RFP-NLS.* The MG132 treatment was performed one day post infiltration with *A. tumefaciens*. It was shown that HY5 accumulates in *A. tumefaciens*-infiltrated tobacco leaves 12h after MG-132 treatment (Liu et al., 2010).

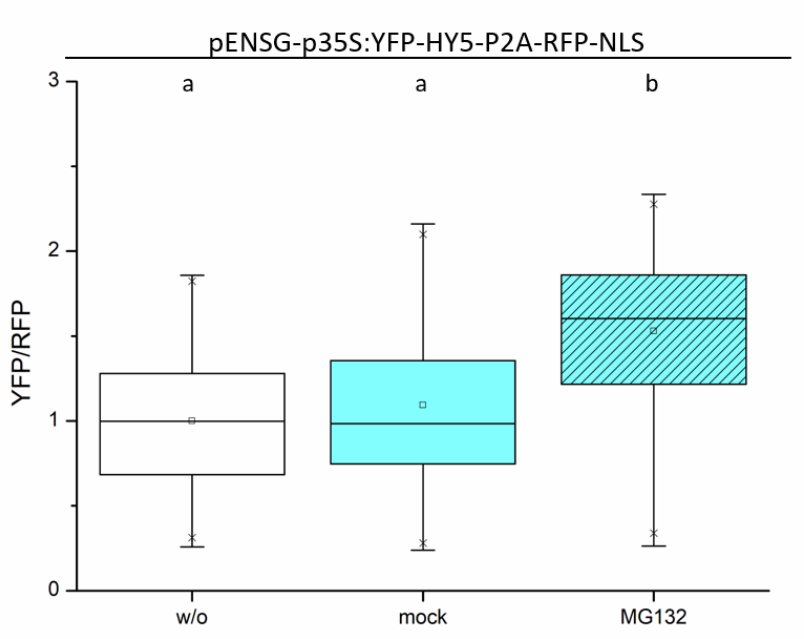

Figure 16. Stability of HY5 in tobacco leaves 16h after MG132 treatment. Box plot graph displaying the normalized YFP/RFP fluorescence ratios of pENSG-p35S:YFP-HY5-P2A-RFP-NLS expressed in non-treated tobacco (n=106, median=1), mock-treated tobacco (n=101, median=0.99) and MG132 treated tobacco (n=107, median=1.6). Each n refers to a single nucleus of tobacco epidermis cells. Statistical analysis was performed by Mann-Whitney U tests and statistical differences are indicated by different letters at the top of each graph ($p \leq 0.05$). In all box plots, the mean is displayed as a small square. Maximum and minimum values are indicated as horizontal lines at the end of the whiskers and the 1% and 99% percentiles are displayed by crosses. Outliers are displayed as small horizontal lines.

The normalized YFP/RFP fluorescence ratio of HY5 did not significantly change upon mock treatment. However, the MG132 treatment led to a statistically significant increase in HY5 stability from 1 to 1.53 ($p=2.8*10^{-16}$). This indicates an influence of MG132 on the proteasomal degradation of HY5 and an effective treatment.

Based on these initial results the same experimental setup was used to test proteasomal degradation of *pENSG-p35S:YFP-GL1-P2A-RFP-NLS* in the presence or absence of GL3. For this experimental setup, the non-treated leaves expressing GL1-P2A and CFP w/o were used to normalize the other fluorescence ratios.

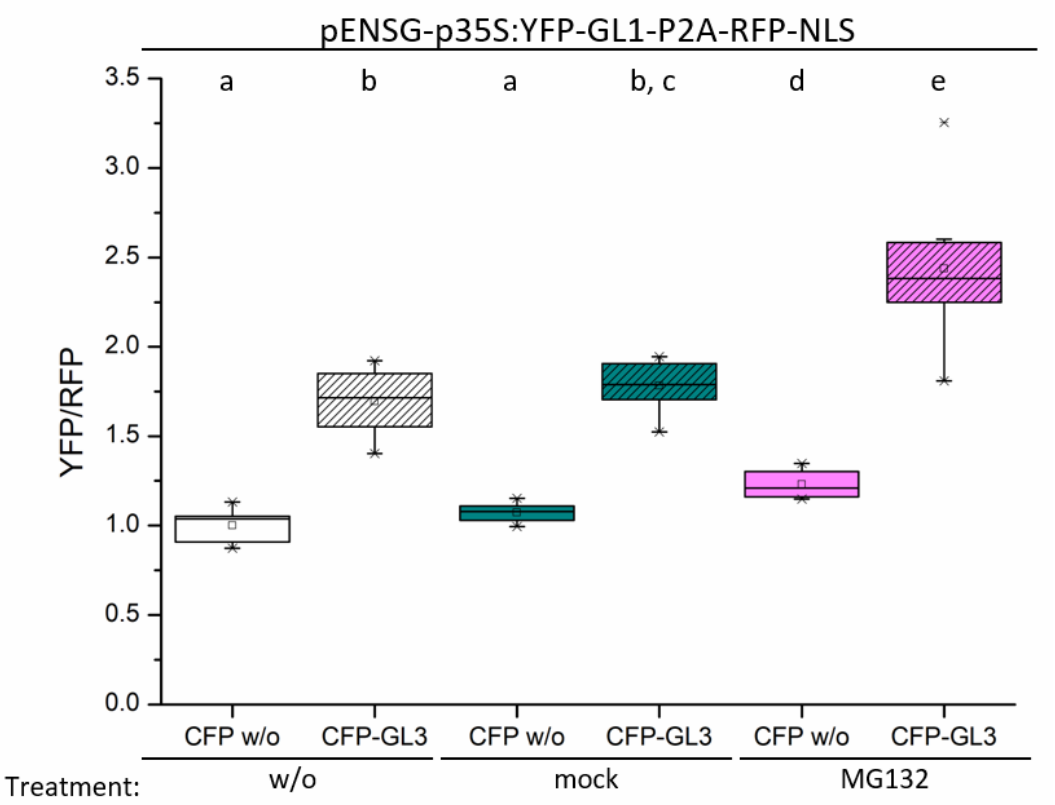

Figure 17. Stability of GL1 in tobacco leaves 16h after MG132 treatment. Box plot graph displaying the normalized YFP/RFP fluorescence ratios of *pENSG-p35S:YFP-GL1-P2A-RFP-NLS* co-expressed with *pENSG-p35S* constructs in not treated leaves (w/o) expressing CFP w/o (n=8, median=1.04) or CFP-GL3 (n=8, median=1.72). The normalized YFP/RFP fluorescence ratios of pENSG-p35S:YFP-GL1-P2A-RFP-NLS co-expressed with pENSG-p35S constructs in mock-treated leaves (mock) expressing CFP w/o (n=8, median=1.08) or CFP-GL3 (n=8, median=1.79). The normalised YFP/RFP fluorescence ratios of *pENSG-p35S:YFP-GL1-P2A-RFP-NLS* co-expressed with *pENSG-p35S* constructs in MG132 treated leaves (MG132) expressing CFP w/o (n=8, median=1.21) or CFP-GL3 (n=8, median=2.38). Each n refers to a single CLSM image with several epidermal cells that are measured as one sample. Statistical analysis was performed by Mann-Whitney U tests, and statistical differences are indicated by different letters at the top of each graph ($p \leq 0.05$). In all box plots, the mean is displayed as a small square. Maximum and minimum values are indicated as horizontal lines at the end of the whiskers, and the 1% and 99% percentiles are displayed by crosses. Outliers are displayed as small horizontal lines.

As shown for the transient expression in leek, the presence of CFP-GL3 led to an increase in GL1-P2A stability. This was the case for all three samples independent of the applied treatment. In the non-treated samples, the mean fluorescence ratio in the samples co-expressing CFP-GL3 increased from 1 to 1.7 ($p=1.6*10^{-4}$), in mock-treated samples, the ratio increased from 1.07 to 1.78 ($p=1.6*10^{-4}$), and in the MG132 treated samples the ratio increased from 1.23 to 2.44 ($p=1.6*10^{-4}$). In general, the MG132 treatment caused an increase in the normalized YFP/RFP fluorescence ratio compared to the mock- and non-treated samples. The samples containing CFP w/o were not statistically different from each other in the cases of no and mock treatment. However, the samples that were MG132 treated displayed a significantly increased ratio compared to the non-treated samples (p=1.6*10-4) and the mock-treated samples ($p=3.1*10^{-4}$). The mean fluorescence ratio of the samples co-expressing CFP-GL3 was not significantly different during no or mock treatment. MG132 treatment, however, led to a

significant increase in the YFP/RFP ratio compared to the other two treatments (p=0.001 non-treated, p= 0.001 mock-treated).

These results prompted the question of the timeline of degradation. The same constructs were used in different infiltration experiments, in which treatment was performed at 4h, 16h, or 14h before imaging. However, no difference in fluorescence ratio upon MG132 treatment was observed at any time point (data not shown). Repetition of the inhibitor treatment experiments in tobacco expressing *pENSG-p35S:YFP-GL1-P2A-RFP-NLS* or *pENSG-p35S:YFP-GL3-P2A-RFP-NLS* with either *CFP w/o* or *CFP-GL3* did not result in any significant changes in YFP/RFP ratio caused by MG132 treatment (Figure 48).

3.1.4. KAKTUS could be the candidate ubiquitin ligase involved in the degradation of trichome patterning proteins

There are indications that GL3 and EGL3 interact with the E3 ubiquitin ligase KAKTUS and thus are degraded via the 26S proteasome (Patra et al., 2013a). Also, for GL1, there are some indications that it is a target of KAKTUS, similar to TTG1 (Jaime, 2007; Patra et al., 2013b). To test the effect of KAK on GL3 stability, *pENSG-p35S:CFP-KAK* was co-expressed with *pENSG-p35S:YFP-GL1-P2A-NLSNLS-mCherry* in leek epidermal cells and normalized to *pENSG-p35S:CFP w/o* (Figure 19). The presence of KAK led to a significant increase in the normalized YFP/mCherry fluorescence ratio of GL3 from 1 to 1.93 ($p=2.5*10^{-6}$). This result contradicts the publications stating a negative effect of KAK on GL3 stability (Patra et al., 2013a). To investigate this finding further, *pENSG-p35S:YFP-GL1-P2A-NLSNLS-mCherry* was co-expressed with *pENSG-p35S:CFP w/o* or *pENSG-p35S:CFP-GL3* in wild type Col-0 or *kak* plants and the YFP/mCherry ratios were examined.

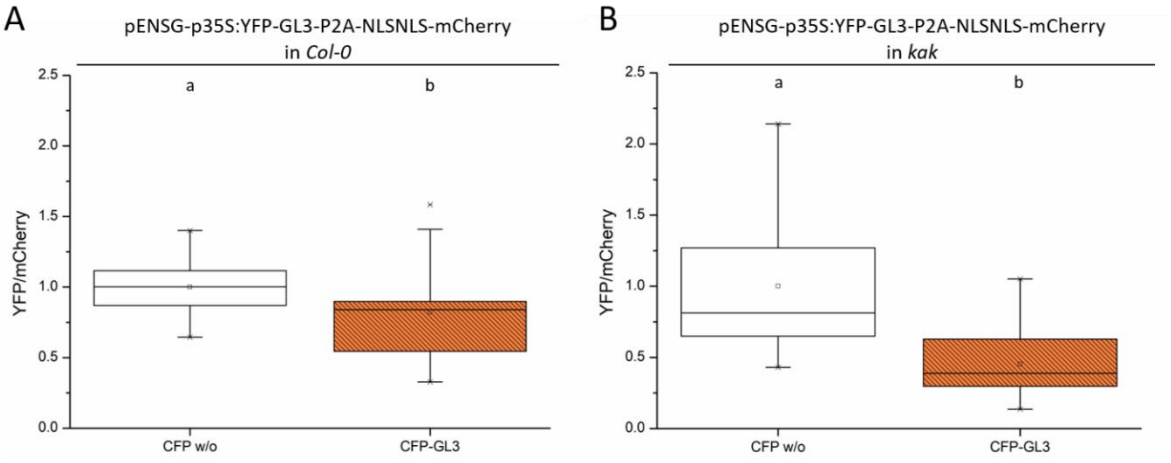

Figure 18. Stability of GL3 in Col-0 and *kak* leaf epidermal cells. A) Box plot graph displaying the normalized YFP/mCherry fluorescence ratios of *pENSG-p35S:YFP-GL3-P2A-NLSNLS-mCherry* co-expressed with *pENSG-p35S* constructs expressing *CFP w/o* (n=10, median=1) or *CFP-GL3* (n=13, median=0.84) in Col-0 leaf epidermal cells. B) Box plot graph displaying the normalized YFP/mCherry fluorescence ratios of *pENSG-p35S:YFP-GL3-P2A-NLSNLS-mCherry* co-expressed with *pENSG-p35S* constructs expressing *CFP w/o* (n=13, median=0.81) or *CFP-GL3* (n=18, median=0.39) in *kak* leaf epidermal cells. Statistical

analysis was performed by Student t-test (A) or Mann-Whitney U test (B), and statistical differences are indicated by compact letter display ($p \leq 0.05$). In all box plots, the mean is displayed as a small square. Maximum and minimum values are indicated as horizontal lines at the end of the whiskers, and the 1% and 99% percentiles are displayed by crosses. Outliers are displayed as small horizontal lines. The experiments in Col-0 and *kak* took place on different days, therefore ratios between both experiments cannot be compared directly.

The co-expression of *pENSG-p35S:YFP-GL3-P2A-NLSNLS-mCherry* (GL3-P2A) with *pENSG-p35S:CFP-GL3* in Col-0 leaf epidermal cells led to a statistically significant increase in normalized mean YFP/mCherry fluorescence ratio compared to the control expressing *pENSG-p35S:CFP w/o*. In the presence of CFP-GL3, GL3-P2A is destabilized, shown by a reduction of the fluorescence ratio of 1 to 0.82 ($p=1.4*10^{-11}$). The same trend could be observed by expressing the same constructs in *kak* leaf epidermal cells. However, in *kak* plants, the decrease in GL3-P2A stability was even more pronounced. The normalized mean YFP/mCherry fluorescence ratio dropped in *kak* plants from 1 to 0.45 ($p=2*10^{-4}$). These findings are in line with the bombardments co-expressing *pENSG-p35S:YFP-GL3-P2A-NLSNLS-mCherry* with *pENSG-p35S:CFP-KAK* (Figure 19), but are contrary to the published results discussed above.

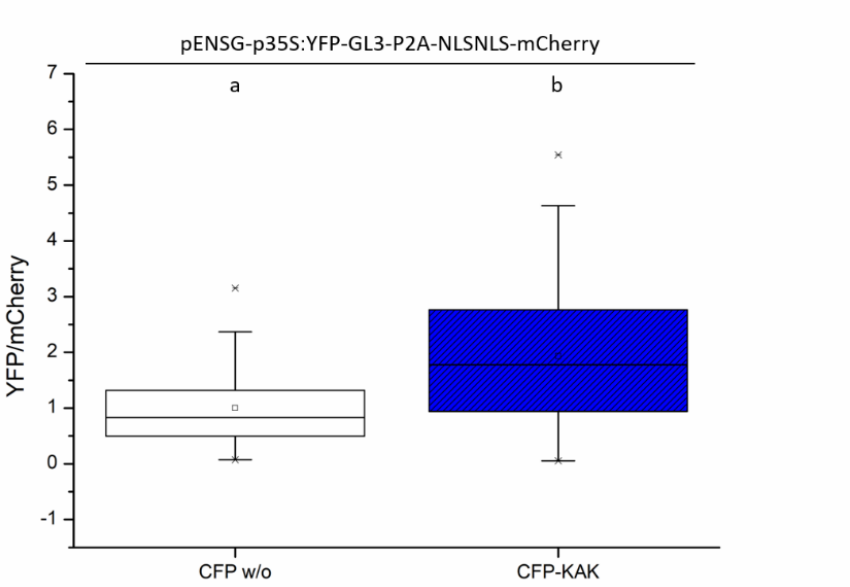

Figure 19. GL3-P2A + CFP-KAK in leek epidermal cells. Box plot graph displaying the normalised YFP/RFP fluorescence ratios of *pENSG-p35S:YFP-HY5-P2A-RFP-NLS* expressed in non-treated tobacco (n=106, median=1), mock treated tobacco (n=101, median=0.99) and MG132 treated tobacco (n=107, median=1.6). Each n refers to a single nucleus of tobacco epidermis cells. Statistical analysis was performed by Mann-Whitney U tests and statistical differences are indicated by different letters at the top of each graph ($p \leq 0.05$). In all box plots the mean is displayed as a small box in the box formed by median, 0.25 and 0.75 quartiles. Maximum and minimum values are indicated as horizontal lines at the end of the whiskers and the 1% and 99% percentiles are displayed by crosses. Outliers are displayed as small horizontal lines.

3.1.5. The different protein stabilities are caused by interactions between the co-expressed proteins

Based on the experimental results obtained so far, it was suspected that the added protein caused the stability changes by protein-protein interaction. This theory was tested by using known interaction

mutants of trichome patterning proteins in transient co-expression experiments. Therefore, interacting and non-interacting (del96GL3) mutants of GL3 (Payne et al., 2000) were co-expressed with *YFP-GL1-P2A-NLSNLS-mCherry* in leek epidermal cells. The truncated version of GL3 was shown to be unable to bind to GL1 in yeast two-hybrid experiments (Payne et al., 2000). If the fluorescence ratio changes were caused by protein interactions, the mutated version should show no difference in the fluorescence ratio compared to the control.

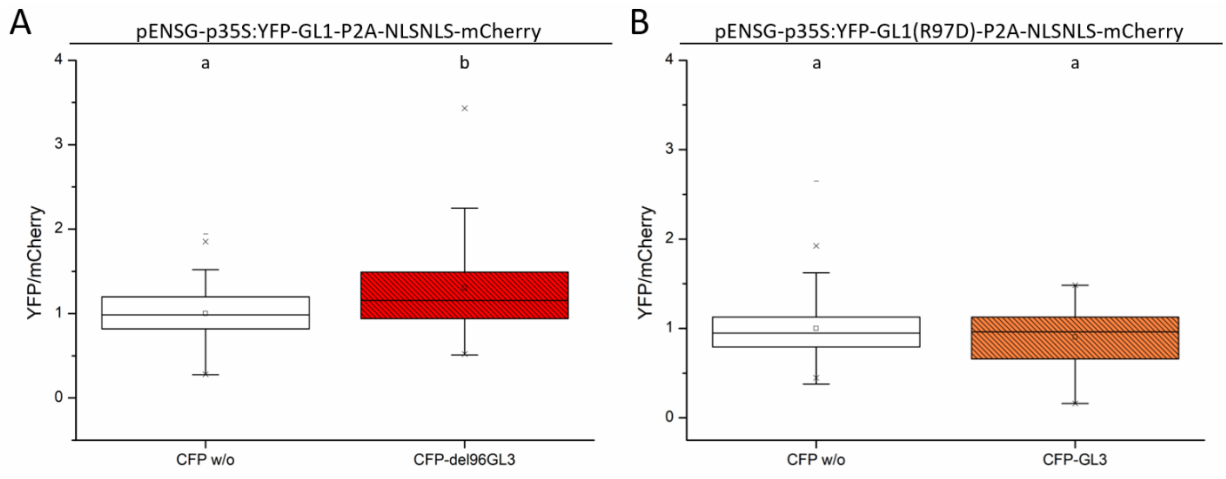

Figure 20. Stability of different GL1 variants in leek epidermal cells. A) Box plot graph displaying the normalized YFP/mCherry fluorescence ratios of *pENSG-p35S:YFP-GL1-P2A-NLSNLS-mCherry* co-expressed with *pENSG-p35S* constructs expressing *CFP w/o* (n=117, median=0.98) and CFP-del96GL3 (n=114, median=1.16) B) Box plot graph displaying the normalized YFP/mCherry fluorescence ratios of *pENSG-p35S:YFP-GL1(R97D)-P2A-NLSNLS-mCherry* co-expressed with *pENSG-p35S* constructs expressing *CFP w/o* (n=128, median=0.95) and *CFP-GL3* (n=90, median=0.96). Statistical analysis was performed by Mann-Whitney U tests, and statistical differences are indicated by different letters at the top of each graph ($p \leq 0.05$). In all box plots, the mean is displayed as a small square. Maximum and minimum values are indicated as horizontal lines at the end of the whiskers, and the 1% and 99% percentiles are displayed by crosses. Outliers are displayed as small horizontal lines.

The co-expression of *pENSG-p35S:YFP-GL1-P2A-NLSNLS-mCherry* and *pENSG-CFP-GL3* led to a statistically significant increase in mean YFP/mCherry fluorescence ratio from 1 to 2 (see Figure 9). If instead a truncated version of GL3 is co-expressed with GL1-P2A (Figure 20 A), the fluorescence ratio also significantly increases, however, the effect is strongly reduced as the ratio only rises to a mean value of 1.3 ($p=2.4*10^{-5}$) compared to the control. This result indicates that the truncated GL3 protein may still be able to interact with GL1 but weaker than the wildtype protein. Additionally, to the interaction impaired GL3 protein, Dustin Firmenich tested the stability changes of a mutated version of GL1 during the course of his bachelor thesis. It was previously shown, that a single amino acid change from arginine to aspartate at position 97 of GL1 leads to the impairment of interaction with GL3 in yeast three-hybrid assays and pulldown experiments (Pesch et al., 2015). The co-expression of *pENSG-p35S:YFP-GL1(R97D)-P2A-NLSNLS-mCherry* and *pENSG-CFP-GL3* in leek epidermal cells led to no significant change in mean YFP/mCherry ratio compared to the control sample (p=0.29; Figure 20, B). This result indicates, that the former observed changes in YFP/mCherry ratios are indeed caused by protein-protein interactions.

3.1.6. MYB23 is differentially stabilized in trichomes and surrounding cells in Col-0

The different effects trichome patterning proteins inflict on each other in leek epidermal cells prompted questions about their reciprocal effects in the endogenous plant organ, i.e., trichomes and epidermal cells of Arabidopsis. This question, however, is not as easily addressed, as the overexpression of trichome patterning genes leads to very drastic changes in trichome patterns. In the case of overexpressing inhibitors, this would lead to glabrous leaves, as shown for the overexpression of TRY, CPC, and ETCs (Kirik, et al., 2004a, b; Schellmann et al., 2002; Tominaga et al., 2008; Wada et al., 1997). Overexpressing activators, such as GL3 and EGL3, leads to the formation of more trichomes (Bernhardt et al., 2003; Payne et al., 2000). A solution to that problem would be the expression of trichome patterning genes under their endogenous promoters. Unfortunately, the expression rate under endogenous promoters is low and restricted to the patterning zone of really young leaves or to trichomes (Friede et al., 2017; Pesch et al., 2014; Pesch & Hülskamp, 2011; Zhang et al., 2003). Luckily, the overexpression of GL1 or MYB23 does not lead to changes in trichome pattern (Kirik et al., 2001; Szymanski & David Marks, 1998). Therefore, *pENSG-p35S:YFP-GL1-P2A-NLSNLS-mCherry* and *pENSG-p35S:YFP-MYB-P2A-NLSNLS-mCherry* were used to generate transgenic lines in Col-0 background. For the *MYB23* construct, several T1 plants could be selected, and some of them showed clear and sufficient signals for microscopic analysis. The YFP and mCherry fluorescence intensities were determined in non-branched trichomes and surrounding cells on small rosette leaves (leaf 3 or 4,Figure 21 A and B). For each trichome, the three surrounding cell tiers were analyzed, and the YFP/mCherry ratio was determined for each cell. The YFP/mCherry ratio of the trichome was used to normalize the ratios in the surrounding cells.

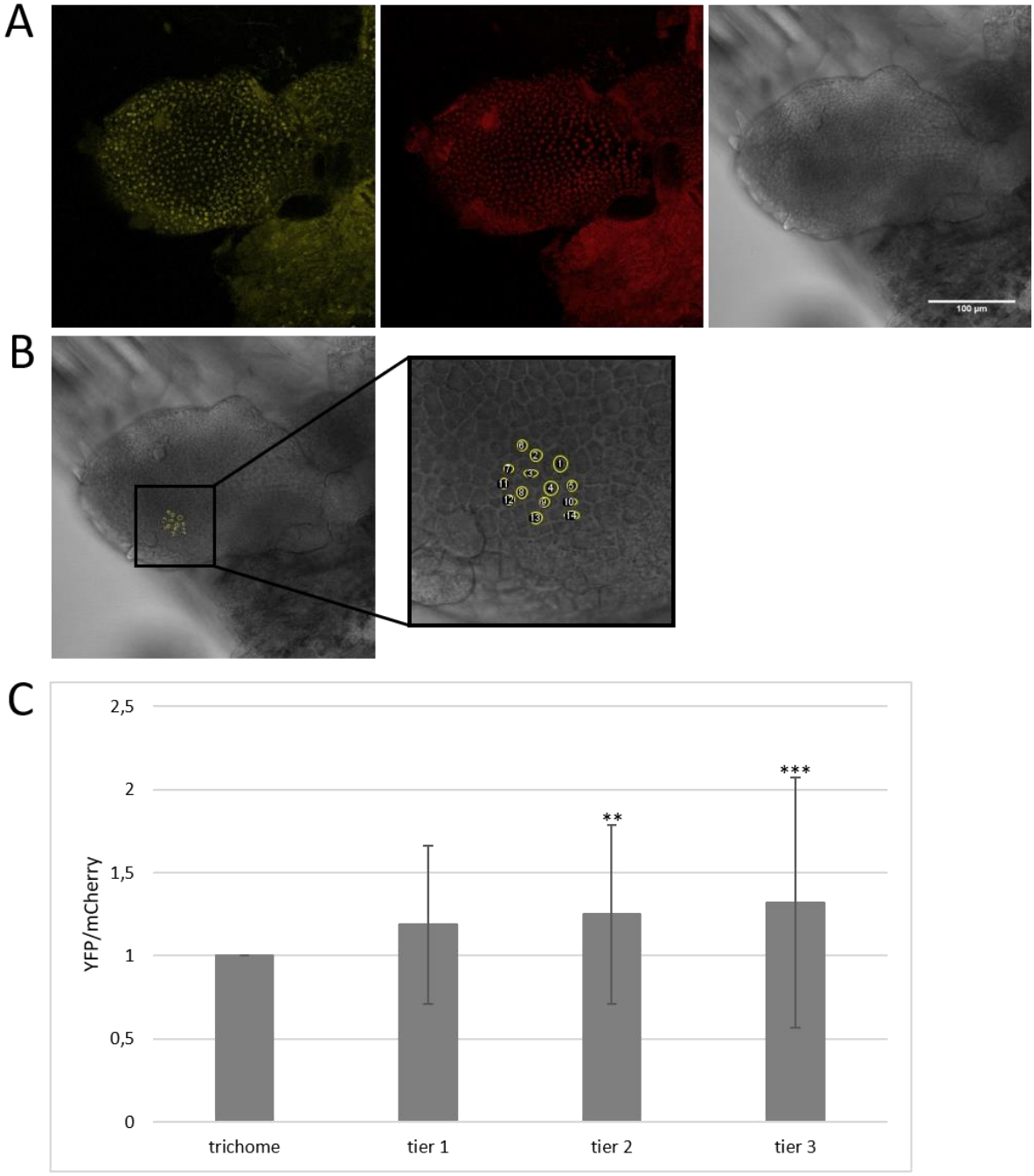

Figure 21. Stability of MYB23 in different epidermal cell types. A) CLSM images of small rosette leaves of Col-0 plants expressing *pENSG-p35S:YFP-MYB-P2A-NLSNLS-mCherry.* YFP-MYB23 is displayed on the left, NLSNLS-mCherry in the middle, and a brightfield image with a scale bar (100 µl) is shown on the right. B) Enlarged CLSM images of Col-0 plants expressing *pENSG-p35S:YFP-MYB-P2A-NLSNLS-mCherry* (brightfield) shown in A) with respective ROIs from fluorescence intensity measurements. C) Bar graph of normalized YFP/mCherry fluorescence ratios in trichomes (n=44) and surrounding cell tiers. Error bars depict standard deviations. Statistical analysis was performed by Mann-Whitney U tests, and statistical differences are indicated by two asterisks (p≤0.01) or three asterisks (p≤0.001).

Measurements were conducted in several lines and upon normalisation the YFP/mCherry ratio in surrounding cells was increased compared to the ratio in trichomes. In the first tier of cells, no change in fluorescence ratio was observed. However, in tier two and three a significantly increased YFP/mCherry ratio was observed. The increase in YFP/mCherry ratio is not as high as observed in the

leek epidermal cell experiments, but it is significantly different from the trichome value. This finding is counter-intuitive, as one would assume, that activators have to be more stable in trichomes compared to epidermal cells. However, the combination of active complexes present in the different cell types may play a role. As specific ratio of activator to inhibitor has to be present to induce trichome formation (Pesch & Hülskamp, 2009). This ratio is not given in epidermal cells, leading to different protein compositions. Additionally, a recent study found differently composed complexes of activators and inhibitors depending on the protein amounts (Zhang et al., 2024). Moreover, the overexpression of MYB23 itself could affect the stability of the different trichome patterning proteins.

3.1.7. Photoconvertible proteins could open an alternative route for protein stability experiments

Ideally, a second method to examine protein stability changes should be used to verify the initial results. An interesting alternative are photoconvertible proteins which change their conformation upon UV irradiation and thus change their emission spectra. A wide variety of photoconvertible proteins are available, such as Kaede, KikGR, monomeric KikGR (mKikGR), EosFP, and Dendra (Ando et al., 2002; Gurskaya et al., 2006; Habuchi et al., 2008; Wiedenmann et al., 2004; Tsutsui et al., 2005). These proteins change fluorescence properties irreversibly from green to red fluorescence upon UV irradiation (Gurskaya et al., 2006; Kaberniuk et al., 2017; Mizuno et al., 2003). In this study, two rather new photoconvertible proteins were tested in more detail, namely Dendra2 and moxDendra2. Both are monomeric proteins, and good conversion rates were reported (Gurskaya et al., 2006; Kaberniuk et al., 2017). In theory, utilizing photoconvertible proteins could enable the analysis of protein production and degradation rates. After conversion, the red protein will be degraded, and the newly appearing green protein will be freshly produced. Hence, degradation and production rates can be determined by measuring fluorescence intensities over time. Unfortunately, a major issue presented by photoconvertible proteins used in this study was the incomplete conversion during microscopy. Even after several rounds of UV irradiation using a high laser intensity, a green signal could be detected (Figure 22). Sometimes repeated irradiation led to cell death, and also photobleaching could not be excluded.

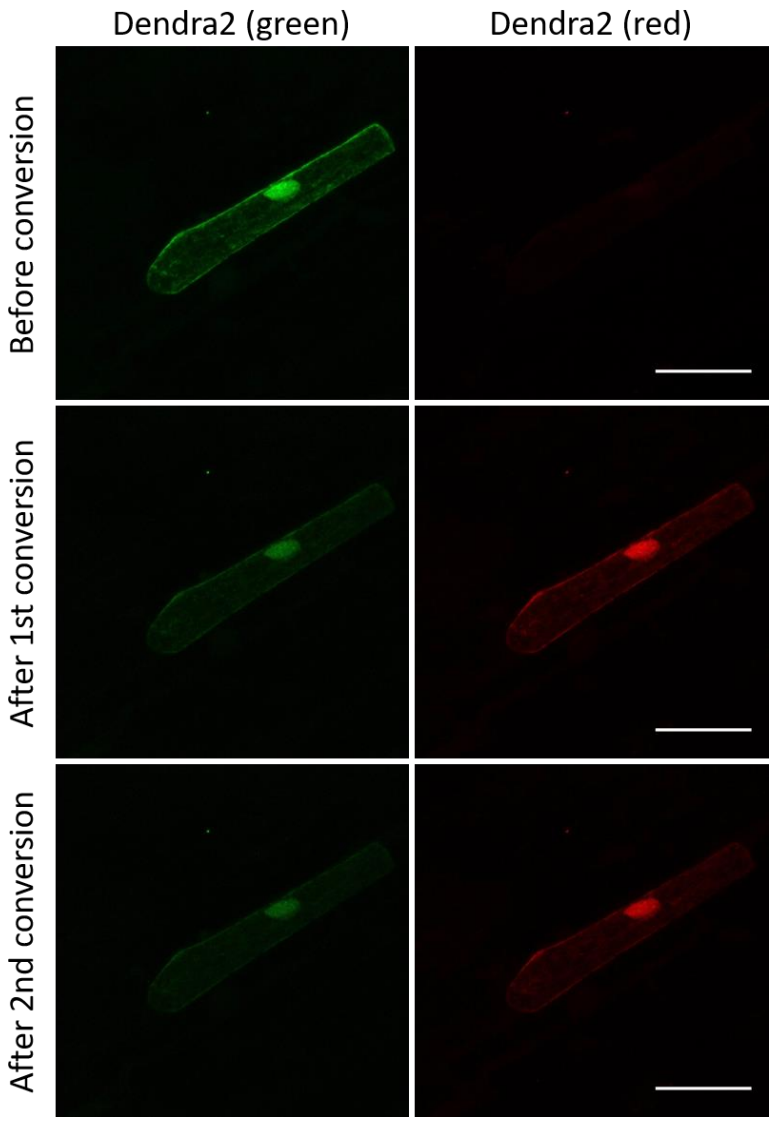

Figure 22. Dendra2 before and after UV conversion. CLSM images of leek epidermal cells transiently expressing p35S:Dendra2. Images all show the same cell, detecting the green and red fluorescent version of Dendra2. Different conversion states were documented before conversion, after a first, and after a second conversion (listed left). The scale bars indicate 50 µm.

To bypass this problem, the full conversion will not be considered a necessary variable for the experiments. The remaining green fluorescent proteins after conversion will be considered as start point “0”, meaning all additional green fluorescence intensity measured will be attributed to new proteins. The red fluorescence intensity after conversion will be tracked over time and any decrease in signal intensity could be attributed to protein degradation. This will allow the use of photoconvertible proteins as tags without complete conversion. For Dendra2 and moxDendra2, the protein degradation rates of tagged proteins could be observed in this fashion. Protein production rates would be harder to determine with this strategy, as apparently, Dendra2 green fluorescent protein populations can alternate between fluorescent and non-fluorescent forms, depending on their protonation state (Chudakov et al., 2007).

In a bachelor thesis associated with this study, the photoconvertible proteins Dendra2 and moxDendra2 were tested for optimized conversion, laser settings, and experiment duration. The results of these experiments can be found in the bachelor thesis of Dustin Firmenich. Based on his results, Dendra2 was chosen for further experiments, due to a better convertibility. In first experiments *Dendra2* tagged *GL1* was transiently expressed in leek epidermal cells. This experiment served the purpose to test the conversion technique and to test the timespan for future experiments. Multiple photoconversions were performed using the microscope UV laser, and green and red fluorescence signals of different cells were tracked over time. The fluorescence intensities were normalized to the intensities detected right after conversion and are shown as percentages in Figure 23.

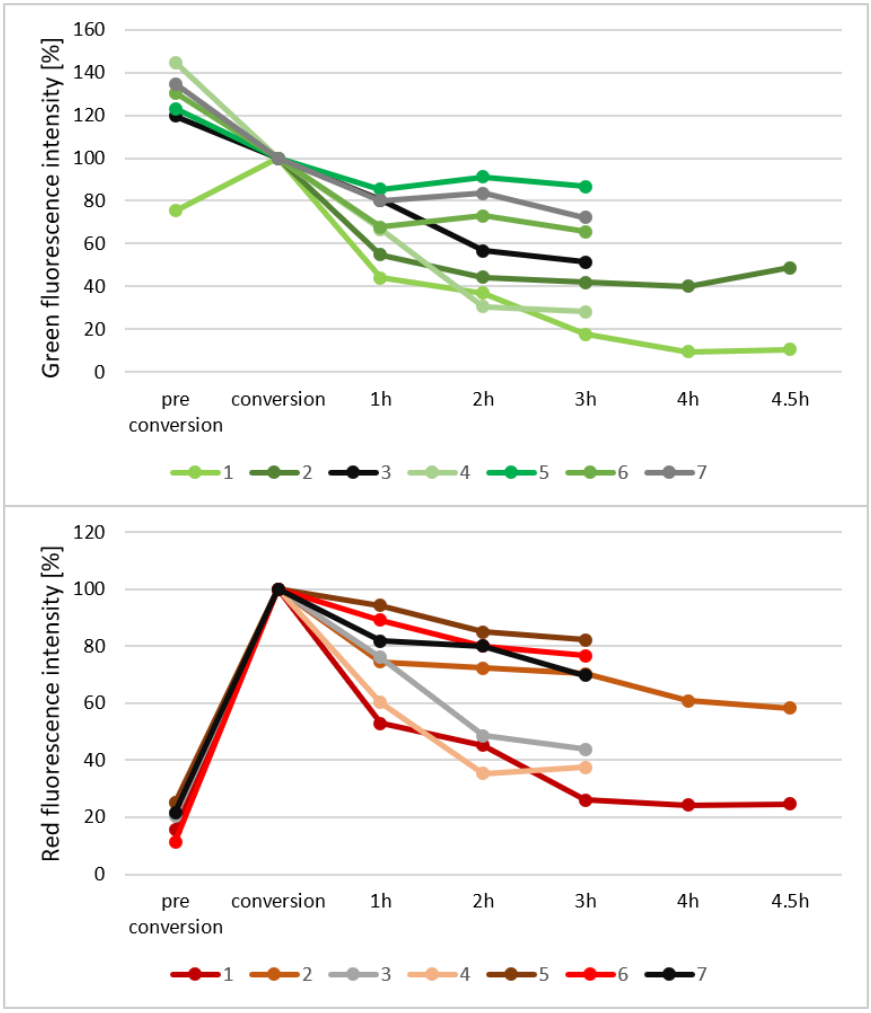

Figure 23. Relative fluorescence intensities of green and red Dendra2-GL1. In leek epidermal cells expressing Dendra2-GL1 both Dendra2 conformations were imaged in seven different cells, before and after UV conversion. The green fluorescence emitting Dendra2 version is displayed in the top graph, the red fluorescence emitting version is shown in the bottom graph. The same cells were imaged after several hours (x-axis), and the relative fluorescence intensity normalized to the fluorescence value after conversion for each individual cell is displayed.

In this experiment, cell death of converted epidermal cells was observed for several cells. These cells were not imaged further, indicated by terminated lines. Nevertheless, a decrease in green signal upon conversion and an increase in red fluorescence intensity could be observed for all cells. Four to five

hours after conversion, the green fluorescence signal slightly increased, and the red signal intensity stagnated. However, a drastic decrease in red signal could be observed 1-3 h after conversion. These first results suggest the suitability of Dendra2 as a fluorescence tag to track protein degradation over time. However, the method of detection could be an issue, as conversion at the CLSM may lead to cell death later in the experiment. Also, protein conversion and image acquisition are time-consuming, and tracking multiple cells on different samples can be challenging.

3.2. Regulatory sequence analysis of trichome patterning genes

Additionally to the trichome patterning regulation at the protein level, a cross-regulatory network at the transcription level takes part in regulating trichome formation (Hülskamp, 2004; Pesch & Hülskamp, 2009; Wang et al., 2021). Though various works analyzing the cross-regulatory network have already been performed and published (Digiuni et al., 2008; Jakoby et al., 2008; Kirik et al., 2005; Morohashi et al., 2007; Morohashi & Grotewold, 2009; Tominaga et al., 2008; Wang et al., 2007, 2008; Zhao et al., 2008), some questions are still open. In this work, several regulatory sequences were analyzed regarding the presence of cis-regulatory elements (CREs). These sequences were analyzed by utilising the plant cis-acting regulatory DNA elements (PLACE) database (Higo et al., 1999). The analyzed sequences were associated with the transcription control of GL1, GL3, ETC1, ETC2, and *ETC3*. PLACE analysis listed all found CREs with corresponding site names, locations, signal sequences, and a unique site number (site #). To summarize and visualize these results more efficiently, different categories were determined, and specific site numbers were assigned for each category. The list of categories with the corresponding site numbers can be found in Table 20. PLACE provides unique site numbers for motifs. These numbers are listed during sequences descriptions and the references to each site number can be found in Table 20. Most motifs were present more than once in each sequence. Therefore, the number of CREs does not automatically match the number of different motif sequences but the total number of CREs found belonging to this category. Furthermore, the sequences analyzed for CREs were also examined in transactivation assays to potentially shed more light on the differential transcriptional regulation of the corresponding genes.

3.2.1. Analysis of regulatory sequences of *GL1*

One of the earliest genes identified as being involved in trichome patterning is *GL1* (Herman & Marks, 1989; Marks & Feldmann, 1989; Oppenheimer et al., 1991). It was identified as a MYB encoding gene and expression under a putative 1.4 kb promoter sequence let to expression in stipules (Oppenheimer et al., 1991). Afterwards, a 3’ enhancer region was proposed to be needed for trichome specific expression and phenotype rescue ability (Larkin et al., 1993). However, also the first intron was suspected to play a role in the regulation of GL1 expression and may be needed for the correct

expression pattern (Wang et al., 2004). In a former study conducted by Martina Pesch, several regulatory sequences were tested for *GL1* expression regulation (Pesch, 2005). In summary, all these different sequences and studies complicate the identification of regulatory sequences of *GL1*. Therefore, an analysis of the regulatory sequences published so far was conducted, followed by PLACE analysis and transactivation assays of these sequences. Moreover, phenotype rescue experiments were performed to identify possible influences of the used plasmid on the rescue efficiency of *GL1* regulatory sequences.

Comparison and in-silico analysis of regulatory sequences involved in GL1 expression

The regulatory sequences used by Oppenheimer and Larkin, as well as Wang and Pesch are illustrated in Figure 24.

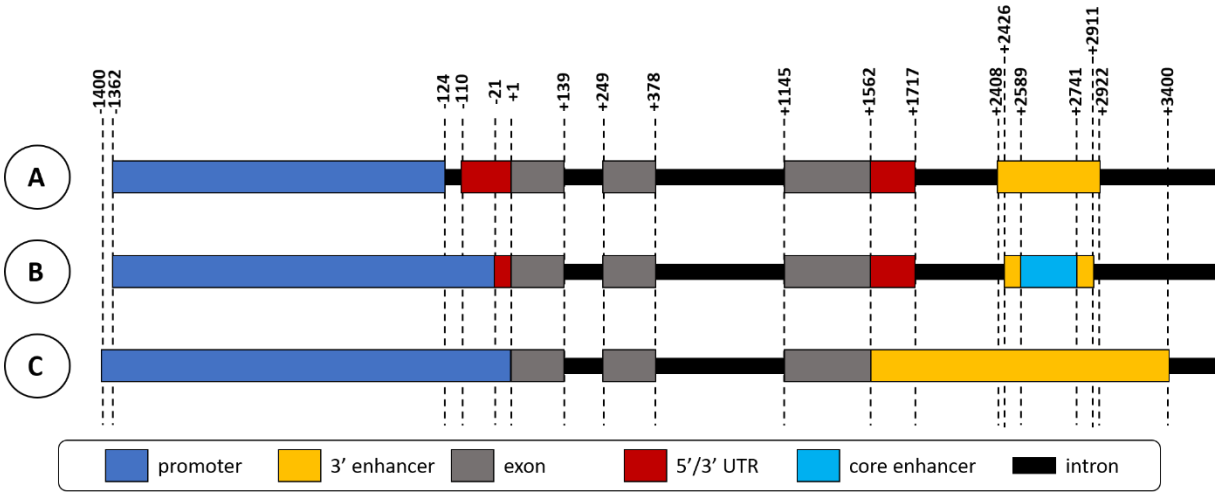

Figure 24. Summary of published regulatory sequences associated with *GL1* expression. Putative regulatory sequences used in the publication A) Pesch, 2005 B) Oppenheimer et al., 1991 & Larkin et al., 1993 C) Wang et al., 2004. Numbers refer to the start of *GL1* coding sequence, positive signs refer to downstream of the ATG of *GL1* and negative signs to upstream. The color code of each depicted sequence category (promoter, 3' enhancer, exon, intron, 5' and 3' UTR, and core enhancer) is listed at the bottom of the figure. The depicted box sizes do not accurately reflect the exact sequence length.

Oppenheimer and colleagues defined the 5' promoter region from -1382 to -21 relative to the start codon of *GL1*. However, this 5' promoter alone did not seem sufficient to express *GL1* correctly (Oppenheimer et al., 1991). Two years later, Larkin and colleagues used the same promoter region combined with a putative 3' enhancer region (+2426 to +2911) to detect GL1 expression in trichomes of young leaves. Subsequently, the sufficient enhancer sequence needed for *gl1* phenotype complementation could be limited to a so-called core enhancer in the region +2589 to +2741 (Larkin et al., 1993). However, in a later study focused on a MYB encoding gene from cotton (*Gossypium* spp), a longer 5' promoter region of *GL1* (-1 to -1400), as well as a longer 3' enhancer element (+1563 to +3400) were used for rescue experiments (Wang et al., 2004). Also, the first intron of *GL1* needed to be included in the rescue constructs to ensure trichome formation in *gl1* plants. Wang et al. analyzed

intron 1 of *GL1*, *WER,* and the cotton *MYB* (*GaMYB2*) regarding CREs and found a conserved MYB motif (Wang et al., 2004). In an independent study, it was also speculated that the first intron may play a role in GL1 expression regulation (Pesch, 2005). However, in the mentioned study different regions for the 5' promoter (-124 to -1362) and 3' enhancer (+2408 to +2922) were used, and the intron was not considered in combination with the other two regulatory elements (Pesch, 2005). The intron was also tested regarding expression pattern and rescue ability, and no expression or trichome formation was observed (Pesch, 2005). In addition to the different regions, Oppenheimer, Larkin, and Pesch used *Landsberg erecta* as the sequence source, whereas Wang used the *Columbia* accession. Moreover, different plasmids were used to generate the rescue constructs. The different properties of these plasmids may also influence the rescue efficiency of the sequence of interest.

As a first step in the examination of the different sequences, a PLACE analysis was performed (Higo et al., 1999). The number of CREs in each category for the promoter sequence used by Wang and colleagues, as well as their used enhancer region and the enhancer region used by Larkin and colleagues are shown in Figure 25.

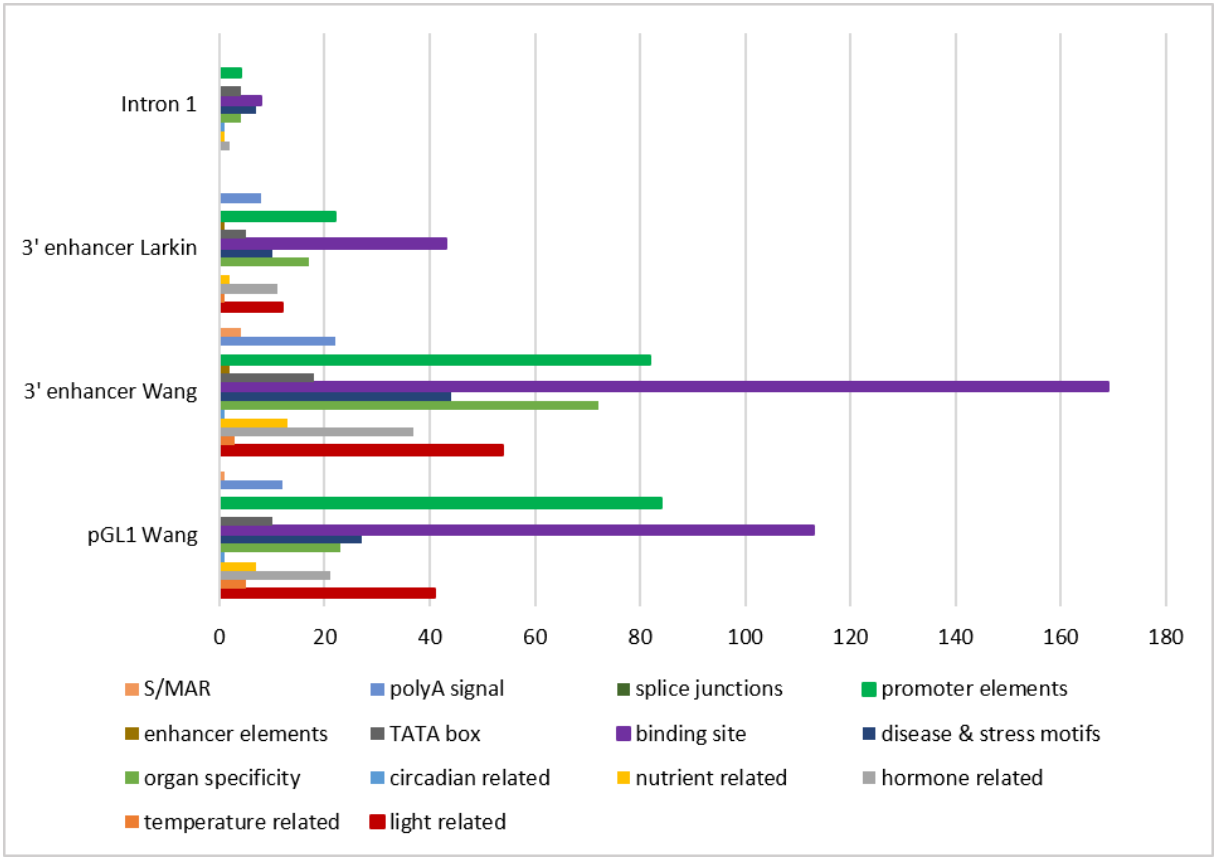

Figure 25. PLACE analysis of GL1 regulatory sequences. Bar graph depicting the number of CREs of each category found in the promoter sequence of *GL1* (sequence from Wang et al., 2004; -14000 to -1), the 3' enhancer region defined by Wang et al., 2004 (+1562 to +3400) and the 3' enhancer region defined by Larkin et al., 1993 (+2426 to +2911). Categories are listed at the bottom of the graph with the corresponding color code.

The first regulatory sequence analyzed via PLACE was the 1400 bp promoter defined by Wang and colleagues. In the sequence, a total of 345 CREs were identified. The majority were classified as binding sites. Out of the 113 identified binding sites, 22 were associated with Dof binding sites (S000265). 20 W-boxes were found that cluster around 26 bp and from 539-715 bp, with one single W-box situated at the C-term at 1296 bp (S000390, S000447, S000310, S000442, S000457). Additionally, 16 MYC-binding sites were identified. They occurred more frequently at four places of the promoter sequence, around 201 bp, 738 bp, 1146 bp, and 1291 bp (S000144, S000407). As MYB-binding sites, 16 motifs were found (S000408, S000176, S000177, S000409, S000180). They were distributed over the whole length of the promoter, with a slightly higher frequency at the end. Interestingly, only three HD-ZIP-associated binding sites were identified, with two of them situated at around 1290 bp (S000292, S000498). Only one circadian-related CRE was identified (S000252), and 7 related to nutrients, all putative nodulin consensus sequences (S000461, S000462). A lot of organ-specific motifs were identified. Out of the 54 CREs, 31 were associated with mesophyll-specific expression (S000449). The other motifs were pollen-, root hair- or seed-specific (S000512, S000353, S000245, S000378, S000273, S000191). Interestingly, 12 poly(A)-signals were identified and are distributed over the whole length of the promoter sequence (S000080, S000088, S000081). In total, 27 disease and stress-related CREs were identified. They are associated with a wide variety of stresses, such as infected root nodules (S000468), general infection response (S000467, S000443), pathogen- and salt-stress (S000453), Ca-responsive elements (S000507), copper- and oxygen-stress (S000493) as well as sulfur-responsive elements (S000499). As TATA boxes, 10 motifs were identified (S000111, S000203, S000109). They are present in the whole sequence of the promoter, but three of them were detected around 880 bp. 53 CREs categorized as general promoter elements were identified. Ten were identified as CAAT promoter consensus sequences (S000028), and 13 were identified as *A. rhizogenes* promoter sequences (S000098). The other motifs were A-boxes (S000130) or motifs found in tobacco, barley, and promoters of anaerobic genes or plastids (S000400, S000477, S000387, S000395, S000296, S000122). Interestingly, also a silencing element was identified (S000391), situated at 197 bp. 21 hormone-related motifs were identified, 12 of them cytokinin-related (S000454). The other CREs were mostly associated with etiolation-induced expression (S000362, S000414, S000415); the rest were classified as I-boxes (S000199, S424, S000124), and even one phyA-repressed motif was found (S000488). As temperature-related motifs, 3 heat-related CREs were identified (S000030, S000506) and two low-temperature-responsive elements (S000250). Finally, no enhancer elements but 1 S/MAR were identified (S00067). Interestingly, in the promoter sequences used by Larkin and Pesch, the most N-terminal W-box cluster, as well as one poly(A) signal, was missing. At the C-term of the promoter,

one TATA-box, a W-box, two HD-ZIP binding sites, and a MYC-binding site cluster are missing in the sequence used by Pesch.

The 3' enhancer sequences analyzed were all partially identical, as the 3' enhancer defined by Wang encompasses the enhancers defined and used by Pesch and Larkin. In the 1838 bp long enhancer used by Wang et al., 521 CREs were identified, of which 132 are present in the 3' enhancer Larkin. In the 3' enhancer of Wang, 169 binding sites were identified. The majority was associated with Dof binding (S000265), followed by GATA boxes (S000039). A total of 25 MYC-binding sites were identified (S000436, S000144, S000407). They form five clusters, situated at 243 bp, 463 bp, 654 bp, 1008 bp, and 1127 bp. These last two clusters are also present in the Larkin and Pesch enhancers. Additionally, 15 MYB-binding sites were identified in the Wang enhancer (S000408, S000176, S000177, S000409, S000180). They are equally distributed over the whole length of the enhancer, but six are present in the last 174 bp. Also, 23 W-boxes were identified (S000039, S000390, S000447, S000310, S000442, S000457, S000508, S000142). They are only present after 630 pb and some of these W-boxes form two clusters at around 1580 bp and 1778 bp. These two W-box cluster, as well as the last six MYB-binding sites are missing in the enhancer regions used by Pesch and Larkin. Additionally, HD-ZIP binding sites were identified, ten in number. Seven of them are situated in the 3' enhancer region used by Larkin, clustering around 1104 bp. In the Wang enhancer, one circadian-related motif was identified (S000252), and none in the smaller sequences. As organ specificity-related CREs 72 motifs were classified in the Wang enhancer. 32 of them are mesophyll-related (S000449), the rest is either pollen-specific (S000245, S000378) or seed-specific (S000148, S000100, S000102, S000277). One was identified as L1-box, meaning L1 layer-specific expression (S000386). In the Larkin enhancer, 17 CREs were organ-specific. The majority was mesophyll-related (S000449), or pollen-specific (S000245, S000378). Poly(A) signals were identified in both enhancer regions, 22 in the Wang enhancer and 8 in the Larkin enhancer (S000080, S000088, S000081). Furthermore, disease and stress-related motifs were identified, 44 in the Wang enhancer and 10 in the Larkin enhancer. In both sequences, the majority was classified as copper- and oxygen-related (S000493), and the rest was infection-related (S000468, S000467, S000453, S000501). Also, TATA boxes were identified in the Wang and Larkin sequences, 18 and 5, respectively. Ten TATA boxes are located upstream of the Larkin enhancer, and three more downstream. In the Larkin enhancer, four TATA boxes are located close to each other. A large number of general promoter elements was identified in the Wang enhancer, 82 in total. Most of them were classified as CAAT promoter consensus sequences (S000028) or found in *A. rhizogenes* promoters and promoter of anaerobic genes (S000098, S000387). Additionally, hormone-related motifs were identified. In the Wang enhancer, in total, 37 CREs were found in this category. The majority was cytokinin-related (S000454), but also ethylene-responsive elements were found

(S000037) and elements related to ABA and GA induction (S000181, S000439, S000174). In the Larkin enhancer, only 11 such CREs were found. Interestingly, no splice junction was found in either sequence. Four S/MARs were identified in the Wang enhancer, and none in the smaller sequence. The Wang enhancer harbors three CREs associated with temperature, two associated with heat (S000030, S000506), and one with cold (S000250). In the Larkin enhancer, only one heat-associated element is situated (S000030). Finally, in the Wang sequence, two enhancer elements were identified (S000494, S000254). One was located at 1182 bp, which is part of the Larkin 3' enhancer sequence, and one was located at 1584 bp.

As a final regulatory sequence, the first intron of *GL1* was analyzed. In the 109 bp, a total of 31 CREs were identified. One was associated with circadian regulation (S000440), and a putative nodulin consensus sequence (S000462) was related to nutrients. Four motifs were categorized as organ-specific, being associated with pollen and mesophyll expression (S000245, S000378, S000273, S000449). No poly(A) signal, temperature-related motif, S/MAR, splice junction, light-regulated CREs, or enhancer element was identified. Only two cytokinin-related CREs were found (S000454). However, four general promoter elements were identified (S000098, S000387, S00460) and four TATA boxes (S000340, S000111, S000109). Additionally, seven motifs related to disease and stress responses were found. They were associated with infected roots, Ca-response, copper- and oxygen-response (S000468, S000507, S000493, S000499, S000501). Finally, 8 binding sites were found. Two were GATA boxes (S000039), two Dof binding sites (S000265), and one a SEF1 (soybean embryo factor1) binding site (S000006). The remaining three are MYB-binding sites (S000176, S000177, S000409), and they all refer to the same location in the intron at around 81 bp.

Phenotypic analysis of pGL1 rescue constructs

To determine the rescue efficiencies of the widest 5' promoter region with and without introns, as well as different enhancer lengths, several rescue constructs were designed using *Col-0* DNA (Figure 26). The constructs were cloned in the PARB vector (Pesch et al., 2014; Pesch & Hülskamp, 2011), which contains a Gateway cassette to insert promoter sequences/regulatory elements upstream of a gene of interest.

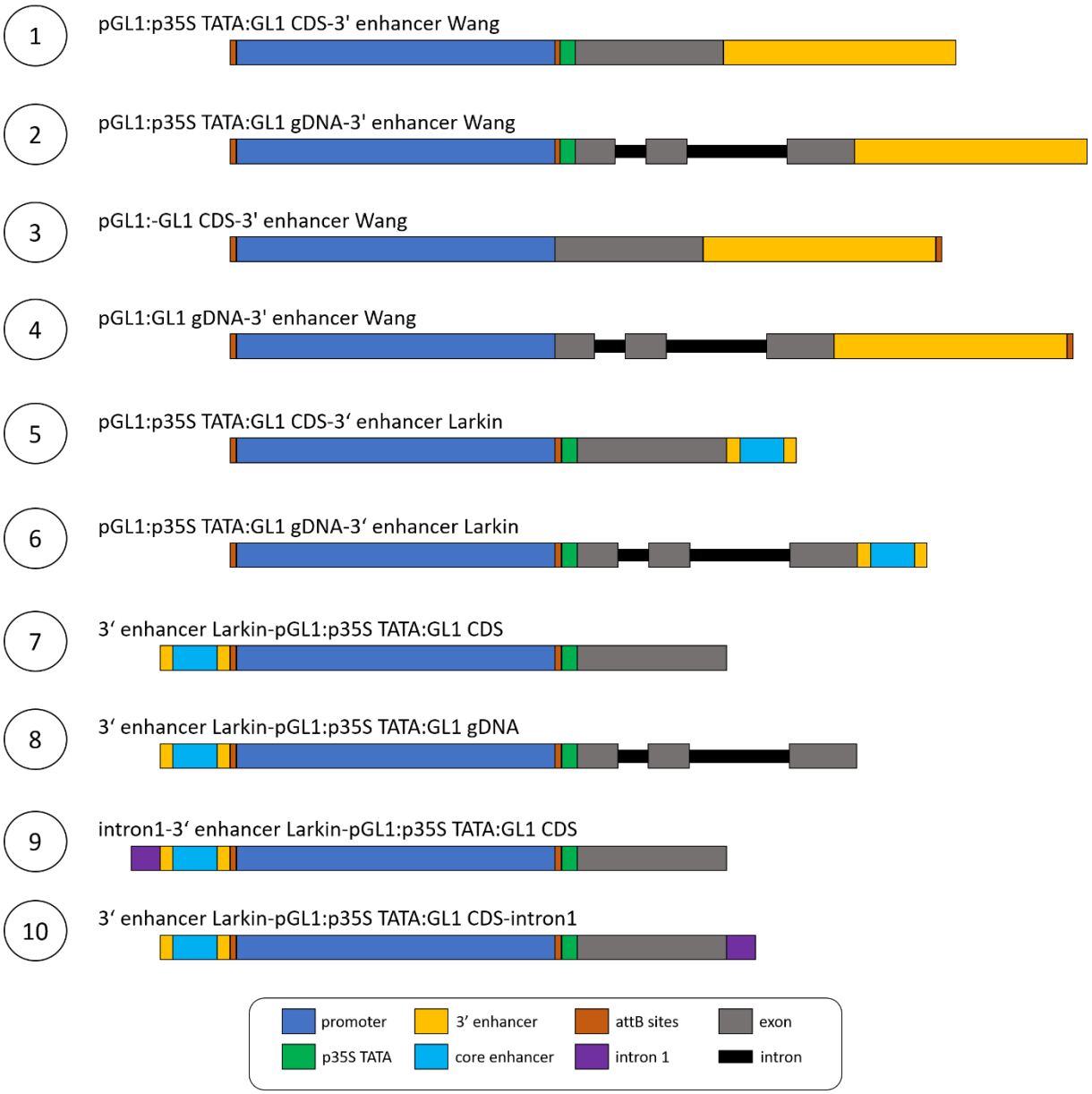

Figure 26. Rescue constructs of GL1 containing different regulatory sequences. The illustrated sequences were cloned in the PARB vector. 1) pGL1:p35S TATA:GL1 CDS-3’ enhancer Wang, 2) pGL1:p35S TATA:GL1 gDNA-3’ enhancer Wang, 3) pGL1:GL1 CDS-3’ enhancer Wang , 4) pGL1:GL1 gDNA-3’ enhancer Wang, 5) pGL1:p35S TATA:GL1 CDS-3’ enhancer Larkin, 6) pGL1:p35S TATA:GL1 gDNA-3’ enhancer Larkin, 7) 3’ enhancer Larkin-pGL1:p35S TATA:GL1 CDS, 8) 3’ enhancer Larkin-pGL1:p35S TATA:GL1 gDNA, 9) intron1-3’ enhancer Larkin-pGL1:p35S TATA:GL1 CDS, 10) 3’ enhancer Larkin-pGL1:p35S TATA:GL1 CDS-intron1. The color code of each depicted sequence category (promoter, 3’ enhancer, attB sites, p35S TATA box, exon, intron, 5’ and 3’ UTR, core enhancer) is listed at the bottom of the figure. The depicted box sizes do not accurately reflect the exact sequence length.

To ensure that artificially introduced sequences, such as the attB cloning sites, or added promoter sequences in the backbone, such as the minimal TATA box of *p35S*, do not influence the rescue ability, different arrangements were chosen. Furthermore, the study conducted by M. Pesch utilized a 5’ promoter region without the 5’ UTR and the endogenous TATA box. The 5’ region used in this study included the 5’ UTR and the TATA box and is identical to the promoter region used by Wang and colleagues (Wang et al., 2004). To ensure the correct transcription and mRNA/RNA procession, in the

previous study the TATA box of the 35S promoter was included (Pesch, 2005). In promoter studies, such a minimal promoter sequence is sometimes included in the constructs (Amack & Antunes, 2020; Jores et al., 2021). Importantly, the TATA box of *p35S* alone does not induce GUS expression in plants (Benfey et al., 1990). But the inclusion of this TATA box led to increased GUS expression (Pesch, 2005). However, because the increase in expression strength is the same for all constructs containing this TATA box, statements regarding expression differences can still be made. In the first construct displayed in Figure 26, the promoter sequence was introduced into the gateway cassette. The coding sequence of *GL1* and the 3' enhancer sequence defined by Wang et al. (2004) were introduced into the vector by classical cloning. The attB2 site and the minimal TATA box of *p35S* are located between *pGL1* and *GL1* CDS. This was also the case for construct 2. The only difference to construct 1 is that the genomic region of *GL1* was used, which will enable the comparison of rescue efficiency based on the presence or absence of intron 1. Additionally, the TATA box of *p35S* was removed from the following two constructs, constructs 3 and 4, to gauge its effect on rescue efficiency. In these constructs *pGL1* was followed by either genomic *GL1* (construct 4) or *GL1* coding sequence (construct 3), followed by the 3' enhancer region defined by Wang and colleagues. These constructs will enable the comparison of rescue efficiencies in the presence or absence of the *GL1* intron, as well as highlight the potential influence of the p35S TATA box in the vector. In construct 5, the same sequences and arrangements were used as in Construct 1, except for the 3' enhancer. In this construct, the 3' enhancer region defined by Larkin et al. (1993) was used. In construct 6, the coding sequence of *GL1* was exchanged for the genomic sequence, compared to construct 5. These two constructs will enable the comparison of rescue efficiencies between different enhancer lengths. In construct 7 and 8, the 3' enhancer defined by Larkin and colleagues was situated in front of the *GL1* promoter that drives the expression of the *GL1* coding sequence (construct 7) or the genomic GL1 sequence (construct 8). These two constructs will enable the comparison between upstream and downstream located 3' enhancers. Finally, in construct 9 and 10, the influence of intron 1 will be tested by including it in construct 7 at different locations. The intron will be situated either upstream of the 3' enhancer sequence (construct 7) or downstream of the *GL1* CDS (construct 10). Rescue experiments were performed by transforming *gl1* plants with each of the ten constructs. The T1 generation was selected for construct presence and up to 50 individual plants were examined regarding their trichome number on leaf 4 of similarly developed plants. The mean trichome number per leaf is illustrated in Figure 27.

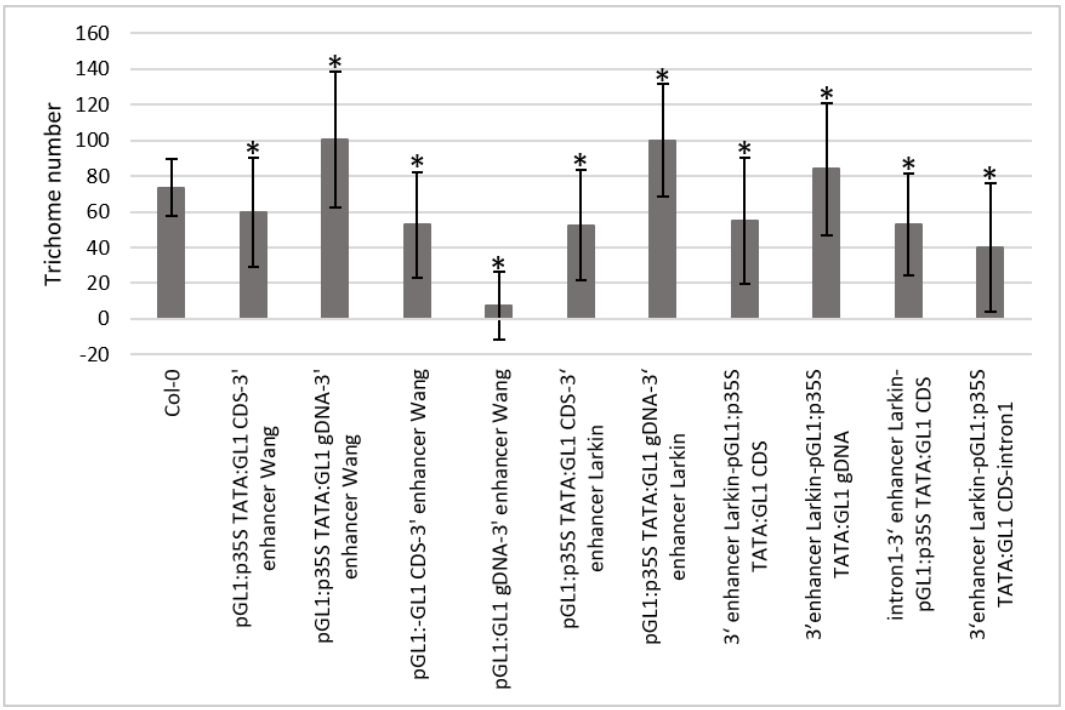

Figure 27. Trichome number of *gl1* T1 plants transformed with *GL1* rescue constructs. Bar graph of trichome numbers on leaf four of *gl1* T1 plants transformed with different GL1 rescue constructs. The rescue constructs and Col-0 are listed on the x-axis, and from left to right refer to 1-10 in Figure 26. Error bars depict standard deviations. Statistical analysis was performed by Mann-Whitney U tests comparing the constructs with Col-0. Statistical differences to Col-0 ($p \leq 0.05$) are indicated by an asterisk.

Interestingly, all tested rescue constructs led to trichome numbers that were statistically different from the control *Col-0*. The *gl1* mutant is glabrous, so any number of trichomes on these T1 plants was induced by the introduced construct. *Col-0* plants possessed 74 trichomes per leaf on average. The introduction of constructs 1 and 2 both caused trichome formation. However, construct 1, containing only the CDS of *GL1*, initiated fewer trichomes (60 trichomes per leaf) than construct 2, which contains the CDS and introns of *GL1*. This construct even caused the formation of more trichomes compared to the control (100 trichomes per leaf). Constructs 3 and 4, which reflect the sequence array found in the *Arabidopsis* genome most closely, also initiated trichomes. However, both constructs induced drastically fewer trichomes than Col-0; 53 and 7, respectively. The constructs containing the shorter 3' enhancer used by Larkin and colleagues, constructs 5 and 6, also led to the formation of trichomes. The construct containing the CDS caused, on average, 52 trichomes, and the construct containing the genomic sequence induced 100 trichomes per leaf. The constructs 7 and 8 also contained the Larkin enhancer, but this time it was situated upstream of the promoter sequence. Both constructs also induced trichome formation, but to differing degrees. Construct 7, containing the CDS of *GL1*, led to the formation of 55 trichomes on average, whereas construct 8 induced, on average, 84 trichomes per leaf. The final two constructs tested were, in principle, construct 7 but with the first intron placed upstream of the promoter (construct 9) or downstream of the CDS (construct 10). Both constructs induced trichomes, but construct 9 induced more than construct 10; 53 and 40, respectively. In

summary, the rescue experiments revealed an over-rescue caused by nearly all constructs containing the gDNA of *GL1*. The constructs containing the CDS always led to fewer trichomes compared to the control. Furthermore, the absence of the 35S TATA box did not induce trichomes close to the number found in *Col-0*, independent of the *GL1* sequence. The construct closest to the *Col-0* trichome number was 8, containing *3'enhancer Larkin-pGL1:p35S TATA:GL1 gDNA*.

The rescue efficiency of GL1 is influenced by a fluorescence tag

Additionally, to the published sequences involved in *GL1* expression control, experiments were planned to investigate which aspects of transcriptional expression are relevant for *GL1*. In a previous study it was shown that *GL1* expression controlled by the promoters of *Arabidopsis thaliana MERISTEM LAYER1* (*AtML1*) and *GL2* rescued the *gl1* trichome phenotype, even better than the expression of *GL1* under its own promoter combined with its 3' enhancer (Pesch, 2005). Interestingly, both GL2 and AtML1 are HD-ZiP proteins, closely related and expressed ubiquitously (Sessions et al., 1999; Szymanski et al., 1998). So, possibly, the accumulation of GL1 in trichomes is not necessary to rescue the *gl1* phenotype. To test this hypothesis, constructs were designed to express *GL1* under different ubiquitous promoters (*pAtML1*, *pUBIQUITIN10* & *p35S*), and the rescue efficiency was examined. For *p35S,* a rescue ability was already shown with a non-tagged version of GL1 (Oppenheimer et al., 1991). The aim was not only to determine the rescue ability and trichome pattern but also to visualize the GL1 location in small leaves. Therefore, the CDS of *GL1* was tagged N-terminally with YFP and, under the control of different promoters, used to transform *gl1* and *gl1 myb23* plants. The *gl1 myb23* double mutants were included in the experiment, as MYB23 could act redundantly to GL1 with respect to its accumulation in trichomes. However, the transformed and herbicide-selected T1 plants did not display a rescued trichome phenotype. Independent of the ubiquitous promoter used, only a small number of trichomes was induced. These results indicate that the N-terminally tagged YFP may influence the rescue ability of GL1.

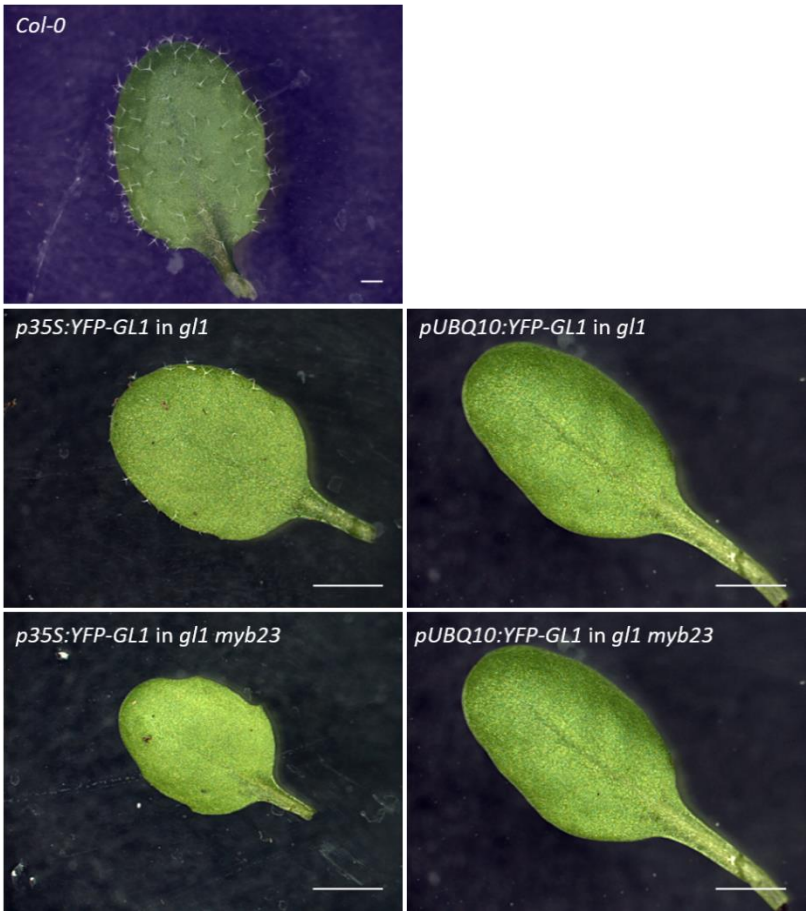

Figure 28. Rosette leaves of Col-0 and *gl1* plants expressing GL1 rescue constructs. Col-0 leaf (top row), leaves of *gl1* (middle row) and *gl1 myb23* (bottom row) T1 plants expressing *pENSG-p35S:YFP-GL1,* and *pENSG-pUBQ10:YFP-GL1* (from left to right). Scale bars refer to 2mm.

Transactivation assays of regulatory sequences of GL1

Additionally to the rescue experiments and the *in-silico* analysis, the examined regulatory sequences were tested regarding their activation through other trichome patterning genes. Therefore, transactivation assays in Arabidopsis cell suspension culture were performed with different regulatory sequences driving the expression of the reporter gene *GUS*. For each assay, the reporter activity in percent was determined by normalizing to the regulatory sequence alone, without other factors being co-expressed. The trichome patterning genes *GL1*, *GL3*, *TTG1*, *TTG2*, *TRY,* and *CPC* were co-expressed with the reporter construct, either alone or in various combinations. The sequences of *pGL1* and 3' enhancer refer to the sequences defined by Wang and colleagues. If the sequences defined by Larkin and colleagues were used, it is stated.

In the first set of transactivation assays, the promoter sequence, the 3' enhancer, and the first intron were examined without additional regulatory sequences (Figure 29). For the promoter sequences, the difference in promoter activity compared to the control was not striking. Most combinations of the trichome patterning genes did not lead to a significant change in promoter activity. However, the addition of the three core activators *GL1*, *GL3*, and TTG1 combined led to a significant increase in promoter activity to around 120%. Also, the co-expression of *TRY* alone led to an increase to 140% β-glucuronidase activity. All other combinations either did not lead to a significant difference in activity.

The 3' enhancer sequence as well was not highly inducible by any of the tested combinations (Figure 29 B). Only the combination co-expressing the three core activators with either *TRY* or *CPC* led to a significant increase in promoter activity to around 130 %. Only *GL3* and *TRY* decrease the promoter activity, but not to a significant degree. All other combinations slightly increased the activity.

The transactivation assay of the first intron alone showed an intriguing change in inducibility (Figure 29, C). The co-expression of neither *GL1*, *GL3*, *TRY*, or *GL1* with *TTG1,* nor all three core activators together, led to a significant change in reporter activity. Interestingly, TTG1 alone increased the activity significantly to 170%, to the same extend as the co-expression of *GL1* with *GL3*. The co-expression of *TTG1* with *GL3* increased the reporter activity significantly to 150%. TTG2 increased the activity slightly to 140%. The most drastic increase was observed by the co-expression of *CPC*, causing an increase to 240%. This change was similar to the co-expression of *CPC* together with the three core enhancers. These three activators, together with TTG2, led to a significant increase in activity to 200%. These observations are different from the observed effects on pGL1 and the 3' enhancer and may hint at a more important role of intron 1 in the expression regulation of *GL1*.

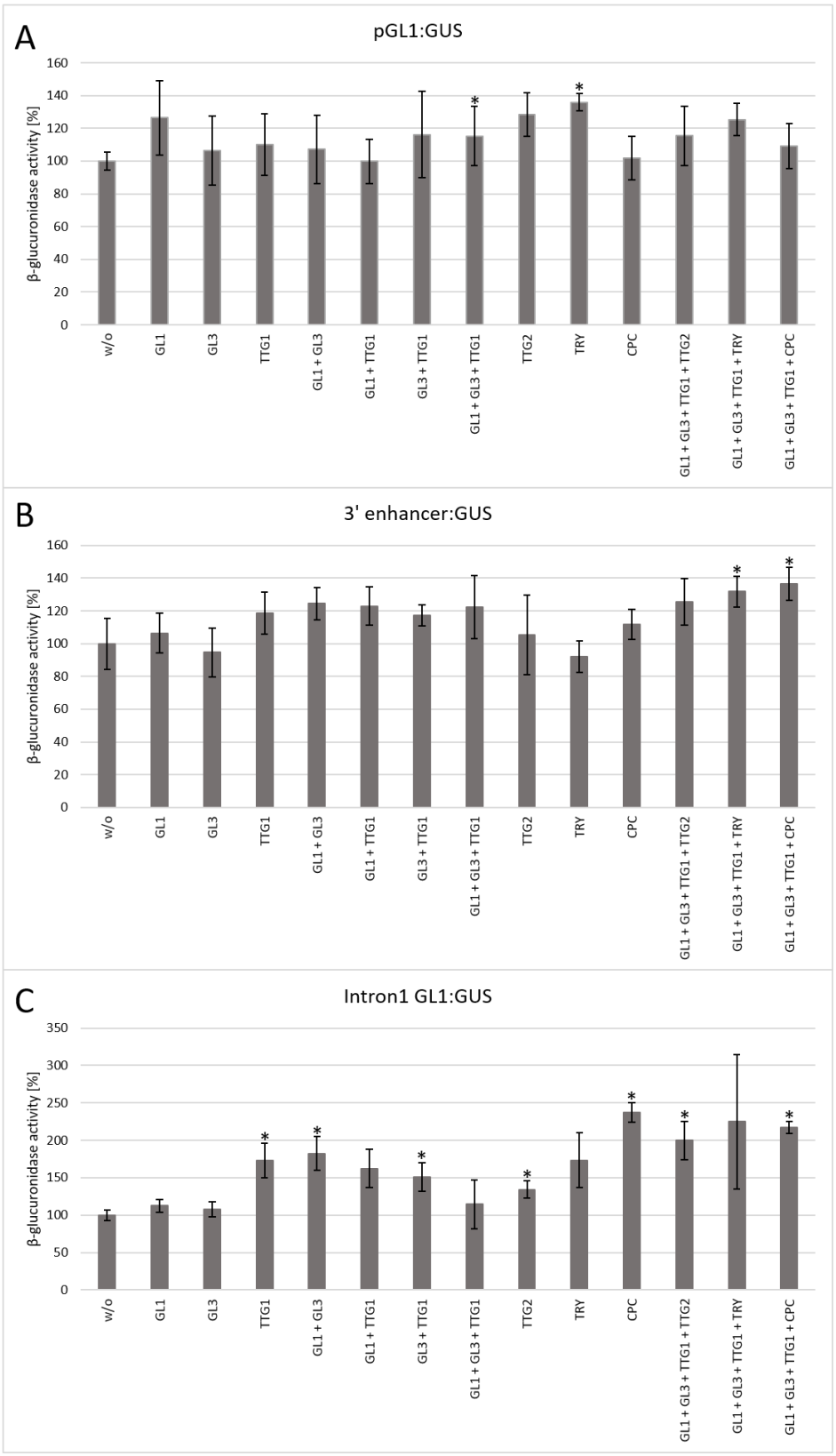

Figure 29. Quantitative GUS assay of regulatory single sequences associated with *GL1* expression. Bar graph depicting the mean β-glucuronidase activity in percent normalized to the promoter construct without co-expression (left bar). The reporter constructs examined were *pGL1:GUS* (A), *3' enhancer:GUS* (B), and *intron1 GL1:GUS* (C) with different *p35S* constructs expressing the trichome patterning genes listed at the x-axis of the graph. Error bars depict standard deviations. Statistical analysis was performed by Student's t-tests. Statistically significant differences towards the reference (w/o) are indicated by asterisks ($p \leq 0.05$).

Additionally to the 3' enhancer sequence, the short 3' enhancer box proposed by Larkin and colleagues was tested in transactivation assays (Figure 30 A). The 3' enhancer box was similarly inducible as the longer enhancer fragment. Only some combinations induced a significantly different promoter activity, although the increase never surpassed 140%. *TTG1* co-expression led to a slight but significant increase in activity to around 120%, neither *GL1* nor *GL3* co-expression significantly changed the promoter activity. Even the combined expression of *GL1* with *GL3* and *GL3* with *TTG1* did not cause significant changes. However, the co-expression of *GL1* and *TTG1* increased the reporter gene activity significantly to 120%, which is similar to the change caused by TTG1 alone. The three core activators did not change the promoter activity significantly. On the other hand, the co-expression of either *TTG2*, *TRY,* or *CPC* led to significant increases in activity. The most drastic change, up to 140%, was caused by *TRY* and *TTG2* addition, whereas *CPC* addition only caused an increase to 120%. Finally, only the co-expression of *TTG2* with the three core activators increased the promoter activity significantly, *TRY* and *CPC* did not.

Also, combinations of the four regulatory sequences were examined in transactivation assays. The 3' enhancer from Wang and colleagues was situated in front of *pGL1* (Figure 30 B). Interestingly, the combination of 3' enhancer and *pGL1* led to distinct and high increases in reporter activity. Several combinations did not change the promoter activity, i.e., the co-expression of *GL1*, *TTG1*, *TTG2*, *TRY*, and CPC alone, as well as *GL1* together with *TTG1*. However, the co-expression of *GL3* alone increased the promoter activity significantly to 250%. Also, the combinations containing *GL3* (*GL1* and *GL3*, *GL3* and *TTG1*, as well as *GL1*, *GL3,* and *TTG1* together) significantly increased the activity to around 330-350%. Even though the co-expression of *TTG2* alone did not induce any changes in promoter activity, co-expressed with the three core activators, the reporter activity increased significantly to approximately 440%. Interestingly, the co-expression of either *TRY* or *CPC* with the core activators seems to counteract their activation potential. The co-expression of the core activators with TRY and CPC led to a significant increase in reporter activity. However, this activity was lower than when the inhibitors were not additionally co-expressed.

Furthermore, *pGL1* with intron1 was tested in transactivation assays (Figure 30 C). Overall the changes in reporter activity were not as drastic as for the combination 3' enhancer and *pGL1*. Moreover, some statistically significant decreases in promoter activity were observed. The co-expression of any single trichome patterning gene did not cause significant changes in promoter activity. However, the co-expression of *GL1* with *TTG1* and the co-expression of all three core activators caused a significant decrease in promoter activity, 85% and 70 %, respectively. Also, the co-expression of the core activators with either *TRY* or *CPC* decreased the reporter gene activity significantly. A reduction of

more than half the promoter activity of the control was observed. These results are strikingly different compared to all other combinations examined so far.

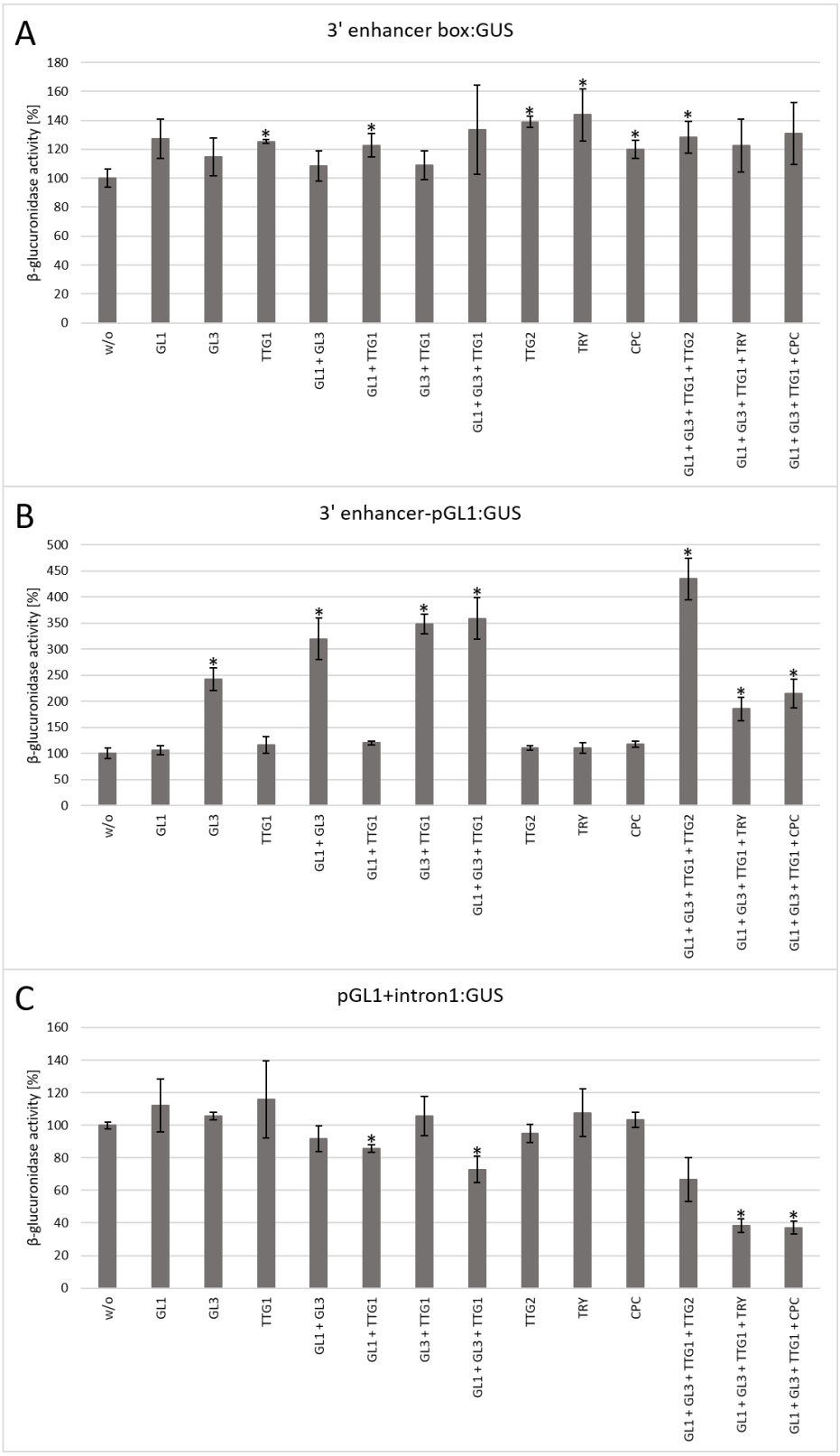

Figure 30. Quantitative GUS assay of regulatory single and combined sequences associated with *GL1* expression. Bar graph depicting the mean β-glucuronidase activity in percent normalized to the promoter construct without co-expression (left bar). The reporter constructs examined were *3' enhancer box:GUS* (A), *3' enhancer-pGL1:GUS* (B) and pGL1+*intron1:GUS* (C) with

different *p35S* constructs expressing the trichome patterning genes listed at the x-axis of the graph. Error bars depict standard deviations. Statistical analysis was performed by Student's t-tests. Statistically significant differences towards the reference (w/o) are indicated by asterisks (p≤0.05).

Two additional arrangements were tested regarding the endogenous position of intron 1. The constructs tested so far artificially placed intron1 directly after *pGL1*. The following two constructs were designed to guarantee intact splicing sites and codon integrity as well as the endogenous placement of the intron flanked by the exons (Reddy, 2007; Shang et al., 2017). The first construct contained *pGL1-Ex1-In1-Ex2(11bp),* and several trichome patterning genes induced a reporter gene activity change (Figure 31, A). Interestingly, the co-expression of GL1, GL3, or *TTG1* alone did not cause differences in reporter activity. However, the co-expression of any combination of these core activators caused a significant increase in promoter activity to a similar degree (around 130-140%). Co-expression of single *TTG2*, *TRY*, or CPC increased the promoter activity significantly and to a slightly higher degree than the core activators. Even combined with the core activators, all three genes caused a significant increase in reporter activity.

The upstream placement of the 3' enhancer did not really change the promoter activity drastically (Figure 31 B). Overall the induced activity changes were in the same range as without the enhancer.

In this assay, the addition of *GL1* and *TTG1* both induced significantly more reporter activity (over 130%), but the co-expression of *GL3* or *CPC* did not lead to any changes. Also, the co-expression of *GL1* with *GL3*, as well as GL1 with TTG1, did not change the promoter activity significantly. However, co-expressing *GL3* and *TTG1*, as well as all three core activators, increased the promoter activity significantly. The addition of *TTG2* and *TRY*, as well as their co-expression with the core activators, led to a significant increase in promoter activity. This was different for the single and combined expression of *CPC*.

As a final construct, the 3' enhancer was placed upstream of pGL1+intron 1, and transactivation assays were performed (Figure 31 C). In these assays, *GL1* and *TTG1*, alone or co-expressed, did not cause any differences in promoter activity. However, the addition of *GL3*, alone or in combination with *GL1* and *TTG1*, increased the reporter activity significantly. This effect was slightly more prominent when all three activators were co-expressed (190%). The co-expression of *TRY* or *CPC*, but not *TTG2*, increased the promoter activity to over 150%. If these three genes were co-expressed with the activator complex, a significant increase in promoter activity was observed. The induction caused by *TRY* or *CPC* combined with the three core activators was similar to their expression without other genes. However, the additional *TTG2* expression combined with *GL1*, *GL3*, and TTG1 led to a significant increase in promoter activity of 240%.

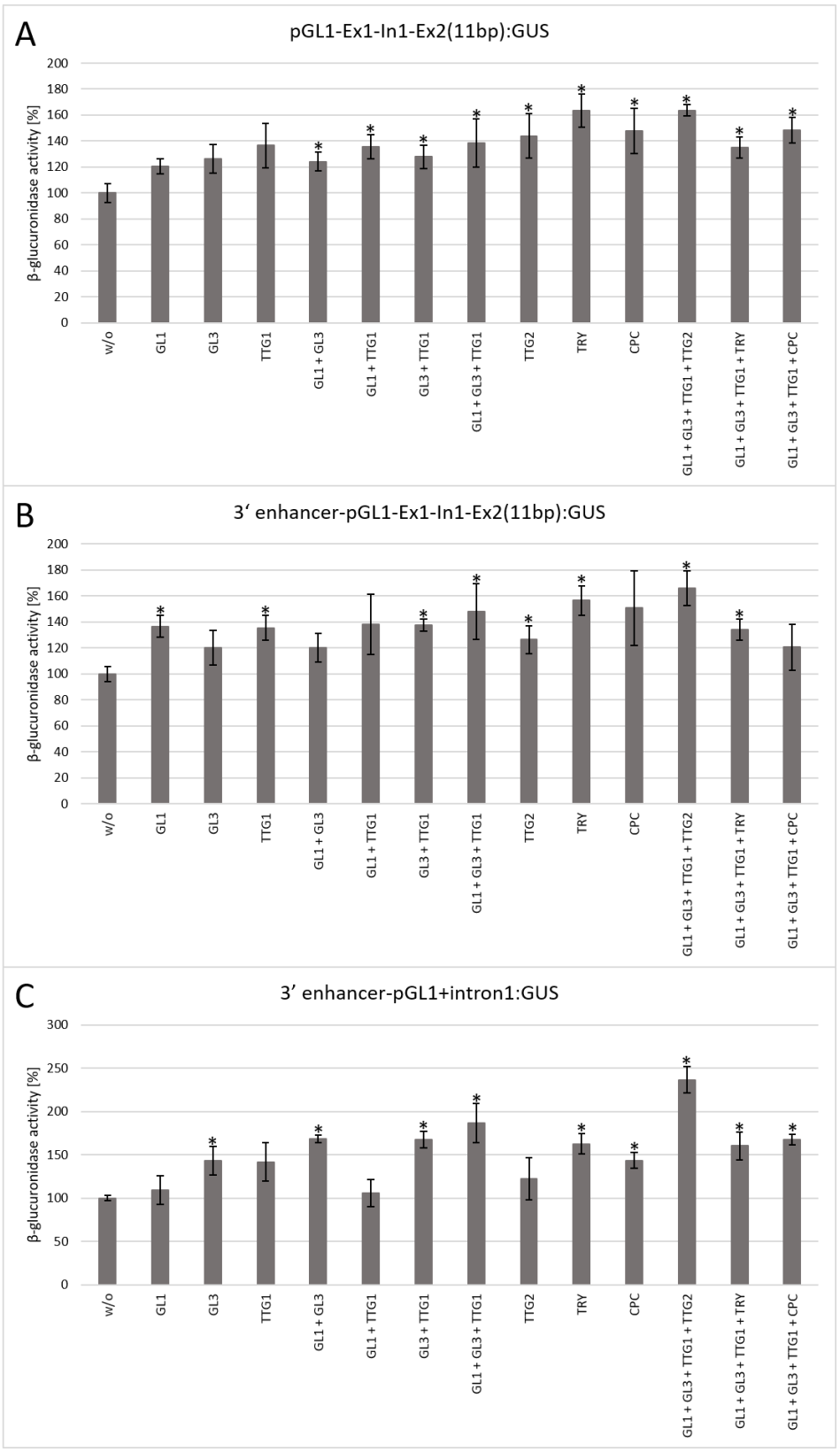

Figure 31. Quantitative GUS assay of combined regulatory sequences associated with *GL1* expression. Bar graph depicting the mean β-glucuronidase activity in percent normalized to the promoter construct without co-expression (left bar). The reporter constructs examined were *pGL1-Ex1-In1-Ex2(11bp):GUS* (A), *3’ enhancer-pGL1-Ex1-In1-Ex2(11bp):GUS* (B) and 3’ enhancer-pGL1+*intron1 GL1:GUS* (C) with different *p35S* constructs expressing the trichome patterning genes listed at the x-axis of the graph. Error bars depict standard deviations. Statistical analysis was performed by Student’s t-tests. Statistically significant differences towards the reference (w/o) are indicated by asterisks (p≤0.05).

3.2.2. Analysis of regulatory sequences of *GL3*

Another interesting promoter in the trichome patterning network is the promoter of *GL3* due to the central role GL3 plays in trichome patterning (Bernhardt et al., 2003, 2005; Zhang et al., 2003). Additionally, only for GL3 expression regulation a negative feedback loop was proposed (Morohashi et al., 2007). For phenotypic rescue of *gl3* plants, it was shown that a 1 kb 5' promoter fragment fused to the genomic *GL3* sequences was sufficient (Bernhardt et al., 2005). An in-depth analysis of the promoter, genomic region, and putative 3' enhancer region further revealed that the 3' enhancer region is not needed for *gl3 egl3* phenotype rescue (Friede et al., 2017). However, the expression of *GL3* CDS under the 1 kb 5' promoter region was not sufficient to rescue the *gl3 egl3* trichome phenotype. Analysis of the *GL3* introns revealed that the second intron seems to play a role in correct *GL3* expression and in rescuing trichome phenotypes of *gl3 egl3* mutants (Friede et al., 2017). Moreover, it was shown that the first 125 nucleotides of the second intron combined with the 1 kb promoter region were sufficient to rescue the trichome phenotype of the double mutant (Friede et al., 2017). In this study, the 1 kb promoter sequence, as well as the second intron, were analyzed regarding their cis-regulatory sequences by PLACE database query (Higo et al., 1999). Furthermore, quantitative GUS assays were performed to examine promoter regulation through various patterning proteins and the effect of specific CRE mutations on expression strength.

In-silico analysis of the promoter and second intron of GL3 regarding cis-regulatory elements

PLACE analysis revealed 249 cis-regulatory elements in the 989 bp of the GL3 promoter. Most motifs found were categorized as binding motifs (Figure 32). Out of the 100 binding motifs, 9 were MYB-related (S000408, S000176, S000409, S000180), 8 were MYC-related (S000409), and 3 were similar to the ASF-1 binding site in the CaMV promoter (S000024). A high number of core sites required for Dof (DNA-binding with one finger) binding were identified (S000265). A high number of core sites required for Dof (DNA-binding with one finger) binding were identified (S000498). Interestingly, also one binding site associated with homeodomain transcription factors was detected (Luo et al., 2005). The MYC-binding sites cluster at around 750 bp of the promoter sequence. Additionally, W-boxes (WRKY binding sites) were identified (S000390, S000447, S000442, S000457). For organ-specific motifs, pollen-specific elements dominate with 19 out of 37 detected motifs. Five TATA boxes were found from nucleotide 532 on (S000203, S000110, S000109). Interestingly, none were found at the N-term of the promoter. Hormone-related motifs were dominated by cytokinin-associates CREs (14 out of 16). The other two motifs are GA- and ABA-associated (S000298, S000174). Three poly(A) signals and no splice junction motifs were identified. 27 CREs associated with disease and stress responses were found. The majority was pathogen- and salt-stress-related, as well as linked to copper and oxygen

stress (S000468, S000453, S000493, S000259). Only one CRE was identified that is regulated through temperature change responses, namely a CCAAT box found in promoters of heat shock genes (S000030). 18 Light-related CREs were also identified, of which some motifs are associated with phytochrome-regulated gene expression (S000198 specific regulation, S000362, S000415). Interestingly, five S/MAR were identified in the promoter sequence (S000067). One cluster is situated at 145 bp and the other two at 682 bp and 711 bp, respectively. 26 motifs were categorized as general promoter elements, with the majority categorized as CAAT consensus sequence (S000028) and promoter elements found in *A. rhizogenes* (S000098). As nutrient-related motifs, two different putative nodulin consensus sequences were identified (S000461, S000462).

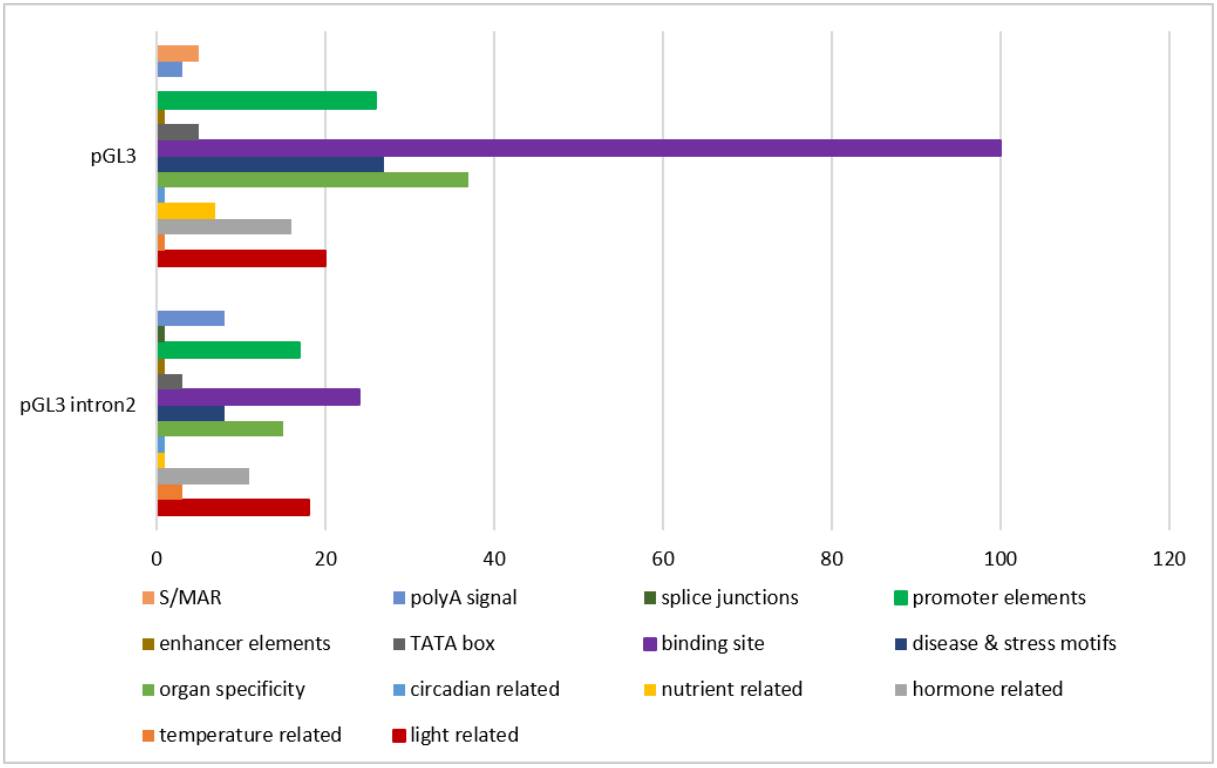

Figure 32. PLACE analysis of pGL3 and second intron. Bar graph depicting the number of CREs of each category found in the promoter sequences of *pGL3* and the second intron of *GL3*. Categories are listed at the bottom of the graph with the corresponding color code.

The second intron of GL3 consists of 579 bp, and 111 CREs were identified via PLACE analysis. In the second intron, fewer binding sites were identified, only 24 out of the 111 motifs. The majority of those binding sites are associated with Dof proteins (S000265). Two motifs are binding sites for homeodomain TFs (S000498). The other binding sites are MYC- or MYB-binding sites, GATA boxes (binding sites for GATA TFs), and W-boxes (S000167, S000408, S000436, S000314, S000039, S000390, S000447). The spatial distribution of these binding motifs is illustrated in Figure 33. Only one circadian and one nutrient-related motif were identified (S000252, S000461). Interestingly, 8 poly(A)-signals (S000080, S000088, S000081) and one splice junction were identified (000086). All three identified

temperature-associated motifs are heat shock-related (S000030, S000506, S000153). A different variety of hormone-related motifs was identified. Some were GA-related (S000181, S000439, S000298). One was identified as an ABA-responsive element (S000402) and one was related to jasmonate production (S000458), as well as six cytokinin-related CREs (S000454). Interestingly, three TATA-boxes were identified at 284-400 bp (S000203, S000110). In total, 15 organ-specific CREs were identified via PLACE analysis. The majority was associated with mesophyll-expression modules and pollen-specific elements (S000245, S000449). Lastly, 17 CREs categorized as promoter elements were identified. The elements were found in promoters of tobacco, *A. rhizogenes,* and several bacteria (S000098, S000070, S000400, S000477, S000387, S000478, S000479, S000395). Four motifs were CAAT promoter consensus sequences (S000028).

The analysis of the second intron of GL3 revealed that the N-terminal part of the intron is needed for rescue ability of GL3 sequences (Friede et al., 2017). Therefore, the N-terminal part of intron 2 was examined regarding binding sites that could alter the expression. Interestingly, all MYB-binding sites were located at the C-terminal part of the intron. Two W-boxes were found in the N-terminal part. This was intriguing, as W-boxes are WRKY-TF binding sites (Eulgem et al., 2000). A WRKY transcription factor that is known to influence the expression of *TRY*, *CPC,* and *GL2* via W-box binding is TRANSPARENT TESTA GLABRA2 (TTG2; Ishida et al., 2007; Pesch et al., 2014). TTG2 plays a role in seed coat mucilage production, seed coat tannin production, and trichome patterning as a downstream gene together with GL2 (Johnson et al., 2002). Interestingly, *TTG2* itself is regulated by WER, GL1, and TTG1 (Ishida et al., 2007). Additionally, TTG2 is involved in the shaping of trichomes by regulating the actin cytoskeleton (Liu et al., 2024). This makes TTG2 and the W-boxes promising candidates for specific *GL3* expression regulation.

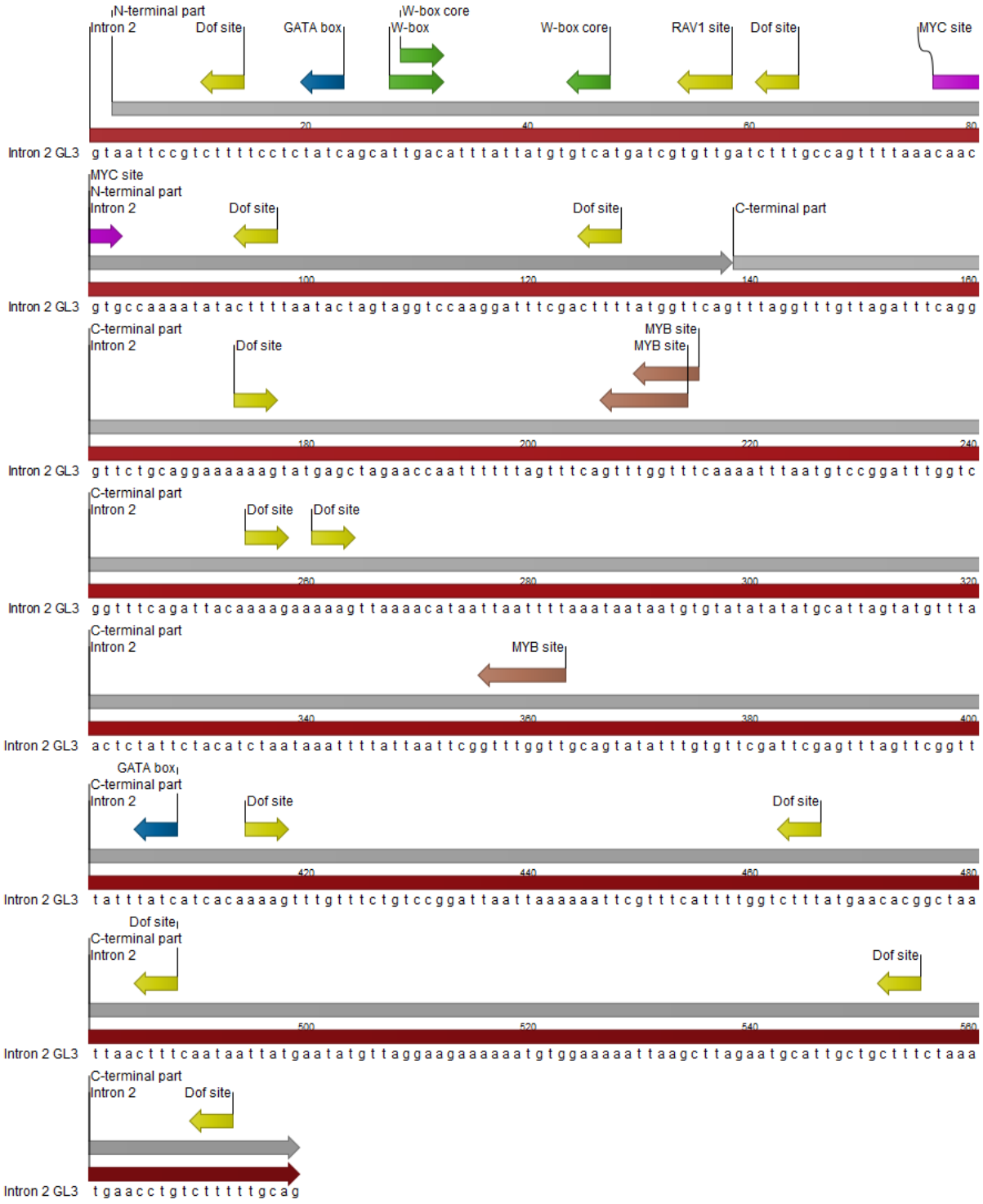

Figure 33. Binding sites detected in intron 2 of *GL3* via PLACE analysis. The nucleotide sequences of intron 2 of GL3 is illustrated in 5' to 3' direction (red arrow), the defined N- and C-terminal part are illustrated as grey arrows. Binding sites are depicted as arrows, the arrow head indicates the motif direction (left = on minus strand, right = on plus strand). Different binding sites are color coded: Dof & RAV1 binding site (yellow; S000265, S000314), GATA box (blue; S000039), MYB site (brown; S000408, S000167), W-box (green; S000390, S000447) and MYC-binding site (purple; S000436).

Transactivation assays of regulatory sequences of GL3 and the influence of mutated W-boxes

To assess the differential regulation of the 989 bp promoter of *GL3* alone and in combination with different intron 2 versions, quantitative GUS assays in dark-grown cell suspension culture of *A. thaliana* were performed. The promoter was tested alone or in combination with the full-length second intron. The same sequence areas as used for successful trichome phenotype rescue were used (Friede et al., 2017). This included exon 1 and 2, as well as 10 bp of exon 3 to guarantee intact splicing sites and codon integrity (Reddy, 2007; Shang et al., 2017). In the N-terminal part of intron 2 (nucleotides 1 to 138, respective to the intron start) both W-boxes were mutated according to published experiments (Eulgem et al., 1999; Pesch et al., 2014). To each reporter construct, different combinations of trichome patterning genes under the control of the p35S promoter were added.

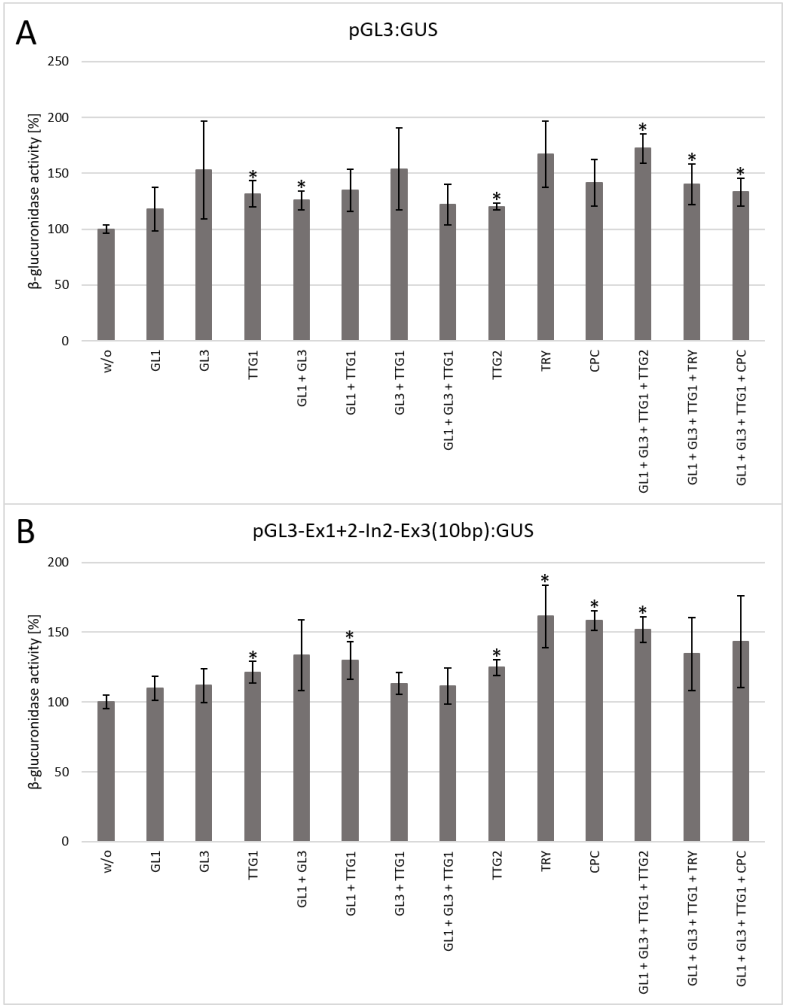

Figure 34. Quantitative GUS assays of pGL3 activity with or without full-length intron 2. A) Bar graph depicting the mean β-glucuronidase activity in percent normalized to the promoter construct without further *p35S* constructs expressing other genes (left bar). The promoter construct used was *pGL3:GUS* with different *p35S* constructs expressing the trichome patterning genes listed at the x-axis of the graph. B) Bar graph depicting the mean β-glucuronidase activity in percent normalized to the promoter construct without added *p35S* constructs (left bar). The promoter construct used was *pGL3-Ex1+2-In2-Ex3(10bp):GUS* with different *p35S* constructs expressing the trichome patterning genes listed at the x-axis of the graph. Error bars depict standard deviations. Statistical analysis was performed by Student's t-tests. Statistically significant differences towards the reference (w/o) are indicated by asterisks ($p \leq 0.05$).

The addition of almost any single activator led to an increase in reporter gene expression under the control of *pGL3* (Figure 34, A). However, this increase was only statistically significant for the addition of TTG1, which led to an increase of approximately 40 %. If two or even all three examined activators, *GL1*, *GL3,* and *TTG1*, were co-expressed with the reporter construct, no drastic changes could be examined in most cases. However, the simultaneous addition of GL1 with GL3 was the only combination causing a statistically significant effect. The single addition of the inhibitors TRY or CPC did not seem to influence *pGL3* expression strength. Interestingly, the co-expression of TTG2 led to a significant increase in reporter gene activity. If all three core activators and TRY, CPC, or TTG2 were co-expressed, the reporter gene activity was significantly increased. The strongest increase was caused by TTG2 addition. However, in general the increase in reporter gene activity was only up to around 50%. Overall, the addition of any patterning gene caused a slight increase in expression, but only some were statistically relevant.

This same general pattern of expression was also observed for the reporter constructs containing the full-length intron 2 additionally to *pGL3* (Figure 34, B). The expression increased only significantly if TTG1 was co-expressed. During this experimental setup, the co-expression of TTG1 with GL1 increased the expression significantly. But all those increases fluctuate around the same percentage range. Interestingly, the addition of TTG2, TRY, and CPC increased the expression significantly. However, upon co-expressing these genes with GL1, GL3, and TTG1, only TTG2 led to a significant increase in gene expression.

Furthermore, the reporter gene expression of the *GL3* promoter, together with the N-terminal part of intron 2, was examined (Figure 35, A). The same trends of expression changes were observed as for the full-length version. Interestingly, in all three different assays, the co-expression of GL1, GL3, and TTG1 led to a smaller increase in expression compared to the addition of TRY or CPC. The co-expression of TTG2 with the other three activators led to a similar increase in expression in all three assays. Expression changes were similar, but in the case of the N-terminal intron being present, they were more often statistically different.

Finally, the construct containing the two mutated W-boxes was tested regarding expression changes (Figure 35, B). Interestingly, the mutation of both W-boxes did not induce any differences compared to the expression of the non-mutated version. The same trends in expression alteration were observed as before, and even the increase range is similar. The only slight differences between all four assays are the statistically significant combinations per assay, but the tendencies and the overall range of expression was not altered. In conclusion, the W-boxes in the N-terminal part of intron 2 do not play a significant role in the expression regulation of *pGL3*.

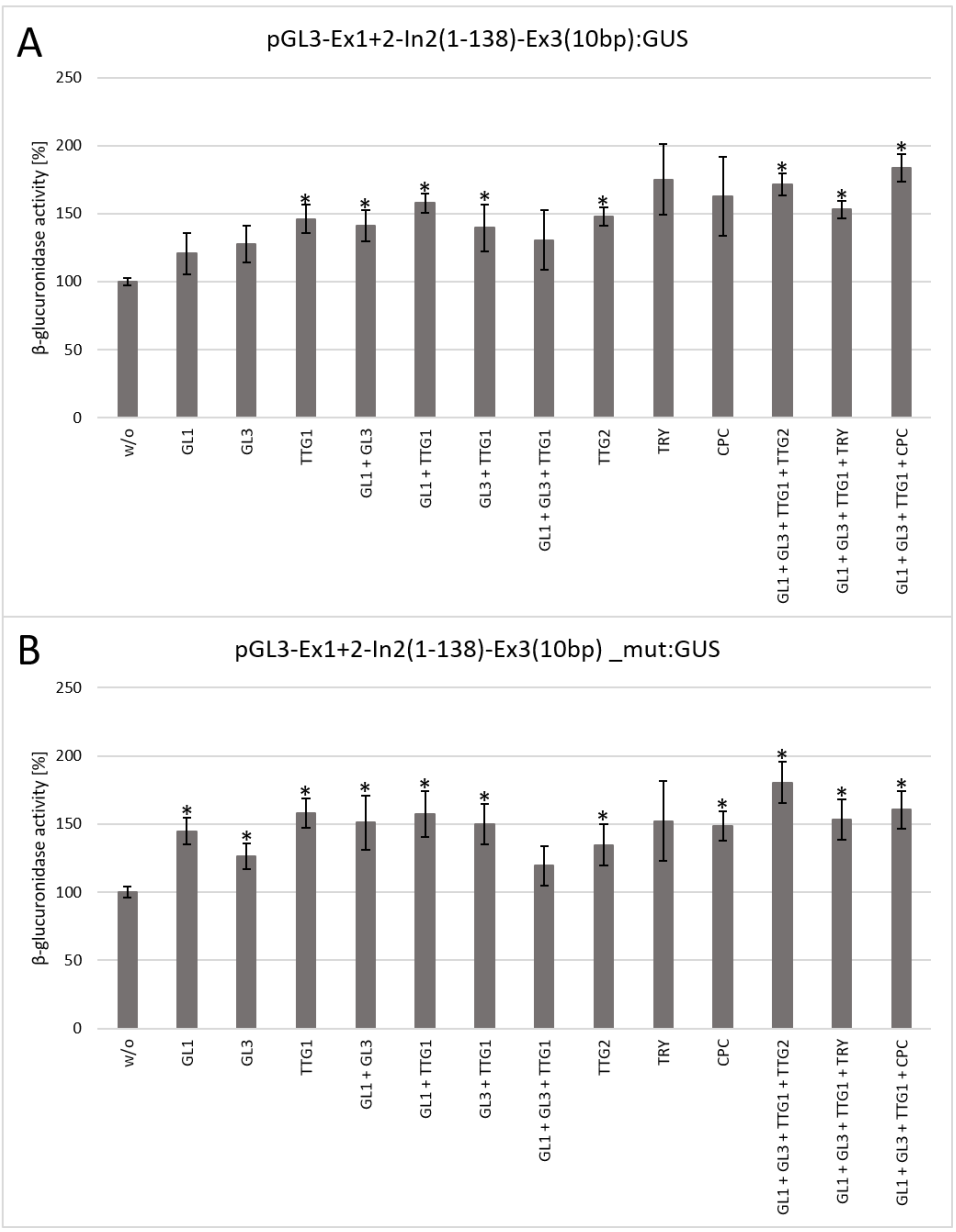

Figure 35. Quantitative GUS assays of pGL3 activity with different versions of the N-terminal part of intron 2. A) Bar graph depicting the mean β-glucuronidase activity in percent normalized to the promoter construct without further *p35S* constructs expressing other genes (left bar). The promoter construct used was *pGL3-Ex1+2-In2(1-138)-Ex3(10bp):GUS* with different *p35S* constructs expressing the trichome patterning genes listed at the x-axis of the graph. B) Bar graph depicting the mean β-glucuronidase activity in percent normalized to the promoter construct without added *p35S* constructs (left bar). The promoter construct used was *pGL3-Ex1+2-In2(1-138)-Ex3(10bp)_mut:GUS* with different *p35S* constructs expressing the trichome patterning genes listed at the x-axis of the graph. Error bars depict standard deviations. Statistical analysis was performed by Student's t-tests. Statistically significant differences towards the reference (w/o) are indicated by asterisks ($p \leq 0.05$).

3.2.3. Analysis of the 5' regulatory sequences of *ETC1*, *ETC2* and *ETC3*

The trichome patterning mechanism not only encompasses the regulation through activators, but also through inhibitors. These inhibitors are closely related and are all members of the same protein family, namely R3MYB proteins (Esch et al., 2004; Gan et al., 2011; Kirik et al., 2004a, b); Schellmann et al., 2007; Simon et al., 2007; Tominaga et al., 2008; Wada, 1997; Wang et al., 2007, 2008; Wester et al., 2009). Regulatory sequences and expression regulation were extensively analyzed for TRY and CPC (Pesch, 2005; Pesch et al., 2014; Pesch & Hülskamp, 2011). However, the closely related genes *ETC1*, *ETC2*, and ETC3 were not studied so far regarding different motifs in their promoter sequences.

Although the three genes are closely related, there are indications of distinct functions (Kirik et al., 2004a, b; Wester et al., 2009). Also, extensive expression data analysis revealed differences in the gene expression of *ETCs* in different mutant backgrounds (Pietsch, 2022). Additionally, *ETC1* and *ETC3* seem to be more closely related to each other and *CPC*. Whereas *ETC2* is more closely related to *TRY* (Simon et al., 2007)Therefore, in this study, the regulatory sequences of ETC1, ETC2, and ETC3 were examined regarding CREs, and quantitative GUS assays were performed to shed light on differences regarding expression regulation.

In-silico analysis of cis-regulatory elements of ETC1, ETC2, and ETC3 promoter regions

All three ETCs were analyzed via PLACE analysis regarding CREs in their promoter regions (Higo et al., 1999). Promoter regions were selected based on published work (Kirik et al., 2004a, b; Wester et al., 2009). For *ETC1*, the promoter region analyzed stretched from -1921 to -1, with respect to ATG of *ETC1*. The *ETC2* promoter encompassed the region from -1638 to -35, respective to gene start, and for *pETC3*, the region from -2372 to +17 was analyzed.

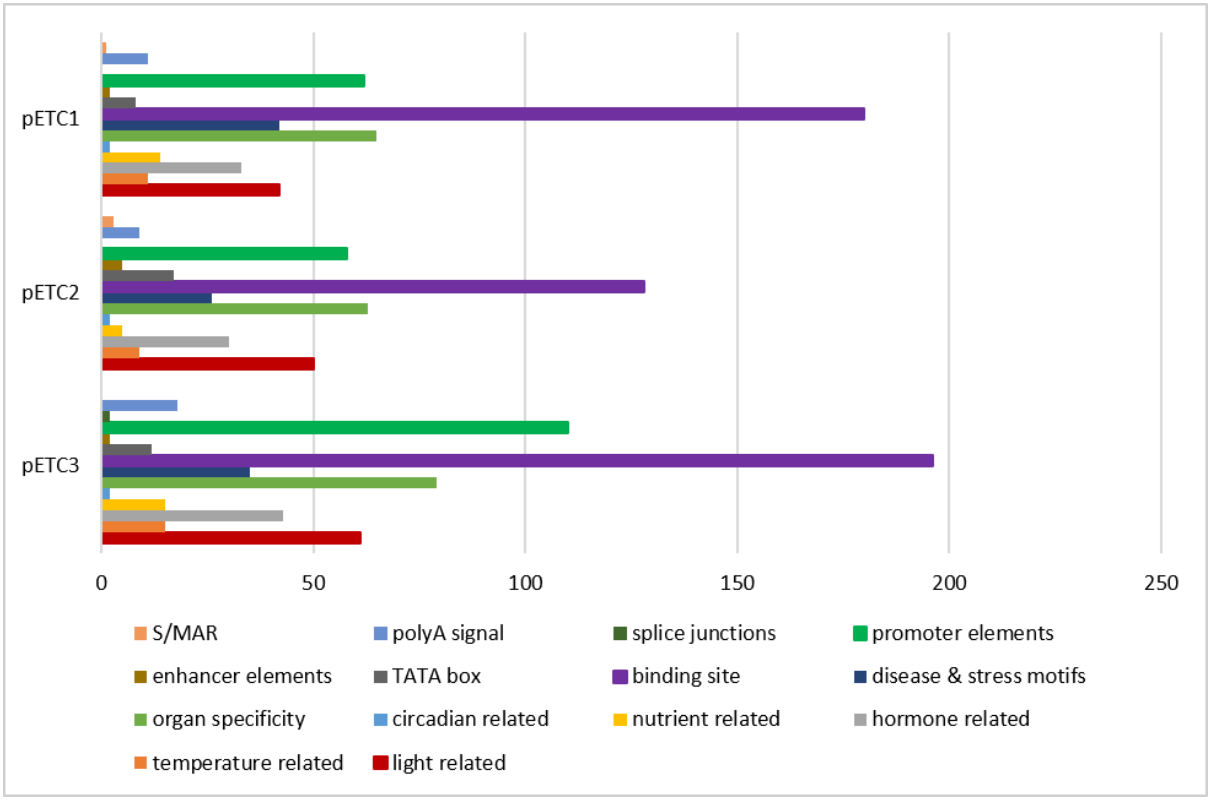

Figure 36. PLACE analysis of the promoter sequences of ETC1, ETC2, and ETC3. Bar graph depicting the number of CREs of each category found in the promoter sequences of ETC1 (-1921 to -1), ETC2 (-1638 to -35), and ETC3 (-2372 to +17). Categories are listed at the bottom of the graph with the corresponding color code.

In the 1921 bp promoter region analyzed for *ETC1* expression control, a total of 473 cis-regulatory elements were identified. The majority of elements were categorized as binding sites. Out of the 180 binding sites identified, 41 were Dof binding sites (S000265), and 44 were MYC binding sites (S000144, S000407), co-called E-boxes (S000144, S000407). The MYC-binding sites were dispersed over the whole promoter length, but they formed a cluster situated around 980-1080 bp. As WRKY-binding sides, 24 sequences were identified (S000390, S000447, S000457, S000442), and 11 were associated with HD-ZIP TF binding (000292, S000498, S000287). None of these motifs formed any significant clusters. Notably, some of the 10 identified MYB-binding sites (S000408, S000177, S000409, S000180) were in close proximity to MYC-binding sites. Additionally, 19 GATA-boxes were identified (S000039). Eight TATA-boxes were identified, located all over the promoter sequence (S000111, S000203, S000110, S000109). Altogether, 42 disease and stress motifs were identified. The majority was associated with copper and oxygen-related responses (S000493), followed by motifs associated with infected root nodules as well as pathogen- and salt-stress (S000468, S000453). Two circadian-related motifs were identified (S000252), and 14 were nutrient-related, with the majority being putative nodulin consensus sequences (S000462). In total, 65 motifs were identified as being associated with organ specificity. The CREs identified were mainly associated with pollen and mesophyll expression (S000378, S000245, S000449). However, two were endosperm-specific, and two were seed-specific

(S000353, S000264). Interestingly, 11 poly(A)-signal were found (S000080, S000088, S000081). 33 hormone-related CREs were identified in this analysis. They are either associated with ABA, cytokinin or GA processes (S000421, S000402, S000181; S000439, S000394, S000438, S000174, S000454). No splice junctions were identified and only one S/MAR (S000067). Interestingly, two enhancer elements were found (S000494). They are position at 678 bp and 1890 bp. Temperature-related motifs were also identified, in total 11. Eight were heat-shock element-related and three were low temperature responsive elements (S000030, S000506, S000250, S000153). Finally, 42 CREs were associated with light-related processed. The majority was associated with light-regulated gene expression or etiolation-induced expression (S000198, S000415, S000414, S000362).

In the 1604 pb of pETC2, in total, 405 CREs were identified. The majority of CREs are classified as binding sites. Out of the 128 sites 32 are associated with MYC-binding (S000144, S000407). They occurred more frequently in the region 130-440 bp. Two more clusters were identified around 878 bp and 1231 bp. GATA-boxes were again highly represented, with 16 CREs (S000039). Interestingly, 13 MYB-binding sites were identified (S000176, S000180, S000409, S000177, S000502) and only 2 HD-ZIP binding sites (S000498, S000292). The MYB-sites are dispersed over the whole promoter sequences, with two little clusters around 800 bp and 1000 bp. 9 poly(A)-signals were found, of which only one was located in the n-terminal promoter region. Two circadian-related motifs were found (S000252), and five nutrient-related putative nodule consensus sequences (S000461, S000462). A total of 63 organ-specific expression motifs were identified, with 34 classified as pollen-specific (S000245, S000378) and 20 mesophyll-related (S000449). Interestingly, three were root hair-specific (S000512), and three seed-specific (S000100, S000264). The same disease and stress motifs found in *pETC1* were also the most represented motifs of this category in *pETC2* (S000453, S000493). However, three motifs were identified as being associated with infection reaction responses (S000467) and four with water stress (S000497, S000413). 17 TATA-boxes were identified, most of them located from 960 bp on, with four located in the last 170 bp (S000340, S000111, S000203, S000110, S000109). A total of 58 promoter elements were found, with the majority being CAAT consensus sequences (S000028) and A-boxes/G-motifs (S000450). The other CREs were connected to motifs found in the promoters of *A. rhizogenes* and tobacco or in anaerobic gene promoters (S000098, S000395, S000477). 30 CREs found were associated with hormone signalling, 18 were classed as cytokinin-related (S000454). The rest was mainly GA-related (S000181, S000439, S000298, S000174). No splice junctions but three S/MAR were identified through analysis (S000067, S000064). In total, 50 light-related motifs were found, the majority being generally associated with light-regulated gene expression or etiolation-induced gene expression (S000198, S000415). Nine heat-related CREs were identified and two associated with cold

responses (S000030, S000506, S000250). Finally, five enhancer elements were identified, situated around 590 bp or from 1115-1483 bp (S000123, S000494, S000254).

The largest promoter sequence with 2389 bp and 590 identified CREs was the *ETC3* promoter. Again, the category containing the most identified motifs was the binding sites. In total 196 binding sites were identified. 42 were Dof-binding sites and 19 were GATA-boxes (S000039, S000265). As for MYB-binding sites, 33 were identified situated along the whole promoter sequence with a slight clustering around 2040-2080 bp (S000408, S000176, S000409, S000502, S000179). Also, 29 MYC-binding sites were identified (S000436, S000144, S000407). They are concentrated at around 1000 bp. Additionally, 21 W-boxes and 11 HD-ZIP binding sites were identified (S000390, S000447, S000442, S000457, S000292, S000498). Both are distributed equally over the promoter length. The typical circadian-related CREs were identified, as well as the putative nodulin consensus sequence (S000252, S000461, S000462). Interestingly, a motif associated with phosphate starvation was found (S000459). In total, 79 organ-specific motifs were identified. The majority, again, was pollen- and mesophyll-specific (S000245, S000378, S000449). Also, some seed/endosperm-related CREs were identified (S000353, S000148, S000264). 18 poly(A)-signals were found, with four situated from 1268-1426 bp and another cluster stretching from 1648 to 2201 bp (S000080, S000088, S000081). Out of the 35 disease and stress motifs, most were infection response-related or copper and oxygen-related (S000468, S000467, S000453, S000418, S000493). The identified 12 TATA-boxes were distributed along the whole sequence with a higher frequency towards the 3'-end of the promoter (S000203, S000110, S000109). A high amount of CREs found were classified as promoter elements. The majority was identified as CAAT consensus sequences of sequences associated with A*. rhizogenes* (S000028, S000098). A sequence absent from *pETC1* and *pETC2* was the quantitative activator region (QAR, S000244) found in *pETC3* at 1452 bp and 1595 bp. Again, the most of the 43 identified hormone-related CREs were cytokinin-related (S000454). Also, motifs involved in ABA, GA, ethylene and jasmonate-related processes were identified (S000181, S000402, S000439, S000458, S000394, S000438, S000037). Two splice junctions were found, one at the very beginning of the promoter sequence and one at 1396 bp (S000086). A total of 61 light-related motifs were identified. The majority was not further specified or etiolation-induced (S000383, S000198, S000415). Interestingly, one CRE was a phyA-repressed motif and some motifs were I-boxes (S000488, S000124). Temperature-related genes were mostly associated with heat responses, 12 out of the 15 CREs (S000030, S000506). Three CREs were associated with low-temperature responses and the vernalization pathway (S000153, S000404). Finally, two enhancer elements were identified, situated at 659 bp and 728 bp (S000123, S000494).

Transactivation assays of pETCs

Additionally to the *in-silico* analysis of the promoter regions of *ETC1*, *ETC2,* and *ETC3*, the same regions were examined regarding expression modulation by other trichome patterning genes (Figure 37). Therefore, quantitative GUS assays were performed using each promoter in a reporter construct expressing *β-glucuronidase*. To each reporter construct, different combinations of trichome patterning genes under the control of the *p35S* promoter were added. The reporter gene expression without any added gene was used to normalize the reporter gene activity.

The activity of the promoter of *ETC1* was increased upon co-expressing *GL1*, *GL3,* and *TTG1*. All three activators led to a significant increase in reporter gene activity to around 150% (Figure 37, A). Interestingly, the co-expression of *GL1* with *GL3*, as well as *GL3* and *TTG1,* led to a similar increase in promoter activity. However, the addition of *GL1* and *TTG1* led to a drastic increase in gene expression up to 250 %. If all three activators were co-expressed with the reporter construct, a similar significant increase was observed as for single activator addition. On the other hand, neither the single addition of *TTG1*, *TRY,* nor *CPC* led to a significant change in promoter activity. Also, if the three activators, *GL1*, *GL3*, and TTG1, were co-expressed with either TTG2, TRY, or *CPC*, no significant change in promoter activity could be observed.

Promoter activity assays of pETC2 showed a slightly different picture. Nearly no co-expressed trichome patterning gene, alone or together with others, led to a significant change in promoter activity (Figure 37, B). However, if the core activators were co-expressed with either *TRY* or *CPC*, the promoter activity increased significantly compared to the control, up to 180%.

Lastly, the promoter of *ETC3* was examined (Figure 37, C). Here, as well as for *pETC2*, only a low number of combinations caused a significant difference in promoter activity compared to the control. Interestingly, only the addition of *TTG1* led to an increase in promoter activity, up to 160%. All other combinations did not change the promoter activity significantly.

To summarize the quantitative GUS assays of the *ETC* promoter regions, it can be said that overall, these promoters seem to be not strongly regulated by the examined trichome patterning proteins. *ETC1* seems to be more susceptible to regulation via the examined proteins; however, these proteins did not cause extreme promoter activity changes, except TTG1. As for *ETC2* and *ETC3*, both promoter regions were not influenced by the examined proteins.

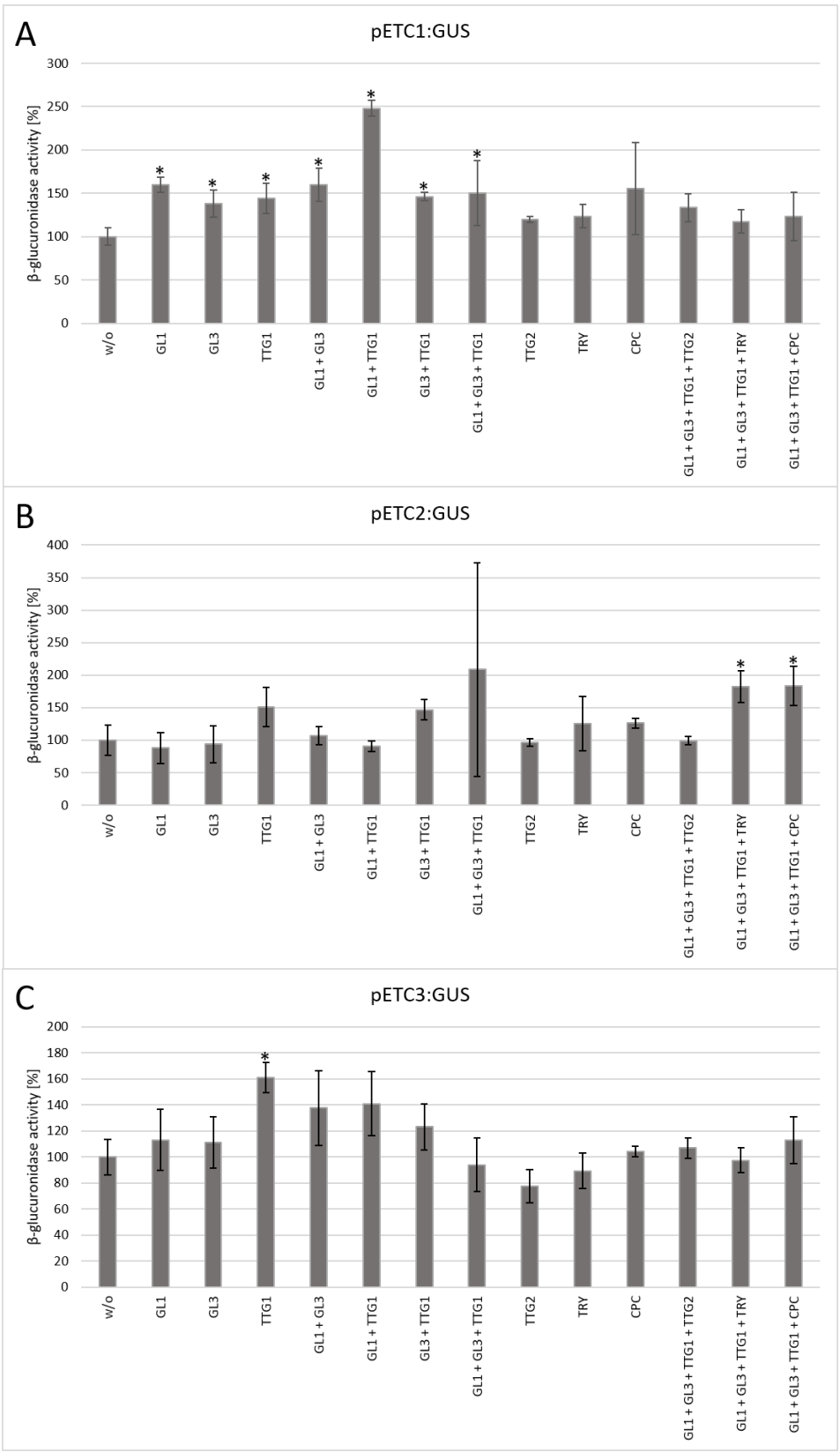

Figure 37. Quantitative GUS assays of *ETC1-3* promoter activity. Bar graph depicting the mean β-glucuronidase activity in percent normalized to the promoter construct without further *p35S* constructs expressing other genes (left bar). The promoter constructs examined were *pETC1:GUS* (A), *pETC2:GUS* (B), and pETC3 (C), with different *p35S* constructs expressing the trichome patterning genes listed at the x-axis of the graph. Error bars depict standard deviations. Statistical analysis was performed by Student's t-tests. Statistically significant differences towards the reference (w/o) are indicated by asterisks ($p \leq 0.05$).

3.3. Interspecies comparison of trichome and root hair patterning MYBs

Different studies in a variety of species indicate the conservation of genes involved in trichome patterning, specifically homeodomain TFs, MYB, and bHLH transcription factors (Chalvin et al., 2020; Han et al., 2022; Schuurink & Tissier, 2020; Wang et al., 2022). In this study, an interspecies comparison of the trichome and root hair patterning R2R3MYBs *GL1*, *MYB23,* and *WER* of *Arabidopsis* and *Cardamine* has been conducted.

In *Arabidopsis*, *GL1* is not expressed in roots but plays a major role in trichome patterning (Hülskamp et al., 1994). *MYB23* is expressed in trichomes and roots, *GL1* only in trichomes, and *WER* only in roots (Hülskamp et al., 1994; Kirik et al., 2001; Lee & Schiefelbein, 1999). Therefore, WER takes over the role of GL1 in forming the MBW complex in roots. In *Arabidopsis*, all three genes are closely related and contain a conserved motif at their C-term in the putative transcription activation domain, which consists of 19 amino acids (Lee & Schiefelbein, 2001). MYB23 and GL1 are very similar in their genetic function, as both promote trichome fate (Kirik et al., 2005; Oppenheimer et al., 1991). However, GL1 plays a role in trichome initiation all over the leaf surface, and MYB23 predominantly at the leaf edges. Also, MYB23 plays a role in trichome branching, which GL1 does not. Interestingly, *MYB23* and *GL1* are redundant and can rescue the phenotype of each other when expressed under the appropriate promoter. *MYB23* expressed under *pGL1* in *gl1* can rescue the phenotype but not when its expression is controlled by its own promoter. This indicates that their specific functions are not due to different protein behavior but different expression properties provided by their promoter and enhancer regions (Kirik et al., 2005). This is also true for comparing GL1 and WER (Lee & Schiefelbein, 2001) and MYB23 and WER (Tominaga-Wada et al., 2012).

A previous study examined the expression levels of the trichome patterning genes R2R3MYBs *GL1*, *MYB23,* and *WER* in different tissues of *Arabidopsis*, *Arabis*, and *Cardamine* (Pietsch, 2022). This analysis revealed an overall low expression of *ChGL1* in all examined tissues. This is very interesting, as a correlation between trichome number and ChGL1 transcript amount was postulated (Fuster-Pons et al., 2024). In contrast, *ChWER* was expressed highly in roots and tiny leaves (Pietsch, 2022), indicating a more pronounced role of *ChWER* in trichome patterning than of *AtWER*. *ChMYB23* was higher expressed in tiny and mature leaves than in seedling, shoot and root (Pietsch, 2022). In Arabis, AaWER was expressed very low compared to the housekeeping gene in nearly every examined tissue, except roots. *AaGL1* was also expressed rather low, except in tiny leaves. *AaWER* and *AaGL1* were extremely low expressed in mature leaves. *AaMYB23* was the only gene that shows increased expression in seedling and shoot (Pietsch, 2022). In Arabidopsis *AtGL1* was higher expressed in seedling and shoot, compared to tiny leaves. It could not be detected in mature leaves or roots. *AtWER* was only expressed

higher in roots. Elevated expression levels for *AtMYB23* were detected in seedling, shoot and mature leaves. In roots *AtMYB23* expression was decreased (Pietsch, 2022).

3.3.1. *In-silico* analysis & comparison of MYBs in *Arabidopsis* and *Cardamine*

All six MYBs are highly similar in their intron-exon structure and their protein structure. The alignments of all six proteins can be found in the appendix (Figure 49).

The proteins share a high percent identity between species, AtGL1 and ChGL1 75.78%, AtMYB23 and ChMYB23 87.16% and AtWER and ChWER 91.14%. A phylogenetic tree was created using the protein sequence alignment created by CLC Main Workbench 22 (Figure 38). In this tree, the GL1, MYB23 and WER proteins are more closely related to their counterparts in the other species than to each other. Interestingly, the two WER proteins diverged from GL1 and MYB23 before the latter two branched off. Regarding their genetic change, ChMYB23 underwent more nucleotide substitutions compared to its *Arabidopsis* counterpart than ChGL1 and ChWER.

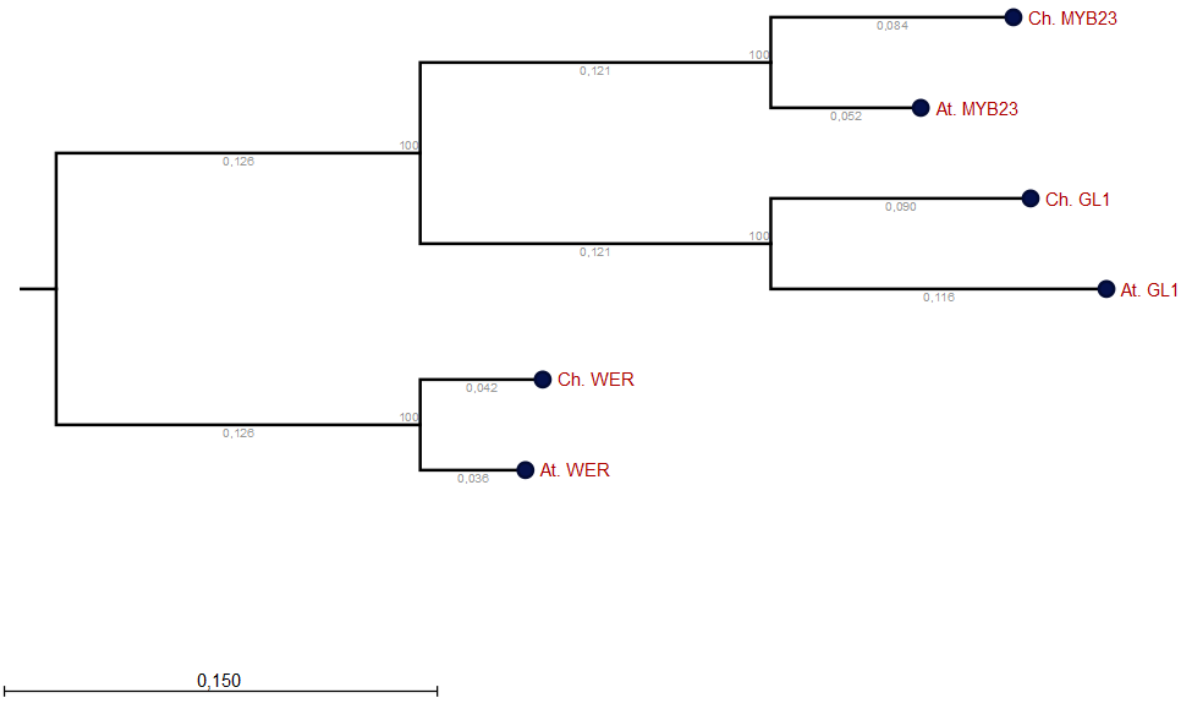

Figure 38. Phylogenetic tree of Arabidopsis & Cardamine MYB protein sequences. Numbers on branches reflect the genetic change in the form of nucleotide substitutions per site, the numbers on internal nodes display the support for the node calculated by bootstrap analysis of 100 replicates.

Due to the high similarity of the proteins of the two species, the potential influence of intron 1 on the expression regulation was examined further by performing PLACE analysis (Figure 40) and sequence alignment of all six first introns (Figure 39). The introns of the orthologous genes are similar in size for *GL1* and *MYB23*. The first intron in *ChWER* is the longest intron (385 bp) followed by *AtWER* (264 bp).

The introns of *AtMYB23* (129 bp) and *ChMYB23* (133 bp), as well as *AtGL1* (109 bp) and *ChGL1* (110 bp) are very similar in size.

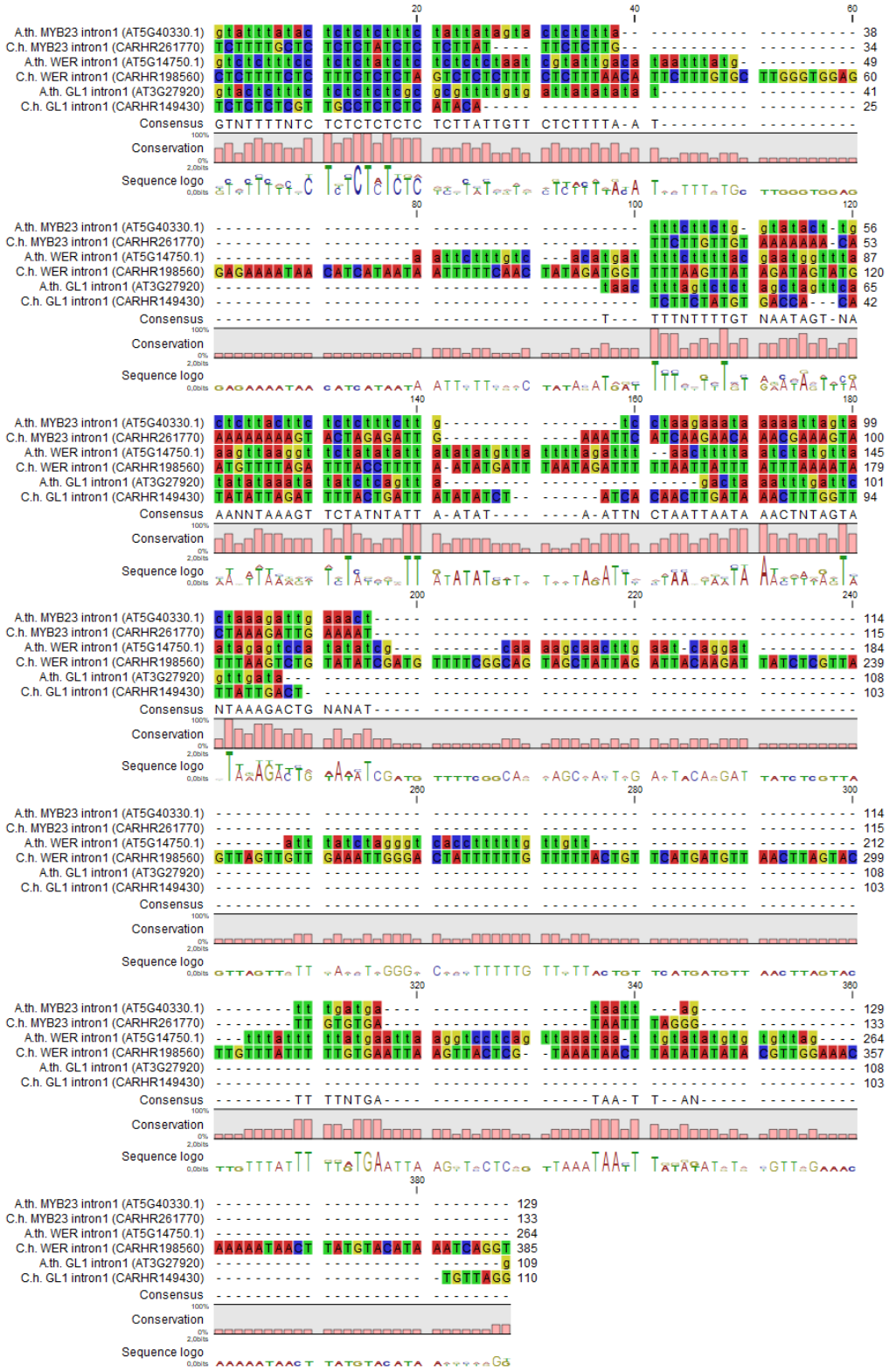

Figure 39. Sequence alignment of the first intron in the MYBs *GL1*, *MYB23* and *WER* from *A. thaliana* & *C. hirsuta*. The sequence name is given left, the nucleotide number right. Similar nucleotides are displayed by different sized letters at the bottom of each row at each given nucleotide position. Alignment was created using CLC DNA Main Workbench 22.

Interestingly, the six introns share some similarity in several regions. The N-term of all introns seems conserved, as well as the sequences corresponding to the intron area at 110 bp to 200 bp of *ChWER*.

3.3.2. The MYB introns display differences regarding CREs

Additionally, PLACE analysis of the first intron of all six MYB was conducted. For *GL1* and maybe *WER* a role in gene expression was proposed for the first intron (Wang et al., 2004). In the first introns of *AtGL1*, *AtMYB23*, and *AtWER*, a total of 31, 42, and 69 CREs were found, respectively. A comparable number was found for the introns in *ChGL1*, *ChMYB23*, and *ChWER* (29, 37, and 88, respectively). As the MYBs share the highest similarity with their corresponding orthologs, the PLACE analysis will be discussed between species (Figure 40).

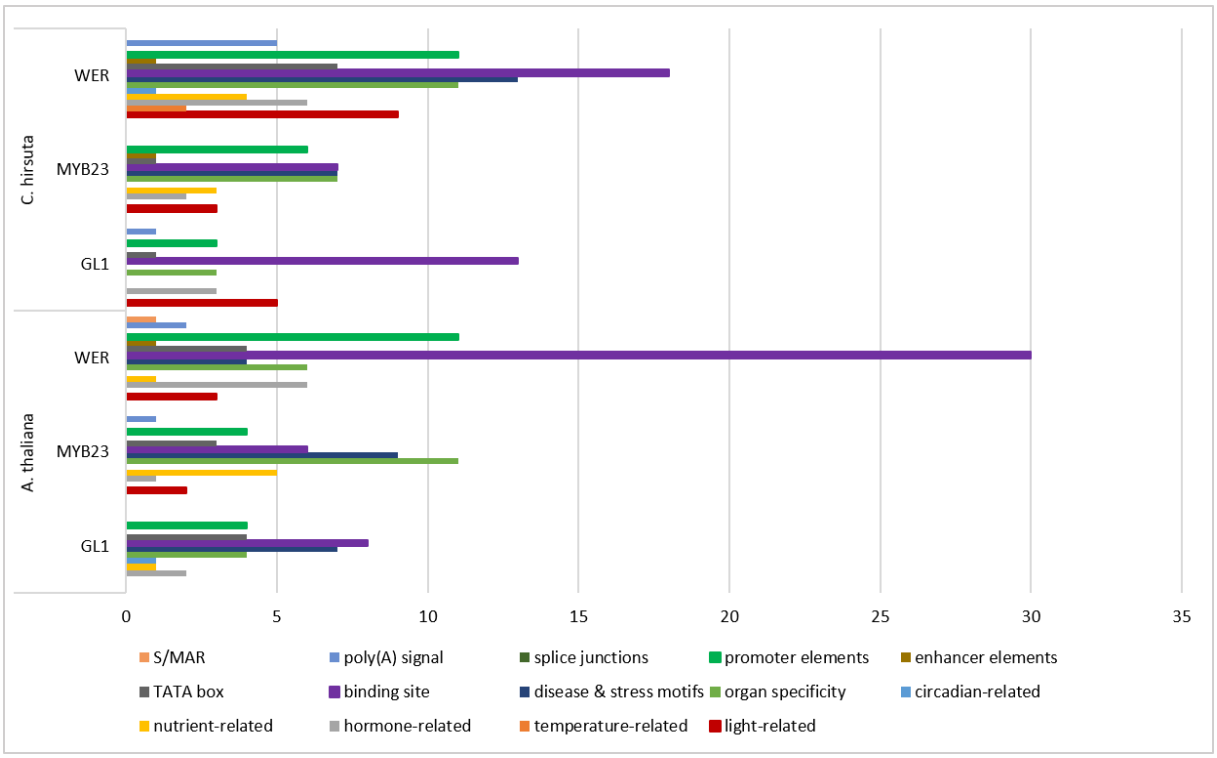

Figure 40. PLACE analysis of first introns of MYBs in *A. thaliana* & *C. hirsuta*. Bar graph depicting the number of CREs of each category found in the first introns of the R2R3MYB transcription factors *GL1*, *MYB23* & *WER* from *A. thaliana* and *C. hirsuta*. Categories are listed at the bottom of the graph with the corresponding color code.

In the *AtGL1* intron, most CREs were identified as binding sites or disease and stress-related. Two of the binding sites are Dof-binding sites (S000265), and one is identified as a SEF1 binding motif from soybean (S000006). No binding motifs associated with WRKY, HD-Zip, or MYC binding were found. Interestingly, three MYB-binding motifs were identified (S000177, S000409, S000176), situated at 81 bp. These motifs were flanked by the two identified GATA boxes (S000039) at 76 bp and 105 bp. The identified disease and response elements were associated with infected root modules, copper and oxygen stress, as well as Ca-responsive elements (S000468, S000507, S000493, S000499, S000501). One circadian-related CRE (S000440), as well as one nutrient-related motif associated with nodulin

(S000462), were found. No motifs were found in the categories Poly(A) signal, splice junction, S/MAR, enhancer elements, temperature- or light-related. Organ-specific elements were predominantly pollen-specific (S000245, S000378). The two hormone-related CREs are associated with cytokinin (S000454). Interestingly, 4 TATA boxes were identified, which were all situated in the C-terminal part of the intron (S000340, S000111, S000109). Four general promoter elements were identified, associated with *A. rhizogenes* promoters or found in CaMV regulatory sequences (S000098, S000460).

In the *ChGL1* intron, a total of 29 CREs were identified. The majority were classified as binding sites, followed by light-related motifs. No motifs associated or classified as enhancer elements, S/MAR, splice junctions, or temperature-, nutrient- and circadian-related were identified. Interestingly, 13 binding sites were identified. Most of them were W-boxes (S000039, S000390, S000447, S000442, S000457). They were situated at 35 bp, around 66-80 bp, and 99 bp. No binding sites for HD-ZIP or MYC proteins were found. Only one MYB-binding site at 90 bp was identified (S000408). However, a variant of the CArG motif, a binding site of AGL15 was identified (S000431). This motif also occurs in the *ChWER* intron. In intron 1 of *ChGL1,* one TATA box was found, located at 61 bp (S000111). Additionally, three promoter elements were found associated with CAAT promoter consensus sequences (S000028), sequences from *A. rhizogenes* (S000098) or plastid promoter elements (S000296). Three hormone-related elements were identified as Ga- and cytokinin-related (S000439, S000454). Interestingly five light-regulated CREs were identified. They were identified as I-boxes or generally associated with light-regulated gene expression (S000383, S000198, S000362, S000491, S000199).

The intron 1 of *AtMYB23* possesses 42 CREs, the majority conferring organ specificity. No CREs identified as enhancer elements, splice junctions or S/MARs were found, as well as no motifs associated with temperature- or circadian-related expression. The 11 organ-specific motifs were either pollen- (S000245) or mesophyll-specific (S000449). The five nutrient-related motifs were all identified as putative nodulin consensus sequences (S0000461, S000462). One poly(A) signal was identified (S000080). Only six binding sites were found, none identified as WRKY-, MYB-, MYC- or HD-ZIP-binding sites. Instead, four Dof-binding sites (S000265), one SEF4 binding site identified in soybean (S000103), and one GATA box at 121 bp (S000039) were determined. The nine disease and stress motifs identified were associated with infection or copper- and oxygen stress (S000468, S000467, S000493). Only one cytokinin-related hormone motif was found (S000454), but two light-regulated CREs (S000198, S000199). Interestingly, three TATA boxes were identified, located all in the N-terminal part of the intron (S000203, S000109). Four general promoter elements were identified, categorized as CAAT promoter consensus sequences (S000028) or as sequences from tobacco or plastid promoters (S000387, S000395, S000296).

In the first intron of *ChMYB23,* a total of 37 CREs were found. None were found in the categories temperature- and circadian-related, as well as splice junctions, poly(A) signal, or S/MAR. Seven CRES were found in each of the categories binding sites, organ specificity, and disease and stress motifs. The same interesting absence of WRKY-, MYC-, MYB- and HD-ZIP-binding sited observed in the *AtMYB23* intron also was observed for the *ChMYB23* intron. The seven identified binding sites were four Dof-sites (S000265), one RAV1 binding site (S000314), and two GATA boxes (S000039) situated at the start and end of the intron sequence. The tree nutrient-related motifs were all putative nodulin consensus sequences (S000461, S000462), and the seven organ-specific motifs were mostly associated with pollen- and mesophyll-specific gene expression (S000353, S000245, S000378, S000449). Seven disease and stress elements were found, associated with infection response and copper and oxygen stress (S000468, S000467, S000493). The single identified TATA box was situated at 23 bp (S000203). As promoter elements, CREs categorized as CAAT promoter consensus sequences (S000028) and as sequences identified from tobacco and anaerobic genes (S000477, S000395) were found. The two hormone-related motifs were associated with cytokinin (S000454). The three light-related motifs were categorized are generally associated with this regulation or as I-boxes (S000198, S000199). Interestingly, an enhancer element was identified at position 74 bp. This enhancer element is associated with MYB-binding (S000494). Enhancer elements were only additionally found in the introns of *AtWER* and *ChWER*.

In *AtWER* the first intron possesses 69 CREs identified by PLACE. With 30 binding sites identified, this is the majority of motifs, followed by 11 promoter elements. Out of the 30 binding sites, seven are Dof-binding sites (S000265), four are GATA boxes (S000039), and one is a RAV1 binding motif (S000314). Three out of the four GATA boxes are located at 158-188 bp. Only two HD-ZIP binding sites were identified (S000498), located at 36 bp and 57 bp, respectively. Five W-boxes were identified (S000390, S000447, S000457), grouped into three areas around 36 bp, 58 bp, and 195 bp. The four MYC-binding sites (S000144, S000407) are exclusively localized around 60 bp. Additionally, five MYB-binding sites were identified (S000408, S000176, S000177, S000409, S000180). They are present at three different locations in the intron, at 81 bp, 181 bp, and 237 bp. No temperature- or circadian-related motifs were identified, as well as no splice junctions. The one nutrient-related element was identified as a putative nodulin consensus sequence (S000462). Six organ-specific CREs were found, conferring predominantly pollen-specific expression (S000245, S000148, S000378, S000273, S000422). Two poly(A) signals were localized at 213 bp and 243 bp (S000080, S000088). Only four disease and stress-related motifs were found. These CREs were associated with infected root nodules (S000468) or water stress (S000413), as well as sulfur-responsive elements (S000499). A total of four TATA boxes were identified, situated around 110 bp, 214 bp, and 242 bp (S000111, S000203). 11 promoter

elements were found, classified as CAAT promoter consensus sequences (S000208) and as elements from *A. rhizogenes* or plastid promoters (S000098, S0000296). The six hormone-related motifs were cytokinin- or ABA-related (S000454, S000174). As light-related elements one I-box was found (S000199) or motifs generally associated with this kind of regulation (S000198). One S/MAR was identified (S000037), and the same enhancer element present in intron 1 of ChMYB23 was localized at 65 bp (S000494).

Finally, the *ChWER* intron was examined. In total, 88 CREs were identified, 18 as binding sites. No splice junctions or S/MARs were found. One circadian-related motif was found (S000252) as well as four nutrient-related putative nodulin consensus sequences (S000462). The 11 organ-specific CREs confer pollen- and mesophyll-specific expression (S000245, S000378, S000449). Five poly(A) signals were found (S000080, S000088, S000081), localized between 77 bp and 304 bp of the intron length. Out of the 18 identified binding sites, no MYC-, WRKY- or HD-ZIP binding sites were found. Only one MYB-binding site, localized at 97 bp, was found (S000408). However, six Dof-sites were found (S000265) and four SEF4 binding sites from soybean (S000103). Also, three GATA boxes were found (S000039), localized at 112 bp, 192 bp, and 230 bp. Interestingly, two variants of the CArG motif were found at 260 bp (S000431). A total of 13 disease and stress elements were identified, the majority being infection-related (000468, S000443) or involved in copper and oxygen stress (S000493). Seven TATA boxes were found (S000111, S000203), localized around 65 bp, 167 bp, and at the C-term around 304-360 bp. All six hormone-related motifs are associated with cytokinin (S000454). The two temperature-related motifs encompassed a motif for heat (S000030) and one motif for cold (S000250). Nine light-related motifs were found, associated with phytochrome (S000149) or identified as I-boxes (S000199). The 11 promoter elements displayed the same variety as described before, with elements identified as CAAT promoter consensus sequences (S000028), promoter elements from *A. rhizogenes* (S000098), and anaerobic promoters (S000477, S000387). Finally, one enhancer element was identified at position 129 bp (S000494). This was the same enhancer element also identified in the introns of *AtWER* and *ChMYB23*.

Overall the introns display a variety of different CREs. They differ unexpectedly regarding the binding sites present in their sequences. Especially both *AtMYB23* and *ChMYB23* as well as *ChWER* are different to the other three MYB introns, as they do not possess a similar amount of MYB-, MYC, WRKY- and HD-ZIP binding sites. Interestingly, they possessed the same enhancer element.

3.3.3. Interspecies rescue experiments of *Cardamine* MYBs in *Arabidopsis* mutants

As *Cardamine* is closely related to *Arabidopsis* (Beilstein et al., 2008, 2010; M. Koch et al., 2001) rescue experiments were performed to shed some light on the evolution of these genes, especially taking into consideration the different expression levels observed in the different species (Pietsch, 2022). Closely related orthologous genes can sometimes rescue the phenotypes of other species (Bernhardt et al., 2003; Galway et al., 1994; Lee & Schiefelbein, 1999; Payne et al., 2000; Wang et al., 2004). To test the rescue ability of the *Cardamine* MYBs in *Arabidopsis*, constructs were generated that included a 1.5 kb putative promoter sequence, the genomic gene sequence, and 1.8 kb putative 3' enhancer fragment of *ChGL1*, *ChMYB23,* and *ChWER*. These constructs were used to transform the *gl1*, *myb23*, and *gl1 myb23 Arabidopsis* mutants, and in the T1 generation, the trichome phenotype rescue ability of each construct was examined. The *gl1* and *gl1 myb23* mutants are nearly glabrous and glabrous, respectively. The *myb23* mutant does not display a difference in trichome number compared to wildtype, but a branching phenotype (Kirik et al., 2005). A total of 50 plants per construct and mutant background were analyzed, and these plants displayed a range of trichome phenotypes (Figure 41 A).

Interestingly, all *Cardamine* constructs induced trichomes in the *gl1* mutant (Figure 41 B). However, only *ChGL1* and *ChMYB23* were able to induce trichomes in the double mutant *gl1 myb23*. The *ChGL1* expressing construct led to the formation of around 30 and 40 trichomes per leaf in *gl1* and *gl1 myb23* plants, respectively. This trichome number is significantly different from the Col-0 reference, with 80 trichomes per leaf. Also, the *ChGL1* construct caused an increase in trichome number in *myb23* compared to Col-0. This was also the case for the ChMYb23 and ChWER construct. None of the *Cardamine* constructs could induce a normal number of trichomes in either *gl1* or *gl1 myb23* plants. The trichomes induced by ChWER in *gl1* were often isolated to the leaf edge (Figure 41 A). Expression of *ChGL1* sometimes led to the formation of trichome clusters, especially in *myb23* plants.

These results indicate, that the *Cardamine MYBs* can induce trichome formation in single *MYB* mutants of *Arabidopsis*. However, none of the *Cardamine* constructs could restore the wildtype trichome pattern or number. Also, *ChGL1* could induce more trichomes in the *gl1* and *gl1 myb23* plants compared to *ChMYB23* and *ChWER*. This is especially interesting, as all *Cardamine* constructs were controlled by their endogenous putative regulatory sequences.

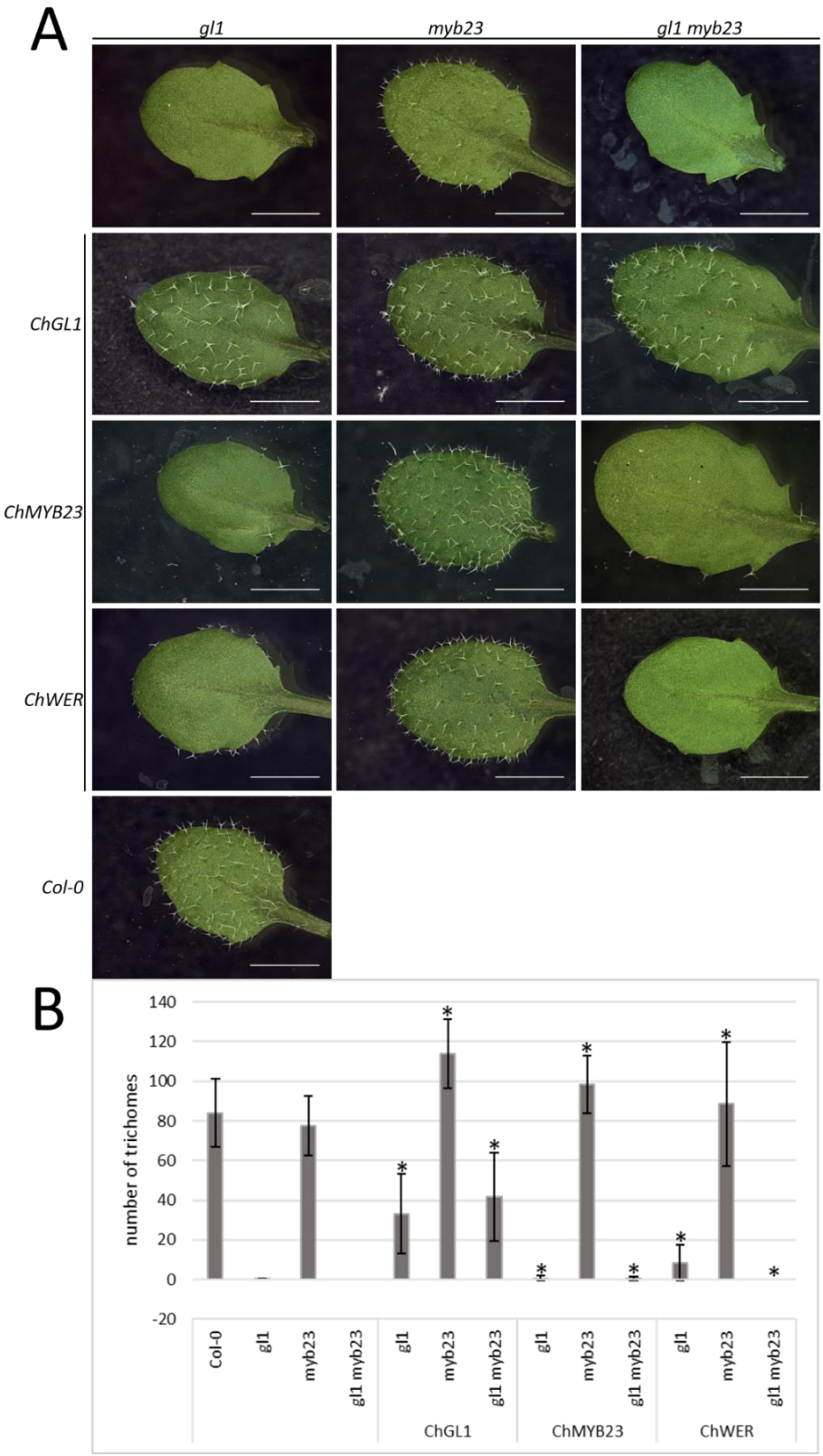

Figure 41. T1 rescue experiments Cardamine. A) Leaves of *MYB* mutants and T1 rescue lines expressing *Cardamine MYB* constructs. B) Trichome number in T1 rescue plants expressing *Cardamine* constructs. Bar graph of trichome number of leave four of Col-0 and mutant plants, as well as *gl1*, *myb23,* and *gl1 myb23* T1 plants transformed with *ChGL1*, *ChMYB23,* and *ChWER* rescue constructs. Error bars depict standard deviations. Statistical analysis was performed by Mann-Whitney U tests comparing the plants expressing the Cardamine constructs with Col-0. Statistical differences to Col-0 ($p \leq 0.05$) are indicated by a black asterisk.

3.4. Experiments to expand the existing patterning models

Biological patterns can be described mathematically, and different patterns can be explained and reproduced by adjusting these mathematical models (Gierer & Meinhardt, 1972; Meinhardt & Gierer, 1974; Turing, 1952). Two trichome patterning models are currently published that are both individually capable of explaining the wildtype trichome pattern (Pesch & Hülskamp, 2009). However, the two published models cannot explain some observed mutant phenotypes. Therefore, in this study, two different sets of phenotypes, namely the weak *ttg1* allele phenotypes and the cluster phenotype of *cpc try* mutants, were examined more closely to help shed light on the underlying mechanisms and enable the adjustment of the mathematical models.

3.4.1. Mutant variants of TTG1 are not depleted in trichome surrounding cells

Mutants of activators and *ttg1* usually show a glabrous phenotype (Koornneef, 1981). However, there are *ttg1* mutants still producing trichomes, even though their number is reduced (Koornneef, 1981; Larkin et al., 1994, 1999; Long & Schiefelbein, 2020; Walker et al., 1999). These so-called weak *ttg1* alleles possess trichomes in an irregular pattern, exhibiting cluster formation (Koornneef, 1981; Larkin et al., 1999; Walker et al., 1999). The different mutant phenotypes suggest that TTG1 is acting as an activator and an inhibitor, and the role in trichome patterning may be influenced by the kind of mutation present in the *ttg1* alleles. In the strong *ttg1* allele *ttg1-1,* the C-terminal 26 amino acids are truncated (Larkin et al., 1994; Walker et al., 1999). Contrarily, in the three weak ttg1 alleles, ttg1-9, ttg1-11, and *ttg1-12*, amino acid exchanges took place. In *ttg1-9* at position 282, serine is replaced by phenylalanine; in *ttg1-11* at position 149, a glycine is replaced by an arginine, and in *ttg1-12,* the same amino acids are exchanged as in *ttg1-11* but at position 43 (Koornneef, 1981; Larkin et al., 1994, 1999; Walker et al., 1999). It was shown that the mutations present in the strong and the weak *ttg1* alleles lead to the reduction or abolishment of TTG1 and GL3 interaction (Balkunde et al., 2011, 2020; Payne et al., 2000). Moreover, TTG1 is recruited by GL3 into the nucleus, which results in the depletion of TTG1 in the trichome surrounding cells (Balkunde et al., 2011; Bouyer et al., 2008). This depletion is one of the key components of the activator depletion model (Bouyer et al., 2008). To examine the nuclear localization of different mutant TTG1 proteins in wild-type plants, transgenic lines expressing YFP-tagged versions of TTG1 under the pTTG1 promoter were generated. These plants were examined regarding the nuclear localization of TTG1 and the depletion in trichome surrounding cell tiers.

Wildtype and mutant TTG1 proteins were localized in the nucleus and the cytoplasm of the trichome and surrounding cells (Figure 51). This was not observed for non-mutated TTG1 in the strong allele *ttg1-13*, where TTG1 was localized in the nucleus in epidermal and trichome cells (Bouyer et al., 2008). This differing behaviour can be explained by the amount of TTG1 present in the different lines. In *ttg1-*

13, no intact TTG1 is available for GL3 interaction, thus no recruitment to the nucleus could take place. The YFP-tagged *TTG1* expressed in wild-type plants needs to compete with endogenous TTG1 for interaction with GL3 and thus recruitment by GL3. Due to the oversaturation of TTG1 compared to GL3, only a part of the fluorescence-tagged TTG1 population is recruited into the nucleus (Balkunde et al., 2020).

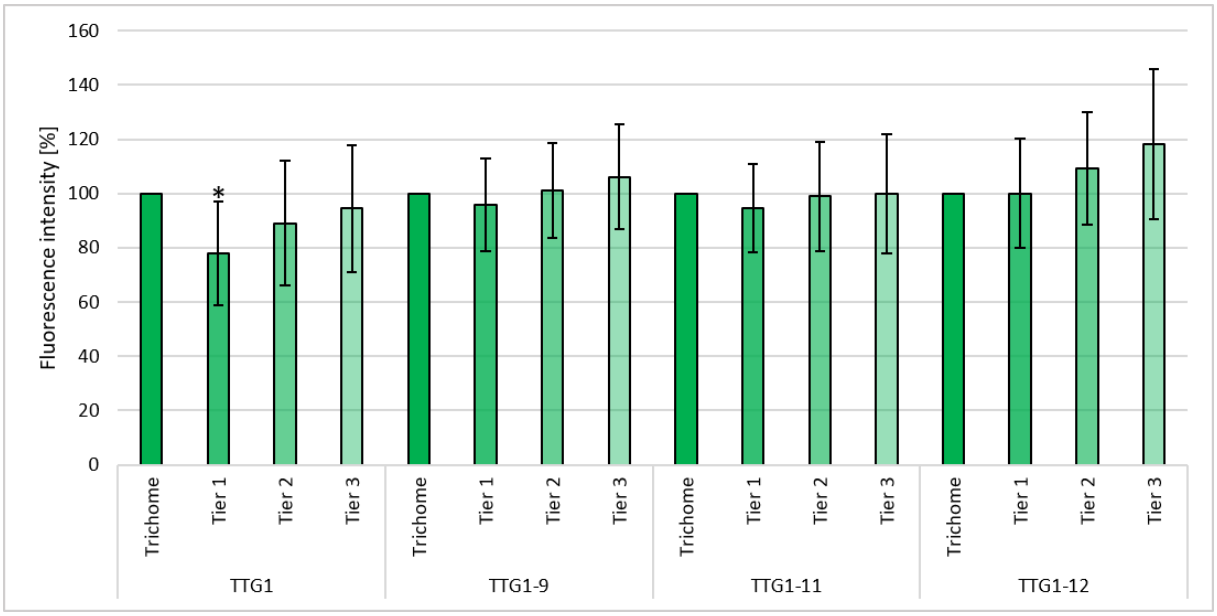

Figure 42. Fluorescence intensity of TTG1 versions in trichomes and surrounding tiers. The fluorescence intensity was normalized to the intensity in the corresponding trichome and is given in percent. The TTG1 versions are listed at the x-axis and standard deviations are represented as black lines at the top of each bar. Statistical analysis was performed by Student's t-tests comparing the normalized fluorescence of each tier with the trichome fluorescence intensity. Statistical differences compared to the trichome fluorescence intensity ($p \leq 0.05$) are indicated by a black asterisk.

Additionally, the depletion of the different TTG1 versions were examined in the wildtype background (Figure 42). The fluorescence intensity in forming, not-branched trichomes, was determined and compared to the fluorescence intensity in the cell tiers surrounding the trichome. Only the wildtype version of TTG1 was depleted in the first cell trier surrounding the trichome. No mutated version examined was depleted in any cell tier. Moreover, the weak *ttg1* alleles did not show any difference regarding their seed color, seed coat mucilage production, or root hair formation (data not shown).

The data provided by the biological experiments enabled the facilitation of a mathematical model that could explain the weak *ttg1* cluster phenotypes, *ttg1* glabrous leaves, and wild-type trichome pattern.

The results presented here regarding weak *ttg1* alleles are part of the publication Balkunde et al., 2020.

3.4.2. Analysis of the *cpc try* double mutant cluster formation

The trichome patterning properties of *cpc*, *try,* and *cpc try* mutants cannot be explained by an additive phenotype alone (Schellmann et al., 2002). A previous study successfully recreated the trichome pattern seen in the *cpc try* mutant using a mathematical model (Deneer, 2022). This model was based on an already published trichome patterning model (Balkunde et al., 2020). However, the published model had to be adjusted in three ways to recreate the *cpc try* pattern: First, the aspect of time had to be introduced by establishing trichome fate in several consecutive patterning rounds. At the end of each patterning cycle, a perturbation was included to mimic the cell differentiation into a trichome. This perturbation could be of two different kinds: Either an increase in trichome patterning gene expression, e.g., caused by endoreduplication cycles, or it could be a decrease in gene expression, e.g., caused by downregulation, as these genes are not required anymore. Only a downregulation in gene expression led to the formation of clusters similar to the size and shape observed in *cpc try* (Deneer, 2022). However, so far, no experimental evidence is available to indicate if a decrease or increase in gene expression is happening. The second aspect that had to be introduced into the model was additional activator mobility (Deneer, 2022). In the published models, TTG1 was the only mobile activator so far. In this new model, also GL1 and GL3 can move between cells. GL3 was observed to be mobile in roots (Savage et al., 2008), but no activator movement in leaf epidermal cells has been observed so far. However, the assumption is based on the criteria for the activator- and inhibitor-containing models from Turing (1952) and Gierer and Meinhardt (1972), in which activators, as well as inhibitors, are mobile. The third aspect that needed to be introduced was a third inhibitor, which was named ETC (Deneer, 2022). ETC incorporates the inhibitors ETC1, ETC2, and ETC3, as they are partially redundant (Wester et al., 2009). In the previously published model, only TRY and CPC were included as inhibitors (Balkunde et al., 2020), however, in the *cpc try* mutant, no inhibitor would have been left active, thus causing patterning problems in the mathematic model. Interestingly, the diffusion rate of ETC had a drastic effect on the number of clusters and their size (Deneer, 2022).

Expression analysis of pCPC:GUS in cpc try mutant leaves

To investigate the nature of the proposed expression perturbation in trichomes, *cpc try* plants were transformed to express *pCPC:GUS* or *pTRY:GUS*. The T2 generation was examined regarding GUS staining of young leaves. For each promoter construct, several lines were examined. For pTRY:GUS no GUS staining could be observed in any examined line (data not shown).

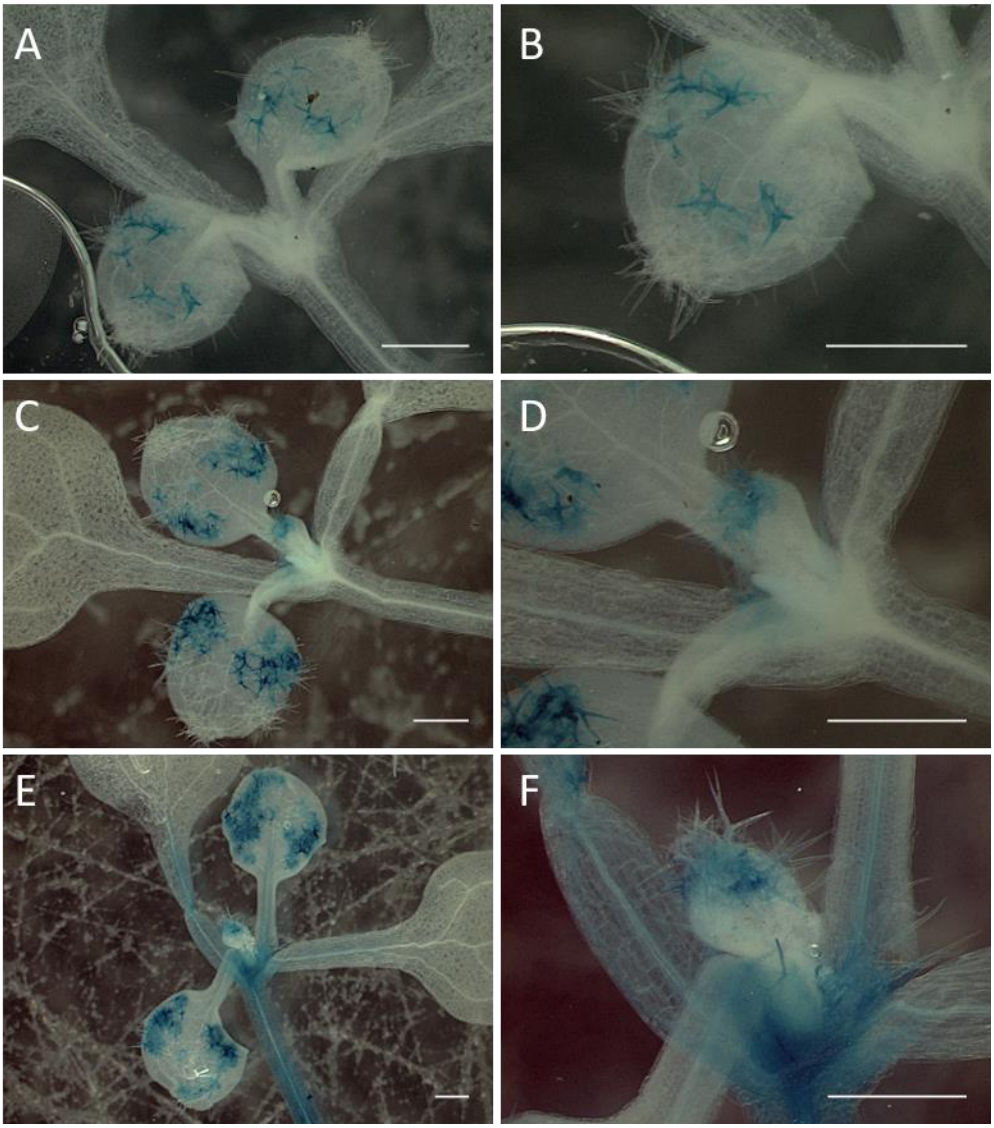

Figure 43. GUS staining of *cpc try* plants expressing *pCPC:GUS*. GUS staining is displayed after 1 h (A, B), after 2 h (C, D) and after 5h (E, F). For each time point, the same sample is shown, but with different magnifications. The scale bar refers to 500 µm.

The GUS staining procedure was performed for different time spans to ensure non-saturated tissue to enable the detection of differences in the GUS staining intensity. Samples from the same time span did not display the same staining pattern (data not shown). Sometimes the small leaves 3 and 4 were partially stained, sometimes not. Overall, the longer the staining procedure was performed, the more intense the GUS staining results were. After 1h of staining, some trichomes on leaves 1 and 2 showed distinct GUS staining (Figure 43 A), whereas the small leaves 3 and 4 did not display any blue staining (Figure 43 B). Interestingly, not all trichomes on the first leaves were stained, but only some discrete trichomes in the middle of trichome clusters. After 2h of staining, more trichomes on leaves 1 and 2 displayed GUS staining. These trichomes were situated more towards the base of the leaf (Figure 43 C). Some, but not all, examined third leaves displayed GUS staining in trichomes situated at the tip of the small leaves (Figure 43 D). The patterning zone was not stained, nor was GUS staining detected in very

small emerging trichomes under these observation parameters. GUS staining procedure for 5h produced even more blue and dark blue trichomes on leaves 1 and 2 (Figure 43 E), as well as stained trichomes in leaf 3 (Figure 43 F). The trichomes at the base of the small leaf did not appear to be stained. However, the detection of faint blue staining signals is quite challenging, and the trichome clusters already present on small emerging leaves contribute to the challenging preparation of the GUS-stained samples.

This irregular staining pattern observed in leaves 1 and 2 may be caused by the insertion site of the pCPC:GUS construct. However, this could be excluded because the same pattern was observed in several lines (data not shown). The stable line displayed in Figure 43 was backcrossed into *Col-0* to determine the expression pattern in these plants and shed light onto the causes for the strange expression pattern in *cpc try*. The same time span for staining was applied, and GUS staining was detected after 3-5 hours (Figure 52). In mature trichomes of leaves 1 and 2, staining could be observed, as well as very faint staining of young trichomes on leaf 3 after 5 h. Overall, these findings seem consistent with the published expression pattern of pCPC:GUS in 2002, but not as pronounced (Schellmann et al., 2002). This is most likely caused by the relatively short staining time.

Tracking cluster formation in growing cpc try leaves

Cluster formation was tracked via dental wax imprints and repeated imaging of the same growing leaf (Schellmann et al., 2002). However, the repeated dental wax application caused the largest central trichome to break off. To track the cluster formation more closely and also examine possible directionality in the cluster formation, stable lines expressing plasma membrane markers were used to perform growth assays. The stable line was kindly provided by Pau Formosa Jordan and was established by Adrienne Roeder (Roeder et al., 2010). The plasma membrane marker *RARE-COLD-INDUCIBLE 2A (RCI2A),* tagged with *mCitrine,* and the nuclear marker *histone 2B* (*H2B*), tagged with *TFP*, were expressed in *Col-0* under the L1-specific promoter *pAtML1*. These plants were microscopically examined on two consecutive days and tissue viability as well as growth were examined. Growth in live samples could be detected after several trials. The increase in leaf size and cell number was evident in two CLSM sessions conducted 16 h apart (Figure 44).

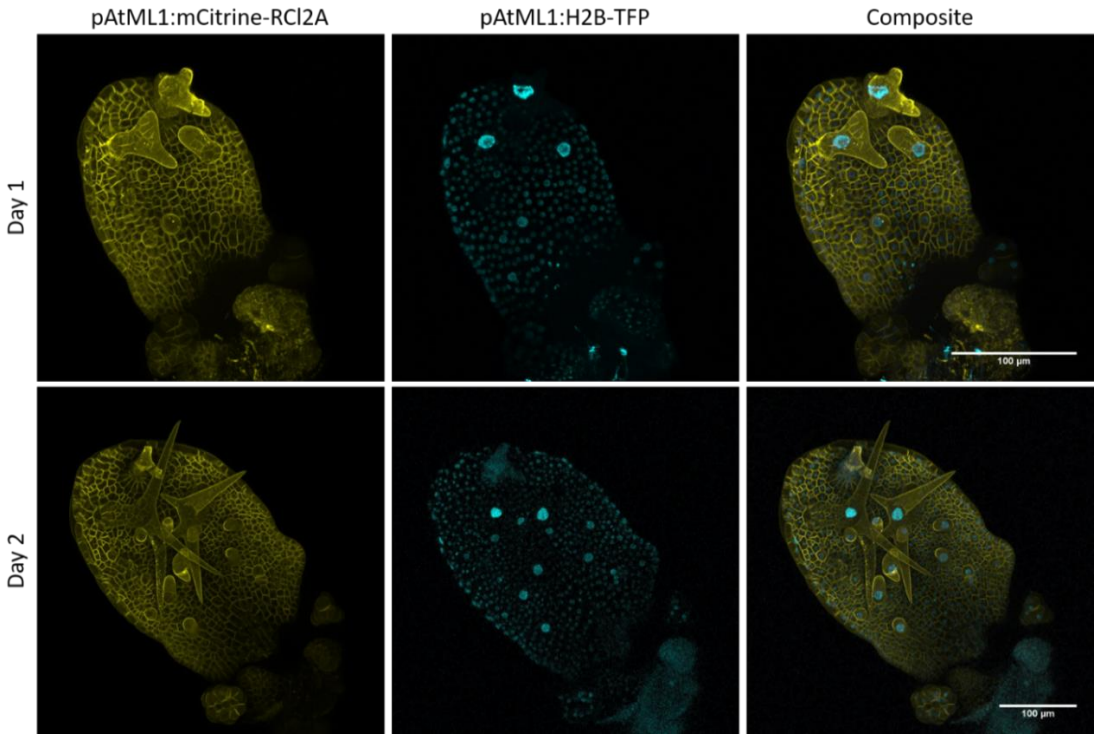

Figure 44. CLSM images of growth tracking in wild-type marker line. Wild-type plants expressing *pATML1:mCitrine-RCI2A (left)* and *pATML1:H2B-TFP* (middle) imaged on day 1 (top row) and day 2 (bottom row). Composite images of the mCitrine and TFP signals are displayed in the right column. Scale bars refer to 100 µm.

The marker line was crossed with *cpc try* plants to establish reporter gene expression in the double mutant. Several plants displaying marker signals in the *cpc try* background could be retrieved. All lines displayed a distinct mCitrine-RCI2A fluorescent signal (Figure 45). However, in most of the lines, no *pATML1:H2B-TFP* expression could be detected. First, growth assays were performed with these new marker lines, and growth occurred after 16 h. However, the dense trichome clusters increased the difficulty of the leaf preparation and often larger trichomes were injured. Additionally, 16 h seems to be too long to track individual growth, as in some samples, the tracking of individual cells was challenging or impossible. Overall, the plasma membrane marker line seems to be an appropriate tool for tracking cluster formation, but the parameters of the cluster formation need to be specified in more detail. CLSM sessions should be conducted in shorter intervals, and especially small leaves should be prepared to minimize damage to leaf tissue.

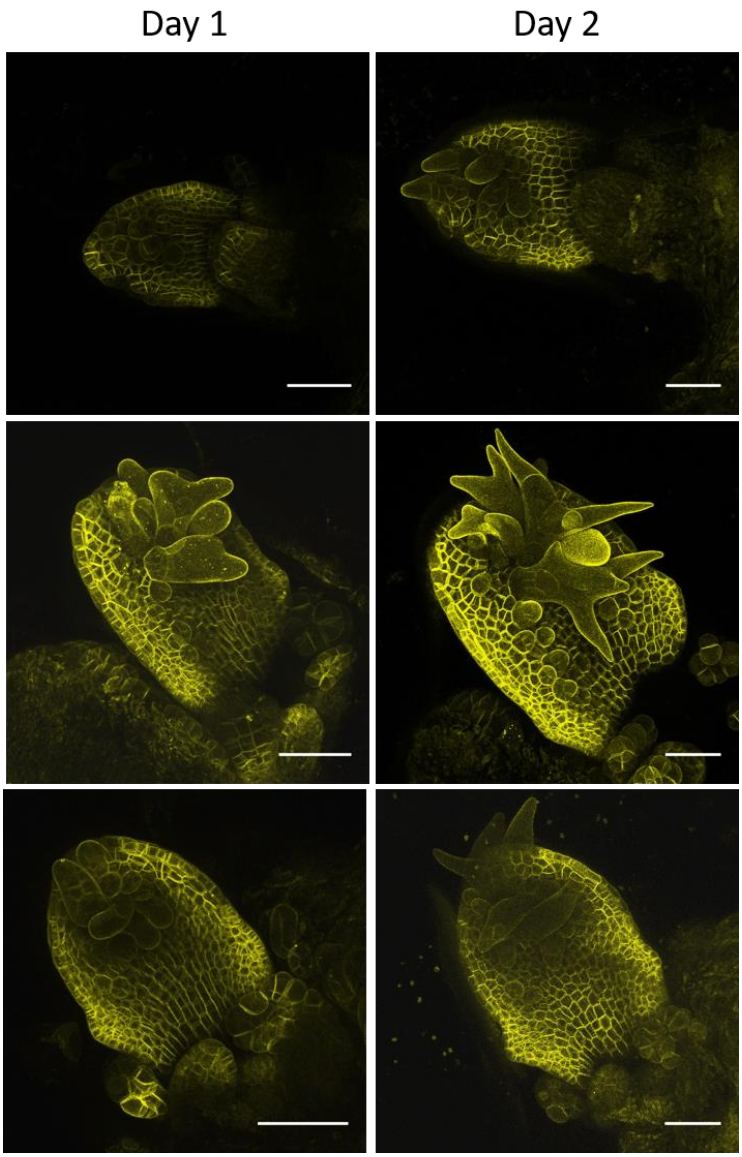

Figure 45. CLSM images of growth tracking in *cpc try* marker line. Wildtype plants expressing *pATML1:mCitrine-RCI2A* imaged on day 1 (left column) and day 2 (right column). Scale bars refer to 100 µm.

4. Discussion

This study aimed to elucidate unresolved questions concerning trichome patterning in *Arabidopsis* rosette leaves. To achieve this, various experimental approaches to examine protein-protein interactions, as well as *in-silico* and *in-vivo* studies observing gene expression, were performed.

4.1. Ratio differences in P2A experiments are caused by protein interactions

In a previous study, the suitability of the P2A sequence to examine differences in fluorescence ratios of equimolar expressed genes has already been verified (Pietsch, 2022). However, the cause for these stability changes has not been addressed until this study. Here, compared to full-length GL3, an N-terminally truncated version of GL3 (Payne et al., 2000) reduced GL1 stability. Additionally, a point-mutated version of GL1 (Pesch et al., 2015) could not be stabilized by GL3 (Figure 20). These two experimental setups suggest protein-protein interactions to be the cause for the detected differences in fluorescence ratios in the P2A experiments, as the only variable was the interaction ability of the protein attached to CFP.

However, there still remained the question regarding the reason behind the different stabilities, meaning what causes the increase in YFP-X protein? Due to the simultaneous transcription of YFP-X and the internal control NLSNLS-mCherry from one plasmid into one mRNA (Ahier & Jarriault, 2014; Kim et al., 2011), an increase in protein amount caused by an increase in production could be ruled out. Also, an unintentional artefact caused by the experimental setup could be excluded, as not only increases in stability were observed but also decreases. This only leaves a decreased protein degradation as a possible reason. Protein degradation is mostly carried out by the ubiquitin-proteasome pathway (Pickart & Eddins, 2004). A link to proteasomal degradation was already published for GL3 and EGL3, as well as TT8 and TTG1 (Patra et al., 2013a, b). No ligase was identified for TTG1 and TT8 degradation, however, the ubiquitin ligase responsible for GL3/EGL3 degradation, KAKTUS, was identified (Patra et al., 2013a, b). Mutations in this gene cause increased trichome branching and an increase in DNA content, indicating a role in endoreduplication control (Downes et al., 2003; El Refy et al., 2004). However, GL3 seems to be also involved in promoting endoreduplication in trichomes, and its absence abolishes the over-branched *kak* phenotype in *kak gl3* (Sako et al., 2010). Also for GL1, an interaction with KAK was shown, and thus, proteasomal degradation is likely (Jaime, 2007). Proteasomal inhibitor treatments showed a slight increase in GL1 stability, which was more pronounced when GL3 was present. This may indicate that GL1 is degraded via the proteasomal pathway, but the MG132 application did not lead to a drastic increase in fluorescence ratio. Moreover, these first results were not reproducible. The results published regarding MG132 treatment often

include Western-Blot analysis and no microscopy (Liu et al., 2010; Patra et al., 2013a, b; Shen et al., 2016). Also, GL3 and EGL3 are degraded rather quickly (Patra et al., 2013b), suggesting that maybe the CLSM may take up too much time to see any effects. Therefore, the proteasomal link cannot be excluded due to a likely unsuitable inhibitor treatment. Alternative treatments should be tested, such as bortezomib or a combination of translation inhibitor cycloheximide and MG132 treatment (Cheng et al., 2020; Patra et al., 2013a). Or the MG132 could be applied to Arabidopsis seedlings expressing the desired P2A constructs, and subsequent Western-Blot analysis could be performed (Seo et al., 2003). However, this may be challenging, as during the course of this study, only some lines expressing MYB23-P2A could be successfully retrieved, while GL1-P2A could not be stably introduced in *Arabidopsis* plants. Therefore, alternative constructs should be used to generate plants expressing the trichome patterning genes with the appropriate tags to conduct these experiments. Protein turnover could be assessed by performing cycloheximide chase experiments, e.g. in yeast (Buchanan et al., 2016). Another alternative could be ubiquitination assays (Saijo et al., 2003).

Additionally to the proteasomal link, the fluorescence ratios of GL3-P2A were examined in the presence or absence of KAK. Both in leek and different *Arabidopsis* lines, the presence of KAK led to an increase in GL3 stability (Figure 19, Figure 18). Although these results verify the interaction of GL3 with KAK through the changed fluorescence stabilities indirectly, they directly contradict the published results regarding KAK and GL3 degradation (Patra et al., 2013b). Additionally, these observations most likely do not reflect the true biological circumstances, as all constructs used in these experiments were expressed under the constitutively active 35S promoter from Cauliflower Mosaic Virus (CaMV; Amack & Antunes, 2020). The artificially high amount of GL3 may not be degraded in the appropriate time, even if KAK is present in the plant. Moreover, other ubiquitin ligases may come into play that can also degrade the targets of KAK in case of its absence. As *kak* mutants are non-lethal, it can be assumed that either no critical amounts of target proteins accumulate in these mutants or that critical amounts are degraded through other ligases. In accordance, the overexpression of GL3 leads to a drastically increased number of trichomes (Zhang et al., 2003), while this phenotype is not observed in *kak* leaves (Downes et al., 2003; El Refy et al., 2004). However, it is still possible that KAK is only responsible for GL3/EGL3 turnover in already established trichomes and not during the early patterning stages. Therefore, the slight increase of GL3 in *kak* mutants may only affect endoreduplication but not the pattern itself.

4.2. The use of viral sequences reveals novel protein interaction effects

In trichome patterning, the interactions between trichome patterning proteins and their effect on the expression of trichome patterning genes were studied extensively (Pesch & Hülskamp, 2009; Wang et

al., 2021). However, if protein-protein interactions affect protein properties directly has only recently been studied (Pietsch, 2022). The viral "self-cleavage" site P2A was established as a useful tool to study protein stability and could be used in this study to examine the stability changes of trichome patterning proteins on each other.

4.2.1. MYB proteins are stabilized by bHLH proteins

Firstly, in this study, the observation previously stated by J. Pietsch that the MYB proteins are stabilized upon bHLH exposure could be confirmed. The presence of GL3 and EGL3 stabilized GL1, MYB23, TRY and CPC. This observation is intriguing, as both *GL3* and *EGL3* are homologs and act redundantly in trichome patterning (Bernhardt et al., 2005; Payne et al., 2000), and only if both are absent a glabrous phenotype is observed (Zhang et al., 2003). However, the protein stability experiments suggest that EGL3 has a higher impact on GL1 stabilization than GL3. The stability effects of GL3 and EGL3 on MYB23 were reversed compared to GL1. MYB23 was drastically more stable in the presence of GL3 compared to the stability in the presence of EGL3. These severe effects of GL3 on MYB23 stability are striking, as only a minor role in the patterning process is attributed to MYB23. It plays a more obvious role in the subsequent branch formation (Kirik et al., 2001, 2005).

However, not only the activator R2R3MYBs were stabilized by GL3/EGL3, but also the two tested inhibitors, TRY and CPC. It is unsurprising that TRY and CPC are similarly stabilized by the same proteins, as they are quite similar in protein sequence (Simon et al., 2007). For both inhibitors, the effect of EGL3 was more pronounced than that of GL3. This differential effect may hint at a stronger involvement of EGL3 in the regulation of short-range trichome inhibition, as TRY is suspected to inhibit trichome formation on shorter distances compared to CPC (Schellmann et al., 2002). Also, EGL3 presence in cells may help to establish non-trichome fate indirectly by stabilizing TRY. As the P2A experiments performed in this study were conducted in leek and not in *Arabidopsis* epidermal cells, the determined ratios do not reflect the endogenous conditions. However, it is known that TRY/CPC interact with GL3/EGL3, thus leading to an inactivation of the active MBW complex (Payne et al., 2000; Pesch et al., 2015; Zhang et al., 2003). Interestingly it was discovered that *EGL3* is slightly higher expressed in *Col-0* plants than *GL3* (Pietsch, 2022). So, possibly, if EGL3 is present in an epidermal cell, the inhibitors are stabilized more, compared to if the same amount of GL3 is present. However, this stabilization is dependent on the amount of patterning proteins present in the cell. Which remains elusive to this day.

4.2.2. GL3 and EGL3 are stabilized differently by the same proteins

EGL3 was stabilized in the presence of TTG1, MYB23, TRY, and CPC. TRY presence only led to a slight increase in stability, while CPC increased the EGL3 stability significantly. This indicates, that the binding of TRY and EGL3 highly increases TRY stability, but not so drastically EGL3 stability. Also, CPC and EGL3

are stabilized similarly in each other's presence, but the stability effect is more pronounced for CPC. No trichome patterning protein led to a decrease in EGL3 stability.

GL3 was stabilized in the presence of EGL3 and MYB23 but was destabilized in the presence of GL1, GL3, and TTG1. Although the destabilizing effects of GL1 and TTG1 may not be extreme enough to cause a change in trichome patterning, the effect of GL3 on its own stability might be significant. Interestingly, the inhibitors did not affect GL3 stability. Overall, the GL3 stability changes are very intriguing as experimental evidence for feedback loops regarding the activator's gene expression is missing. These feedback loops, however, are requirements for all patterning models based on Turing's postulated models (Balkunde et al., 2011, 2020; Meinhardt, 2012; Turing, 1952)

4.3. Different protein stabilities could offer an alternative for the missing feedback loop

The models explaining trichome patterning rely on feedback loops regarding the activation of the activators and inhibitors (Balkunde et al., 2020; Pesch & Hülskamp, 2009). However, this positive feedback loop is missing so far for the trichome patterning mechanism. It was assumed that such a feedback loop would take the form of gene expression regulation, meaning the activators would activate their own gene expression. In the case of trichome patterning, this makes sense, as most of the core patterning proteins classified as activators are transcription factors (Pesch & Hülskamp, 2009). So far, however, only a feedback loop for the inhibitors has been reported. It was shown that TRY and CPC are both activated by the activators GL1, GL3, and TTG1. Additionally, TTG2 added to the trimeric active complex increases the activation of *TRY* and *CPC* expression even more (Pesch et al., 2014). Nonetheless, such a positive effect on the own expression rate has not yet been found for activators. For *GL3,* it was even postulated that it has a negative effect on its own expression. Morohashi and colleagues suggested a negative effect of GL3 on its own expression. However, they used *GL3* fused to a glucocorticoid hormone receptor domain (GR), and upon exposure to a ligand of this receptor domain, trichomes were initiated in *gl3 egl3* plants. However, the pattern was not checked regarding the rescue efficiency (Morohashi et al., 2007). In 2005, Bernhardt and colleagues also postulated a potential negative influence of GL3 on its own expression, as GL3 needs to be present to inhibit *GL3* gene expression and RNA accumulation in cells at the N-position (non-root hair cells; Bernhardt et al., 2005). In the GUS assays performed in this study, no negative effect of GL3 on its own expression could be observed. If any effect was observed, the co-expression of GL3 led to an increase in reporter gene activity. However, the mutation of the two W-boxes in the second intron did not cause a decrease in gene expression. If the W-boxes were mutated, more combinations showed a significant increase in gene expression compared to the non-mutated version. However, the observed increase was in a

similar percent range and thus the statistical differences are most likely caused by more consistent samples in these experiments. For *pGL3* overall, the expression increased in all tested promoter versions when TTG1 was co-expressed. Also, the co-expression of TTG2 led to a significant increase in gene expression, even when both W-boxes were mutated. This suggests, that TTG2 may bind to other CREs in the regulatory sequences associated with *GL3*. In the tested promoter, additional W-boxes are present that could allow TTG2 binding. In the N-terminal part of intron 2 an additional binding sites is present, apart from the Dof- and RAV1-sites, that was not yet tested regarding its effect on *GL3* expression. This MYC-binding site may indicate another protein involved in *GL3* expression regulation or may even hint to the MYC-related bHLH containing trichome patterning gene *MYC1* (Symonds et al., 2011). In this study MYC1 was not included in any assay and therefore an effect of *GL3* expression cannot be verified. The co-expression of GL1, GL3, TTG1 and TTG2 also increased the reporter gene expression in all four tested *GL3* constructs. These findings indicate, that the direct protein-DNA interactions of the activators slightly increase the GL3 expression. However, the increased reporter gene activities did not exceed 160 %, which seems to be rather low compared to effects observed for TRY and CPC for example (Pesch et al., 2014). Low expression changes seem to be in line with the overall low expression of GL3 in the patterning zone and in emerging trichomes (Friede et al., 2017). Yet, alternatively to gene expression regulation, another mechanism could take place.

The positive feedback loop ultimately leads to an increase in activator amount. However, this may not be caused by increased expression rate but by increased protein stability. The increased stability would lead to a higher protein amount for an elongated period of time, which could have the same effect as increased gene expression. However, this theory is currently being tested by T. Bergmann through adjusting our already published and established mathematic models. The postulated feedback loops lead to an exponential increase in activators in the models (Balkunde et al., 2020; Zhang et al., 2024) and it remains to be seen if the prolonged presence of proteins may lead to the same effect.

4.4. Differential complex formation may influence protein stabilities

The generated P2A data was acquired from experiments performed in leek epidermal cells, with only two interaction partners. Of course, this does not reflect the protein composition in *Arabidopsis's* epidermal cells. Therefore, stable lines expressing R2R3MYB-P2A constructs in *Arabidopsis* were created. Unfortunately, only MYB23-P2A stable lines that displayed the fluorescence proteins in the expected cellular locations were retrieved. Fluorescence ratios of MYB23-P2A in developing trichomes and surrounding cells revealed an increase in MYB23 stability with increasing distance to the trichomes. These results were highly surprising, as one would assume that activators are more stable in and close to trichomes due to their role in initiating trichome fate.

The observation could be explained by different variants of MBW complexes in the different cell types. A recent study showed that competition between GL1 and TTG1 for GL1 binding in the presence of TRY leads to the formation of different complexes when all interaction partners are present in equimolar amounts (Zhang et al., 2024). Dimers consisting of GL1-GL3, GL1-TTG1, GL1-TRY, and GL3-GL3 make up the majority of detected complexes, with 21.2 %, 12 %, 5.8 %, and 2.7 %, respectively. The assumed "classic" MBW complex consisting of GL1-GL3-TTG1 only amounted to 5.8 % of total complexes (Zhang et al., 2024). A lot of different complex compositions included GL3 homodimers bound by the three other proteins in different arrangements. In this study, only the four mentioned proteins were tested in HEK cells, so one can only imagine the vast variety of protein complexes present at any given moment in trichome patterning. Thus, these complexes can influence the protein stability of their own components and, therefore, the patterning process. Also, these different complexes may help to explain how a seemingly low expressed and rapidly degraded core patterning protein, such as GL3 (Friede et al., 2017; Patra et al., 2013a, b), plays such an important role in patterning. Maybe the free GL3 is degraded rapidly, but as soon as it is bound by other trichome patterning proteins, it is not accessible for the proteasomal degradation cascade. The homodimerization of GL3, however, could even lead to a decrease in GL3 stability, which may be counteracted by the other bound proteins in the complex or even be reinforced. These mechanisms could also apply to the other patterning proteins incorporated in complexes. Therefore, in the stable lines expressing MYB23-P2A differential regulation could take place, depending on the complex compositions.

Nevertheless, it has to be taken into consideration that MYB23 in the stable line created in this study is expressed constitutively via the *35S* promoter. Therefore, the endogenous protein proportions are askew, and the observed MYB23 stability changes do not necessarily reflect the endogenous situation. However, overexpression lines of *MYB23* do not display a trichome phenotype (Tominaga-Wada et al., 2012).Also, the MYB23-P2A lines do not possess any obvious trichome phenotype. To exclude a systematic effect caused by the P2A construct, a transgenic plant expressing *pENSG-p35S:YFP-NLSNLS-P2A-NLSNLS-mCherry* should be generated, and fluorescence ratios should be determined. If no increase in stability with increased trichome distance is observed, the stability effect observed in the MYB23-P2A line could be understood as caused by biological factors.

4.5. Alternative strategies to examine protein stabilities

The performed P2A experiments do not reflect the correct *in-vivo* conditions. However, the endogenous expression of trichome patterning genes is relatively low and protein amount measurements on a single cell level are challenging (Xie & Ding, 2022). As an alternative strategy to determine protein stabilities in the form of production and degradation rates, photoconvertible

proteins were explored. Dendra2 is a promising candidate to be utilized in transient expression to determine protein degradation over time. However, the tested conversion and detection with CLSM may limit the sample examination due to being time-consuming and also lead to decreased sample size due to phototoxicity (Icha et al., 2017). An alternative would be the detection of green and red fluorescence Dendra2 species using a plate reader (Heidary et al., 2017). Heidary and colleagues utilized HEK cells expressing Dendra2 and an LED flood array emitting 405 nm light, intense enough to successfully convert the Dendra2 protein from the green to the red fluorescence emitting form. The HEK cells were easily accessible for this treatment and fluorescence intensity measurements, as they were placed onto 96-well plates (Heidary et al., 2017). This strategy could most likely be adapted to converse cell suspension culture or *Arabidopsis* protoplasts transformed with trichome patterning proteins fused to Dendra2. Alternatively, the assay could be established in HEK cells expressing the fusion proteins, or tobacco-infiltrated leaf discs could be used for conversion in a 96-well plate.

Implementing the acquired P2A data into the patterning models will be challenging, as the data only reflect the different stabilities in the isolated presence of one other patterning protein. Furthermore, the high expression of both constructs may influence the behaviours observed for these proteins. Ideally, protein amounts in the appropriate tissue could be determined in different developmental stages and compared between proteins. In recent years different techniques to measure protein amounts with a single-cell resolution in planta were developed and may be suitable (Clark et al., 2022; Cookson et al., 2009; Komatsubara et al., 2019; Levy & Slavov, 2018; Misra et al., 2014; Montenegro-Johnson et al., 2015; Rosenfeld et al., 2005; Xie & Ding, 2022).

4.6. The exact regulatory sequences of *GL1* remain somewhat elusive

Different studies are available claiming to have identified the regulatory sequences of *GL1* (Larkin et al., 1993; Oppenheimer et al., 1991; Pesch, 2005; Wang et al., 2004). However, all studies used slightly different sequences, vectors, or even ecotypes. Here, an array of different rescue constructs was analyzed to shed more light on the underlying regulatory elements. Interestingly, nearly all constructs containing introns induced more trichomes compared to the CDS-containing constructs. This indicates a role of the introns in expression regulation, most likely through CRMs. An enhancer role of the first intron seems unlikely, as the constructs containing the first intron up- or downstream of the 3' enhancer or *GL1* CDS, respectively, did not induce enough trichomes to rescue the *gl1* phenotype. This indicates a location-dependent role of intron 1, which excludes the intron as a classic enhancer element (Schmitz et al., 2022).

Comparing the 3' enhancer defined by Wang or Larkin does not reveal any difference in rescue efficiency. This indicates that the shorter enhancer defined by Larkin already encompasses all

necessary CREs. This would include, for example, MYC-binding sites, several HD-ZIP motifs, and MYB-binding sites. Interestingly, the Larkin enhancer includes one enhancer element (Kucho et al., 2003) with MYB-binding site properties. In the Wang 3' enhancer, another enhancer element is present, the so-called quantitative-element (Hamilton et al., 1998). Considering the similar rescue efficiencies of both 3' enhancers, these elements are probably not functional or necessary in the examined vector arrangements. Additionally, the position of the Larkin 3' enhancer did not lead to differences in rescue efficiency.

The most surprising result was the reduced rescue ability of the constructs most closely reflecting the endogenous situation. In constructs without a p35S TATA box but with the endogenous order of the regulatory sequences, the genomic *GL1* sequence generated significantly fewer trichomes than the CDS sequence. This reduction in trichome number may be explained by a silencer motif present in the introns that may be overridden in the presence of another enhancer element, such as the TATA box of p35S (Schmitz et al., 2022). Alternatively, these results may indicate that the endogenous sequences may not be fully known due to the insufficient rescue ability. In the 2004 study of Wang and colleagues, a full recovery of the *gl1* phenotype was observed using the endogenous sequence including the intron containing *GL1*. However, the used construct possessed a *p35S* enhancer element upstream of the inserted *pGL1* sequence (Wang et al., 2004). The rescue experiments performed in this study indicate, that the *p35S* TATA box leads to an over rescue of the trichome phenotype. Without such an enhancing sequence, the so far published sequences do not induce enough trichomes to fully rescue *gl1*. So maybe the endogenous position of *GL1* enables the correct expression strength.

4.7. Transactivation assays indicate qualitative differences in expression regulation of *GL1* and the *ETCs*

Transactivation assays revealed some qualitative differences between the different regulatory sequences of *GL1*. Both tested 3' enhancer sequences alone induced only a small difference in reporter gene expression. This solidifies the categorization as an enhancer element (Schmitz et al., 2022). The first intron seemed to act as a kind of silencer when combined only with *pGL1*. Especially the addition of *TRY* and *CPC*, in combination with the three activators, led to a nearly abolished promoter activity. Interestingly, this silencing behaviour of intron 1 was not observed when placed more endogenously between exon 1 and 2 with intact splicing sites. These observations reinforce the complicated nature of expression regulation via CREs and CRMs and their organization relative to each other (Brooks et al., 2023; Schmitz et al., 2022).

If 3' enhancer and *pGL1*, as well as the first intron, were present in the reporter construct, the co-expression of the three activators led to an increase in reporter gene expression, and this effect could be muted by the additional expression of either *TRY* or *CPC*. These results suggest a positive feedback loop of *GL1* on its own expression. However, this effect is dependent on the presence of *GL3* and *TTG1*. The addition of *TTG2* increased the reporter gene expression even more, indicating a role of *TTG2* not only in *TRY* and *CPC* regulation but also in *GL1* (Pesch et al., 2014). Moreover, there are hints to a more elaborate role for GL2 in gene regulation of trichome patterning genes, apart from its role as downstream gene (Pietsch, 2022). Classically, GL2, as well as TTG2, were defined as downstream genes of the trichome patterning active complex (Ishida et al., 2007; Johnson et al., 2002; Masucci & Schiefelbein, 1996; Rerie et al., 1994).

Additionally to *GL1*, the gene expression of the closely related R3MYB inhibitors *ETC1*, *ETC2* and *ETC3* was examined. All three genes seem to be very similar regarding their expression regulation. However, pETC1 seem to be more sensitive towards activation through the tested activators, compared to pETC2 and pETC3. PLACE analysis revealed several motifs present in all three promoter sequences, which is highly likely as these motifs are commonly known transcription factor binding sites or associated with stress responses (Marand et al., 2017, 2023; Schmitz et al., 2022) . Also, the distribution regarding motif classes was very similar in all three promoter sequences. This would explain the similar transactivation results. However, the number of binding sites of specific transcription factor classes differed between the promoter sequences. Especially the stark reduction in WRKY binding sites in pETC2 may hint to a differential regulation. To really decipher important CREs and CRMs in *ETC* regulation, promoter deletion studies should be conducted. For example, the different predicted enhancer elements need to be tested regarding their actual functionality.

In the extensive qPCR study conducted by J. Pietsch, *ETC1*, *ETC2,* and *ETC3* were drastically different expressed in various patterning mutants (Pietsch, 2022). *ETC2* seems to be regulated differently than *ETC1* and *ETC3*, as it is often upregulated when the other two ETCs, or the other tested inhibitors in general, are downregulated. Interestingly, *ETC2* is downregulated in the *etc1* and *etc3* single mutants, but not vice versa. Additionally, the simultaneous loss of *ETC1* and *ETC3* leads to an even more drastic decrease in *ETC2* expression (Pietsch, 2022). The qPCR results, as well as the transactivation assays, indicate a slightly different regulation of the three ETCs.

However, in the GUS assays conducted in this study neither any ETC nor GL2 was tested regarding the effect on reporter gene activity. This should definitely be tested in future studies, as the expression data suggest an influence of these proteins on gene expression. Also, the different binding sites may indicate differential regulation. Further promoter deletion studies combined with transactivation assays could shed more light on the underlying mechanisms.

These transactivation results need to be verified by repeating the GUS assays and also via different experiments, such as duel-luciferase assays in protoplasts for example (Wehner et al., 2011). Additionally, the influence of other trichome patterning proteins on *GL1* and *ETC* expression could be examined, such as GL2. Additionally, the influence of the *ETCs*, *MYB23, TT8* and *MYC1* were not studied in transactivation assays but the qPCR results indicate an influence of some of these gene on GL1, ETC1, ETC2 and ETC3 expression (Pietsch, 2022). Also, the different binding sites in the pETCs may indicate differential regulation. Further promoter deletion studies combined with transactivation assays could shed more light on the underlying mechanisms.

4.8. Interspecies rescue experiments reveal conserved functions

In the closely related Brassicaceae species *Arabidopsis* and *Cardamine*, trichome patterning seems to rely on the same set of genes (Fuster-Pons et al., 2024; Pietsch, 2022). The rescue experiments using *Cardamine* MYB constructs to rescue *Arabidopsis* phenotypes revealed some conserved functions between the two sets of MYBs. Although none of the *Cardamine* MYBs could rescue the trichome phenotypes to the wild-type level, *ChGL1* was able to induce trichomes in both *gl1* as well as *gl1 myb23* plants. Though it is known that closely related MYB genes from different species can rescue interspecies phenotypes, such as the R gene from maize or cotton MYBs in *Arabidopsis* (Bernhardt et al., 2003; Payne et al., 2000; Wang et al., 2004), the partial rescue of *gl1* and *gl1 myb23* by *ChGL1* was surprising as, in a former study, *ChGL1* was found to be expressed at a low level in small leaves where patterning takes place (Pietsch, 2022).

ChMYB23 and *ChWER* could only induce trichomes in *gl1*. Interestingly, the trichomes induced by *ChWER* are often situated at the leaf margin, indicating a different expression pattern compared to *ChGL1*. This observation is not surprising, as not only gene function needs to be somewhat conserved between species, but also the regulatory sequences to confer at least some degree of correct expression parameters. To assess the impact of protein function and expression patterns independently in future experiments, promoter swap constructs could be generated to express the ChMYBs under the endogenous *Arabidopsis* regulatory sequences and the *Arabidopsis* MYBs under the *Cardamine* regulatory sequences.

Additionally to the rescue experiments, the first introns of the six different MYB TFs were examined regarding CREs. If focused on binding motifs for four protein classes, MYB, MYC, WRKY, and HD-ZIP, the comparison revealed an absence of any predicted binding motif in intron 1 of *AtMYB23* and *ChMYB23*. This may indicate that these intron sequences do not play a role in orchestrating gene expression by binding members of the four protein classes. However, in the first intron of *ChMYB23* an enhancer element was predicted, which is also described as an MYB-binding site (Kucho et al.,

2003). This enhancer element may correspond to the predicted MYB-binding sites in the C-terminus of *AtGL1* and *AtWER*, as well as the MYB-binding site predicted for *ChGL1*. Interestingly, the same enhancer element found in *ChMYB23* was also found in both At*WER* and *ChWER* introns. However, so far, no statement regarding the influence of the first intron on the expression of each gene can be stated. This needs to be examined experimentally, through different rescue constructs containing the introns or even mutating specific CREs. The role of introns in gene expression is rather interesting, as for *GL1* and *MYB23* such a role in Arabidopsis is postulated (Wang et al., 2004). For *TRY* and *GL3* studies were published to suggest an influence of the second intron on gene expression (Friede et al., 2017; Meng et al., 2021). For *TRY* an enhancer element was identified which is suspected to be involved in gene regulation regarding flowering time and trichome development (Meng et al., 2021).

In *Arabidopsis,* MYBs can replace each other functionally by being under the control of the appropriate regulatory sequences (Kirik et al., 2005; Lee & Schiefelbein, 2001; Tominaga-Wada et al., 2012). In *Cardamine,* neither trichome patterning nor root hair formation has so far been extensively studied, with only recently linking GL1 amount to trichome number and revealing the presence of two cortical layers in the root (Di Ruocco et al., 2018; Fuster-Pons et al., 2024). Therefore, not many genes are identified as playing a role in both patterning processes in *Cardamine*, and no gene exchange studies were conducted. However, the rescue experiments conducted in this study reveal some conserved functions of interspecies MYBs. Even ChWER could induce trichomes under its endogenous regulatory sequences. This is different from the situation in *Arabidopsis* but is in accordance with the qPCR experiments performed by J. Pietsch, which showed that contrary to *Arabidopsis*, *ChWER* was detected in tiny leaves (Pietsch, 2022). This indicates an involvement of *ChWER* in trichome patterning, and in cross-species experiments, this study could show that regulatory sequences are present in controlling *ChWER* that leads to leaf expression. Additionally, *ChWER* was able to induce some trichomes in *Arabidopsis*. The location of the initiated trichomes, however, indicates differences in the information regarding the location of expression.

4.9. Patterning models help to frame biological questions and experimental design

The intriguing trichome phenotypes of the weak *ttg1* alleles and the *cpc try* double mutants led to the testing of published trichome patterning models regarding their ability to reconstruct the observed trichome pattern (Deneer, 2022). These models were not able to recreate the observed pattern without adjusting different parameters, which were validated in experiments or are planned to be examined in detail. In the weak *ttg1* alleles, the depletion of TTG1 in trichome surrounding cells was

abolished, leading ultimately to the fusion of the activator-depletion and activator-inhibitor model in a new publication (Balkunde et al., 2020).

Still, open questions remain regarding the *cpc try* mutant. The methods used in this study to gain insight into the mechanisms causing the phenotype may need optimization. The GUS stainings revealed difficulties regarding staining sensitivity, and due to the dense trichome clusters, the preparation of the stained samples is challenging. Therefore, the expression of a bright fluorophore under the endogenous *TRY* or *CPC* promoter may enable a better examination. The observed distinct staining of single trichomes on leaves 1 and 2 may not be representative of the trichome pattern as those leaves display a different trichome pattern than the following leaves (Pesch, 2005; Schnittger & Hülskamp, 2002). However, this staining pattern was not observed in the backcrosses in *Col-0*, indicating that the specific properties of the *cpc try* mutant induce this expression pattern. The stained trichomes somehow differ regarding their *CPC* expression compared to the other trichomes, although similarly developed trichomes at the leaf tip do not display staining. *CPC* is expressed in the patterning zone and in trichomes in wild-type plants, indicating trichome-specific expression (Schellmann et al., 2002). Also, the established marker line in *cpc try* mutants will help to examine the cluster formation in more detail. The time span between CLSM sessions has to be determined more closely, but the method for growth tracking was successfully established based on the method published by the Roeder lab, and growth can be tracked reliably.

4.10. Perspectives

Trichome patterning is a complex process involving a high number of genes and cross-regulation networks. In this study, some of these interactions could be examined more closely. Especially the protein stability changes seem to be a promising new hint at pattern regulation. The results obtained in this study need to be verified by other methods but could ultimately help to adapt the mathematic models based on experimental data. Another very interesting parameter for trichome patterning is the total amount of each trichome patterning protein at different developmental stages. This could be determined by utilizing single-cell resolution methods in living tissue. These approaches are challenging, but in recent years, some new techniques have been developed that could help solve some of the big open questions. The close interplay between mathematic modelling and experimental approaches will continue to unravel the mysteries underlying trichome patterning. Furthermore, the potential positive feedback loop of GL1 combined with GL3 and TTG1 on its own expression is a very interesting result. Utilizing additional methods to examine these results in more detail will shed light on the regulation of *GL1* expression. However, the question regarding the necessary regulatory sequences for *GL1* expression is not resolved completely. Further experiments need to be conducted,

such as promoter deletion studies and also using an increased enhancer sequence to hopefully find the missing elements to generate the correct *GL1* expression. A detailed analysis of the regulatory element that confers trichome-specific expression needs to be performed to gain more insight into spatial expression regulation. Additionally, the timeline of GL1 expression may be an interesting field of research, as data suggest that pGL2-mediated expression of *GL1* rescues *gl1* trichome phenotypes (Pesch, 2005). Moreover, overexpression lines of trichome patterning genes have not been analyzed so far regarding expression changes. Thus, qPCR analysis of these lines would increase the knowledge about gene expression regulation during trichome patterning. The interspecies rescue experiment revealed some conservation between MYB function across the two examined species. Further promoter swap experiments, as well as the establishment of *Cardamine* mutants impaired in trichome or root hair formation, would facilitate the understanding of the evolution of these patterning processes.

5. Bibliography

Abe, H., Urao, T., Ito, T., Seki, M., Shinozaki, K., & Yamaguchi-Shinozaki, K. (2003). Arabidopsis AtMYC2 (bHLH) and AtMYB2 (MYB) function as transcriptional activators in abscisic acid signaling. *Plant Cell*, *15*(1), 63–78. https://doi.org/10.1105/tpc.006130

Abe, H., Yamaguchi-Shinozaki, K., Urao, T., Lwasaki, T., Hosokawa, D., & Shinozakic, K. (1997). Role of Arabidopsis MYC and MYB Homologs in Drought-and Abscisic Acid-Regulated Gene Expression. In *The Plant Cell* (Vol. 9). American Society of Plant Physiologists. https://academic.oup.com/plcell/article/9/10/1859/5986524

Abe, M., Takahashi, T., & Komeda, Y. (2001). Identification of a cis-regulatory element for L1 layer-specific gene expression, which is targeted by an L1-specific homeodomain protein. *Plant Journal*, *26*(5), 487–494. https://doi.org/10.1046/j.1365-313X.2001.01047.x

Ahier, A., & Jarriault, S. (2014). Simultaneous expression of multiple proteins under a single promoter in Caenorhabditis elegans via a versatile 2A-based toolkit. *Genetics*, *196*(3), 605–613. https://doi.org/10.1534/genetics.113.160846

Allen, R. D., Bernier, F., Lessard, P. A., & Beachy', R. N. (1989). Nuclear Factors lnteract with a Soybean ,&Conglycinin En hancer. In *The Plant Cell* (Vol. 1).

Amack, S. C., & Antunes, M. S. (2020). CaMV35S promoter – A plant biology and biotechnology workhorse in the era of synthetic biology. In *Current Plant Biology* (Vol. 24). Elsevier B.V. https://doi.org/10.1016/j.cpb.2020.100179

Andersson, R., & Sandelin, A. (2020). Determinants of enhancer and promoter activities of regulatory elements. In *Nature Reviews Genetics* (Vol. 21, Issue 2, pp. 71–87). Nature Research. https://doi.org/10.1038/s41576-019-0173-8

Ando, R., Hama, H., Yamamoto-Hino, M., Mizuno, H., & Miyawaki, A. (2002). An optical marker based on the UV-induced green-to-red photoconversion of a fluorescent protein. *Proceedings of the National Academy of Sciences*, *99*(20), 12651–12656. https://doi.org/10.1073/pnas.202320599

Ando, R., Mizuno, H., & Miyawaki, A. (2004). Regulated fast nucleocytoplasmic shuttling observed by reversible protein highlighting. *Genome Biology*, *5*(8). https://doi.org/10.1186/gb-2004-5-8-r55

Arteaga, N., Méndez-Vigo, B., Fuster-Pons, A., Savic, M., Murillo-Sánchez, A., Picó, F. X., & Alonso-Blanco, C. (2022). Differential environmental and genomic architectures shape the natural diversity for trichome patterning and morphology in different Arabidopsis organs. *Plant Cell and Environment*, *45*(10), 3018–3035. https://doi.org/10.1111/pce.14308

Atkins, J. F., Wills, N. M., Loughran, G., Wu, C. Y., Parsawar, K., Ryan, M. D., Wang, C. H., & Nelson, C. C. (2007). A case for "StopGo": Reprogramming translation to augment codon meaning of GGN by promoting unconventional termination (Stop) after addition of glycine and then allowing continued translation (Go). *RNA*, *13*(6), 803–810. https://doi.org/10.1261/rna.487907

Baker, S. S., Wilhelm, K. S., & Thomashow, M. F. (1994). The 5'-region of Arabidopsis thaliana corl5a has cis-acting elements that confer cold-, drought-and ABA-regulated gene expression. In *Plant Molecular Biology* (Vol. 24).

Balkunde, R., Bouyer, D., & Hülskamp, M. (2011). Nuclear trapping by Gl3 controls intercellular transport and redistribution of TTG1 protein in Arabidopsis. *Development*, *138*(22), 5039–5048. https://doi.org/10.1242/dev.072454

Balkunde, R., Deneer, A., Bechtel, H., Zhang, B., Herberth, S., Pesch, M., Jaegle, B., Fleck, C., & Hülskamp, M. (2020). Identification of the Trichome Patterning Core Network Using Data from

Weak ttg1 Alleles to Constrain the Model Space. *Cell Reports*, *33*(11). https://doi.org/10.1016/j.celrep.2020.108497

Balkunde, R., Pesch, M., & Hülskamp, M. (2010). Trichome patterning in arabidopsis thaliana. From genetic to molecular models. In *Current Topics in Developmental Biology* (Vol. 91, Issue C, pp. 299–321). Academic Press Inc. https://doi.org/10.1016/S0070-2153(10)91010-7

Baranowskij, N., Frohberg, C., Prat, S., & Willmitzer, L. (1994). A novel DNA binding protein with homology to Myb oncoproteins containing only one repeat can function as a transcriptional activator. *EMBO Journal*, *13*(22), 5383–5392. https://doi.org/10.1002/j.1460-2075.1994.tb06873.x

Barthlott W, Wiersch S, Colic ZC, Koch K. Classification of trichome types within species of the water fern Salvinia, and ontogeny of the egg-beater trichomes. Botany. 2009;87(9):830–6.

Bate, N., & Twell, D. (1998). Functional architecture of a late pollen promoter: pollen-specific transcription is developmentally regulated by multiple stage-specific and co-dependent activator elements. In *Plant Molecular Biology* (Vol. 37).

Baumann, K., De Paolis, A., Costantino, P., & Gualberti, G. (1999). The DNA Binding Site of the Dof Protein NtBBF1 Is Essential for Tissue-Specific and Auxin-Regulated Expression of the rolB Oncogene in Plants. In *The Plant Cell* (Vol. 11). www.plantcell.org

Baumgarten, L., Pieper, B., Song, B., Mane, S., Lempe, J., Lamb, J., Cooke, E. L., Srivastava, R., Strütt, S., Žanko, D., Casimiro, P. G. P., Hallab, A., Cartolano, M., Tattersall, A. D., Huettel, B., Filatov, D. A., Pavlidis, P., Neuffer, B., Bazakos, C., … Tsiantis, M. (2023). Pan-European study of genotypes and phenotypes in the Arabidopsis relative Cardamine hirsuta reveals how adaptation, demography, and development shape diversity patterns. *PLoS Biology*, *21*(7 July). https://doi.org/10.1371/journal.pbio.3002191

Beilstein, M. A., Al-Shehbaz, I. A., Mathews, S., & Kellogg, E. A. (2008). Brassicaceae phylogeny inferred from phytochrome A and ndhF sequence data: Tribes and trichomes revisited. *American Journal of Botany*, *95*(10), 1307–1327. https://doi.org/10.3732/ajb.0800065

Beilstein, M. A., Nagalingum, N. S., Clements, M. D., Manchester, S. R., & Mathews, S. (2010). Dated molecular phylogenies indicate a Miocene origin for Arabidopsis thaliana. *Proceedings of the National Academy of Sciences of the United States of America*, *107*(43), 18724–18728. https://doi.org/10.1073/pnas.0909766107

Benfey, P. N., Ren, L., & Chua, N.-H. (1990). Combinatorial and synergistic properties of CaMV 35S enhancer subdomains. In *The EMBO Journal* (Vol. 9, Issue 6).

Bernard, P., & Couturier, M. (1992). *Cell Killing by the F Plasmid CcdB Protein Involves Poisoning of DNA-Topoisomerase II Complexes*.

Bernhardt, C., Lee, M. M., Gonzalez, A., Zhang, F., Lloyd, A., & Schiefelbein, J. (2003). The bHLH genes GLABRA3 (GL3) and ENHANCER OF GLABRA3 (EGL3) specify epidermal cell fate in the Arabidopsis root. *Development*, *130*(26), 6431–6439. https://doi.org/10.1242/dev.00880

Bernhardt, C., Zhao, M., Gonzalez, A., Lloyd, A., & Schiefelbein, J. (2005). The bHLH genes GL3 and EGL3 participate in an intercellular regulatory circuit that controls cell patterning in the Arabidopsis root epidermis. *Development*, *132*(2), 291–298. https://doi.org/10.1242/dev.01565

Borevitz, J. O., Xia, Y., Blount, J., Dixon, R. A., & Lamb, C. (2000). Activation Tagging Identifies a Conserved MYB Regulator of Phenylpropanoid Biosynthesis. In *The Plant Cell* (Vol. 12). www.plantcell.org

Boter, M., Ruíz-Rivero, O., Abdeen, A., & Prat, S. (2004). Conserved MYC transcription factors play a key role in jasmonate signaling both in tomato and Arabidopsis. *Genes and Development*, *18*(13), 1577–1591. https://doi.org/10.1101/gad.297704

Bouyer, D., Geier, F., Kragler, F., Schnittger, A., Pesch, M., Wester, K., Balkunde, R., Timmer, J., Fleck, C., & Hülskamp, M. (2008). Two-dimensional patterning by a trapping/depletion mechanism: The role of TTG1 and GL3 in Arabidopsis trichome formation. *PLoS Biology*, *6*(6), 1166–1177. https://doi.org/10.1371/journal.pbio.0060141

Boyle, B., Brisson, N. Repression of the Defense Gene PR-10a by the Single-Stranded DNA Binding Protein SEBF, The Plant Cell, Volume 13, Issue 11, November 2001, Pages 2525–2537, https://doi.org/10.1105/tpc.010231

Brooks, E. G., Elorriaga, E., Liu, Y., Duduit, J. R., Yuan, G., Tsai, C. J., Tuskan, G. A., Ranney, T. G., Yang, X., & Liu, W. (2023). Plant Promoters and Terminators for High-Precision Bioengineering. In *BioDesign Research* (Vol. 5). American Association for the Advancement of Science. https://doi.org/10.34133/bdr.0013

Broun, P. (2005). Transcriptional control of flavonoid biosynthesis: A complex network of conserved regulators involved in multiple aspects of differentiation in Arabidopsis. *Current Opinion in Plant Biology*, *8*(3 SPEC. ISS.), 272–279. https://doi.org/10.1016/j.pbi.2005.03.006

Brown, J. W. S. (1986). A catalogue of splice junction and putative branch point sequences from plant introns. In *Nucleic Acids Research* (Vol. 14). https://academic.oup.com/nar/article/14/24/9549/1454446

Buchanan, B. W., Lloyd, M. E., Engle, S. M., & Rubenstein, E. M. (2016). Cycloheximide chase analysis of protein degradation in Saccharomyces cerevisiae. *Journal of Visualized Experiments*, *2016*(110). https://doi.org/10.3791/53975

Burke, T. W., & Kadonaga, J. T. (1996). *Drosophila TFIID binds to a conserved downstream basal promoter element that is present in many TATA-box-deficient promoters*.

Busk, P. K., Jensen, A. B., & Pages, M. (1997). Regulatory elements in vivo in the promoter of the abscisic acid responsive gene rab17 from maize. *Plant Journal*, *11*(6), 1285–1295. https://doi.org/10.1046/j.1365-313X.1997.11061285.x

Campos-Ortega, J. A. (1993). *Mechanisms of Early Neurogenesis in Drosophila melanogaster*.

Cercós, M., Gómez-Cadenas, A., & Ho, T. H. D. (1999). Hormonal regulation of a cysteine proteinase gene, EPB-1, in barley aleurone layers: Cis- and trans-acting elements involved in the co-ordinated gene expression regulated by gibberellins and abscisic acid. *Plant Journal*, *19*(2), 107–118. https://doi.org/10.1046/j.1365-313X.1999.00499.x

Chakravarthy, S., Tuori, R. P., D'Ascenzo, M. D., Fobert, P. R., Després, C., & Martin, G. B. (2003). The Tomato Transcription Factor Pti4 Regulates Defense-Related Gene Expression via GCC Box and Non-GCC Box cis Elements. *Plant Cell*, *15*(12), 3033–3050. https://doi.org/10.1105/tpc.017574

Chalvin, C., Drevensek, S., Dron, M., Bendahmane, A., & Boualem, A. (2020). Genetic Control of Glandular Trichome Development. In *Trends in Plant Science* (Vol. 25, Issue 5, pp. 477–487). Elsevier Ltd. https://doi.org/10.1016/j.tplants.2019.12.025

Chan, C.-S., Guo, L., & Shih, M.-C. (2001). Promoter analysis of the nuclear gene encoding the chloroplast glyceraldehyde-3-phosphate dehydrogenase B subunit of Arabidopsis thaliana. In *Plant Molecular Biology* (Vol. 46).

Cheng, M. C., Enderle, B., Kathare, P. K., Islam, R., Hiltbrunner, A., & Huq, E. (2020). PCH1 and PCHL Directly Interact with PIF1, Promote Its Degradation, and Inhibit Its Transcriptional Function

during Photomorphogenesis. *Molecular Plant*, *13*(3), 499–514. https://doi.org/10.1016/j.molp.2020.02.003

Chopra, D., Mapar, M., Stephan, L., Albani, M. C., Deneer, A., Coupland, G., Willing, E. M., Schellmann, S., Schneeberger, K., Fleck, C., Schrader, A., & Hülskamp, M. (2019). Genetic and molecular analysis of trichome development in Arabis alpina. *Proceedings of the National Academy of Sciences of the United States of America*, *116*(24), 12078–12083. https://doi.org/10.1073/pnas.1819440116

Chopra, D., Wolff, H., Span, J., Schellmann, S., Coupland, G., Albani, M. C., Schrader, A., & Hülskamp, M. (2014). Analysis of TTG1 function in Arabis alpina. *BMC Plant Biology*, *14*(1). https://doi.org/10.1186/1471-2229-14-16

Chudakov, D. M., Matz, M. V., Lukyanov, S., & Lukyanov, K. A. (2010). Fluorescent proteins and their applications in imaging living cells and tissues. In *Physiological Reviews* (Vol. 90, Issue 3, pp. 1103–1163). https://doi.org/10.1152/physrev.00038.2009

Ciechanover, A. (1998). EMBO MEMBER'S REVIEW The ubiquitin-proteasome pathway: on protein death and cell life. In *The EMBO Journal* (Vol. 17, Issue 24).

Cirillo, L. A., Lin, F. R., Cuesta, I., Friedman, D., Jarnik, M., & Zaret, K. S. (2002). Opening of Compacted Chromatin by Early Developmental Transcription Factors HNF3 (FoxA) and GATA-4 binding of GAL4 to the GAL1 promoter in yeast precedes recruitment of SAGA (Dudley et al., 1999). It remains to be determined how these and other transcription factors recognize their binding sites within silent chromatin and whether they require other proteins for initial binding. In *Molecular Cell* (Vol. 9).

Clark, N. M., Elmore, J. M., & Walley, J. W. (2022). To the proteome and beyond: advances in single-cell omics profiling for plant systems. *Plant Physiology*, *188*(2). https://doi.org/10.1093/plphys/kiab429

Colot, V., Robert, L. S., Kavanagh, T. A., Bevan, M. W., & Thompson, R. D. (1987). Localization of sequences in wheat endosperm protein genes which confer tissue-specific expression in tobacco. *The EMBO Journal*, *6*(12), 3559–3564. https://doi.org/10.1002/j.1460-2075.1987.tb02685.x

Cookson, N. A., Cookson, S. W., Tsimring, L. S., & Hasty, J. (2009). Cell cycle-dependent variations in protein concentration. *Nucleic Acids Research*, *38*(8), 2676–2681. https://doi.org/10.1093/nar/gkp1069

Cristina, M. Di, Sessa, G., Dolan, L., Linstead, P., Baima, S., Ruberti, I., & Morelli, G. (1996). The Arabidopsis Athb-10 (GLABRA2) is an HD-Zip protein required for regulation of root hair development. *The Plant Journal*.

Dalin, P., Ågren, J., Björkman, C., Huttunen, P., & Kärkkäinen, K. (2008). Leaf trichome formation and plant resistance to herbivory. In *Induced Plant Resistance to Herbivory* (pp. 89–105). Springer Netherlands. https://doi.org/10.1007/978-1-4020-8182-8_4

Daniels, R. W., Rossano, A. J., Macleod, G. T., & Ganetzky, B. (2014). Expression of multiple transgenes from a single construct using viral 2A peptides in Drosophila. *PLoS ONE*, *9*(6). https://doi.org/10.1371/journal.pone.0100637

Davies, J. (2017). Using synthetic biology to explore principles of development. In *Development (Cambridge)* (Vol. 144, Issue 7, pp. 1146–1158). Company of Biologists Ltd. https://doi.org/10.1242/dev.144196

Debeaujon, I., Nesi, N., Perez, P., Devic, M., Grandjean, O., Caboche, M., & Lepiniec, L. (2003). Proanthocyanidin-Accumulating Cells in Arabidopsis Testa: Regulation of Differentiation and Role in Seed Development. *Plant Cell*, *15*(11), 2514–2531. https://doi.org/10.1105/tpc.014043

Degenhardt, J., & Tobin', E. M. (1996). A DNA Binding Activity for One of Two Closely Defined Phytochrome Regulatory Elements in an Lhcb Promoter 1s More Abundant in Etiolated Than in Green Plants. In *The Plant Cell* (Vol. 8). American Society of Plant Physiologists. https://academic.oup.com/plcell/article/8/1/31/5985068

De Laat, W., & Duboule, D. (2013). Topology of mammalian developmental enhancers and their regulatory landscapes. In *Nature* (Vol. 502, Issue 7472, pp. 499–506). https://doi.org/10.1038/nature12753

de Lima, J. G. S., & Lanza, D. C. F. (2021). 2a and 2a-like sequences: Distribution in different virus species and applications in biotechnology. In *Viruses* (Vol. 13, Issue 11). MDPI. https://doi.org/10.3390/v13112160

Della Rosa, M., & Spivakov, M. (2020). Silencers in the spotlight. In *Nature Genetics* (Vol. 52, Issue 3, pp. 244–245). Nature Research. https://doi.org/10.1038/s41588-020-0583-8

Deneer, A. (2022). *Mathematical modelling of trichome patterning*.

Digiuni, S., Schellmann, S., Geier, F., Greese, B., Pesch, M., Wester, K., Dartan, B., Mach, V., Srinivas, B. P., Timmer, J., Fleck, C., & Hulskamp, M. (2008). A competitive complex formation mechanism underlies trichome patterning on Arabidopsis leaves. *Molecular Systems Biology*, *4*(217), 1–11. https://doi.org/10.1038/msb.2008.54

Di Ruocco, G., Bertolotti, G., Pacifici, E., Polverari, L., Tsiantis, M., Sabatini, S., Costantino, P., & Dello Ioio, R. (2018). Differential spatial distribution of miR165/6 determines variability in plant root anatomy. *Development (Cambridge)*, *145*(1). https://doi.org/10.1242/dev.153858

Donald, R. G., & Cashmore, A. R. (1990). Mutation of either G box or I box sequences profoundly affects expression from the Arabidopsis rbcS-1A promoter. *The EMBO Journal*, *9*(6), 1717–1726. https://doi.org/10.1002/j.1460-2075.1990.tb08295.x

Donnelly, M. L. L., Hughes, L. E., Luke, G., Mendoza, H., Ten Dam, E., Gani, D., & Ryan, M. D. (2001a). The "cleavage" activities of foot-and-mouth disease virus 2A site-directed mutants and naturally occurring "2A-like" sequences. *Journal of General Virology*, *82*(5), 1027–1041. https://doi.org/10.1099/0022-1317-82-5-1027

Donnelly, M. L. L., Luke, Garry, Mehrotra, A., Li, X., Hughes, L. E., Gani, D., & Ryan, M. D. (2001b). Printed in Great Britain Analysis of the aphthovirus 2A/2B polyprotein ' cleavage ' mechanism indicates not a proteolytic reaction, but a novel translational effect : a putative ribosomal ' skip '. In *Journal of General Virology* (Vol. 82). www.microbiologyresearch.org

Downes, B. P., Stupar, R. M., Gingerich, D. J., & Vierstra, R. D. (2003). The HECT ubiquitin-protein ligase (UPL) family in Arabidopsis: UPL3 has a specific role in trichome development. *Plant Journal*, *35*(6), 729–742. https://doi.org/10.1046/j.1365-313X.2003.01844.x

Dubouzet, J. G., Sakuma, Y., Ito, Y., Kasuga, M., Dubouzet, E. G., Miura, S., Seki, M., Shinozaki, K., & Yamaguchi-Shinozaki, K. (2003). OsDREB genes in rice, Oryza sativa L., encode transcription activators that function in drought-, high-salt- and cold-responsive gene expression. *Plant Journal*, *33*(4), 751–763. https://doi.org/10.1046/j.1365-313X.2003.01661.x

Dunn, M. A., White, A. J., Vural, S., & Hughes, M. A. (1998). Identification of promoter elements in a low-temperature-responsive gene (blt4.9) from barley (Hordeum vulgare L.). In *Plant Molecular Biology* (Vol. 38).

Ellerstr6m, M., Sffdberg, K., Ezcurra, I., & Rask, L. (1996). Functional dissection of a napin gene promoter: identification of promoter elements required for embryo and endosperm-specific transcription. In *Plant Molecular Biology* (Vol. 32). Kluwer Academic Publishers.

Elliott, K. A., & Shirsat, A. H. (1998). Promoter regions of the extA extensin gene from Brassica napus control activation in response to wounding and tensile stress. In *Plant Molecular Biology* (Vol. 37).

Elmayan, T., & Tepfer, M. (1995). Evaluation in tobacco of the organ specificity and strength of the rolL) promoter, domain A of the 35S promoter and the 35S 2 promoter. In *Transgenic Research* (Vol. 4).

El Refy, A., Perazza, D., Zekraoui, L., Valay, J. G., Bechtold, N., Brown, S., Hülskamp, M., Herzog, M., & Bonneville, J. M. (2004). The Arabidopsis KAKTUS gene encodes a HECT protein and controls the number of endoreduplication cycles. *Molecular Genetics and Genomics*, *270*(5), 403–414. https://doi.org/10.1007/s00438-003-0932-1

Ericson, M. L., Murén, E., Gustavsson, H. -O, Josefsson, L. -G, & Rask, L. (1991). Analysis of the promoter region of napin genes from Brassica napus demonstrates binding of nuclear protein in vitro to a conserved sequence motif. *European Journal of Biochemistry*, *197*(3), 741–746. https://doi.org/10.1111/j.1432-1033.1991.tb15966.x

Esch, J. J., Chen, M. A., Hillestad, M., & Marks, M. D. (2004). Comparison of TRY and the closely related At1g01380 gene in controlling Arabidopsis trichome patterning. *Plant Journal*, *40*(6), 860–869. https://doi.org/10.1111/j.1365-313X.2004.02259.x

Eulgem, T., Rushton, P. J., Robatzek, S., & Somssich, I. E. (2000). *The WRKY superfamily of plant transcription factors* (Vol. 5, Issue 5).

Eulgem, T., Rushton, P. J., Schmelzer, E., Hahlbrock, K., & Somssich, I. E. (1999). Early nuclear events in plant defence signalling: rapid gene activation by WRKY transcription factors. In *The EMBO Journal* (Vol. 18, Issue 17). https://www.embopress.org

Ezcurra, I., Wycliffe, P., Stålberg, K., & Rask, L. (1999). Interaction between composite elements in the napA promoter: both the B-box ABA-responsive complex and the RY/G complex are necessary for seed-specific expression. In *Plant Molecular Biology* (Vol. 40).

Fehlberg, V., Vieweg, M. F., Dohmann, E. M. N., Hohnjec, N., Pühler, A., Perlick, A. M., & Küster, H. (2005). The promoter of the leghaemoglobin gene VfLb29: Functional analysis and identification of modules necessary for its activation in the infected cells of root nodules and in the arbuscule-containing cells of mycorrhizal roots. *Journal of Experimental Botany*, *56*(413), 799–806. https://doi.org/10.1093/jxb/eri074

Fernández, V., Sancho-Knapik, D., Guzmán, P., Peguero-Pina, J. J., Gil, L., Karabourniotis, G., Khayet, M., Fasseas, C., Heredia-Guerrero, J. A., Heredia, A., & Gil-Pelegrín, E. (2014). Wettability, Polarity, And water absorption of holm oak leaves: Effect of leaf side and age. *Plant Physiology*, *166*(1), 168–180. https://doi.org/10.1104/pp.114.242040

Feys, B. J., Wiermer, M., Bhat, R. A., Moisan, L. J., Medina-Escobar, N., Neu, C., Cabral, A., & Parker, J. E. (2005). Arabidopsis SENESCENCE-ASSOCIATED GENE101 stabilizes and signals within an ENHANCED DISEASE SUSCEPTIBILITY1 complex in plant innate immunity. *Plant Cell*, *17*(9), 2601–2613. https://doi.org/10.1105/tpc.105.033910

Folkers, U., Berger, J., & Hülskamp, M. (1997). Cell morphogenesis of trichomes in *Arabidopsis*: differential control of primary and secondary branching by branch initiation regulators and cell growth. *Development*, *124*, 3779–3786.

Forde, B. G., Heyworth, A., Pywell, J., & Kreis, M. (1985). Nucleotide sequence of a Bl bordein gene and the identification of possible upstream regulatory elements in endosperm storage protein genes from barley, wheat and maize. In *Nucleic Acids Research* (Vol. 13). https://academic.oup.com/nar/article/13/20/7327/2377651

Foster R, Izawa T, Chua NH. Plant bZIP proteins gather at ACGT elements. FASEB J. 1994 Feb;8(2):192-200. doi: 10.1096/fasebj.8.2.8119490. PMID: 8119490.

Freemont, P. S. (2000). Ubiquitination: RING for destruction? Ubiquitination targets proteins for degradation and is a potent regulator of cellular protein function. Recent results implicate the RING finger domain in specific ubiquitination events; it is possible that all RING proteins act as E3 ubiquitin protein ligases, with implications for a variety of biological areas. In *Current Biology* (Vol. 10).

Friede, A., Zhang, B., Herberth, S., Pesch, M., Schrader, A., & Hülskamp, M. (2017). The second intron is essential for the transcriptional control of the Arabidopsis thaliana GLABRA3 gene in leaves. *Frontiers in Plant Science*, *8*. https://doi.org/10.3389/fpls.2017.01382

Fujiwara, T., & Beachy, R. N. (1994). Tissue-specific and temporal regulation of a fl-conglycinin gene: roles of the RY repeat and other cis-acting elements. In *Plant Molecular Biology* (Vol. 24).

Fulgione, A., & Hancock, A. M. (2018). Archaic lineages broaden our view on the history of Arabidopsis thaliana. In *New Phytologist* (Vol. 219, Issue 4, pp. 1194–1198). John Wiley and Sons Inc. https://doi.org/10.1111/nph.15244

Fusada, N., Masuda, T., Kuroda, H., Shimada, H., Ohta, H., & Takamiya, K. I. (2005). Identification of a novel cis-element exhibiting cytokinin-dependent protein binding in vitro in the 5'-region of NADPH-protochlorophyllide oxidoreductase gene in cucumber. *Plant Molecular Biology*, *59*(4), 631–645. https://doi.org/10.1007/s11103-005-0579-x

Fuster-Pons, A., Murillo-Sánchez, A., Méndez-Vigo, B., Marcer, A., Pieper, B., Torres-Pérez, R., Oliveros, J. C., Tsiantis, M., Picó, F. X., & Alonso-Blanco, C. (2024). The trichome pattern diversity of Cardamine shares genetic mechanisms with Arabidopsis but differs in environmental drivers. *Plant Physiology*. https://doi.org/10.1093/plphys/kiae213

Galway, M. E., Masucci, J. D., Lloyd, A. M., Walbot, V., Davis, R. W., & Schiefelbein, J. W. (1994). The TTG Gene Is Required to Specify Epidermal Cell Fate and Cell Patterning in the Arabidopsis Root. *Developmental Biology*, 740–754.

Gan, L., Xia, K., Chen, J. G., & Wang, S. (2011). Functional characterization of TRICHOMELESS2, a new single-repeat R3 MYB transcription factor in the regulation of trichome patterning in Arabidopsis. *BMC Plant Biology*, *11*. https://doi.org/10.1186/1471-2229-11-176

Gasser SM, Amati BB, Cardenas ME, Hofmann JF. Studies on scaffold attachment sites and their relation to genome function. Int Rev Cytol. 1989;119:57-96. doi: 10.1016/s0074-7696(08)60649-x. PMID: 2695485.

Ghysen, A., Dambly-Chaudi~re, C., Jan, L. Y., & Jan, Y.-N. (1993). *Cell interactions and gene interactions in peripheral neurogenesis*.

Gierer, A., & Meinhardt, H. (1972). A Theory of Biological Pattern Formation. *Kybernetik*, *12*, 30–39.

Gilmartin, P. M., Sarokin, L., Memelink, J., & Chua, N.-H. (1990). Molecular Light Switches for Plant Genes. In *The Plant Cell* (Vol. 2). https://academic.oup.com/plcell/article/2/5/369/5970451

Giuliano, G., Picherskycd, E., Malikce, V. S., Timkoc'f, M. P., Scolnik5, P. A., & Cashmorea'c', A. R. (1988). An evolutionarily conserved protein binding sequence upstream of a plant light-regulated gene (gel retardation assay/DNA binding protein/tomato/Arabidopsis/small subunit of ribulose 1,5-bisphosphate carboxylase/oxygenase genes). In *Proc. Nati. Acad. Sci. USA* (Vol. 85). https://www.pnas.org

Glickman, M. H., & Ciechanover, A. (2002). The Ubiquitin-Proteasome Proteolytic Pathway: Destruction for the Sake of Construction. *Physiol Rev.* https://doi.org/10.1152/physrev.00027.2001.-Between

Goldberg, A. L. (2003). *Protein degradation and protection against misfolded or damaged proteins*. www.nature.com/nature

Gonzalez, A., Zhao, M., Leavitt, J. M., & Lloyd, A. M. (2008). Regulation of the anthocyanin biosynthetic pathway by the TTG1/bHLH/Myb transcriptional complex in Arabidopsis seedlings. *Plant Journal*, *53*(5), 814–827. https://doi.org/10.1111/j.1365-313X.2007.03373.x

Gowik, U., Burscheidt, J., Akyildiz, M., Schlue, U., Koczor, M., Streubel, M., & Westhoff, P. (2004). cis-regulatory elements for mesophyll-specific gene expression in the C4 plant Flaveria trinervia, the promoter of the C4 phosphoenolpyruvate carboxylase gene. *Plant Cell*, *16*(5), 1077–1090. https://doi.org/10.1105/tpc.019729

Grace, M. L., Chandrasekharan, M. B., Hall, T. C., & Crowe, A. J. (2004). Sequence and Spacing of TATA Box Elements Are Critical for Accurate Initiation from the β-Phaseolin Promoter. *Journal of Biological Chemistry*, *279*(9), 8102–8110. https://doi.org/10.1074/jbc.M309376200

Greese, B., Wester, K., Bensch, R., Ronneberger, O., Timmer, J., HüLskamp, M., & Fleck, C. (2012). Influence of cell-to-cell variability on spatial pattern formation. *IET Systems Biology*, *6*(4), 143–153. https://doi.org/10.1049/iet-syb.2011.0050

Groll, M., & Huber, R. (2003). Substrate access and processing by the 20S proteasome core particle. In *International Journal of Biochemistry and Cell Biology* (Vol. 35, Issue 5, pp. 606–616). Elsevier Ltd. https://doi.org/10.1016/S1357-2725(02)00390-4

Grotewold, E., Drummond, B. J., Bowen, B., & Peterson, T. (1994). The myb-Homologous P Gene Controls Phlobaphene Pigmentation in Maize Floral Organs by Directly Activating a Flavonoid Biosynthetic Gene Subset. In *Cell* (Vol. 76).

Guan, X., Pang, M., Nah, G., Shi, X., Ye, W., Stelly, D. M., & Chen, Z. J. (2014). MiR828 and miR858 regulate homoeologous MYB2 gene functions in Arabidopsis trichome and cotton fibre development. *Nature Communications*, *5*. https://doi.org/10.1038/ncomms4050

Gubler, F., Kalla, R., Robertqa, J. K., & Jacobsena, J. V. (1995). Gibbemllin-Regulated Expmssion of a myb Gene in Barley Aleurone Cells: Evidence for Myb Transactivation of a High-pl a-Amylase Gene Promoter. In *The Plant Cell* (Vol. 7). https://academic.oup.com/plcell/article/7/11/1879/5985005

Guerfel, M., Baccouri, O., Boujnah, D., Chaïbi, W., & Zarrouk, M. (2009). Impacts of water stress on gas exchange, water relations, chlorophyll content and leaf structure in the two main Tunisian olive (Olea europaea L.) cultivars. *Scientia Horticulturae*, *119*(3), 257–263. https://doi.org/10.1016/j.scienta.2008.08.006

Gurskaya, N. G., Verkhusha, V. V., Shcheglov, A. S., Staroverov, D. B., Chepurnykh, T. V., Fradkov, A. F., Lukyanov, S., & Lukyanov, K. A. (2006). Engineering of a monomeric green-to-red photoactivatable fluorescent protein induced by blue light. *Nature Biotechnology*, *24*(4), 461–465. https://doi.org/10.1038/nbt1191

Haberle, V., & Stark, A. (2018). Eukaryotic core promoters and the functional basis of transcription initiation. In *Nature Reviews Molecular Cell Biology* (Vol. 19, Issue 10, pp. 621–637). Nature Publishing Group. https://doi.org/10.1038/s41580-018-0028-8

Habuchi, S., Tsutsui, H., Kochaniak, A. B., Miyawaki, A., & van Oijen, A. M. (2008). mKikGR, a monomeric photoswitchable fluorescent protein. *PLoS ONE*, *3*(12). https://doi.org/10.1371/journal.pone.0003944

Hamilton, D. A., Schwarz, Y. H., & Mascarenhas, J. P. (1998). A monocot pollen-specific promoter contains separable pollen-specific and quantitative elements. In *Plant Molecular Biology* (Vol. 38).

Hanahan, D. (1983). Studies on Transformation of Escherichia coli with Plasmids. In *J. Mol. Biol* (Vol. 166).

Han, G., Li, Y., Yang, Z., Wang, C., Zhang, Y., & Wang, B. (2022). Molecular Mechanisms of Plant Trichome Development. In *Frontiers in Plant Science* (Vol. 13). Frontiers Media S.A. https://doi.org/10.3389/fpls.2022.910228

Harline, K., & Roeder, A. H. K. (2023). An optimized pipeline for live imaging whole Arabidopsis leaves at cellular resolution. *Plant Methods*, *19*(1). https://doi.org/10.1186/s13007-023-00987-2

Harris, R. E., Setiawan, L., Saul, J., & Hariharan, I. K. (2016). *Localized epigenetic silencing of a damage-activated WNT enhancer limits regeneration in mature Drosophila imaginal discs*. https://doi.org/10.7554/eLife.11588.001

Hattori, T., Totsuka, M., Hobo, T., Kagaya, Y., & Yamamoto-Toyoda, A. (2002). Experimentally Determined Sequence Requirement of ACGT-Containing Abscisic Acid Response Element. In *Plant Cell Physiol* (Vol. 43, Issue 1).

Hay, A. S., Pieper, B., Cooke, E., Mandáková, T., Cartolano, M., Tattersall, A. D., Ioio, R. D., McGowan, S. J., Barkoulas, M., Galinha, C., Rast, M. I., Hofhuis, H., Then, C., Plieske, J., Ganal, M., Mott, R., Martinez-Garcia, J. F., Carine, M. A., Scotland, R. W., … Tsiantis, M. (2014). Cardamine hirsuta: A versatile genetic system for comparative studies. *Plant Journal*, *78*(1), 1–15. https://doi.org/10.1111/tpj.12447

Hay, A., & Tsiantis, M. (2016). Cardamine hirsuta: A comparative view. In *Current Opinion in Genetics and Development* (Vol. 39, pp. 1–7). Elsevier Ltd. https://doi.org/10.1016/j.gde.2016.05.005

Heidary, D. K., Fox, A., Richards, C. I., & Glazer, E. C. (2017). A high-throughput screening assay using a photoconvertable protein for identifying inhibitors of transcription, translation, or proteasomal degradation. *SLAS Discovery*, *22*(4), 399–407. https://doi.org/10.1177/2472555216684333

Hepworth, S. R., Valverde, F., Ravenscroft, D., Mouradov, A., & Coupland, G. (2002). Antagonistic regulation of flowering-time gene SOC1 by CONSTANS and FLC via separate promoter motifs. *The EMBO Journal*, 4327–4337.

Herman, P. L., & David Marks', M. (1989). Trichome Development in Arabidopsis thaliana. II. Isolation and Complementation of the GLABROUSI Gene. In *The Plant Cell* (Vol. 1).

Hershko, A., & Ciechanover, A. (1998). THE UBIQUITIN SYSTEM. In *Annu. Rev. Biochem* (Vol. 67).

Higo, K., Ugawa, Y., & Korenaga, T. (1999). Plant cis-acting regulatory DNA elements (PLACE) database: 1999. In *Nucleic Acids Research* (Vol. 27, Issue 1).

Hofmann, M., Eggeling, C., Jakobs, S., & Hell, S. W. (2005). *Breaking the diffraction barrier in fluorescence microscopy at low light intensities by using reversibly photoswitchable proteins*. www.pnas.orgcgidoi10.1073pnas.0506010102

Hong, J. C., Cheong, Y. H., Nagao, R. T., Bahk, J. D., Key, J. L., & Cho, M. J. (1995). Isolation of two soybean G-box binding factors which interact with a G-box sequence of an auxin-responsive gene. *The Plant Journal*, *8*(2), 199–211. https://doi.org/10.1046/j.1365-313x.1995.08020199.x

Huang, C. H., Sun, R., Hu, Y., Zeng, L., Zhang, N., Cai, L., Zhang, Q., Koch, M. A., Al-Shehbaz, I., Edger, P. P., Pires, J. C., Tan, D. Y., Zhong, Y., & Ma, H. (2016). Resolution of brassicaceae phylogeny using nuclear genes uncovers nested radiations and supports convergent morphological evolution. *Molecular Biology and Evolution*, *33*(2), 394–412. https://doi.org/10.1093/molbev/msv226

Huang, N., Sutliff, T. D., Litts, J. C., & Rodriguez, R. L. (1990). Classification and characterization of the rice-amylase muitigene family. In *Plant Molecular Biology* (Vol. 14).

Hudson, M. E., & Quail, P. H. (2003). Identification of Promoter Motifs Involved in the Network of Phytochrome A-Regulated Gene Expression by Combined Analysis of Genomic Sequence and Microarray Data. *Plant Physiology*, *133*(4), 1605–1616. https://doi.org/10.1104/pp.103.030437

Hufford, M. B., Lubinksy, P., Pyhäjärvi, T., Devengenzo, M. T., Ellstrand, N. C., & Ross-Ibarra, J. (2013). The Genomic Signature of Crop-Wild Introgression in Maize. *PLoS Genetics*, *9*(5). https://doi.org/10.1371/journal.pgen.1003477

Hu, J., Li, B., & Kihara, D. (2005). Limitations and potentials of current motif discovery algorithms. *Nucleic Acids Research*, *33*(15), 4899–4913. https://doi.org/10.1093/nar/gki791

Hülskamp, M. (2004). Plant trichomes: a model for cell differentiation. *Nature Reviews. Molecular Cell Biology*, *5*(6), 471–480. https://doi.org/10.1038/nrm1404

Hülskamp, M., Misŕa, S., & Jürgens, G. (1994). Genetic dissection of trichome cell development in Arabidopsis. *Cell*, *76*(3), 555–566. https://doi.org/10.1016/0092-8674(94)90118-X

Hülskamp, M., & Schnittger, A. S. (1998). Spatial regulation of trichome formation in Arabidopsis thaliana. In *CELL & DEV ELOPMENTAL BI OLOGY* (Vol. 9).

Hülskamp, M., Schnittger, A. & Folkers, U. Pattern formation and cell differentiation: trichomes in Arabidopsis as a genetic model system. Int. Rev. Cytol. 186, 147–178 (1999).

Hwang, Y.-S., Karrer, E. E., Thomas, B. R., Chen, L., & Rodriguez, R. L. (1998). Three cis-elements required for rice-amylase Amy3D expression during sugar starvation. In *Plant Molecular Biology* (Vol. 36).

Icha, J., Weber, M., Waters, J. C., & Norden, C. (2017). Phototoxicity in live fluorescence microscopy, and how to avoid it. In *BioEssays* (Vol. 39, Issue 8). John Wiley and Sons Inc. https://doi.org/10.1002/bies.201700003

Ishida, T., Hattori, S., Sano, R., Inoue, K., Shirano, Y., Hayashi, H., Shibata, D., Sato, S., Kato, T., Tabata, S., Okada, K., & Wada, T. (2007). Arabidopsis TRANSPARENT TESTA GLABRA2 is directly regulated by R2R3 MYB transcription factors and is involved in regulation of GLABRA2 transcription in epidermal differentiation. *Plant Cell*, *19*(8), 2531–2543. https://doi.org/10.1105/tpc.107.052274

Ishiguro, S., & Nakamura, K. (1994). *Characterization of a cDNA encoding a novel DNA.binding protein, SPF1, that recognizes SP8 sequences in the 5' upstream regions of genes coding for sporamin and p-amylase from sweet potato*.

Itzhaki, H., Maxson, J. M., & Woodsont, W. R. (1994). An ethylene-responsive enhancer element is involved in the senescence-related expression of the carnation glutathione-S-transferase (GSTI) gene (Dianhus caryophyllusplant hormone/flower senescence/transcription). In *Proc. Nadl. Acad. Sci. USA* (Vol. 91). https://www.pnas.org

Jaime, E. G. (2007). *Analysis of trichome pattern formation in Arabidopsis thaliana: The role of KAKTUS in protein degradation*.

Jakoby, M. J., Falkenhan, D., Mader, M. T., Brininstool, G., Wischnitzki, E., Platz, N., Hudson, A., Hülskamp, M., Larkin, J., & Schnittger, A. (2008). Transcriptional profiling of mature Arabidopsis trichomes reveals that NOECK encodes the MIXTA-like transcriptional regulator MYB106. *Plant Physiology*, *148*(3), 1583–1602. https://doi.org/10.1104/pp.108.126979

Jiao, W. B., Accinelli, G. G., Hartwig, B., Kiefer, C., Baker, D., Severing, E., Willing, E. M., Piednoel, M., Woetzel, S., Madrid-Herrero, E., Huettel, B., Hümann, U., Reinhard, R., Koch, M. A., Swan, D., Clavijo, B., Coupland, G., & Schneeberger, K. (2017). Improving and correcting the contiguity of long-read genome assemblies of three plant species using optical mapping and chromosome conformation capture data. *Genome Research*, *27*(5), 778–786. https://doi.org/10.1101/gr.213652.116

Jiao, Y., Ma, L., Strickland, E., & Deng, X. W. (2005). Conservation and divergence of light-regulated genome expression patterns during seedling development in rice and Arabidopsis. *Plant Cell*, *17*(12), 3239–3256. https://doi.org/10.1105/tpc.105.035840

Johannesson, H., Wang, Y., & Engström, P. (2001). DNA-binding and dimerization preferences of Arabidopsis homeodomain-leucine zipper transcription factors in vitro. In *Plant Molecular Biology* (Vol. 45).

Johnson, C. S., Kolevski, B., & Smyth, D. R. (2002). Transparent Testa Glabra2, a trichome and seed coat development gene of arabidopsis, encodes a WRKY transcription factor. *Plant Cell*, *14*(6), 1359–1375. https://doi.org/10.1105/tpc.001404

Johnson HB. Plant pubescence: An ecological perspective. Bot Rev. 1975; 41(3):233–58.

Jores, T., Tonnies, J., Wrightsman, T., Buckler, E. S., Cuperus, J. T., Fields, S., & Queitsch, C. (2021). Synthetic promoter designs enabled by a comprehensive analysis of plant core promoters. *Nature Plants*, *7*(6), 842–855. https://doi.org/10.1038/s41477-021-00932-y

Joshi, C. P. (1987). Putative poly(A)denylation signals in nuclear genes of higher plants: a compilation and analysis. In *Nucleic Acids Research* (Vol. 15). https://academic.oup.com/nar/article/15/23/9627/2378186

Judd WS, Campbell CS, Kellogg EA, Stevens PF. Plant sytematics, a phylogenetic approach. Massachusetts (USA): Sinauer Associates; 1999.

Kaberniuk, A. A., Morano, N. C., Verkhusha, V. V., & Snapp, E. L. (2017). moxDendra2: an inert photoswitchable protein for oxidizing environments. *Chemical Communications*, *53*(13), 2106–2109. https://doi.org/10.1039/c6cc09997a

Kagaya, Y., Ohmiya, K., & Hattori, T. (1999). RAV1, a novel DNA-binding protein, binds to bipartite recognition sequence through two distinct DNA-binding domains uniquely found in higher plants. In *Nucleic Acids Research* (Vol. 27, Issue 2).

Kamiya, N., Nagasaki, H., Morikami, A., Sato, Y., & Matsuoka, M. (2003). Isolation and characterization of a rice WUSCHEL-type homeobox gene that is specifically expressed in the central cells of a quiescent center in the root apical meristem. *Plant Journal*, *35*(4), 429–441. https://doi.org/10.1046/j.1365-313X.2003.01816.x

Kaplan, B., Davydov, O., Knight, H., Galon, Y., Knight, M. R., Fluhr, R., & Fromm, H. (2006). Rapid transcriptome changes induced by cytosolic Ca2+ transients reveal ABRE-related sequences as Ca2+-responsive cis elements in Arabidopsis. *Plant Cell*, *18*(10), 2733–2748. https://doi.org/10.1105/tpc.106.042713

Kapoor, S., & Sugiura, M. (1999). Identification of Two Essential Sequence Elements in the Nonconsensus Type II PatpB-290 Plastid Promoter by Using Plastid Transcription Extracts from Cultured Tobacco BY-2 Cells. In *The Plant Cell* (Vol. 11). www.plantcell.org

Karabourniotis, G., Papadopoulos, K., Papamarkou, M., & Manetas, Y. (1992). Ultraviolet-B radiation absorbing capacity of leaf hairs. *Physiologia Plantarum*, *86*(3), 414–418. https://doi.org/10.1111/j.1399-3054.1992.tb01337.x

Kaufmann, K., Pajoro, A., & Angenent, G. C. (2010). Regulation of transcription in plants: Mechanisms controlling developmental switches. In *Nature Reviews Genetics* (Vol. 11, Issue 12, pp. 830–842). https://doi.org/10.1038/nrg2885

Kim, D. W., Lee, S. H., Choi, S. B., Won, S. K., Heo, Y. K., Cho, M., Park, Y. Il, & Cho, H. T. (2006). Functional conservation of a root hair cell-specific cis-element in angiosperms with different root hair distribution patterns. *Plant Cell*, *18*(11), 2959–2970. https://doi.org/10.1105/tpc.106.045229

Kim, J. H., Lee, S. R., Li, L. H., Park, H. J., Park, J. H., Lee, K. Y., Kim, M. K., Shin, B. A., & Choi, S. Y. (2011). High cleavage efficiency of a 2A peptide derived from porcine teschovirus-1 in human cell lines, zebrafish and mice. *PLoS ONE*, *6*(4). https://doi.org/10.1371/journal.pone.0018556

Kim, S. Y., Chung, H. J., & Thomas, T. L. (1997). Isolation of a novel class of bZIP transcription factors that interact with ABA-responsive and embryo-specification elements in the Dc3 promoter using a modified yeast one-hybrid system. *Plant Journal*, *11*(6), 1237–1251. https://doi.org/10.1046/j.1365-313X.1997.11061237.x

Kirik, V., Lee, M. M., Wester, K., Herrmann, U., Zheng, Z., Oppenheimer, D., Schiefelbein, J., & Hulskamp, M. (2005). Functional diversification of MYB23 and GL1 genes in trichome morphogenesis and initiation. *Development*, *132*(7), 1477–1485. https://doi.org/10.1242/dev.01708

Kirik, V., Schnittger, A., Radchuk, V., Adler, K., Hülskamp, M., & Bäumlein, H. (2001a). Ectopic expression of the Arabidopsis AtMYB23 gene induces differentiation of trichome cells. *Developmental Biology*, *235*(2), 366–377. https://doi.org/10.1006/dbio.2001.0287

Kirik, V., Simon, M., Huelskamp, M., & Schiefelbein, J. (2004a). The ENHANCER of TRY and CPC1 gene acts redundantly with TRIPTYCHON and CAPRICE in trichome and root hair cell patterning in Arabidopsis. *Developmental Biology*, *268*(2), 506–513. https://doi.org/10.1016/j.ydbio.2003.12.037

Kirik, V., Simon, M., Wester, K., Schiefelbein, J., & Hulskamp, M. (2004b). Enhancer of try and CPC 2 (ETC2) reveals redundancy in the region-specific control of trichome development of Arabidopsis. *Plant Molecular Biology*, *55*(3), 389–398. https://doi.org/10.1007/s11103-004-0893-8

Klemm, S. L., Shipony, Z., & Greenleaf, W. J. (2019). Chromatin accessibility and the regulatory epigenome. In *Nature Reviews Genetics* (Vol. 20, Issue 4, pp. 207–220). Nature Publishing Group. https://doi.org/10.1038/s41576-018-0089-8

Klinedinst, S., Pascuzzi, P., Redman, J., Desai, M., & Arias, J. (2000). A xenobiotic-stress-activated transcription factor and its cognate target genes are preferentially expressed in root tip meristems. In *Plant Molecular Biology* (Vol. 42).

Koch, M. A., Kiefer, C., Ehrich, D., Vogel, J., Brochmann, C., & Mummenhoff, K. (2006). Three times out of Asia Minor: The phylogeography of Arabis alpina L. (Brassicaceae). *Molecular Ecology*, *15*(3), 825–839. https://doi.org/10.1111/j.1365-294X.2005.02848.x

Koch, M., Haubold, B., & Mitchell-Olds, T. (2001). Molecular systematics of the brassicaceae: Evidence from coding plastidic matK and nuclear Chs sequences. *American Journal of Botany*, *88*(3), 534–544. https://doi.org/10.2307/2657117

Ko, J. H., Beers, E. P., & Han, K. H. (2006). Global comparative transcriptome analysis identifies gene network regulating secondary xylem development in Arabidopsis thaliana. *Molecular Genetics and Genomics*, *276*(6), 517–531. https://doi.org/10.1007/s00438-006-0157-1

Komatsubara, A. T., Goto, Y., Kondo, Y., Matsuda, M., & Aoki, K. (2019). Single-cell quantification of the concentrations and dissociation constants of endogenous proteins. *Journal of Biological Chemistry*, *294*(15), 6062–6072. https://doi.org/10.1074/jbc.RA119.007685

Koncz, C., & Schell, J. (1986). *The promoter of TL-DNA gene 5 controls the tissue-specific expression of chimaeric genes carried by a novel type of Agrobacterium binary vector* (Vol. 204).

Koornneef, M. (1981). The complex syndrome of ttg mutanis. Arabidopsis Information Service, 18, 45-51.

Koornneef, M., Dellaert, L. W. M., & Van Der Veen, J. H. (1982). EMS-and radiation-induced mutation frequencies at individual loci in Arabidopsis thaliana (L.) Heynh. In *Mutation Research* (Vol. 93).

Kopp, F., & Mendell, J. T. (2018). Functional Classification and Experimental Dissection of Long Noncoding RNAs. In *Cell* (Vol. 172, Issue 3, pp. 393–407). Cell Press. https://doi.org/10.1016/j.cell.2018.01.011

Kucho, K. I., Yoshioka, S., Taniguchi, F., Ohyama, K., & Fukuzawa, H. (2003). Cis-acting Elements and DNA-Binding Proteins Involved in CO 2-Responsive Transcriptional Activation of Cah1 Encoding a Periplasmic Carbonic Anhydrase in Chlamydomonas reinhardtii. *Plant Physiology*, *133*(2), 783–793. https://doi.org/10.1104/pp.103.026492

Kumari, S., & Ware, D. (2013). Genome-wide computational prediction and analysis of core promoter elements across plant monocots and dicots. *PLoS ONE*, *8*(10). https://doi.org/10.1371/journal.pone.0079011

Lacombe, E., Van Doorsselaere, J., Boerjan, W., Boudet, A. M., & Grima-Pettenati, J. (2000). Characterization of cis-elements required for vascular expression of the cinnamoyl CoA reductase gene and for protein-DNA complex formation. *Plant Journal*, *23*(5), 663–676. https://doi.org/10.1046/j.1365-313X.2000.00838.x

Laloum, T., De Mita, S., Gamas, P., Baudin, M., & Niebel, A. (2013). CCAAT-box binding transcription factors in plants: Y so many? In *Trends in Plant Science* (Vol. 18, Issue 3, pp. 157–166). https://doi.org/10.1016/j.tplants.2012.07.004

Lambert, S. A., Jolma, A., Campitelli, L. F., Das, P. K., Yin, Y., Albu, M., Chen, X., Taipale, J., Hughes, T. R., & Weirauch, M. T. (2018). The Human Transcription Factors. In *Cell* (Vol. 172, Issue 4, pp. 650–665). Cell Press. https://doi.org/10.1016/j.cell.2018.01.029

Larkin, J. C., David Marks, M., Nadeau, J., & Sackc, F. (1997). Epidermal Cell Fate and Patterning in Leaves. In *The Plant Cell* (Vol. 9). American Society of Plant Physiologists.

Larkin, J. C., Oppenheimer, D. G., Lloyd, A. M., Paparozzi, E. T., & David Marks, M. (1994). Roles of the GLABROUS1 and TRANSPARENT TESTA GLABRA Genes in Arabidopsis Trichome Development. In *The Plant Cell* (Vol. 6).

Larkin, J. C., Walker, J. D., Bolognesi-Winfield, A. C., Gray, J. C., & Walker, A. R. (1999). *Allele-Specific Interactions Between ttg and gl1 During Trichome Development in Arabidopsis thaliana*.

Larkin, J. C., Young, N., Prigge, M., & Marks, M. D. (1996). The control of trichome spacing and number in *Arabidopsis*. *Development*, *122*, 997–1005.

Larkin, J., Oppenheimer, D., Pollock, S., & Marks, M. (1993). Arabidopsis GLABROUS1 Gene Requires Downstream Sequences for Function. *The Plant Cell*, *5*(12), 1739–1748. https://doi.org/10.1016/0168-9525(94)90210-0

Leavitt RG. 1904. Trichomes of the root in vascular cryptograms and angiosperms. Proceedings of the Boston Society of Natural History 31: 273±313.

Lee, C. R., Svardal, H., Farlow, A., Exposito-Alonso, M., Ding, W., Novikova, P., Alonso-Blanco, C., Weigel, D., & Nordborg, M. (2017). On the post-glacial spread of human commensal Arabidopsis thaliana. *Nature Communications*, *8*. https://doi.org/10.1038/ncomms14458

Lee, M. M., & Schiefelbein, J. (1999). *WEREWOLF, a MYB-Related Protein in Arabidopsis, Is a Position-Dependent Regulator of Epidermal Cell Patterning*.

Lee, M. M., & Schiefelbein, J. (2001). Developmentally distinct MYB genes encode functionally equivalent proteins in Arabidopsis. *Development*, *128*(9), 1539–1546. http://www.ncbi.nlm.nih.gov/pubmed/11290293

Lelievre, J.-M., & Nielsen, N. C. (1992). 5'-CATGCAT-3' Elements Modulate the Expression of Glycinin Genes. In *Plant Physiol* (Vol. 98). https://academic.oup.com/plphys/article/98/1/387/6087713

Lescot, M., Déhais, P., Thijs, G., Marchal, K., Moreau, Y., Van De Peer, Y., Rouzé, P., & Rombauts, S. (2002). PlantCARE, a database of plant cis-acting regulatory elements and a portal to tools for in silico analysis of promoter sequences. In *Nucleic Acids Research* (Vol. 30, Issue 1). http://sphinx.rug.ac.be:8080/PlantCARE/.

Lessard, P. A., Allen, R. D., Bernier, F., Crispino, J. D., Fujiwara, T., & Beachy, R. N. (1991). Multiple nuclear factors interact with upstream sequences of differentially regulated fl-conglycinin genes. In *Plant Molecular Biology* (Vol. 16).

Levin DA (1973) The role of trichomes in plant defense. Q Rev Biol 48: 3-15.

Levine, B., Mizushima, N., & Virgin, H. W. (2011). Autophagy in immunity and inflammation. In *Nature* (Vol. 469, Issue 7330, pp. 323–335). https://doi.org/10.1038/nature09782

Levy, E., & Slavov, N. (2018). Single cell protein analysis for systems biology. In *Essays in Biochemistry* (Vol. 62, Issue 4, pp. 595–605). Portland Press Ltd. https://doi.org/10.1042/EBC20180014

Lewis, J. E., Brameld, J. M., Hill, P., Barrett, P., Ebling, F. J. P., & Jethwa, P. H. (2015). The use of a viral 2A sequence for the simultaneous over-expression of both the vgf gene and enhanced green fluorescent protein (eGFP) in vitro and in vivo. *Journal of Neuroscience Methods*, *256*, 22–29. https://doi.org/10.1016/j.jneumeth.2015.08.013

Liang, G., He, H., Li, Y., Ai, Q., & Yu, D. (2014). MYB82 functions in regulation of trichome development in Arabidopsis. *Journal of Experimental Botany*, *65*(12), 3215–3223. https://doi.org/10.1093/jxb/eru179

Li, E., Liu, H., Huang, L., Zhang, X., Dong, X., Song, W., Zhao, H., & Lai, J. (2019). Long-range interactions between proximal and distal regulatory regions in maize. *Nature Communications*, *10*(1). https://doi.org/10.1038/s41467-019-10603-4

Li JL, Zeng LT, Liao YY, Tang J, Yang Z. Evaluation of the contribution of trichomes to metabolite compositions of tea (Camellia sinensis) leaves and their products. LWT Food Sci Technol. 2020

Li, S. F., Milliken, O. N., Pham, H., Seyit, R., Napoli, R., Preston, J., Koltunow, A. M., & Parish, R. W. (2009). The Arabidopsis MYB5 Transcription Factor Regulates Mucilage Synthesis, Seed Coat Development, and Trichome Morphogenesis. *The Plant Cell Online*, *21*(1), 72–89. https://doi.org/10.1105/tpc.108.063503

Li, S. F., Santini, J. M., Nicolaou, O., & Parish, R. W. (1996). A novel myb-related gene from Arabidopsis thaliana. *FEBS Letters*, *379*(2), 117–121. https://doi.org/10.1016/0014-5793(95)01461-6

Liu, L., Wang, Y., Cao, W., Yang, L., Zhang, C., Yuan, L., Wang, D., Wang, W., Zhang, H., Schiefelbein, J., Yu, F., & An, L. (2024). TRANSPARENT TESTA GLABRA2 defines trichome cell shape by modulating actin cytoskeleton in Arabidopsis thaliana. *Plant Physiology*. https://doi.org/10.1093/plphys/kiae091

Liu, L., Zhang, Y., Tang, S., Zhao, Q., Zhang, Z., Zhang, H., Dong, L., Guo, H., & Xie, Q. (2010). An efficient system to detect protein ubiquitination by agroinfiltration in Nicotiana benthamiana. *Plant Journal*, *61*(5), 893–903. https://doi.org/10.1111/j.1365-313X.2009.04109.x

Logemann, E., Parniske, M., & Hahlbrockt, K. (1995). Modes of expression and common structural features of the complete phenylalanine ammonia-lyase gene family in parsley (cinnamate 4-hydroxylase/4-coumarate:CoA ligase/fungal elicitor/UV light/wounding). In *Plant Biology* (Vol. 92). https://www.pnas.org

Loke, J. C., Stahlberg, E. A., Strenski, D. G., Haas, B. J., Wood, P. C., & Qingshun, Q. L. (2005). Compilation of mRNA poly(A)denylation signals in Arabidopsis revealed a new signal element and potential secondary structures. *Plant Physiology*, *138*(3), 1457–1468. https://doi.org/10.1104/pp.105.060541

Long, Y., & Schiefelbein, J. (2020). Novel TTG1 Mutants Modify Root-Hair Pattern Formation in Arabidopsis. *Frontiers in Plant Science*, *11*. https://doi.org/10.3389/fpls.2020.00383

Loppes, R., & Radoux, M. (2001). Identification of short promoter regions involved in the transcriptional expression of the nitrate reductase gene in Chlamydomonas reinhardtii. In *Plant Molecular Biology* (Vol. 45).

Lu, C. A., Ho, T. H. D., Ho, S. L., & Yu, S. M. (2002). Three novel MYB proteins with one DNA binding repeat mediate sugar and hormone regulation of α-amylase gene expression. *Plant Cell*, *14*(8), 1963–1980. https://doi.org/10.1105/tpc.001735

Luo, H., Song, F., Goodman, R. M., & Zheng, Z. (2005a). Up-regulation of OsBIHD1, a rice gene encoding BELL homeodomain transcriptional factor, in disease resistance responses. *Plant Biology*, *7*(5), 459–468. https://doi.org/10.1055/s-2005-865851

Maeda, K., Kimura, S., Demura, T., Takeda, J., & Ozeki, Y. (2005). DcMYB1 acts as a transcriptional activator of the carrot phenylalanine ammonia-lyase gene (DcPAL1) in response to elicitor treatment, UV-B irradiation and the dilution effect. *Plant Molecular Biology*, *59*(5), 739–752. https://doi.org/10.1007/s11103-005-0910-6

Mandel, C. R., Bai, Y., & Tong, L. (2008). Protein factors in pre-mRNA 3'-end processing. In *Cellular and Molecular Life Sciences* (Vol. 65, Issues 7–8, pp. 1099–1122). https://doi.org/10.1007/s00018-007-7474-3

Mapar, M., Chopra, D., Stephan, L., Schrader, A., Sun, H., Schneeberger, K., Albani, M., Coupland, G., & Hülskamp, M. (2021). Genetic and Molecular Analysis of Root Hair Development in Arabis alpina. *Frontiers in Plant Science*, *12*. https://doi.org/10.3389/fpls.2021.767772

Marand, A. P., Eveland, A. L., Kaufmann, K., & Springer, N. M. (2023). *Annual Review of Plant Biology cis-Regulatory Elements in Plant Development, Adaptation, and Evolution*. https://doi.org/10.1146/annurev-arplant-070122

Marand, A. P., Zhang, T., Zhu, B., & Jiang, J. (2017). Towards genome-wide prediction and characterization of enhancers in plants. *Biochimica et Biophysica Acta - Gene Regulatory Mechanisms*, *1860*(1), 131–139. https://doi.org/10.1016/j.bbagrm.2016.06.006

Marks, D. M., & Feldmann, K. A. (1989). Trichome Development in Arabidopsis thaliana. 1. T-DNA Tagging of the GLABROUSI Gene. In *The Plant Cell* (Vol. 1). https://academic.oup.com/plcell/article/1/11/1043/5970265

Marks, M. D. (1997). MOLECULAR GENETIC ANALYSIS OF TRICHOME DEVELOPMENT IN ARABIDOPSIS. In *Annu. Rev. Plant Physiol. Plant Mol. Biol* (Vol. 48).

Martínez-Hernández, A., López-Ochoa, L., Argüello-Astorga, G., & Herrera-Estrella, L. (2002). Functional properties and regulatory complexity of a minimal RBCS light-responsive unit activated by phytochrome, cryptochrome, and plastid signals. *Plant Physiology*, *128*(4), 1223–1233. https://doi.org/10.1104/pp.010678

Maruyama-Nakashita, A., Nakamura, Y., Watanabe-Takahashi, A., Inoue, E., Yamaya, T., & Takahashi, H. (2005). Identification of a novel cis-acting element conferring sulfur deficiency response in Arabidopsis roots. *Plant Journal*, *42*(3), 305–314. https://doi.org/10.1111/j.1365-313X.2005.02363.x

Masucci, J. D., Rerie, W. G., Foreman, D. R., Zhang, M., Galway, M. E., Marks, M. D., & Schiefelbein, J. W. (1996). The homeobox gene GLABRA2 is required for position-dependent cell differentiation in the root epidermis of Arabidopsis thaliana. *Development*, *122*, 1253–1260.

Masucci, J. D., & Schiefelbein, J. W. (1996). Hormones Act Downstream of TTG and GL2 to Promote Root Hair Outgrowth during Epidermis Development in the Arabidopsis Root. In *The Plant Cell* (Vol. 8). American Society of Plant Physiologists.

Matarasso, N., Schuster, S., & Avni, A. (2005). A novel plant cysteine protease has a dual function as a regulator of 1-aminocyclopropane-1-carboxylic acid synthase gene expression. *Plant Cell*, *17*(4), 1205–1216. https://doi.org/10.1105/tpc.105.030775

Maxwell, B. B., Andersson, C. R., Poole, D. S., Kay, S. A., & Chory, J. (2003). HY5, Circadian Clock-Associated 1, and a cis-Element, DET1 Dark Response Element, Mediate DET1 Regulation of Chlorophyll a/b-Binding Protein 2 Expression. *Plant Physiology*, *133*(4), 1565–1577. https://doi.org/10.1104/pp.103.025114

Meinhardt, H. (2012). Turing's theory of morphogenesis of 1952 and the subsequent discovery of the crucial role of local self enhancement and long-range inhibition. In *Interface Focus* (Vol. 2, Issue 4, pp. 407–416). Royal Society. https://doi.org/10.1098/rsfs.2011.0097

Meinhardt, H., & Gierer, A. (1974). Applications of a theory of biological pattern formation based on lateral inhibition. *Journal of Cell Science*, *15*(2), 321–346.

Meinhardt, H., & Gierer, A. (2000). Pattern formation by local self-activation and lateral inhibition. In *BioEssays* (Vol. 22). John Wiley & Sons, Inc.

Melaragno, J. E., Mehrotra, B., & Coleman, A. W. (1993). Relationship between Endopolyploidy and Cell Size in Epidermal Tissue of Arabidopsis. *The Plant Cell*, *5*(11), 1661–1668. https://doi.org/10.1105/tpc.5.11.1661

Meng, F., Zhao, H., Zhu, B., Zhang, T., Yang, M., Li, Y., Han, Y., & Jiang, J. (2021). Genomic editing of intronic enhancers unveils their role in fine-tuning tissue-specific gene expression in Arabidopsis thaliana. *Plant Cell*, *33*(6), 1997–2014. https://doi.org/10.1093/plcell/koab093

Mikami, K., Tabata, T., Kawata, T., Nakayama, T., & Iwabuchi, M. (1987). Nuclear protein(s) binding to the conserved DNA hexameric sequence postulated to regulate transcription of wheat histone genes. *FEBS Letters*, *223*(2), 273–278. https://doi.org/10.1016/0014-5793(87)80303-4

Miki, T., Parkl, J. A., Nagaog, K., Murayama, N., & Horiuchi, T. (1992). Control of Segregation of Chromosomal DNA by Sex Factor F in Escherichia coli Mutants of DNA Gyrase Subunit A Suppress ZetD (ccdB) Product Growth Inhibition. In *J. Mol. Biol* (Vol. 225).

Misra, B. B., Assmann, S. M., & Chen, S. (2014). Plant single-cell and single-cell-type metabolomics. In *Trends in Plant Science* (Vol. 19, Issue 10, pp. 637–646). Elsevier Ltd. https://doi.org/10.1016/j.tplants.2014.05.005

Mizuno, H., Mal, T. K., Tong, K. I., Ando, R., Furuta, T., Ikura, M., & Miyawaki, A. (2003a). Photo-induced peptide cleavage in the green-to-red conversion of a fluorescent protein. *Molecular Cell*, *12*(4), 1051–1058. https://doi.org/10.1016/S1097-2765(03)00393-9

Mohanty, B., Krishnan, S. P. T., Swarup, S., & Bajic, V. B. (2005). Detection and preliminary analysis of motifs in promoters of anaerobically induced genes of different plant species. *Annals of Botany*, *96*(4), 669–681. https://doi.org/10.1093/aob/mci219

Molina, C., & Grotewold, E. (2005). Genome wide analysis of Arabidopsis core promoters. *BMC Genomics*, *6*. https://doi.org/10.1186/1471-2164-6-25

Montenegro-Johnson, T. D., Stamm, P., Strauss, S., Topham, A. T., Tsagris, M., Wood, A. T. A., Smith, R. S., & Bassel, G. W. (2015). Digital single-cell analysis of plant organ development using 3dcellatlasopen. *Plant Cell*, *27*(4), 1018–1033. https://doi.org/10.1105/tpc.15.00175

Moon, J., Parry, G., & Estelle, M. (2004). The ubiquitin-proteasome pathway and plant development. In *Plant Cell* (Vol. 16, Issue 12, pp. 3181–3195). American Society of Plant Biologists. https://doi.org/10.1105/tpc.104.161220

Morita, A., Umemura, T. A., Kuroyanagi, M., Futsuhara, Y., Perata, P., & Yamaguchi, J. (1998). Functional dissection of a sugar-repressed α-amylase gene (RAmy1A) promoter in rice embryos. *FEBS Letters*, *423*(1), 81–85. https://doi.org/10.1016/S0014-5793(98)00067-2

Morohashi, K., & Grotewold, E. (2009). A systems approach reveals regulatory circuitry for Arabidopsis trichome initiation by the GL3 and GL1 selectors. *PLoS Genetics*, *5*(2). https://doi.org/10.1371/journal.pgen.1000396

Morohashi, K., Zhao, M., Yang, M., Read, B., Lloyd, A., Lamb, R., & Grotewold, E. (2007). Participation of the arabidopsis bHLH factor GL3 in trichome initiation regulatory events. *Plant Physiology*, *145*(3), 736–746. https://doi.org/10.1104/pp.107.104521

Müller, M., & Knudsen, S. (1993). The nitrogen response of a barley C-hordein promoter is controlled by positive and negative regulation of the GCN4 and endosperm box. *Plant Journal*, *4*(2), 343–355. https://doi.org/10.1046/j.1365-313X.1993.04020343.x

Nag, R., Maity, M. K., & DasGupta, M. (2005). Dual DNA binding property of ABA insensitive 3 like factors targeted to promoters responsive to ABA and auxin. *Plant Molecular Biology*, *59*(5), 821–838. https://doi.org/10.1007/s11103-005-1387-z

Nakagawa, T., Kurose, T., Hino, T., Tanaka, K., Kawamukai, M., Niwa, Y., Toyooka, K., Matsuoka, K., Jinbo, T., & Kimura, T. (2007). Development of series of gateway binary vectors, pGWBs, for realizing efficient construction of fusion genes for plant transformation. *Journal of Bioscience and Bioengineering*, *104*(1), 34–41. https://doi.org/10.1263/jbb.104.34

Nakamura, M., Tsunoda, T., & Obokata, J. (2002). Photosynthesis nuclear genes generally lack TATA-boxes: A tobacco photosystem I gene responds to light through an initiator. *Plant Journal*, *29*(1), 1–10. https://doi.org/10.1046/j.0960-7412.2001.01188.x

Nakashima, K., Fujita, Y., Katsura, K., Maruyama, K., Narusaka, Y., Seki, M., Shinozaki, K., & Yamaguchi-Shinozaki, K. (2006). Transcriptional regulation of ABI3- and ABA-responsive genes including RD29B and RD29A in seeds, germinating embryos, and seedlings of Arabidopsis. *Plant Molecular Biology*, *60*(1), 51–68. https://doi.org/10.1007/s11103-005-2418-5

Nasmyth, K., Adolf, G., Lydall, D., & Seddon', A. (1990). The Identification of a Second Cell Cycle Control on the HO Promoter in Yeast: Cell Cycle Regulation of SW15 Nuclear Entry. In *Cell* (Vol. 62).

Nesi, N., Debeaujon, I., Jond, C., Pelletier, G., Caboche, M., & Lepiniec, L. (2000). The TT8 Gene Encodes a Basic Helix-Loop-Helix Domain Protein Required for Expression of DFR and BAN Genes in Arabidopsis Siliques. In *Source: The Plant Cell* (Vol. 12, Issue 10). https://www.jstor.org/stable/3871198?seq=1&cid=pdf-

Nesi, N., Jond, C., Debeaujon, I., Caboche, M., & Lepiniec, L. (2001). The Arabidopsis TT2 Gene Encodes an R2R3 MYB Domain Protein That Acts as a Key Determinant for Proanthocyanidin Accumulation in Developing Seed. In *The Plant Cell* (Vol. 13). www.plantcell.org

Ngan, C. Y., Wong, C. H., Tjong, H., Wang, W., Goldfeder, R. L., Choi, C., He, H., Gong, L., Lin, J., Urban, B., Chow, J., Li, M., Lim, J., Philip, V., Murray, S. A., Wang, H., & Wei, C. L. (2020). Chromatin interaction analyzes elucidate the roles of PRC2-bound silencers in mouse development. *Nature Genetics*, *52*(3), 264–272. https://doi.org/10.1038/s41588-020-0581-x

Nibert, M. L. (2007). "2A-like" and "shifty heptamer" motifs in penaeid shrimp infectious myonecrosis virus, a monosegmented double-stranded RNA virus. *Journal of General Virology*, *88*(4), 1315–1318. https://doi.org/10.1099/vir.0.82681-0

Nolis, I. K., Mckay, D. J., Mantouvalou, E., Lomvardas, S., Merika, M., & Thanos, D. (2009). *Transcription factors mediate long-range enhancer-promoter interactions*. www.pnas.org/cgi/content/full/

Oates, A. C., Morelli, L. G., & Ares, S. (2012). Patterning embryos with oscillations: Structure, function and dynamics of the vertebrate segmentation clock. In *Development* (Vol. 139, Issue 4, pp. 625–639). https://doi.org/10.1242/dev.063735

Ogawa, M., Hanada, A., Yamauchi, Y., Kuwahara, A., Kamiya, Y., & Yamaguchi, S. (2003). Gibberellin biosynthesis and response during Arabidopsis seed germination. *Plant Cell*, *15*(7), 1591–1604. https://doi.org/10.1105/tpc.011650

Ogo, Y., Itai, R. N., Nakanishi, H., Inoue, H., Kobayashi, T., Suzuki, M., Takahashi, M., Mori, S., & Nishizawa, N. K. (2006). Isolation and characterization of IRO2, a novel iron-regulated bHLH transcription factor in graminaceous plants. *Journal of Experimental Botany*, *57*(11), 2867–2878. https://doi.org/10.1093/jxb/erl054

Ohgishi, M., Oka, A., Morelli, G., Ruberti, I., & Aoyama, T. (2001). Negative autoregulation of the Arabidopsis homeobox gene ATHB-2. *Plant Journal*, *25*(4), 389–398. https://doi.org/10.1046/j.1365-313X.2001.00966.x

Oka, R., Zicola, J., Weber, B., Anderson, S. N., Hodgman, C., Gent, J. I., Wesselink, J. J., Springer, N. M., Hoefsloot, H. C. J., Turck, F., & Stam, M. (2017). Genome-wide mapping of transcriptional enhancer candidates using DNA and chromatin features in maize. *Genome Biology*, *18*(1). https://doi.org/10.1186/s13059-017-1273-4

O'Neill, S. D., Kumagai, M. H., Majumdar, A., Huang, N., Sutliff, T. D., & Rodriguez, R. L. (1990). *The a-amylase genes in Oryza sativa: Characterization of cDNA clones and mRNA expression during seed germination* (Vol. 221).

Onodera, Y., Suzuki, A., Wu, C. Y., Washida, H., & Takaiwa, F. (2001). A Rice Functional Transcriptional Activator, RISBZ1, Responsible for Endosperm-specific Expression of Storage Protein Genes through GCN4 Motif. *Journal of Biological Chemistry*, *276*(17), 14139–14152. https://doi.org/10.1074/jbc.M007405200

Oppenheimer, D. G., Herman, P. L., Sivakumaran, S., Esch, J., & Marks, M. D. (1991). A myb gene required for leaf trichome differentiation in Arabidopsis is expressed in stipules. *Cell*, *67*(3), 483–493. https://doi.org/10.1016/0092-8674(91)90523-2

Pajoro, A., Madrigal, P., Muiño, J. M., Matus, J. T., Jin, J., Mecchia, M. A., Debernardi, J. M., Palatnik, J. F., Balazadeh, S., Arif, M., Ó'Maoiléidigh, D. S., Wellmer, F., Krajewski, P., Riechmann, J. L., Angenent, G. C., & Kaufmann, K. (2014). Dynamics of chromatin accessibility and gene regulation by MADS-domain transcription factors in flower development. *Genome Biology*, *15*(3). https://doi.org/10.1186/gb-2014-15-3-r41

Pang, B., & Snyder, M. P. (2020). Systematic identification of silencers in human cells. *Nature Genetics*, *52*(3), 254–263. https://doi.org/10.1038/s41588-020-0578-5

Park, H. C., Kim, M. L., Kang, Y. H., Jeon, J. M., Yoo, J. H., Kim, M. C., Park, C. Y., Jeong, J. C., Moon, B. C., Lee, J. H., Yoon, H. W., Lee, S.-H., Chung, W. S., Chae, O. L., Lee, S. Y., Hong, J. C., & Cho, M. J. (2004). Pathogen- and NaCl-induced expression of the SCaM-4 promoter is mediated in part by a GT-1 box that interacts with a GT-1-like transcription factor. *Plant Physiology*, *135*(4), 2150–2161. https://doi.org/10.1104/pp.104.041442

Patra, B., Pattanaik, S., & Yuan, L. (2013a). Proteolytic degradation of the flavonoid regulators, TRANSPARENT TESTA8 and TRANSPARENT TESTA GLABRA1, in Arabidopsis is mediated by the ubiquitin/26sproteasome system. *Plant Signaling and Behavior*, *8*(10). https://doi.org/10.4161/psb.25901

Patra, B., Pattanaik, S., & Yuan, L. (2013b). Ubiquitin protein ligase 3 mediates the proteasomal degradation of GLABROUS 3 and ENHANCER of GLABROUS 3, regulators of trichome development and flavonoid biosynthesis in Arabidopsis. *Plant Journal*, *74*(3), 435–447. https://doi.org/10.1111/tpj.12132

Patterson, G. H., & Lippincott-Schwartz, J. (2002). A photoactivatable GFP for selective photolabeling of proteins and cells. *Science*, *297*(5588), 1873–1877. https://doi.org/10.1126/science.1074950

Pauli, S., Rothnie, H. M., Chen, G., He, X., & Hohn, T. (2004). The Cauliflower Mosaic Virus 35S Promoter Extends into the Transcribed Region. *Journal of Virology*, *78*(22), 12120–12128. https://doi.org/10.1128/jvi.78.22.12120-12128.2004

Payne, C. T., Zhang, F., & Lloyd, A. M. (2000). GL3 encodes a bHLH protein that regulates trichome development in arabidopsis through interaction with GL1 and TTG1. *Genetics*, *156*(3), 1349–1362.

Pesch, M. (2005). *Trichom- und Wurzelhaar-Musterbildung in Arabidopsis thaliana: Vergleichende Promotoranalyze der Aktivatoren GLABRA1 und WEREWOLF sowie der Inhibitoren TRIPTYCHON und CAPRICE*.

Pesch, M., Dartan, B., Birkenbihl, R., Somssich, I. E., & Hülskamp, M. (2014). Arabidopsis TTG2 regulates TRY expression through enhancement of activator complex-triggered activation. *Plant Cell*, *26*(10), 4067–4083. https://doi.org/10.1105/tpc.114.129379

Pesch, M., & Hülskamp, M. (2004). Creating a two-dimensional pattern de novo during Arabidopsis trichome and root hair initiation. *Current Opinion in Genetics and Development*, *14*(4), 422–427. https://doi.org/10.1016/j.gde.2004.06.007

Pesch, M., & Hülskamp, M. (2009). One, two, three...models for trichome patterning in Arabidopsis? In *Current Opinion in Plant Biology* (Vol. 12, Issue 5, pp. 587–592). https://doi.org/10.1016/j.pbi.2009.07.015

Pesch, M., & Hülskamp, M. (2011). Role of TRIPTYCHON in trichome patterning in Arabidopsis. *BMC Plant Biology*, *11*. https://doi.org/10.1186/1471-2229-11-130

Pesch, M., Schultheiß, I., Klopffleisch, K., Uhrig, J. F., Koegl, M., Clemen, C. S., Simon, R., Weidtkamp-Peters, S., & Hülskamp, M. (2015). Transparent testa glabra1 and glabra1 compete for binding to glabra3 in arabidopsis. *Plant Physiology*, *168*(2), 584–597. https://doi.org/10.1104/pp.15.00328

Pickart, C. M., & Eddins, M. J. (2004). Ubiquitin: Structures, functions, mechanisms. In *Biochimica et Biophysica Acta - Molecular Cell Research* (Vol. 1695, Issues 1–3, pp. 55–72). https://doi.org/10.1016/j.bbamcr.2004.09.019

Piechulla, B., Merforth, N., & Rudolph, B. (1998). Identification of tomato Lhc promoter regions necessary for circadian expression. In *Plant Molecular Biology* (Vol. 38).

Pietsch, J. (2022). *Cross-regulatory interactions of trichome patterning genes in Arabidopsis thaliana and related species*.

Planchais, S., Perennes, C., Glab, N., Mironov, V., Inzé, D., & Bergounioux, C. (2002). Characterization of cis-acting element involved in cell cycle phase-independent activation of Arath;CycB1;1 transcription and identification of putative regulatory proteins. In *Plant Molecular Biology* (Vol. 50).

Plesch, G., Ehrhardt, T., & Mueller-Roeber, B. (2001). Involvement of TAAAG elements suggests a role for Dof transcription factors in guard cell-specific gene expression. *Plant Journal*, *28*(4), 455–464. https://doi.org/10.1046/j.1365-313X.2001.01166.x

Porto, M. S., Pinheiro, M. P. N., Batista, V. G. L., Dos Santos, R. C., De Albuquerque Melo Filho, P., & De Lima, L. M. (2014). Plant promoters: An approach of structure and function. In *Molecular*

Biotechnology (Vol. 56, Issue 1, pp. 38–49). Humana Press Inc. https://doi.org/10.1007/s12033-013-9713-1

Quevedo, M., Meert, L., Dekker, M. R., Dekkers, D. H. W., Brandsma, J. H., van den Berg, D. L. C., Ozgür, Z., IJcken, W. F. J. van, Demmers, J., Fornerod, M., & Poot, R. A. (2019). Mediator complex interaction partners organize the transcriptional network that defines neural stem cells. *Nature Communications*, *10*(1). https://doi.org/10.1038/s41467-019-10502-8

Quinn, J. M., & Merchant ', S. (1995). Two Copper-Responsive Elements Associated with the Chlamydomonas Cyc6 Gene Function as Targets for Transcri pt ional Act ivators. In *The Plant Cell* (Vol. 7). American Society of Plant Physiologists. https://academic.oup.com/plcell/article/7/5/623/5984929

Ramsay, N. A., & Glover, B. J. (2005). MYB-bHLH-WD40 protein complex and the evolution of cellular diversity. In *Trends in Plant Science* (Vol. 10, Issue 2, pp. 63–70). Elsevier Ltd. https://doi.org/10.1016/j.tplants.2004.12.011

Rapp, W. D., & Stern, D. B. (1992). A conserved 1 1 nucleotide sequence contains an essential promoter element of the maize mitochondrial atp1 gene. In *The EMBO Journal* (Vol. 1, Issue 3).

Reddy, A. S. N. (2007). Alternative splicing of pre-messenger RNAs in plants in the genomic era. In *Annual Review of Plant Biology* (Vol. 58, pp. 267–294). https://doi.org/10.1146/annurev.arplant.58.032806.103754

Rerie, W. G., Feldmann, K. A., & David Marks, M. (1994). *The GLABRA2 gene encodes a homeo domain protein required for normal tnchome development in Arabidopsis*.

Rg Wiedenmann, J., Ivanchenko, S., Oswald, F., Schmitt, F., Rö Cker ‡, C., Salih, A., Spindler, K.-D., & Ulrich Nienhaus, G. (2004). *EosFP, a fluorescent marker protein with UV-inducible green-to-red fluorescence conversion*. www.pnas.orgcgidoi10.1073pnas.0403668101

Ricci, W. A., Lu, Z., Ji, L., Marand, A. P., Ethridge, C. L., Murphy, N. G., Noshay, J. M., Galli, M., Mejía-Guerra, M. K., Colomé-Tatché, M., Johannes, F., Rowley, M. J., Corces, V. G., Zhai, J., Scanlon, M. J., Buckler, E. S., Gallavotti, A., Springer, N. M., Schmitz, R. J., & Zhang, X. (2019). Widespread long-range cis-regulatory elements in the maize genome. *Nature Plants*, *5*(12), 1237–1249. https://doi.org/10.1038/s41477-019-0547-0

Rieping, M., & Sehfffl, F. (1992). *Synergistic effect of upstream sequences, CCAAT box elements, and HSE sequences for enhanced expression of chimaeric heat shock genes in transgenic tobacco* (Vol. 231).

Rogers, H. J., Bate, N., Combe, J., Sullivan, J., Sweetman, J., Swan, C., Lonsdale, D. M., & Twell, D. (2001). Functional analysis of cis-regulatory elements within the promoter of the tobacco late pollen gene g10. In *Plant Molecular Biology* (Vol. 45).

Rosenfeld, N., Young, J. W., Alon, U., Swain, P. S., & Elowitz, M. B. (2005). Gene regulation at the single-cell level. *Science*, *307*(5717), 1962–1965. https://doi.org/10.1126/science.1106914

Rubio, V., Linhares, F., Solano, R., Martín, A. C., Iglesias, J., Leyva, A., & Paz-Ares, J. (2001). A conserved MYB transcription factor involved in phosphate starvation signaling both in vascular plants and in unicellular algae. *Genes and Development*, *15*(16), 2122–2133. https://doi.org/10.1101/gad.204401

Rushton, P. J., Macdonald, H., Huttly, A. K., Lazarus, C. M., & Hooley, R. (1995). Members of a new family of DNA-binding proteins bind to a conserved cis-element in the promoters of a-Amy2 genes. In *Plant Molecular Biology* (Vol. 29).

Rushton, P. J., Somssich, I. E., Ringler, P., & Shen, Q. J. (2010). WRKY transcription factors. In *Trends in Plant Science* (Vol. 15, Issue 5, pp. 247–258). Elsevier Ltd. https://doi.org/10.1016/j.tplants.2010.02.006

Rushton, P. J., Torres1, J. T., Parniske2, M., Wernert, P., Hahlbrock, K., & Somssich3, E. (1996). Interaction of elicitor-induced DNA-binding proteins with elicitor response elements in the promoters of parsley PR1 genes. In *The EMBO Journal* (Vol. 15, Issue 20).

Ryan, M. D., King, A. M. Q., & Thomas, G. P. (1991). Cleavage of foot-and-mouth disease virus polyprotein is mediated by residues located within a 19 amino acid sequence. *Journal of General Virology*, *72*(11), 2727–2732. https://doi.org/10.1099/0022-1317-72-11-2727

Sablowski, R. W., Moyano, E., Culianez-Macia, F. A., Schuch, W., Martin, C., & Bevan, M. (1994). A flower-specific Myb protein activates transcription of phenylpropanoid biosynthetic genes. *The EMBO Journal*, *13*(1), 128–137. https://doi.org/10.1002/j.1460-2075.1994.tb06242.x

Saijo, Y., Sullivan, J. A., Wang, H., Yang, J., Shen, Y., Rubio, V., Ma, L., Hoecker, U., & Deng, X. W. (2003). The COP1-SPA1 interaction defines a critical step in phytochrome A-mediated regulation of HY5 activity. *Genes and Development*, *17*(21), 2642–2647. https://doi.org/10.1101/gad.1122903

Sakai, H., Aoyama, T., & Oka, A. (2000). Arabidopsis ARR1 and ARR2 response regulators operate as transcriptional activators . *The Plant Journal*, *24*(6), 703–711. https://doi.org/10.1111/j.1365-313x.2000.00909.x

Sako, K., Maki, Y., Imai, K. K., Aoyama, T., Goto, D. B., & Yamaguchi, J. (2010). Control of endoreduplication of trichome by RPT2a, a subunit of the 19S proteasome in Arabidopsis. *Journal of Plant Research*, *123*(5), 701–706. https://doi.org/10.1007/s10265-010-0321-x

Samalova, M., Fricker, M., & Moore, I. (2006). Ratiometric fluorescence-imaging assays of plant membrane traffic using polyproteins. *Traffic*, *7*(12), 1701–1723. https://doi.org/10.1111/j.1600-0854.2006.00502.x

Satoh, R., Fujita, Y., Nakashima, K., Shinozaki, K., & Yamaguchi-Shinozaki, K. (2004). A Novel Subgroup of bZIP Proteins Functions as Transcriptional Activators in Hypoosmolarity-Responsive Expression of the ProDH Gene in Arabidopsis. In *Plant Cell Physiol* (Vol. 45, Issue 3). http://www.dna.affrc.go.jp/htdocs/PLACE

Savage, N. saint, Walker, T., Wieckowski, Y., Schiefelbein, J., Dolan, L., & Monk, N. A. M. (2008). A mutual support mechanism through intercellular movement of CAPRICE and GLABRA3 can pattern the Arabidopsis root epidermis. *PLoS Biology*, *6*(9), 1899–1909. https://doi.org/10.1371/journal.pbio.0060235

Scheffner, M., Nuber, U., & Huibregtse, J. M. (1995). Protein ubiquitination involving an E1-E2-E3 enzyme ubiquitin thioester cascade. In *14. Seufert, W. & Jentsch, S. EMBO J* (Vol. 248, Issue 6). Green and Wiley.

Schellmann, S., Hülskamp, M., & Uhrig, J. (2007). Epidermal pattern formation in the root and shoot of *Arabidopsis*. *Biochemical Society Transactions*, *35*, 146–148. https://doi.org/10.1042/BST0350146

Schellmann, S., Schnittger, A., Kirik, V., Wada, T., Okada, K., Beerman, A., Thumfahrt, J., Jürgens, G., & Hülskamp, M. (2002). TRIPTYCHON and CAPRICE mediate lateral inhibition during trichome and root hair patterning in Arabidopsis. *EMBO Journal*, *21*(19), 5036–5046. https://doi.org/10.1093/emboj/cdf524

Schiefelbein, J. (2003). Cell-fate specification in the epidermis: a common patterning mechanism in the root and shoot. *Current Opinion in Plant Biology*, *6*, 74–78. https://doi.org/10.1016/S1369-5266(02)00002-X

Schmitz, R. J., Grotewold, E., & Stam, M. (2022). Cis-regulatory sequences in plants: Their importance, discovery, and future challenges. In *Plant Cell* (Vol. 34, Issue 2, pp. 718–741). Oxford University Press. https://doi.org/10.1093/plcell/koab281

Schnittger, A., Folkers, U., Schwab, B., Jürgens, G., & Hülskamp, M. (1999). Generation of a spacing pattern: the role of triptychon in trichome patterning in Arabidopsis. *The Plant Cell*, *11*(6), 1105–1116. https://doi.org/10.1105/tpc.11.6.1105

Schnittger, A., & Hülskamp, M. (2002). Trichome morphogenesis: A cell-cycle perspective. *Philosophical Transactions of the Royal Society B: Biological Sciences*, *357*(1422), 823–826. https://doi.org/10.1098/rstb.2002.1087

Schnittger, A., Jürgens, G., & Hülskamp, M. (1998). Tissue layer and organ specificity of trichome formation are regulated by GLABRA1 and TRIPTYCHON in Arabidopsis. *Development*, *125*, 2283–2289.

Schuurink, R., & Tissier, A. (2020). Glandular trichomes: micro-organs with model status? In *New Phytologist* (Vol. 225, Issue 6, pp. 2251–2266). Blackwell Publishing Ltd. https://doi.org/10.1111/nph.16283

Schwentker, M. A., Bock, H., Hofmann, M., Jakobs, S., Bewersdorf, J., Eggeling, C., & Hell, S. W. (2007). Wide-field subdiffraction RESOLFT microscopy using fluorescent protein photoswitching. *Microscopy Research and Technique*, *70*(3), 269–280. https://doi.org/10.1002/jemt.20443

Seol, J. H., Feldman, R. M. R., Zachariae, W., Shevchenko, A., Correll, C. C., Lyapina, S., Chi, Y., Galova, M., Claypool, J., Sandmeyer, S., Nasmyth, K., Shevchenko, A., & Deshaies, R. J. (1999). Cdc53/cullin and the essential Hrt1 RING-H2 subunit of SCF define a ubiquitin ligase module that activates the E2 enzyme Cdc34. *GENES & DEVELOPMENT*, 1614–1626.

Seo, S., Seto, H., Koshino, H., Yoshida, S., & Ohashi, Y. (2003). A diterpene as an endogenous signal for the activation of defense responses to infection with Tobacco mosaic virus and wounding in tobacco. *Plant Cell*, *15*(4), 863–873. https://doi.org/10.1105/tpc.010231

Sessa, G., Morelli, G., & Ruberti, I. (1993). The Athb-1 and −2 HD-Zip domains homodimerize forming complexes of different DNA binding specificities. *The EMBO Journal*, *12*(9), 3507–3517. https://doi.org/10.1002/j.1460-2075.1993.tb06025.x

Shang, X., Cao, Y., & Ma, L. (2017). Alternative splicing in plant genes: A means of regulating the environmental fitness of plants. In *International Journal of Molecular Sciences* (Vol. 18, Issue 2). MDPI AG. https://doi.org/10.3390/ijms18020432

Shen, Q., Hu, T., Bao, M., Cao, L., Zhang, H., Song, F., Xie, Q., & Zhou, X. (2016). Tobacco RING E3 Ligase NtRFP1 Mediates Ubiquitination and Proteasomal Degradation of a Geminivirus-Encoded βC1. *Molecular Plant*, *9*(6), 911–925. https://doi.org/10.1016/j.molp.2016.03.008

Shirley, B. W., Kubasek, W. L., Storz, G., Bruggemann, E., Koornneef, M., Ausubel, F. M., & Goodman, H. M. (1995). Analysis of Arabidopsis mutants deficient in flavonoid biosynthesis. *The Plant Journal*, *8*(5), 659–671. https://doi.org/10.1046/j.1365-313x.1995.08050659.x

Shirsat, A., Wilford, N., Croy, R., & Boulter, D. (1989). *Sequences responsible for the tissue specific promoter activity of a pea legumin gene in tobacco* (Vol. 215).

Shlyueva, D., Stampfel, G., & Stark, A. (2014). Transcriptional enhancers: From properties to genome-wide predictions. In *Nature Reviews Genetics* (Vol. 15, Issue 4, pp. 272–286). Nature Publishing Group. https://doi.org/10.1038/nrg3682

Simon, M., Lee, M. M., Lin, Y., Gish, L., & Schiefelbein, J. (2007). Distinct and overlapping roles of single-repeat MYB genes in root epidermal patterning. *Developmental Biology*, *311*(2), 566–578. https://doi.org/10.1016/j.ydbio.2007.09.001

Simpson, S. D., Nakashima, K., Narusaka, Y., Seki, M., Shinozaki, K., & Yamaguchi-Shinozaki, K. (2003). Two different novel cis-acting elements of erd1, a clpA homologous Arabidopsis gene function in induction by dehydration stress and dark-induced senescence. *Plant Journal*, *33*(2), 259–270. https://doi.org/10.1046/j.1365-313X.2003.01624.x

Smale, S. T., & Kadonaga, J. T. (2003). The RNA polymerase II core promoter. In *Annual Review of Biochemistry* (Vol. 72, pp. 449–479). https://doi.org/10.1146/annurev.biochem.72.121801.161520

Smalle, J., & Vierstra, R. D. (2004). The ubiquitin 26S proteasome proteolytic pathway. In *Annual Review of Plant Biology* (Vol. 55, pp. 555–590). https://doi.org/10.1146/annurev.arplant.55.031903.141801

Stalberg, K., Ellerström, M., Ezcurra, I., Ablov, S., & Rask, L. (1996). Disruption of an overlapping E-box/ABRE motif abolished high transcription of the napA storage-protein promoter in transgenic Brassica napus seeds. In *Planta* (Vol. 199). Springer-Verlag.

Stougaard, J., Jorgensen, J.-E., Christensen, T., Kiihle, A., & Marcker, K. A. (1990). *Interdependence and nodule specificity of c/s-acting regulatory elements in the soybean leghemoglobin lbc3 and N23 gene promoters* (Vol. 220).

Stracke, R., Werber, M., & Weisshaar, B. (2001). The R2R3-MYB gene family in Arabidopsis thaliana. *Current Opinion in Plant Biology*.

Straub, P. F., Shen, Q., & David Ho, T. (1994). Structure and promoter analysis of an ABA-and stress-regulated barley gene, HVA1. In *Plant Molecular Biology* (Vol. 26).

Sugimoto, K., Takeda, S., & Hirochika, H. (2003). Transcriptional activation mediated by binding of a plant GATA-type zinc finger protein AGP1 to the AG-motif (AGATCCAA) of the wound-inducible Myb gene NtMyb2. *Plant Journal*, *36*(4), 550–564. https://doi.org/10.1046/j.1365-313X.2003.01899.x

Sun, C., Palmqvist, S., Olsson, H., Borén, M., Ahlandsberg, S., & Jansson, C. (2003). A novel WRKY transcription factor, SUSIBA2, participates in sugar signaling in barley by binding to the sugar-responsive elements of the iso1 promoter. *Plant Cell*, *15*(9), 2076–2092. https://doi.org/10.1105/tpc.014597

Sutoh, K., & Yamauchi, D. (2003). Two cis-acting elements necessary and sufficient for gibberellin-upregulated proteinase expression in rice seeds. *Plant Journal*, *34*(5), 635–645. https://doi.org/10.1046/j.1365-313X.2003.01753.x

Symonds, V. V., Hatlestad, G., & Lloyd, A. M. (2011). Natural allelic variation defines a role for ATMYC1: Trichome cell fate determination. *PLoS Genetics*, *7*(6). https://doi.org/10.1371/journal.pgen.1002069

Szymczak, A. L., & Vignali, D. A. A. (2005). Development of 2A peptide-based strategies in the design of multicistronic vectors. In *Expert Opinion on Biological Therapy* (Vol. 5, Issue 5, pp. 627–638). https://doi.org/10.1517/14712598.5.5.627

Szymczak, A. L., Workman, C. J., Wang, Y., Vignali, K. M., Dilioglou, S., Vanin, E. F., & Vignali, D. A. A. (2004). Correction of multi-gene deficiency in vivo using a single "self-cleaving" 2A peptide-based retroviral vector. *Nature Biotechnology*, *22*(5), 589–594. https://doi.org/10.1038/nbt957

Tang, W., & Perry, S. E. (2003). Binding site selection for the plant MADS domain protein AGL15. An in vitro and in vivo study. *Journal of Biological Chemistry*, *278*(30), 28154–28159. https://doi.org/10.1074/jbc.M212976200

Tan, Y., Barnbrook, M., Wilson, Y., Molnár, A., Bukys, A., & Hudson, A. (2020). Shared Mutations in a Novel Glutaredoxin Repressor of Multicellular Trichome Fate Underlie Parallel Evolution of

Antirrhinum Species. *Current Biology*, *30*(8), 1357-1366.e4. https://doi.org/10.1016/j.cub.2020.01.060

Tatematsu, K., Ward, S., Leyser, O., Kamiya, Y., & Nambara, E. (2005). Identification of cis-elements that regulate gene expression during initiation of axillary bud outgrowth in Arabidopsis. In *Plant Physiology* (Vol. 138, Issue 2, pp. 757–766). American Society of Plant Biologists. https://doi.org/10.1104/pp.104.057984

Tattini, M., Gravano, E., Pinelli, P., Mulinacci, N., & Romani, A. (2000). Flavonoids accumulate in leaves and glandular trichomes of Phillyrea latifolia exposed to excess solar radiation. *New Phytologist*, *148*(1), 69–77. https://doi.org/10.1046/j.1469-8137.2000.00743.x

Teakle, G. R., Manfield, I. W., Graham, J. F., & Gilmartin, P. M. (2002). Arabidopsis thaliana GATA factors: organisation, expression and DNA-binding characteristics. In *Plant Molecular Biology* (Vol. 50).

Teng, S., Keurentjes, J., Bentsink, L., Koornneef, M., & Smeekens, S. (2005). Sucrose-specific induction of anthocyanin biosynthesis in Arabidopsis requires the MYB75/PAP1 gene. *Plant Physiology*, *139*(4), 1840–1852. https://doi.org/10.1104/pp.105.066688

Terzaghi, W. B., & Cashmore, A. R. (1995). LIGHT-REGULATED TRANSCRIPTION. In *Annu. Rev. Plant Physiol. Plant Mol. Biol* (Vol. 46).

Theobald WL, Krahulik JL, Rollins RC. Trichome description and classification. Anatomy of the dicotyledons I. Oxford: Clarendon Press; 1980. p. 40–53.

Thomas', M. S., & Flavel12, R. B. (1990). ldentification of an Enhancer Element for the Endosperm-Specific Expression of High Molecular Weight Glutenin. In *The Plant Cell* (Vol. 2). American Society of Plant Physiologists. https://academic.oup.com/plcell/article/2/12/1171/5983228

Thum, K. E., Kim, M., Morishige, D. T., Eibl, C., Koop, H.-U., & Mullet, J. E. (2001). Analysis of barley chloroplast psbD light-responsive promoter elements in transplastomic tobacco. In *Plant Molecular Biology* (Vol. 47).

Tjaden, G., Edwards3, J. W., & Coruni, G. M. (1995). cis Elements and frans-Acting Factors Affecting Regulation of a Nonphotosynthetic Light-Regulated Gene for Chloroplast Glutamine Synthetase'. In *Plant Physiol* (Vol. 108). https://academic.oup.com/plphys/article/108/3/1109/6069798

Tominaga, R., Iwata, M., Sano, R., Inoue, K., Okada, K., & Wada, T. (2008). Arabidopsis CAPRICE-LIKE MYB 3 (CPL3) controls endoreduplication and flowering development in addition to trichome and root hair formation. *Development*, *135*(7), 1335–1345. https://doi.org/10.1242/dev.017947

Tominaga-Wada, R., Nukumizu, Y., Sato, S., Kato, T., Tabata, S., & Wada, T. (2012). Functional divergence of MYB-related genes, WEREWOLF and AtMYB23 in Arabidopsis. *Bioscience, Biotechnology and Biochemistry*, *76*(5), 883–887. https://doi.org/10.1271/bbb.110811

Tompa, M., Li, N., Bailey, T. L., Church, G. M., De Moor, B., Eskin, E., Favorov, A. V., Frith, M. C., Fu, Y., Kent, W. J., Makeev, V. J., Mironov, A. A., Noble, W. S., Pavesi, G., Pesole, G., Régnier, M., Simonis, N., Sinha, S., Thijs, G., … Zhu, Z. (2005). Assessing computational tools for the discovery of transcription factor binding sites. In *Nature Biotechnology* (Vol. 23, Issue 1, pp. 137–144). Nature Publishing Group. https://doi.org/10.1038/nbt1053

Toyofuku, K., Umemura, T., & Yamaguchi, J. (n.d.). *Promoter elements required for sugar-repression of the RAmy3D gene for K-amylase in rice*.

Tsutsui, H., Karasawa, S., Shimizu, H., Nukina, N., & Miyawaki, A. (2005). Semi-rational engineering of a coral fluorescent protein into an efficient highlighter. *EMBO Reports*, *6*(3), 233–238. https://doi.org/10.1038/sj.embor.7400361

Turing, A. M. (1952). The Chemical Basis of Morphogenesis. In *Philosophical Transactions of the Royal Society of London. Series B, Biological Sciences* (Vol. 237, Issue 641). http://www.jstor.org/about/terms.html.

Tutin TG, Burges NA, Chater AO JRE, Heywood VH, Moore DM, Valentine DH, Walters SM, Webb DA, Akeroyd JR, Newton ME, et al. Flora Europaea. New York: Cambridge University Press; 1993.

Ulmasov, T., Hagen, G., & Guilfoyle, T. J. (1999). Dimerization and DNA binding of auxin response factors. *Plant Journal*, *19*(3), 309–319. https://doi.org/10.1046/j.1365-313X.1999.00538.x

Urao, T., Yamaguchi-Shinozaki ~', K., Mitsukawa, N., Shibata, D., & Shinozaki, K. (1996). Molecular cloning and characterization of a gene that encodes a MYC-related protein in Arabidopsis. In *Plant Molecular Biology* (Vol. 32). Kluwer Academic Publishers.

Urao, T., Yamaguchi-Shinozaki, K., Satorni Urao, C., & Shinozaki, K. (1993). to the Conserved MYB Recognition Sequence. In *The Plant Cell* (Vol. 5).

Uriu, K. (2016). Genetic oscillators in development. In *Development Growth and Differentiation* (Vol. 58, Issue 1, pp. 16–30). Blackwell Publishing. https://doi.org/10.1111/dgd.12262

Vandepoele, K., Vlieghe, K., Florquin, K., Hennig, L., Beemster, G. T. S., Gruissem, W., Van De Peer, Y., Inzé, D., & De Veylder, L. (2005). Genome-wide identification of potential plant E2F target genes. In *Plant Physiology* (Vol. 139, Issue 1, pp. 316–328). American Society of Plant Biologists. https://doi.org/10.1104/pp.105.066290

Van Der Fits, L., Deakin, E. A., Harry, J., Hoge, C., & Memelink, J. (2000). The ternary transformation system: constitutive virG on a compatible plasmid dramatically increases Agrobacterium-mediated plant transformation. In *Plant Molecular Biology* (Vol. 43).

Vieweg, M. F., Frühling, M., Quandt, H.-J., Heim, U., Bäumlein, H., Pühler, A., Küster, H., & Perlick, A. M. (2004). The Promoter of the Vicia faba L. Leghemoglobin Gene VfLb29 Is Specifically Activated in the Infected Cells of Root Nodules and in the Arbuscule-Containing Cells of Mycorrhizal Roots from Different Legume and Nonlegume Plants. In *Molecular Plant-Microbe Interactions MPMI* (Vol. 17, Issue 1).

Villain, P., Gis Mache, R., & Zhou, D.-X. (1996). *The Mechanism of GT Element-mediated Cell Type-specific Transcriptional Control**. http://www-jbc.stanford.edu/jbc/

Voges, D., Zwickl, P., & Baumeister, W. (1999). *THE 26S PROTEASOME: A MOLECULAR MACHINE DESIGNED FOR CONTROLLED PROTEOLYSIS*.

Voinnet, O., Pinto, Y. M., & Baulcombe, D. C. (1999). Suppression of gene silencing: A general strategy used by diverse DNA and RNA viruses of plants. *Proceedings of the National Academy of Sciences of the United States of America*, *96*(24), 14147–14152. https://doi.org/10.1073/pnas.96.24.14147

von Gromoff, E. D., Schroda, M., Oster, U., & Beck, C. F. (2006). Identification of a plastid response element that acts as an enhancer within the Chlamydomonas HSP70A promoter. *Nucleic Acids Research*, *34*(17), 4767–4779. https://doi.org/10.1093/nar/gkl602

Wada, T., Tachibana, T., Shimura, Y., & Okada, K. (1997). Epidermal Cell Differentiation in Arabidopsis Determined by a Myb Homolog, CPC. *Science*, *277*(5329), 1113–1116. https://doi.org/10.1126/science.277.5329.1113

Walker, A. R., Davison, P. A., Bolognesi-Winfield, A. C., James, C. M., Srinivasan, N., Blundell, T. L., Esch, J. J., David Marks, M., & Gray, J. C. (1999). The TRANSPARENT TESTA GLABRA1 Locus, Which Regulates Trichome Differentiation and Anthocyanin Biosynthesis in Arabidopsis, Encodes a WD40 Repeat Protein. In *The Plant Cell* (Vol. 11). www.plantcell.org

Wang, G., Feng, H., Sun, J., & Du, X. (2013). Induction of cotton ovule culture fibre branching by co-expression of cotton BTL, cotton SIM, and Arabidopsis STI genes. *Journal of Experimental Botany*, *64*(14), 4157–4168. https://doi.org/10.1093/jxb/ert222

Wang, M., Cheng, D., Peng, J., & Pickart, C. M. (2006). Molecular determinants of polyubiquitin linkage selection by an HECT ubiquitin ligase. *EMBO Journal*, *25*(8), 1710–1719. https://doi.org/10.1038/sj.emboj.7601061

Wang, S., & Chen, J. G. (2008). Arabidopsis transient expression analysis reveals that activation of GLABRA2 may require concurrent binding of GLABRA1 and GLABRA3 to the promoter of GLABRA2. *Plant and Cell Physiology*, *49*(12), 1792–1804. https://doi.org/10.1093/pcp/pcn159

Wang, S., Hubbard, L., Chang, Y., Guo, J., Schiefelbein, J., & Chen, J.-G. (2008). Comprehensive analysis of single-repeat R3 MYB proteins in epidermal cell patterning and their transcriptional regulation in Arabidopsis. *BMC Plant Biology*, *8*, 81. https://doi.org/10.1186/1471-2229-8-81

Wang, S., Kwak, S.-H., Zeng, Q., Ellis, B. E., Chen, X.-Y., Schiefelbein, J., & Chen, J.-G. (2007). TRICHOMELESS1 regulates trichome patterning by suppressing GLABRA1 in Arabidopsis. *Development (Cambridge, England)*, *134*, 3873–3882. https://doi.org/10.1242/dev.009597

Wang, S., Wang, J. W., Yu, N., Li, C. H., Luo, B., Gou, J. Y., Wang, L. J., & Chen, X. Y. (2004a). Control of plant trichome development by a cotton fiber MYB gene. *Plant Cell*, *16*(9), 2323–2334. https://doi.org/10.1105/tpc.104.024844

Wang, X., Shen, C., Meng, P., Tan, G., & Lv, L. (2021). Analysis and review of trichomes in plants. In *BMC Plant Biology* (Vol. 21, Issue 1). BioMed Central Ltd. https://doi.org/10.1186/s12870-021-02840-x

Wang, Y., Zhou, Q., Meng, Z., Abid, M. A., Wang, Y., Wei, Y., Guo, S., Zhang, R., & Liang, C. (2022). Multi-Dimensional Molecular Regulation of Trichome Development in Arabidopsis and Cotton. In *Frontiers in Plant Science* (Vol. 13). Frontiers Media S.A. https://doi.org/10.3389/fpls.2022.892381

Wang, Z.-Y., Kenigsbuch, D., Sun, L., Harel, E., Ong, M. S., & Tobin4, E. M. (1997). A Myb-Related Transcription Factor 1s lnvolved in the Phytochrome Regulation of an Arabidopsis Lhcb Gene. In *The Plant Cell* (Vol. 9). American Society of Plant Physiologists. https://academic.oup.com/plcell/article/9/4/491/5977084

Weber, B., Zicola, J., Oka, R., & Stam, M. (2016). Plant Enhancers: A Call for Discovery. In *Trends in Plant Science* (Vol. 21, Issue 11, pp. 974–987). Elsevier Ltd. https://doi.org/10.1016/j.tplants.2016.07.013

Wehner, N., Hartmann, L., Ehlert, A., Böttner, S., Oñate-Sánchez, L., & Dröge-Laser, W. (2011). High-throughput protoplast transactivation (PTA) system for the analysis of Arabidopsis transcription factor function. *Plant Journal*, *68*(3), 560–569. https://doi.org/10.1111/j.1365-313X.2011.04704.x

Weiher H, König M, Gruss P. Multiple point mutations affecting the simian virus 40 enhancer. Science. 1983 Feb 11;219(4585):626-31. doi: 10.1126/science.6297005. PMID: 6297005.

Wester, K., Digiuni, S., Geier, F., Timmer, J., Fleck, C., & Hülskamp, M. (2009). Functional diversity of R3 single-repeat genes in trichome development. *Development*, *136*(9), 1487–1496. https://doi.org/10.1242/dev.021733

Wilkinson, K. D. (2000). Ubiquitination and deubiquitination: Targeting of proteins for degradation by the proteasome. *Seminars in Cell and Developmental Biology*, *11*(3), 141–148. https://doi.org/10.1006/scdb.2000.0164

Willing, E.-M., Rawat, V., Mandáková, T., Maumus, F., James, G. V., Nordström, K. J. V., et al. (2015). Genome expansion of Arabis alpina linked with retrotransposition and reduced symmetric DNA methylation. Nat. Plants 1:14023. doi: 10.1038/nplants.2014.23

Wu, C. Y., Washida, H., Onodera, Y., Harada, K., & Takaiwa, F. (2000). Quantitative nature of the prolamin-box, ACGT and AACA motifs in a rice glutelin gene promoter: Minimal cis-element requirements for endosperm-specific gene expression. *Plant Journal*, *23*(3), 415–421. https://doi.org/10.1046/j.1365-313X.2000.00797.x

Wu, S., Koizumi, K., MacRae-Crerar, A., & Gallagher, K. L. (2011). Assessing the utility of photoswitchable fluorescent proteins for tracking intercellular protein movement in the Arabidopsis root. *PLoS ONE*, *6*(11). https://doi.org/10.1371/journal.pone.0027536

Xiao, J., Jin, R., Yu, X., Shen, M., Wagner, J. D., Pai, A., Song, C., Zhuang, M., Klasfeld, S., He, C., Santos, A. M., Helliwell, C., Pruneda-Paz, J. L., Kay, S. A., Lin, X., Cui, S., Garcia, M. F., Clarenz, O., Goodrich, J., … Wagner, D. (2017). Cis and trans determinants of epigenetic silencing by Polycomb repressive complex 2 in Arabidopsis. *Nature Genetics*, *49*(10), 1546–1552. https://doi.org/10.1038/ng.3937

Xie, H., & Ding, X. (2022). The Intriguing Landscape of Single-Cell Protein Analysis. In *Advanced Science* (Vol. 9, Issue 12). John Wiley and Sons Inc. https://doi.org/10.1002/advs.202105932

Xue, P. (2002). *Characterisation of the DNA-binding profile of barley HvCBF1 using an enzymatic method for rapid, quantitative and high-throughput analysis of the DNA-binding activity*.

Xu, N., Hagen, G., & Guilfoyle, T. (1997). Multiple auxin response modules in the soybean SAUR 15A promoter. In *Plant Science* (Vol. 126).

Yamagata, H., Yonesu, K., Hirata, A., & Aizono, Y. (2002). TGTCACA motif is a novel cis-regulatory enhancer element involved in fruit-specific expression of the cucumisin gene. *Journal of Biological Chemistry*, *277*(13), 11582–11590. https://doi.org/10.1074/jbc.M109946200

Yamamoto, S., Nakano, T., Suzuki, K., & Shinshi, H. (2004). Elicitor-induced activation of transcription via W box-related cis-acting elements from a basic chitinase gene by WRKY transcription factors in tobacco. *Biochimica et Biophysica Acta - Gene Structure and Expression*, *1679*(3), 279–287. https://doi.org/10.1016/j.bbaexp.2004.07.005

Yamamoto, Y., Ichida, H., Abe, T., Suzuki, Y., Sugano, S., & Obokata, J. (2007). Differentiation of core promoter architecture between plants and mammals revealed by LDSS analysis. *Nucleic Acids Research*, *35*(18), 6219–6226. https://doi.org/10.1093/nar/gkm685

Yamamoto, Y. Y., Yoshitsugu, T., Sakurai, T., Seki, M., Shinozaki, K., & Obokata, J. (2009). Heterogeneity of Arabidopsis core promoters revealed by high-density TSS analysis. *Plant Journal*, *60*(2), 350–362. https://doi.org/10.1111/j.1365-313X.2009.03958.x

Yamauchi, D. (2001). A TGACGT Motif in the 5¢ ¢ ¢ ¢-Upstream Region of a a a a-Amylase Gene from Vigna mungo is a cis-Element for Expression in Cotyledons of Germinated Seeds. In *Plant Cell Physiol* (Vol. 42, Issue 6).

Yanagisawa, S. (2004). Dof Domain Proteins: Plant-Specific Transcription Factors Associated with Diverse Phenomena Unique to Plants. In *Plant Cell Physiol* (Vol. 45, Issue 4). https://academic.oup.com/pcp/article/45/4/386/1922047

Yan, A., Pan, J., An, L., Gan, Y., & Feng, H. (2012). The responses of trichome mutants to enhanced ultraviolet-B radiation in Arabidopsis thaliana. *Journal of Photochemistry and Photobiology B: Biology*, *113*, 29–35. https://doi.org/10.1016/j.jphotobiol.2012.04.011

Yang, P., Fu, H., Walker, J., Papa, C. M., Smalle, J., Ju, Y. M., & Vierstra, R. D. (2004). Purification of the Arabidopsis 26 S proteasome: Biochemical and molecular analyzes revealed the presence of

multiple isoforms. *Journal of Biological Chemistry*, *279*(8), 6401–6413. https://doi.org/10.1074/jbc.M311977200

Yang, T., & Poovaiah, B. W. (2002). A calmodulin-binding/CGCG box DNA-binding protein family involved in multiple signaling pathways in plants. *Journal of Biological Chemistry*, *277*(47), 45049–45058. https://doi.org/10.1074/jbc.M207941200

Yin, Y., Chen, L., & Beachy, R. (1997). Promoter elements required for phloem-specific gene expression from the RTBV promoter in rice. *Plant Journal*, *12*(5), 1179–1188. https://doi.org/10.1046/j.1365-313X.1997.12051179.x

Yukawa, Y., Sugita, M., Choisne, N., Small, I., & Sugiura, M. (2000). The TATA motif, the CAA motif and the poly(T) transcription termination motif are all important for transcription re-initiation on plant tRNA genes. *Plant Journal*, *22*(5), 439–447. https://doi.org/10.1046/j.1365-313X.2000.00752.x

Zhang, B., Deneer, A., Fleck, C., & Hülskamp, M. (2024). Quantitative analysis of MBW complex formation in the context of trichome patterning. *Frontiers in Plant Science*, *15*. https://doi.org/10.3389/fpls.2024.1331156

Zhang, B., & Schrader, A. (2017). TRANSPARENT TESTA GLABRA 1-Dependent Regulation of Flavonoid Biosynthesis. *Plants*, *6*(4), 65. https://doi.org/10.3390/plants6040065

Zhang, C. C., Laurent, S., Sakr, S., Peng, L., & Bédu, S. (2006). Heterocyst differentiation and pattern formation in cyanobacteria: A chorus of signals. In *Molecular Microbiology* (Vol. 59, Issue 2, pp. 367–375). https://doi.org/10.1111/j.1365-2958.2005.04979.x

Zhang, F., Gonzalez, A., Zhao, M., Payne, C. T., & Lloyd, A. (2003). A network of redundant bHLH proteins functions in all TTG1-dependent pathways of Arabidopsis. *Development*, *130*(20), 4859–4869. https://doi.org/10.1242/dev.00681

Zhang, L., Gurskaya, N. G., Merzlyak, E. M., Staroverov, D. B., Mudrik, N. N., Samarkina, O. N., Vinokurov, L. M., Lukyanov, S., & Lukyanov, K. A. (2007). Method for real-time monitoring of protein degradation at the single cell level. In *BioTechniques* (Vol. 42, Issue 4, pp. 446–450). https://doi.org/10.2144/000112453

Zhao, H., Wang, X., Zhu, D., Cui, S., Li, X., Cao, Y., & Ma, L. (2012). A single amino acid substitution in IIIf subfamily of basic helix-loop-helix transcription factor AtMYC1 leads to trichome and root hair patterning defects by abolishing its interaction with partner proteins in Arabidopsis. *Journal of Biological Chemistry*, *287*(17), 14109–14121. https://doi.org/10.1074/jbc.M111.280735

Zhao, J., Hyman, L., & Moore, C. (1999). Formation of mRNA 3 Ends in Eukaryotes: Mechanism, Regulation, and Interrelationships with Other Steps in mRNA Synthesis. In *MICROBIOLOGY AND MOLECULAR BIOLOGY REVIEWS* (Vol. 63, Issue 2). https://journals.asm.org/journal/mmbr

Zhao, M., Morohashi, K., Hatlestad, G., Grotewold, E., & Lloyd, A. (2008). The TTG1-bHLH-MYB complex controls trichome cell fate and patterning through direct targeting of regulatory loci. *Development*, *135*(11), 1991–1999. https://doi.org/10.1242/dev.016873

Zhao, X., Qiao, L., & Wu, A. M. (2017). Effective extraction of Arabidopsis adherent seed mucilage by ultrasonic treatment. *Scientific Reports*, *7*, 1–8. https://doi.org/10.1038/srep40672

Zhous, D.-X., Li, Y.-F., Rocipon, M., & Mache, R. (1992). *THE JOURNAL OF BIOLOGICAL CHEMISTRY Sequence-specific Interaction between S l F, a Spinach Nuclear Factor, and a Negative &-Element Conserved in Plastid-related Genes** (Vol. 267, Issue 33).

Zhu, Q., Ordiz, M. I., Dabi, T., Beachy, R. N., & Lamb, C. (2002). Rice TATA binding protein interacts functionally with transcription factor IIB and the RF2a bZIP transcriptional activator in an

enhanced plant in vitro transcription system. *Plant Cell*, *14*(4), 795–803. https://doi.org/10.1105/tpc.010364

Zhu, Y., Cai, X. L., Wang, Z. Y., & Hong, M. M. (2003). An Interaction between a MYC Protein and an EREBP Protein Is Involved in Transcriptional Regulation of the Rice Wx Gene. *Journal of Biological Chemistry*, *278*(48), 47803–47811. https://doi.org/10.1074/jbc.M302806200

Zimmermann, I. M., Heim, M. A., Weisshaar, B., & Uhrig, J. F. (2004). Comprehensive identification of Arabidopsis thaliana MYB transcription factors interacting with R/B-like BHLH proteins. *Plant Journal*, *40*(1), 22–34. https://doi.org/10.1111/j.1365-313X.2004.02183.x

6. Appendix

Table 17. List of entry vectors used in this study.

Plasmid	Provided/generate by
pDONR201 GW	L. Stephan
pDONR207 GW	L. Stephan
pENTR-GUS	S. Schellmann
pENTR1A- w/o ccdB	J. Pietsch
pENTR4-CPC	I. Schultheiß Araújo
pDONR201-TRY	I. Schultheiß Araújo
pDONR201-GL3	I. Schultheiß Araújo
pENTR1A-GL1	I. Schultheiß Araújo
pENTR4-TTG1	I. Schultheiß Araújo
pDONR207-pETC1	this study
pDONR207-pETC2	this study
pDONR207-pETC3	this study
pDONR207-TRY	I. Schultheiß Araújo
pDONR207-GL3 w/o stop	I. Schultheiß Araújo
pDONR201-TTG2 with stop	this study
pDONR207-TTG2 with stop	this study
pDONR201-pCPC_minimal	this study
pDONR201-pTRY_minimal	this study
pDONR207-pTRY_minimal	this study
pDONR207-pCPC_minimal	this study
pDONR201-MYB23 w/o stop	this study
pDONR201-EGL3 w/o stop	this study
pDONR201-CPC_truncated	this study
pDONR207-CPC_truncated	this study
pDONR201-enhancer+pGL1	this study
pDONR207-enhancer+pGL1	this study
pDONR201-GL1 w/o stop	I. Schultheiß Araújo
pDONR201-pGL1 Wang	this study
pDONR221-HY5	this study
pDONR207-pGL1 Wang	this study
pDONR201-GL1-R97D	this study
pDONR207-GL1-R97D	this study
pDONR201-Ex1+2-In2-Ex3(10bp)_GL3	this study
pDONR207-Ex1+2-In2-Ex3(10bp)_GL3	this study
pDONR201-Δ96 GL3	this study
pDONR207-Δ96 GL3	this study
pDONR201-Ex1+2-In2(1-138)-Ex3(10bp)_GL3	this study
pDONR207-Ex1+2-In2(1-138)-Ex3(10bp)_GL3	this study
pDONR201-pGL1 Wang-GL1 gDNA-3‘ enhancer Wang	this study
pDONR201-pGL1 Wang:GL1 CDS-3‘ enhancer Wang	this study
pDONR201-GL1-R97D w/o stop	this study

pDONR207-pGL3	this study
pDONR207-pGL3-EX1+2-In2-Ex3(10bp)	this study
pDONR207-Intron1_GL1	this study
pDONR207-3'enhancer Wang	this study
pDONR207-3'enhancer box Larkin	this study
pDONR207-pGL3-EX1+2-IN2(1-138)-Ex3(10bp)	this study
pDONR207-pGL3-EX1+2-IN2(1-138)-Ex3(10bp)_Mut.1&2	this study
pDONR207-pGL1 Wang-Ex1+In1-Ex2(11bp)	this study
pDONR207-pGL1+Intron1	this study

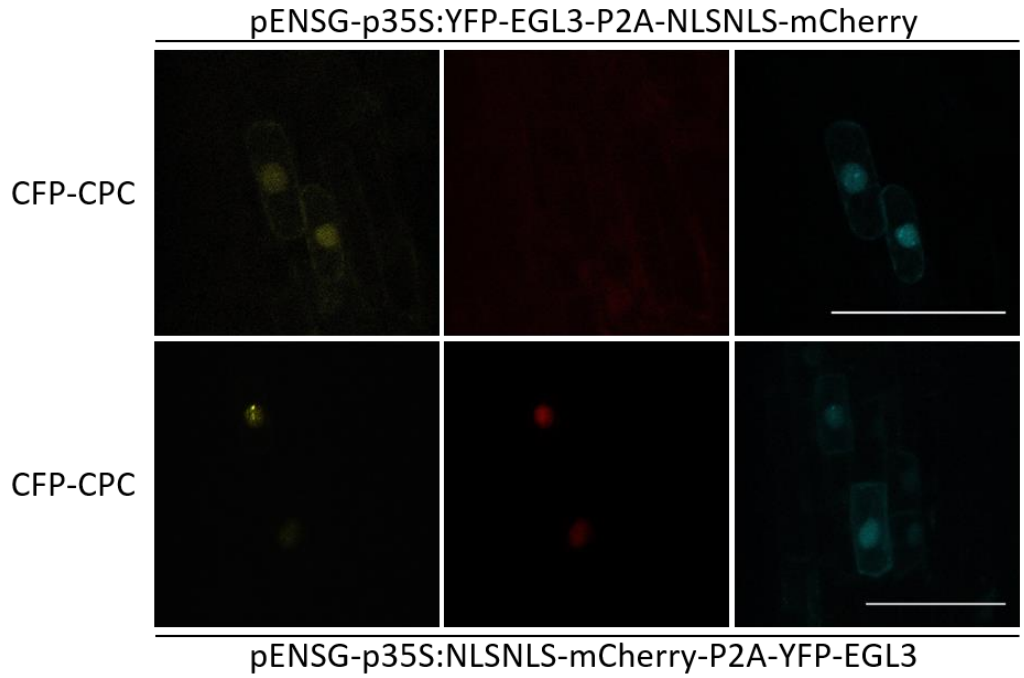

Figure 46. Subcellular localization of EGL3 in the presence CPC. CLSM images of leek epidermal cells transiently expressing *pENSG-p35S:YFP-EGL3-P2A-NLSNLS-mCherry* and *pENSG-p35S:CFP-CPC* (top row) or *pENSG-p35S:NLSNLS-mCherry-P2A-YFP-EGL3* and *pENSG-p35S:CFP-CPC* (bottom row). YFP-EGL3 is displayed in the left column, NLSNLS-mCherry in the middle column and CFP-CPC in the right column. The scale bar indicates 100 µm.

A

Score	Expect	Method	Identities	Positives	Gaps
904 bits(2336)	0.0	Compositional matrix adjust.	474/637(74%)	528/637(82%)	41/637(6%)

```
Query  9    MATGQNRTTVPENLKKHLAVSVRNIQWSYGIFWSVSASQSGVLEWGDGYYNGDIKTRKTI  68
Sbjct  1    ....E...-..D....Q.....................P.....................  59

Query  69   QASEIKADQLGLRRSEQLSELYESLSVAESSSSGVAAGSQVTRRASAAALSPEDLADTEW  128
Sbjct  60   ..A.V.I.....E.....R.......L....A..---S.................T....  116

Query  129  YYLVCMSFVFNIGEGMPGRTFANGEPIWLCNAHTADSKVFSRSLLAKSAAVKTVVCFPFL  188
Sbjct  117  ..............I..GALS..........E.......T........SLQ........  176

Query  189  GGVVEIGTTEHITEDMNVIQCVKTSFLEAPDPYATILPARSDYHIDNVLDPQQILGDEIY  248
Sbjct  177  ...L........K.......S...L.....-..T..-ST....Q--EIF..---.S.DK.  229

Query  249  APMFSTEPFPTASPSRTTNGFDQEHEQVADDHDSFMTERITGGASQVQSWQLMDDELSNC  308
Sbjct  230  T.V.I..A...T.----.S..E..P.----.....IND---..........FVGE.I...  278

Query  309  VHQSLNSSDCVSQTFVEGAAGRVAYGARKSRVQRLGQIQEQQRNVKTLSFDPRNDDVHYQ  368
Sbjct  279  I..............-.TT..L.CDP....I.........SNH.NM------D......  331

Query  369  SVISTIFKTNHQLILGPQFRNCDKQSSFTRWKKSSSSSSGTATVTAPSQGMLKKIIFDVP  428
Sbjct  332  G........T.........Q.F..R.......R...----VK.LGEK..K.I...L.E..  387

Query  429  RVHQKEKLMLDSPEARDETGNHAVLEKKRREKLNERFMTLRKIIPSINKIDKVSILDDTI  488
Sbjct  388  LMNK..E.LP.T..---......LS.................S.....S...........  444

Query  489  EYLQELERRVQELESCRESTDTETRGTMTMKRKKPCDAGERTSANCANNETGNGKKVSVN  548
Sbjct  445  ....D.QK...........A.....I..-......D.EE..A....M.SK----R.G.DV  499

Query  549  NVGEAEPADTGFTGLTDNLRIGSFGNEVVIELRCAWREGVLLEIMDVISDLHLDSHSVQS  608
Sbjct  500  ....D....I.YA........S.L..............I...........N........  559

Query  609  STGDGLLCLTVNCKHKGSKIATPGMIKEALQRVAWIC  645
Sbjct  560  .................T....T...Q..........  596
```

B

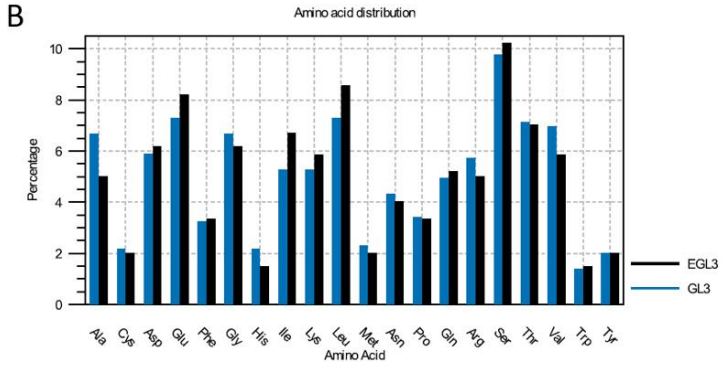

Figure 47. Amino acid alignment and amino acid distribution of GL3 and EGL3. A) The protein sequence alignment of GL3 and EGL3 via protein BLAST. B) Amino acid distribution of GL3 and EGL3 created via CLC Main Workbench22.

Table 18. YFP/mCherry ratios of P2A constructs in leek epidermal cells. Ratio changes to 0.5 or 1.5 may already be biological significant, as they influence the trichome pattern in models (personal communication, A. Deneer).

	CFP-GL1	CFP-GL3	CFP-TTG1	CFP-TRY	CFP-CPC	CFP-EGL3	CFP-MYB23
YFP-GL1-P2A	0.9	2	0.9	1.5	1.4	5.6	0.7
YFP-GL3-P2A	0.8	0.6	0.7			2.6	3.1
P2A-YFP-TTG1	0.7	2.9	0.5	1.3	1.7	3.5	1.4
YFP-TRY-P2A	1.3	2	1.2	1.25		8.2	
YFP-CPC-P2A		1.9		1.5	1.2	4.1	2.3
YFP-MYB23-P2A		6.6	0.9			2.6	1.8
P2A-YFP-EGL3	1.3		1.8	1.5	3.4		1.9

Table 19. Fluorescence percentages of transformed leek epidermal cells expressing *Dendra2-GL1*.

	pre-conversion	conversion	1h	2h	3h	4h	4.5h
Green_1	75.39	100.00	44.06	36.79	17.53	9.61	10.52
Green_2		100.00	54.95	44.28	41.91	39.94	48.74
Green_3	119.68	100.00	80.38	56.65	51.36		
Green_4	144.60	100.00	66.59	30.69	28.16		
Green_5	122.97	100.00	85.29	91.21	86.74		
Green_6	130.47	100.00	67.83	72.95	65.76		
Green_7	134.66	100.00	80.07	83.53	72.16		
Red_1	15.46	100.00	52.84	45.23	26.07	24.21	24.61
Red_2		100.00	74.49	72.24	70.35	60.78	58.32
Red_3	20.23	100.00	75.97	48.55	43.71		
Red_4	25.24	100.00	60.25	35.36	37.58		
Red_5	25.01	100.00	94.22	84.83	82.12		
Red_6	11.29	100.00	89.06	79.94	76.60		
Red_7	21.67	100.00	81.85	79.95	69.73		

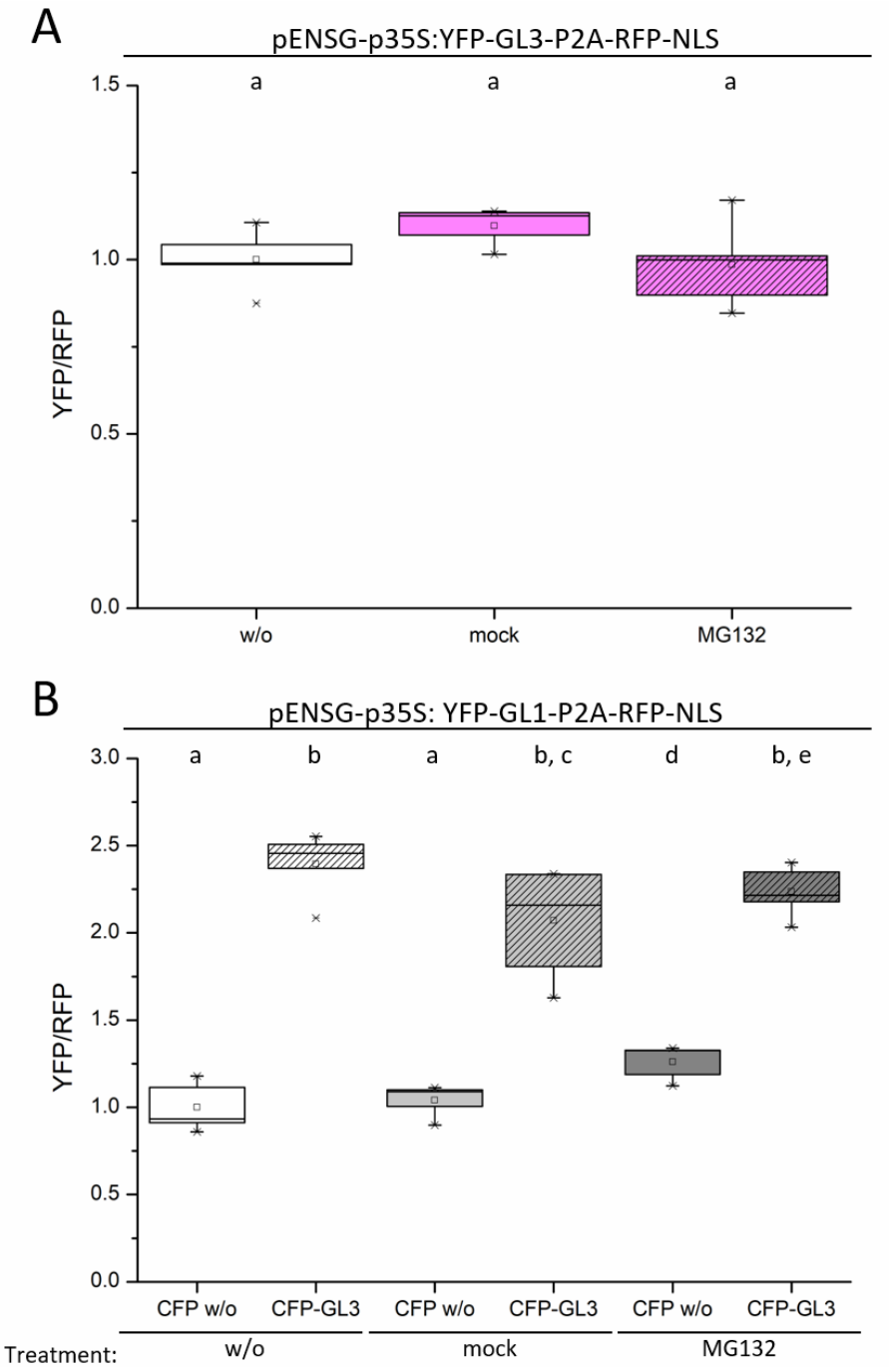

Figure 48. MG132 treatment in tobacco using GL1-P2A and GL3-P2A constructs. A) Box plot graph displaying the normalised YFP/RFP fluorescence ratios of *pENSG-p35S:YFP-GL3-P2A-RFP-NLS* expressed in non-treated tobacco (n=5, median=1), mock treated tobacco (n=5, median=1.13) and MG132 treated tobacco (n=5, median=1. B) Box plot graph displaying the normalised YFP/RFP fluorescence ratios of *pENSG-p35S:YFP-GL1-P2A-RFP-NLS* expressed in non-treated tobacco (n=8, median=1), mock treated tobacco (n=8, median=1.08) and MG132 treated tobacco (n=8, median=1.21). Each n refers to an image of several tobacco epidermis cells. Statistical analysis was performed by OneWayANOVA for A, and Mann-Whitney U tests for B. Statistical differences are indicated by different letters at the top of each graph ($p \leq 0.05$). In all box plots the mean is displayed as a small box in the box formed by median, 0.25 and 0.75 quartiles. Maximum and minimum values are indicated as horizontal lines at the end of the whiskers and the 1% and 99% percentiles are displayed by crosses. Outliers are displayed as small horizontal lines

Table 20. List of CREs detected by PLACE with corresponding category, site number and reference.

Category	Description	Site #	Reference
circadian-related	circadian gene expression regulation	S000252	(Piechulla et al., 1998)
circadian-related	CDA-1 (CAB2 DET1-associated factor 1) binding site in DtRE (dark response element) f of chlorophyll a/b-binding protein2 (CAB2) gene	S000440	(Maxwell et al., 2003)
nutrient-related	putative nodulin consensus sequence	S000461	(Stougaard et al., 1990)
nutrient-related	putative nodulin consensus sequence	S000462	(Stougaard et al., 1990)
nutrient-related	GLM (GCN4-like motif) found in the promoter of barley B1- and c-hordein gene; Involved in the nitrogen response	S000451	(Müller & Knudsen, 1993)
nutrient-related	OsIRO2-binding core sequence; G-box plus G, Fe defieneicy	S000505	(Ogo et al., 2006)
nutrient-related	PHR1-binding sequence found in the upstream regions of phosphate starvation responsive genes (PSR1)	S000459	(Rubio et al., 2001)
organ specificity	Root Hair-specific cis-Elements	S000512	(Kim et al., 2006)
organ specificity	endosperm specific expression	S000353	(C. Y. Wu et al., 2000)
organ specificity	pollen specific element	S000245	(Bate & Twell, 1998)
organ specificity	element for seed specific expression	S000148	(Ellerström et al., 1996)
organ specificity	GTGA motif, pollen specific, tobacco	S000378	(Rogers et al., 2001)
organ specificity	tissue specific expression & induction of auxin, agrobacterium	S000273	(Baumann et al., 1999)
organ specificity	R-GATA (GATA motif binding factor) binding site, phloem-specific gene expression	S000191	(Yin et al., 1997)
organ specificity	RY repeat motif, quantitative seed expression	S000102	(Nag et al., 2005)
organ specificity	RY repeat (CATGCAY) or legumin box found in seed-storage protein genes	S000100	(Fujiwara & Beachy, 1994)
organ specificity	RY repeat found in RY/G box f napA gene in Brassica napus, seed specific expression	S000264	(Ezcurra et al., 1999)
organ specificity	Prolamine box found in the rice GluB-1 gene promoter, endosperm	S000354	(C. Y. Wu et al., 2000)
organ specificity	L1 box, L1 layer-specific expression	S000386	(M. Abe et al., 2001)
organ specificity	GCN4 motif found in GluB-1 gene in rice, endosperm-specific expression	S000277	(Onodera et al., 2001)
organ specificity	BS1 (binding site 1) found in E. gunnii Cinnamoyl-CoA reductase (CCR) gene promoter; required for vascular expression	S000352	(Lacombe et al., 2000)
organ specificity	TGACGT motif high level expression of alpha-Amylase in the cotyledons of the germinated seeds	S000377	(Yamauchi, 2001)

organ specificity	TGTCACA motif, novel enhancer element necessary for fruit-specific expression of the cucumisin gene	S000422	(Yamagata et al., 2002)
organ specificity	key component of expression module of Mem1 (mesophyll expression module 1) in Flaveria	S000449	(Gowik et al., 2004)
poly(A) signal	Poly(A) signal	S000080	(Loke et al., 2005)
poly(A) signal	Plant poly(A) signal	S000088	(Joshi, 1987)
poly(A) signal	poly (A) signal found in rice alpha-amylase	S000081	(O'Neill et al., 1990)
binding site	MYB binding site	S000167	(Sablowski et al., 1994)
binding site	MYB binding site	S000408	(Abe et al., 2003)
binding site	MYC binding site	S000436	(Zhu et al., 2003)
binding site	binding site for TF RAV1	S000314	(Kagaya et al., 1999)
binding site	GATA Box	S000039	(Teakle et al., 2002)
binding site	W-box	S000390	(Eulgem et al., 2000)
binding site	core W-box	S000447	(Eulgem et al., 1999)
binding site	W-box, WRKY binding site	S000310	(Rushton et al., 1995)
binding site	W-box element; *Hordeum vulgare* (barley)	S000442	(Sun et al., 2003)
binding site	W-box, tobacco	S000457	(Eulgem et al., 1999)
binding site	SEF4 binding site, soy bean	S000103	(Allen et al., 1989)
binding site	MYB binding site, animal & Arabidopsis	S000176	(Urao et al., 1993)
binding site	SPBF binding site (SP8b); amylase	S000184	(Ishiguro & Nakamura, 1994)
binding site	SEF1 (soybean embryo factor 1), binding motif; soy bean	S000006	(Lessard et al., 1991)
binding site	putative "core" sequences of box-L-like sequence in carrots	S000492	(Maeda et al., 2005)
binding site	Binding site for ATMYB2, an Arabidopsis MYB homolog	S000177	(Urao et al., 1993)
binding site	MYB recognition site in promoters	S000409	(Abe et al., 2003)
binding site	ARF (auxin response factor) binding site found in the promoters of primary/early auxin response genes of A. thaliana	S000270	(Ulmasov et al., 1999)
binding site	E-box, MYC binding site	S000144	(Stalberg et al., 1996)

binding site	MYC binding site	S000407	(H. Abe et al., 2003)
binding site	S1F binding site	S000215	(Zhous et al., 1992)
binding site	S1F box, plastid protein regulation	S000223	(Zhous et al., 1992)
binding site	variant of CArG motif; Binding site for AGL15 (AGAMOUS-like 15)	S000431	(Tang & Perry, 2003)
binding site	Critical for GT-1 binding to box II of rbcS	S000125	(Gilmartin et al., 1990)
binding site	Core motif of MybSt1 (a potato MYB homolog) binding site	S000180	(Baranowskij et al., 1994)
binding site	"CACGTG motif"; "G-box"; Binding site of Arabidopsis GBF4	S000042	(Yamamoto et al., 2007)
binding site	bZIP transcription factors, DPBF-1 and 2	S000292	(Kim et al., 1997)
binding site	disease resistance response, binding site homeodomain TF	S000498	(Luo et al., 2005)
binding site	SEF3 binding site, SEF=soybean embryo factor	S000115	(Allen et al., 1989)
binding site	amylase box, amylase element in grains	S000021	(Huang et al., 1990)
binding site	TATCCAY motif; RAmy3D alpha-amylase gene promoter in rice	S000256	(Toyofuku et al., 1998)
binding site	Binding consensus sequence of an Arabidopsis TF RAV1	S000315	(Kagaya et al., 1999)
binding site	Binding site of the Arabidopsis homeobox gene (ATHB-2; HD-Zip protein) found in its own promoter	S000373	(Ohgishi et al., 2001)
binding site	Core element in LeCp binding cis-element	S000465	(Matarasso et al., 2005)
binding site	W box from tobacco	S000508	(Yamamoto et al., 2004)
binding site	Recognition sequence of Arabidopsis Athb-1 protein; HD-Zip motif	S000317	(Sessa et al., 1993)
binding site	Consensus binding sequence for Arabidopsis class I HDZIP protein	S000371	(Johannesson et al., 2001)
binding site	E2F consensus sequence of all different E2F-DP-binding motifs	S000476	(Vandepoele et al., 2005)
binding site	ElRE (Elicitor Responsive Element), W box	S000142	(Rushton et al., 1996)
binding site	AG-motif, AGP1 (GATA-type zinc finger protein) binding site	S000444	(Sugimoto et al., 2003)
binding site	ASF-1 binding site in CaMV 35S promoter	S000024	(Klinedinst et al., 2000)
binding site	bZIP proteins SGBF-1 and SGBF-2 binding site in soybean	S000287	(Hong et al., 1995)
binding site	Target sequence of WUS in the intron of AGAMOUS gene in Arabidopsis	S000433	(Kamiya et al., 2003)

binding site	Myb core in the 18 bp sequence which is able to activate reporter gene without leading to M-phase-specific expression	S000502	(Planchais et al., 2002)
binding site	rbcS general consensus sequence; G box; I box	S000127	(Donald & Cashmore, 1990)
binding site	Box A; Consensus; One of three putative cis-acting elements (boxes P, A, and L) of phenylalanine ammonia-lyase	S000137	(Logemann et al., 1995)
binding site	Target sequence of LEAFY in the intron of AGAMOUS gene in Arabidopsis	S000432	(Kamiya et al., 2003)
binding site	Core of consensus maize P (myb homolog) binding site; MYB binding site	S000179	(Grotewold et al., 1994)
binding site	Core site required for binding of Dof proteins in maize	S000265	(Yanagisawa, 2004)
disease & stress motifs	promoters activated in infected cells of root nodules	S000468	(Vieweg et al., 2004)
disease & stress motifs	organ specific element (OSE), disease/infection reaction response	S000467	(Fehlberg et al., 2005)
disease & stress motifs	promoter motif soy bean; pathogen- & salt-stress	S000453	(Park et al., 2004)
disease & stress motifs	Ca responsive element	S000507	(Kaplan et al., 2006)
disease & stress motifs	Core motif of DRE/CRT (dehydration-responsive element/C-repeat)	S000418	(Dubouzet et al., 2003)
disease & stress motifs	binding site of dehydration-responsive element (DRE)	S000497	(Xue, 2002)
disease & stress motifs	copper & oxygen response	S000493	(Quinn & Merchant, 1995)
disease & stress motifs	core of sulfur-responsive element (SURE)	S000499	(Maruyama-Nakashita et al., 2005)
disease & stress motifs	Pti4(ERF) regulates defence-related gene expression	S000443	(Chakravarthy et al., 2003)
disease & stress motifs	CGCG box; Ca++/calmodulin binds to all AtSRs	S000501	(Yang & Poovaiah, 2002)
disease & stress motifs	Pyrimidine box found in rice alpha-amylase (RAmy1A) gene, partially involved in sugar repression	S000259	(Morita et al., 1998)
disease & stress motifs	MYC recognition sequence; water-stress	S000413	(Simpson et al., 2003)
disease & stress motifs	Binding site for MYB (ATMYB2) in dehydration-responsive gene rd22	S000175	(Abe et al., 1997)
TATA box	TATA-like motif; Phaseolus vulgaris; maize (Zea mays)	S000340	(Yukawa et al., 2000)
TATA box	TATA box, sweet potato & pea	S000111	(Grace et al., 2004)
TATA box	TATA box	S000203	(Tjaden et al., 1995)

TATA box	TATA box	S000110	no reference
TATA box	TATA box	S000109	(Shirsat et al., 1989)
promoter elements	CAAT promoter consensus sequence	S000028	(Shirsat et al., 1989)
promoter elements	promoter element *A. rhizogenes*	S000098	(Elmayan & Tepfer, 1995)
promoter elements	promoter element in *B. napus*	S000070	(Ericson et al., 1991)
promoter elements	promoter element of bacterial enzyme	S000400	(Zhu et al., 2002)
promoter elements	promoter element of anearobic genes	S000477	(Mohanty et al., 2005)
promoter elements	promoter element, guard cell specific expression	S000387	(Plesch et al., 2001)
promoter elements	promoter element of anearobic genes	S000478	(Mohanty et al., 2005)
promoter elements	promoter element of anearobic genes	S000479	(Mohanty et al., 2005)
promoter elements	promoter element tobacco	S000395	(Nakamura et al., 2002)
promoter elements	promoter element, amylase enzymes	S000020	(Huang et al., 1990)
promoter elements	silencing element binding factors (SEBF)	S000391	Boyle & Brisson, 2001
promoter elements	BoxII, plastid promoter element	S000296	(Kapoor & Sugiura, 1999)
promoter elements	Pro- or hypoosmolarity-responsive element	S000450	(Satoh et al., 2004)
promoter elements	A-box; ACGT element; G motif	S000130	Foster, 1994
promoter elements	Motif (IVD) found in the *Chlamydomonas* (C.R.) Nia1 gene promoter	S000375	(Loppes & Radoux, 2001)
promoter elements	Sequence found in NDE element in soybean; auxin response	S000370	(Xu et al., 1997)
promoter elements	the -300 element in B-hordein gene of barley	S000122	(Colot et al., 1987)
promoter elements	QAR (quantitative activator region	S000244	(Elliott & Shirsat, 1998)
promoter elements	Conserved 11 nt sequence found in the maize (Z.m.) mitochondrial promoter	S000301	(Rapp & Stern, 1992)
promoter elements	sugar-repressive element (SRE)	S000470	(Tatematsu et al., 2005)
promoter elements	cell-cycle-specific activation of transcription	S000031	(Nasmyth et al., 1990)
promoter elements	CT-rich motif (inverted GAGA) found in a 60-nucleotide region (S1) downstream of the transcription start site of the CaMV 35S RNA	S000460	(Pauli et al., 2004)
promoter elements	TGTAAAG core motif in "-300 elements"	S000001	(Forde et al., 1985)

promoter elements	CGACG element found in the GC-rich regions of the rice Amy3D and Amy3E amylase genes	S000205	(Hwang et al., 1998)
promoter elements	RY repeat motif (CATGCAT) in soy bean glycinin gene	S000105	(Lelievre & Nielsen, 1992)
promoter elements	promoter element of anearobic genes	S000480	(Mohanty et al., 2005)
promoter elements	Motif in -300 elements of alpha-zein genes of maize	S000002	(Thomas & Flavel, 1990)
promoter elements	T-box according to the nomenclature of ACGT elements by Foster	S000132	Foster, 1994
promoter elements	hexamer motif found in promoter of wheat (T.a.) histone genes H3 and H4; Binding with HBP-1A and HBP-1B	S000053	(Mikami et al., 1987)
promoter elements	cis-element identified among the promoters of the "core xylem gene set"	S000510	(Ko et al., 2006)
promoter elements	Conserved in many storage-protein gene promoters	S000143	(Stalberg et al., 1996)
hormone-related	ABA responsive element	S000402	(Busk et al., 1997)
hormone-related	Central element of gibberellin (GA) response complex (GARC)	S000181	(Gubler et al., 1995)
hormone-related	GARE (GA-responsive element)	S000439	(Ogawa et al., 2003)
hormone-related	Pyrimidine box, promoter element, required for GA induction	S000298	(Cercós et al., 1999)
hormone-related	T/G box, jasmonate production	S000458	(Boter et al., 2004)
hormone-related	putative element for ABA-responsive expression	S000394	(Hattori et al., 2002)
hormone-related	Gibberellin-responsive element (GARE)	S000420	(Sutoh & Yamauchi, 2003)
hormone-related	Sequence present in 24 genes in the GA-down regulated d1 cluster	S000438	(Nakashima et al., 2006)
hormone-related	ERE (ethylene responsive element)" of tomato	S000037	(Itzhaki et al., 1994)
hormone-related	TATCCA element; Binding sites of OsMYBS1, OsMYBS2 and OsMYBS3 which mediate sugar and hormone regulation	S000403	(Lu et al., 2002)
hormone-related	Binding site for MYC (rd22BP1) in Arabidopsis dehydration-resposive gene, ABA-induction	S000174	(Abe et al., 1997)
hormone-related	CAREs (CAACTC regulatory elements) gibberellin; seed	S000421	(Sutoh & Yamauchi, 2003)
hormone-related	Gibberellin-responsive element (GARE) in promoter region of a cystein proteinase (REP-1) gene in rice	S000419	(Sutoh & Yamauchi, 2003)
hormone-related	ABA responsive element, ABRE3	S000135	(Straub et al., 1994)

hormone-related	ARR1-binding element	S000454	(Sakai et al., 2000)
splice junctions	3' intron-exon splice junctions	S000086	(Brown, 1986)
light-related	Tbox, Light-regulated gene expression	S000383	(Chan et al., 2001)
light-related	Light-regulated gene expression	S000198	(Villain et al., 1996)
light-related	promoter motif, phytochrome regulation, etiolation	S000362	(Degenhardt & Tobin, 1996)
light-related	etiolation-induced expression	S000414	(Simpson et al., 2003)
light-related	etiolation-induced expression	S000415	(Simpson et al., 2003)
light-related	phyA-repressed motifs; light response	S000488	(Hudson & Quail, 2003)
light-related	promoter element cytokinin, chloroplast	S000491	(Fusada et al., 2005)
light-related	I-box, light specific regulation	S000199	(Terzaghi & Cashmore, 1995)
light-related	-10 promoter element" found in the barley (H.v.) chloroplast	S000392	(Thum et al., 2001)
light-related	I-box core motif in the CAMs (conserved DNA modular arrays) associated with light-responsive promoter regions	S000424	(Martínez-Hernández et al., 2002)
light-related	I-box, light specific regulation	S000124	(Giuliano b et al., 1988)
light-related	"REbeta" found in *Lemna gibba Lhcb21* gene promoter; Required for phytochrome regulation	S000363	(Degenhardt & Tobin, 1996)
light-related	CCA1 binding site, CCA1 protein (myb-related TF), regulation by phytochrome	S000149	(Wang et al., 1997)
light-related	Sequences Over-Represented in Light-Induced Promoters (SORLIPs), phyA-induced motifs	S000486	(Hudson & Quail, 2003)
light-related	Sequences Over-Represented in Light-Induced Promoters (SORLIPs), phyA-induced motifs	S000482	(Jiao et al., 2005)
temperature-related	CCAAT box, element in promoters of heat shock protein genes	S000030	(Rieping & Sehfffl, 1992)
temperature-related	heat shock responsive element, *Clamydomonas*	S000506	(von Gromoff et al., 2006)
temperature-related	Core of low temperature responsive element (LTRE)	S000153	(Baker et al., 1994)
temperature-related	LTRE-1, low-temperature-responsive element, barley	S000250	(Dunn et al., 1998)
temperature-related	CArG consensus; in promoter of SOC1; vernalization (low-temperature) pathway	S000404	(Hepworth et al., 2002)
scaffold/matrix attachment sites	T-Box; Motif found in SAR (scaffold attachment region; or matrix attachment region, MAR)	S000067	(Gasser et al., 1989)

scaffold/matrix attachment sites	ARS element; Motif found in SAR (MAR)	S000064	(Gasser et al., 1989)
enhancer elements	SV40 core enhancer; Similar sequences found in rbcS genes	S000123	Weiher, 1983
enhancer elements	enhancer element, MYB-binding site	S000494	(Kucho et al., 2003)
enhancer elements	Q(quantitative)-element; pollen-specific maize gene, enhancer function	S000254	(Hamilton et al., 1998)

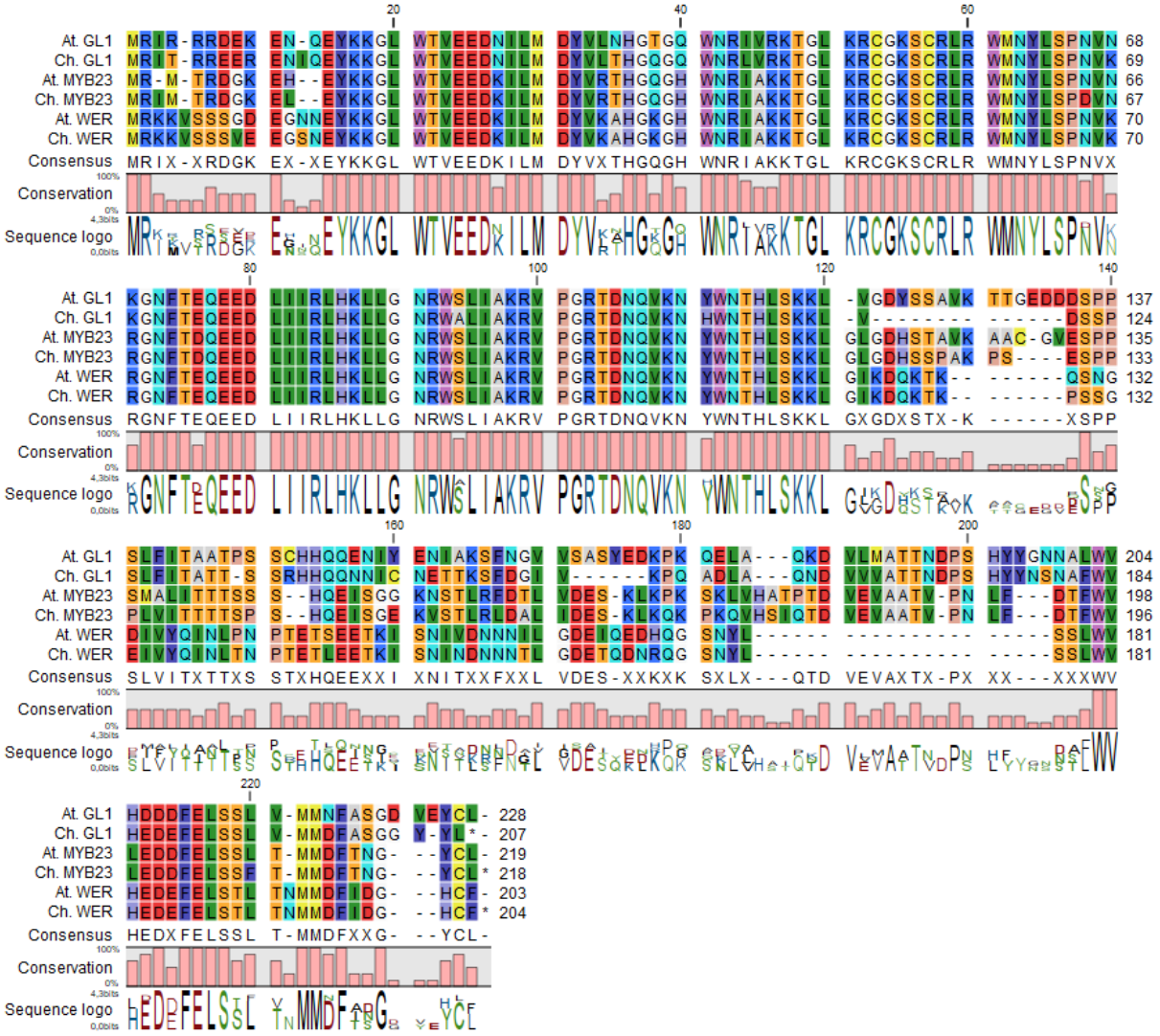

Figure 49. Alignment of the protein sequences of the MYBs *GL1*, *MYB23* and *WER* from *A. thaliana* & *C. hirsuta*. The name is given left, the nucleotide number right. Similar nucleotides are displayed by different sized letters at the bottom of each row at each given nucleotide position. Alignment was created using CLC DNA Main Workbench 22.

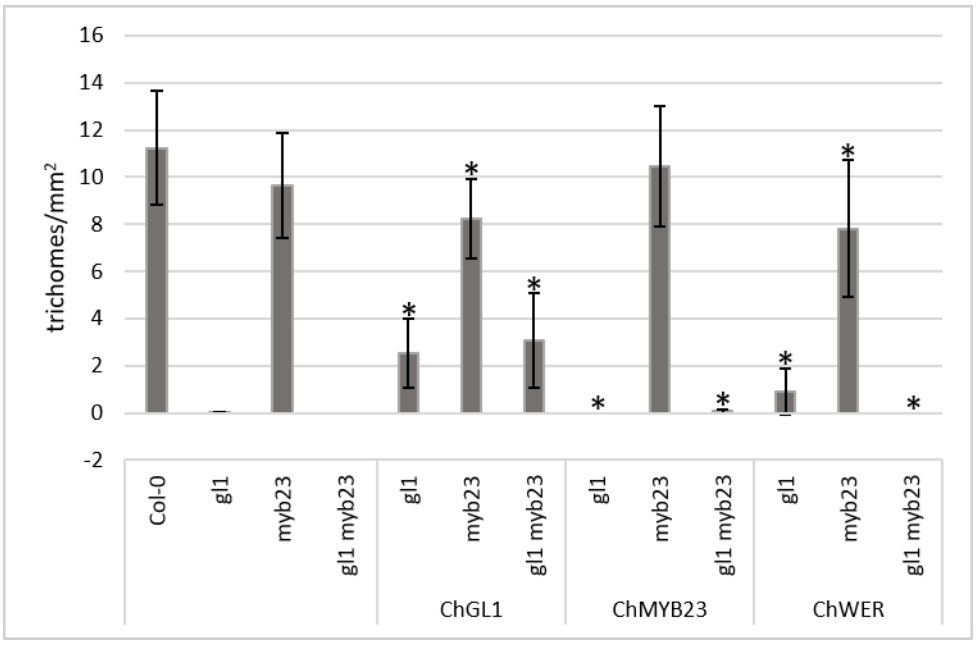

Figure 50. Trichome density in T1 rescue plants expressing Cardamine constructs. Trichome density in T1 rescue plants expressing *Cardamine* constructs. Bar graph of trichome number of leave four of Col-0 and mutant plants, as well as *gl1*, *myb23,* and *gl1 myb23* T1 plants transformed with *ChGL1*, *ChMYB23,* and *ChWER* rescue constructs. Error bars depict standard deviations. Statistical analysis was performed by Mann-Whitney U tests comparing the plants expressing the Cardamine constructs with Col-0. Statistical differences to Col-0 ($p \leq 0.05$) are indicated by a black asterisk.

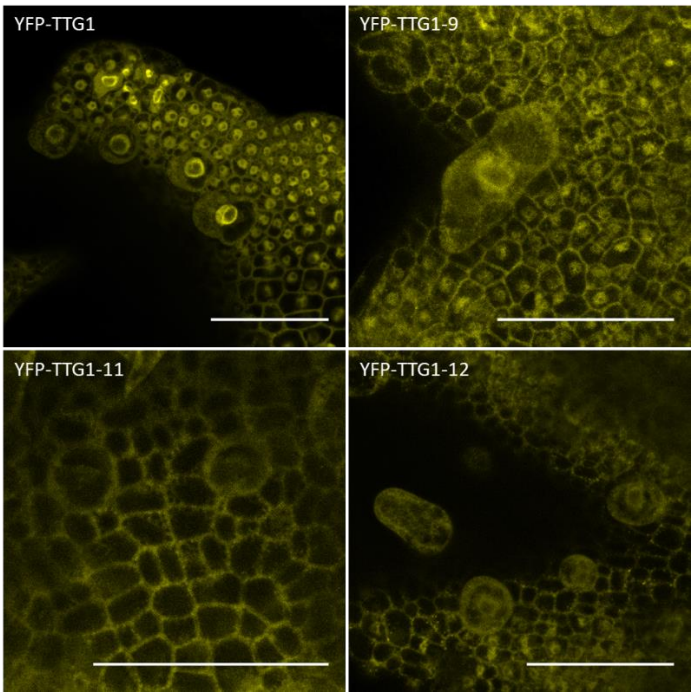

Figure 51. Cellular localization of TTG1 and TTG1 mutant versions. Scale bar is 50 µm.

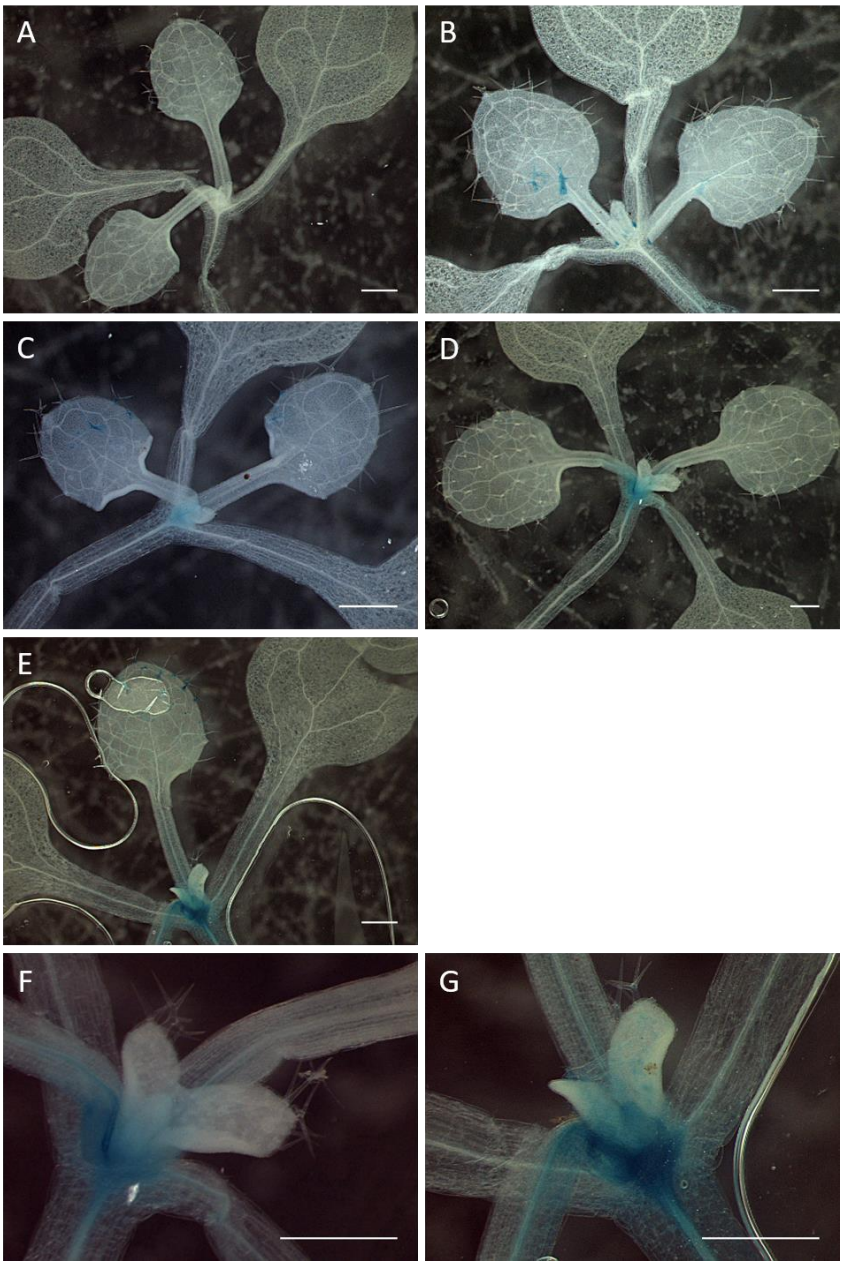

Figure 52. GUS staining of back-crossed Col-0 plants expressing *pCPC:GUS* from cpc try line GUS staining is displayed after 1h (A, B), after 2 h (C, D, F) and after 5h (E, G). For each time point, the same sample is shown, but with different magnifications. The scale bar refers to 500 µm.

Acknowledgements

First and foremost, I want to thank my supervisor **Prof. Dr. Martin Hülskamp**. Thank you for providing me with the opportunity to research such an interesting topic as trichome patterning. Over the years I always felt supported and understood, but also provided with complex biological questions. Thank you for always having an open ear.

Also, I want to thank **Prof. Dr. Ute Höcker** and **Prof. Dr. Kay Hofmann** cordially for agreeing to be part of my examination committee.

Moreover, I want to thank my TAC, **Prof. Dr. Ute Höcker**, **Prof. Dr. Matias Zurbriggen** and **Dr. Swen Schellmann** for the highly appreciated questions and ideas regarding my different project. Thank you for listening to my rather long talks.

The biggest thank you has to go to **Dr. Lisa Stephan**, without you I would not be here. Thank you from the bottom of my heart for believing in me! Since by Bachelor student days you were always there, answering questions, giving creative ideas and problem-solving strategies. Also, your proof-reading of this thesis was an existential part of its creation process.

Even though we are no colleagues anymore, we are still friends. Dear **Dr. Eva Koebke and Dr. Jessica Pietsch**, I am very grateful to have worked a long time of my academic career besides you two and engaged in interesting work or not work-related conversation.

I also want to thank my fellow PhD students **Barbara**, **Helen** and **Andrii** for the very nice working environment, the friendships and also the differentiated discussions regarding our research topics.

Without **Dr. Anna Deneer** and **Toquinha Bergmann**, the development of trichome patterning models and tte discussion about the interplay between modelling and biological experiments would be just half as fun and informative.

Without the help of **Sabine**, **Roswitha**, **Sonja**, **Neda** and **Birgit** our Lab would probably not be running so smoothly. Thank you very much for the scientific expertise, the haring of experiences and being an essential part of this group. Also thank you **Irene** and **Bastian**, especially for the help regarding the cell suspension culture, but not exclusively.

Thank you, **Birgit**, for your extraordinary help in the past years! Without you these projects would not have advanced as was as they did. Especially your cloning skills came in handy!

Also, I am really grateful for **Dr. Marc Jakoby** for providing great ideas and sharing the plethora of experimental procedures performed by yourself. I really appreciate the feedback and suggestion regarding my different projects.

Dustin Firmenich, thank you for your outstanding work during your Bachelor thesis and for being such a bright, kind and funny person to be around.

My fellow Bachelor companions, **Christiane Schuh** and **Lucas Aschenbrenner**, thank you for your support and your year-long friendship.

I also want to thank my **family** and **friends**, who always believed in me and supported by dream to become a biologist unconditionally. Especially my parents enabled my studies in Cologne and always showed me their support.

Last, but not least, I want to thank my wonderful husband! Without you **Micha**, I would have had significantly more nervous breakdowns during my PhD. You always have my back and would listen to my lab stories, long or short. Thank you for always cheering me on.

Declaration of academic integrity

Erklärung zur Dissertation
gemäß der Promotionsordnung vom 12. März 2020

Hiermit versichere ich an Eides statt, dass ich die vorliegende Dissertation selbstständig und ohne die Benutzung anderer als der angegebenen Hilfsmittel und Literatur angefertigt habe. Alle Stellen, die wörtlich oder sinngemäß aus veröffentlichten und nicht veröffentlichten Werken dem Wortlaut oder dem Sinn nach entnommen wurden, sind als solche kenntlich gemacht. Ich versichere an Eides statt, dass diese Dissertation noch keiner anderen Fakultät oder Universität zur Prüfung vorgelegen hat; dass sie - abgesehen von unten angegebenen Teilpublikationen und eingebundenen Artikeln und Manuskripten - noch nicht veröffentlicht worden ist sowie, dass ich eine Veröffentlichung der Dissertation vor Abschluss der Promotion nicht ohne Genehmigung des Promotionsausschusses vornehmen werde. Die Bestimmungen dieser Ordnung sind mir bekannt. Darüber hinaus erkläre ich hiermit, dass ich die Ordnung zur Sicherung guter wissenschaftlicher Praxis und zum Umgang mit wissenschaftlichem Fehlverhalten der Universität zu Köln gelesen und sie bei der Durchführung der Dissertation zugrundeliegenden Arbeiten und der schriftlich verfassten Dissertation beachtet habe und verpflichte mich hiermit, die dort genannten Vorgaben bei allen wissenschaftlichen Tätigkeiten zu beachten und umzusetzen. Ich versichere, dass die eingereichte elektronische Fassung der eingereichten Druckfassung vollständig entspricht.

Teilpublikationen:

Balkunde R, Deneer A, Bechtel H, Zhang B, Herberth S, Pesch M, Jaegle B, Fleck C, Hülskamp M. Identification of the Trichome Patterning Core Network Using Data from Weak ttg1 Alleles to Constrain the Model Space. Cell Rep. 2020 Dec 15;33(11):108497. doi: 10.1016/j.celrep.2020.108497. PMID: 33326794.

28.06.24 Hanna Bechtel Bechtel

Datum, Name und Unterschrift